Real-Time Monitoring and Characterization of Smart Cement and Soil with Polymer Modification to Control Gas Leakage and Corrosion.

by
Guru Prasad Panda

A dissertation submitted to the Material Science Department,
Cullen College of Engineering
in partial fulfillment of the requirements for the degree of

Doctor of Philosophy

in Material Science Engineering.

Chair of Committee: Dr. Cumaraswamy Vipulanandan

Committee Member: Dr. Gangbing Song

Committee Member: Dr. Gino J. Lim

Committee Member: Dr. George K. Wong

Committee Member: Dr. Yandi Hu

University of Houston
May 2020

ACKNOWLEDGMENTS

This study was made possible by the support, assistance, and valuable feedbacks by my guide Dr Cumaraswamy Vipulanandan. I express my sincere gratitude towards my Professor for his unequivocal support. I would like to extend my appreciation to Dr. Gangbing Song, Dr. Gino J Lim, Dr. Yandi Hu and Dr. George K. Wong for serving in my dissertation committee and for providing me valuable advices into my research. I would like to thank my Department Chair Dr Karim Alamgir, for his support.

I am thankful to Almighty, which manifests itself through nature for being able to write these lines. I thank all my teachers who nurtured and made me. I thank my friends for their valuable feedbacks throughout this period. I also thank our previous department manager, Miranda Vernon-Harrison and present manger Chrisdolyn Dawson for their help and guidance during the PhD. I thank all UH staff members for their support and kind help.

Without the affection and inspiration of my father Dr Chittaranajan Panda and my mother Dr Priti Lata Panda ,this journey would have never started.Finally , I thank my wife Namrata Dash for her enduring support during the journey.

ABSTRACT

In Oil and Gas, downhole sensing and monitoring of cementing activities is extremely difficult. Smart cement with an electrical impedance method provides a new mechanism to monitor cementing activities. In this research, the rheological properties of cement slurries at different temperatures, the effect of polymer addition has been investigated. With different additives, the sensing properties of smart Class H cement is monitored for field applications. Research is done on different types of cement additives to check their efficacy to control shrinkage, impact retardation, gas prevention capacity, sensing properties, and their overall effect on mechanical properties.

Another major problem in the oil industry is gas leakage. In this research, the hydration mechanism of cement affected by gas migration is put forward. The gas leak in cement slurry at various stages of curing and effect on electrical properties in investigated A novel method to quantify gas leak is proposed, which would accurately differentiate the efficiency of cement slurries to prevent gas leakage. Detection and quantification of gas leakage on cement at high temperature and high pressure are investigated by using sensing smart cement and electrical impedance concept.

In this study, polymer stabilization of clay has been investigated. Using electrical properties, the effect of polymer on clay soil was investigated. Polymer stabilization provides a rapid and cost-effective alternative to lime treatment. In this research, the quantification of electrical properties of soil due to polymer application is done, which could be applied on the field for quality control. Additionally, for detecting artificial ground

freezing, the electrical impedance method is verified.The change in electrical properties of soil is quantified by the electric measurements.

In this research, the corrosion of cement composites and steel is evaluated using electrical impedance method. The corrosion kinetics occurring inside the material are quantified by using an equivalent electric impedance method.

Table of Contents

List of Tables

List of Figure

CHAPTER 1

Introduction

1.1) Monitoring Oil Well Cement Behavior.

In the past decade, shale gas resources have been exploited. Application of hydraulic fracturing and horizontal drilling has given a vast new energy resource. However, the cement sheath, behind the casing is vulnerable to failure due all these activities. Failure of cement sheath located in gas formation leads to gas migration in from the reservoir to wellbore. Sustained casing pressure may cause safety issues to personnel, damage equipment, and may cause environmental hazards. Many researchers have worked on the failure mechanism of cement sheath due to sustained pressure, gas leakage, exposure to cyclic load and due to hydraulic fracturing. One of the major problems faced in oil and gas industry is the real-time detection and monitoring of the physical phenomenon happening below. Existing methods of used in the industry such as acoustic measurement have limitations (Gowida et al., 2018). A new method proposed by Vipulanandan, using smart cement with EIS measuring technique can be used to detect the downhole cement sheath conditions.

A highly sensitive chemo-piezo cement invented by Vipulanandan (2014) and improvised electrical impedance method is used to monitor the cement behavior under different conditions of curing, under different stress conditions and under gas leakage at various time intervals. Resistivity change of the smart cement due to addition of additives, setting time, curing duration under different conditions, application of stress, fluid loss and under gas leakage has been quantified in this research. Using resistivity as monitoring method smart cement with different additives have been characterized.

1.2) Additive to Enhance Properties and Control Gas Leakage.

To retard the cementing process, drilling industry uses different combinations of retarders to delay the thickening time. In this research, cellulose is used to retard the cementing process. Although it is known to retarding properties, but it has adverse effects on the cement slurry. In this this research an optimum mix of cellulose was used with smart cement to achieve the desired setting time and compressive strength. Cellulose effect on the setting time, rheology, compressive strength and piezoresistive behavior has been investigated. Another, bigger problem in oil well cements is shrinkage (Lyomov et al., 1977). To reduce the plastic shrinkage, extremely low percentage of polypropylene fiber has been used. The effect of polypropylene fiber on the resistivity, curing time, compressive strength and piezoresistive behavior has been investigated.

Gas leakage through cement sheath is a complex problem. Many researchers have proposed different cementing formulation to mitigate gas leak problem in oil industry based on the fluid loss, static gel strength, and slurry response number (Bonett et al., 1996). In this research, gas migration test is performed on neat cement slurry of different water/cement ratios at various curing time to know the critical conditions at which gas starts to leak under sustained pressure. As cement transits from slurry state to solid-state, significant change happens in cement pore structure and it directly affects the gas leak. To quantify the gas leak rate, the resistivity change during the process is monitored. Gas leakage test was performed on the smart cement modified with carboxylated styrene butadiene at various stages of curing.

1.3) Using Rheology as Quality Control

Cement slurry used in oil well is an amalgamation of various additives. Rheology of the cement slurry becomes essential to know the flowability and pumpability of cement. Cement slurry is viscoelastic material and shows different thixotropic behavior under addition of different admixtures. In this thesis, cement rheological behavior is modeled, thixotropic and anti-thixotropic behavior is discussed. A new concept of energy for any cementing formulation has been introduced and it can be used to decide pumping operations.

1.4) Expansive Soil Stabilization By Polymer Treatment.

Around one-fourth of surface area in the USA is made of expansive soil and is found in all states. Expansive soil, as the name suggests expands or shrinks due to change of moisture content. Expansive soil causes severe damage to houses, building, roads, and pipelines. Wet and dry cycles in clay lead to volumetric changes, which lead to soil expansion or contraction. Due to this, superstructure build over clays soil gets damaged. As per ASCE estimate, one fourth of all homes in USA have some damage caused by expansive soils. Wiggins (1977) reported that building loses from the expansive soil would be over by 4.5 billion dollars at today's age

To overcome the swelling problem caused by clay soil, two primary soil stabilization methods are mechanical and chemical techniques. Many techniques of soil stabilization by chemical additives, squeezing control, overloading and moisture control have been suggested. Commonly used binder for soil stabilization are cement, fly ash, lime, blast furnace slag, bitumen. Another class of derivatives call nontraditional are used.

Nontraditional additives such as polymer-based product, lignosulfonate products, enzymes and resin are used to control the stabilize the soil.

In 2012, Vipulanandan proposed a new method to control swelling soil. This method involves applying water-soluble polyacrylamide polymer into clay soil. In this research, the percentage of polymer addition has been optimized to give better results. Polymer addition affects the electrical resistivity of the treated soil. To monitor the soil treatment, electrical resistivity may be used as a monitoring tool. Electrical resistivity measures the material property, and it can be correlated with the swelling potential of the soil, plasticity index, activity index of the soil.

1.5) Detecting Soil Freezing

Soil freezing affects the resistivity and this can be used to know the soil condition. Resistivity change can be employed to know the soil condition while freezing.

1.6) Detection of Corrosion in Cement Composites.

Detect and quantify corrosion in cement composites and steel at high temperature by applying electrical impedance method.

1.7) Objective

The overall objective of the studies on the oil well cement with different additives, gas leak studies and rheology are

1. Investigate the effect of cellulose addition on the short term and long-term electrical resistivity of smart cement, the retarding effect of cellulose, piezoresistive behavior of cellulose on smart cement.

2. Characterize the effect of polypropylene fiber on the short term and long-term electrical properties curing, shrinkage, compressive behavior and piezoresistive behavior of smart cement.
3. Quantify the effect of carboxylated styrene butadiene on the resistivity, curing, compressive strength, piezoresistive behavior, fluid loss, permeability and gas leak rate on smart cement.
4. Investigate the effect of different w/c ratios on electrical resistivity due to one day curing and their piezoresistive behavior, effect of gas migration on the fluid loss at different curing times, phase diagram of hydrating cement, effect of gas migration on electrical resistivity.
5. Characterize the rheological behavior of different cement slurries using Bingham Plastic and Vipulanandan rheological model.
6. Electrical Characterization of Polymer Treated Expansive Soil.
7. Characterize the mechanical and electrical properties of soft clay soil while freezing and thawing.
8. Detection of Corrosion in Cement Composites by Using Electrical Impedance Method.

1.8) **Organization**

The dissertation would be organized in the following chapters.

Chapter 2

In chapter 2, a comprehensive literature review is presented about oil well cement slurry properties, expansive soil treatment.

Chapter 3

Material, method and Mathematical model used to conduct the studies has been discussed.

Chapter 4

In chapter 4, the effect of temperature and polymer addition on smart slurries at various temperatures were investigated.

Chapter 5

Chapter 5 presents the details of experimental work done on smart cement modified by polymer. Material Behavior were characterized using electrical resistivity, sensing capabilities were examined by piezo resistivity test.

Chapter 6

This chapter summarizes the finding of gas migration test on cement slurry of different water cement ratios. The effect of gas leak phenomenon is described in cement slurry at various stages of curing by the phase diagram. The electrical behavior of cement due to gas migration is explained.

Chapter 7

This chapter presents the electrical characterization of polymer treated clay soil. Additionally, the application of electrical impedance method to monitor artificial ground freezing of soil is investigated.

Chapter 8

This chapter summarizes the corrosion of cement composites using electrical impedance method.

CHAPTER 2 BACKGROUND AND LITERATURE REVIEW

2.1) Oil well cement

In oil well, cementing is a critical operation. Good cementing job decides the long-term stability of well, ensures safe production activities, and in the long run, saves contamination of soil. Cementing standards and methodology has been developed over time to ensure proper cementing jobs in oil wells. Depending on the formation, well type (oil, gas, or geothermal), gas zone, different types and varieties of cementing jobs are performed. The cementing systems are listed below (Saleh, 2016)

1) Deepwater Cementing Systems-This cementing system should have all the characteristics to stop the flow of shallow water/gas, high rapid development of gel strength and low viscosity

2) Heavyweight Cementing Systems-Heavy weight cementing system should be selected if the formations categorized as high pressure.

3) Lightweight Cementing Systems. The lightweight cement system makes sure that the density of the cement is kept at a minimum level so that the losses to the formation can be avoided.

4) Self-Healing System-These cement system has a built-in capability of repairing the cracks and thereby maintaining its integrity without any remedial operation.

5) Foam Cementing Systems-This cementing system comprises of cement slurry, foaming agent and a gas. On mixing and shearing, tiny and discrete bubbles get created which are not interconnected and form a less dense cement matrix with characteristics such as high strength and low permeability.

To characterize a cement slurry behavior, initial density, rheological behavior, gel strength, fluid loss, free water tests are needed. For mechanical properties, compressive strength, tension test is required. In this chapter, the previous models used by the researcher to describe the heat of hydration behavior of cement slurries, rheological properties, the compressive strength of cement with additives, models to describe the stress-strain behavior and permeability of slurry at various stages of curing has been put forward. One of the challenging problems in the oil industry is gas leakage and the existing method to describe gas-tight cement slurry and its limitations have been reviewed.

Another important aspect is the real-time monitoring of gas oil wells including cement hydration. Real-time monitoring is necessary to detect and sense gas migration. Acoustic logs measure the cement quality from the degree of acoustic coupling of the cement to casing and formation. (Gowida et al., 2018). Although properly run CBL provides reliable well integrity and zonal isolation but does not detect gas leakage and cement hydration. To detect real-time gas leakage, smart cement developed by Vipulanandan can be used as a monitoring tool with electrochemical Impedance measurements (Vipulanandan et al., 2012). For continuous monitoring of cement behavior from preparation to solidification, resistivity as a monitoring method has been used extensively in this research. The work of many researchers on the electrical resistance and resistivity application for concrete has been investigated in detail. In the research, use of electrical resistivity as a monitoring tool for measuring the physical properties of cement is well established. In this research, the changes in electrical resistivity of smart cement due to setting, uniaxial load, curing in different conditions and gas leakage through cement have been quantified separately.

Table 2-1 Key feature of API Oil Well Cement

Cement Class	A	B	C	D	G	H
Recommend w/c, % mass fraction of cement	46	46	56	38	44	38
Recommend rage of depth, m (ft)	0 to 1830 (0 to 6000)	0 to 1830 (0 to 6000)	0 to 1830 (0 to 6000)	1830 to 3050 (6000 to 10000)	0 to 2440 (0 to 8000)	0 to 2440 (0 to 8000)
Availability O Grade-I MSR- II HSR- III	Type I	Type	Type I, II and Type III	Type II and Type III	Type II and Type III	Type II and Type III
Other Features	Intended for use when special properties are not required	1.Intended for use when conditions require moderate or high sulfate resistance 2.Lower C_3A content than Class A	1.Intended for use when conditions require high early strength 2.The C_3S content and surface area are relatively high	1.Required under conditions of moderately high temperature and pressure 2. Retarded cement and retardation is achieved by reducing C_3S and C_3A, and increasi[ng] the particle size of cement grains.	1.Basic well cement 2.Thickening times controllable with additives to prevent loss of circulation up to 250-degree F (120 degree C)	1. Basic well cement 2. The surface area is coarser than that of class G. 3.Thickening Times controllable with additives to prevent loss of circulation up to 450-degree F (230 degree C) Ref-API Specification 10A,2002; Nelson and Michaux,2006; Lafarge Halliburton,2009

A number of admixtures are added into cement, which can broadly be classified into accelerators, extenders, bond improving and expanding agents, fluid loss additives, anti-gas migration cement, anti-foam, and defoaming agents, additives and mixture to prevent lost circulation, density increasing agents, free water control and solid suspending agents and speciality cement blends.In table 2-2,a summary is presented to control the special problems in Cement.

Table 2-2 Summary of Additives to Control Special Problem.

Purpose	Actions or Agents.
1)Gel Strength	Preparation of Spacers
2)Permeability Control	Silica Flour, Gas Bubble Producing Additives
3)Corrosion Control	Various Nitrogen Compounds,polyoxylated Amines, Amides
4)Radioactive wastes	Helpful In Finding the Regions of Actual Placement of Cement.
5)Strength Increasers	Nylon, Metal Fibers
6)Defoamers	Controlled Inclusion of Air During Mixing.
7)Encapsulation.	Controlled Mixing of Various Additives.

To have enhanced properties of cement, cement are modified by polymers to have customized properties. Based on the polymer used,Cement modified with polymers has better abrasion resistance, impact resistance, tensile strength, and flexural strength. Presently, oil well cement slurries are modified by different types of polymer.

Table 2-3 Admixtures used in Oil Well Cement.

Dispersants	Viscosity Control	Retarders	Accelerators.
1)Poly(oxyethylene) sulfonate	1)Latex	1)Scleroglucan	1)Propylene carbonate
2)Acetone formaldehyde cyanide	2)Scleroglucan	2)Copolymer isobutene and maleic anhydride (MA)	2)Sodium and calcium chlorides
3)Polyoxethylated octylphenol	3)Calcium Lignosulfonate	3)Amino-N-([alkylidene] phosphonic acid) derivatives	3)Aluminum oxide and aluminum sulfate
4)Copolymers of MA and 2-hydroxypropyl acrylate	4)Phenol-formaldehyde resin modified with furfuryl alcohol	4)Alkanolamines-hydroxy carboxy acid salts (e.g., tartaric acid and ethanolamine)	4)Sodium sulfate
5)Allyloxybenzene sulfonate.	5)Hectorite clay	5)Phosphonocarboxylic acids	5)Calcium chloride
6)Ferrous lignosulfonate, ferrous sulfate, and tannic acid	6)Sulfonic acid copolymer castor oil	6)Dicyclopentadiene bis(methylamine) methylenephosphonate	6)2,4,6-Thihydroxybenzoic acid
7)Alkali lignosulfonate		7)Lignosulfonate derivatives	7)Disodium 4,5-dihydroxy-m-benzenedisulfonate
8)Acetone, formaldehyde polycondensate		8)Carbohydrates grafted with vinyl polymers	8)Formic acid esters
9)2,4-Pentanedione-1,5-sodium disulfonate		9)Carboxymethyl hydroxyethyl cellulose	9)Formamide
10)Melamine sulfonate polymer		10)Wellan gum	10)Monoethanolamine
11)Poly (vinyl sulfonate)		11)Borax based	11)Diethanolamine
12)Styrene sulfonate polymer		12)Carrageenan	12)Triethanolamine
13)Poly(ethyleneimine) phosphonate		13)Polyethylene amine derivatives and amides	
14)Casein with poly(saccharide)s		14)Copolymers from maleic acid, 2-acrylamide-2-methyl-1-propane sulfonic acid (AMPS) and others	
15)Dialdeyhde starch		15)Ethylenediamine tetramethylene phosphonic acid, poly(oxyethylene) phosphonic acid, or citric acid	
		16)Poly (acrylic acid) phosphinate	

2.2) Chemical Reactions Occurring in Class H Cement

The main components of Class H Cement are tricalcium silicate(C_3S), dicalcium silicate(C_2S) and tetra calcium aluminoferrite. (C_4AF). The C_3A content for class H cement is quite low, so the fast reaction which occurs due to C_3A can be neglected. The hydration mechanism involved in class H cement is completely different from other Portland cement due to the absence of (C_3A). Tricalcium aluminate (C_3A) initially liberates a lot of heat and its presence (C_3A) makes it susceptible to sulfate attack. Tricalcium silicate hydrates and hardens rapidly and it is responsible for cement initial strength gain whereas C_2S hydrates and hardens slowly with strength development occurring after one week. The hydration of reaction of C_3S and C_2S can be represented by this equation

(C_2S, C_3S) + Water= C-S-H+ portlandite.

$CzS + (z-x+y)\ H \rightarrow Cx-S-Hy + (z-x)\ CH$ (1.1) where z =2,3 for C_2S and C_3S, respectively.

When C_3S and C_2S react with water after which it is transformed into calcium silicate hydrate and hydrated lime ($Ca(OH)_2$).The exact chemical composition and morphology of the calcium silicate hydrate vary, so it is written in the very vague formulation C-S-H. The crystalline form of hydrated lime found in hydrated cement paste is called portlandite. The hydration of C_3S liberates more portlandite than the hydration of C_2S, as C_3S is richer in calcium.

There are several phases of heat of hydration in an oil well cement which primarily can be divided into five phases namely pre-induction period, induction period, acceleration period, deceleration period and the diffusion period. In the pre-induction or initial fast reaction period, cement comes in contact with water and it lasts only for few minutes.

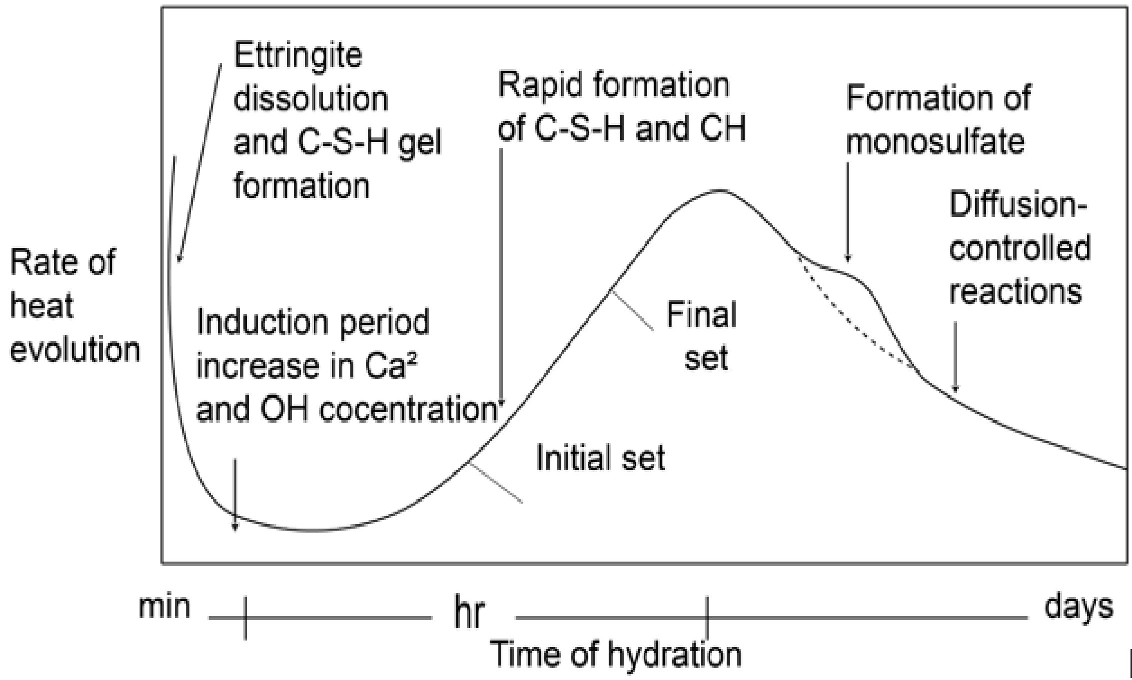

Figure 2-1 Heat of Hydration of Normal Portland Cement.

The induction period corresponds to a very low reaction rate, mainly due to the slow dissolution of the clinker grains and can extend from minutes to several hours. The dissolution mechanisms depend on the concentration of the different species, which is the driving force of the reaction (J . Cheung et al., 2011). After the induction period follows the acceleration period, where rapid hydration occurs, and cement begins to develop strength. The duration of curing period is strongly influenced by the curing conditions. During this phase, the peak hydration is achieved. After the peak, deceleration phase starts. Then comes the deceleration period where the hydration decelerates. The diffusion period is after when the cement is set, slow reaction takes place inside.

2.3) Rheology of Cement

Cement rheology is needed to understand the material behavior. Understanding the rheology is essential to know the viscosity, yield shear stress and gel strength. The cement slurry is viscoelastic material, where the continuous change in viscosity occurs due to cement hydration. Cement slurry shows both shear thickening and shear thinning behavior with different types of admixtures.

Main objectives to do rheology tests are as follows

1) It provides an insight into the interaction occurring among the ingredients in the material.

2) The rheological test can be used as a quality control index. Cement slurries can be accepted or rejected if it does not match a requisite behavior based on rheological tests.

3) It can be used to evaluate the pumpability or mixability of cement slurry.

4) With the addition of some special additives, it becomes essential to know if the slurry can transfer large particles. The addition of fibers affects the rheology significantly; thus, it is crucial to the rheological properties.

5) Slurries rheological behavior changes considerably when it is exposed to high temperature. At the bottom of the borehole, the cement slurry is exposed to harsh environments such as high temperature and pressure.

6) To design processing equipment such as selecting the appropriate pump to provide sufficient power for material to flow over a certain distance in pipelines. The relationship between the pump and flow in the pipeline is governed by the rheological properties of the material.

Cement is thixotropic or anti thixotropic fluid is not well defined in the literature. Thixotropy is discussed as the changes in the area within the up and down curve (Quanji et al., 2010). The area under the hysteresis curve general defines if the material is thixotropic or anti thixotropic

Table 2-4 Various Rheological Models used describe strain rate -shear stress.

Model Used.		Model Parameters
Newtonian Model	$\eta = \frac{\tau}{\dot{\gamma}}$	
Bingham Plastic Model	$\tau = \tau_0 + \mu_p \times \dot{\gamma}$	Two parameter Model
Modified Bingham Model	$\tau = \tau_0 + \mu_p \times \dot{\gamma} + C\dot{\gamma}^2$	Three Parameter Model
Power Law Model	$\tau = k \times \dot{\gamma}^n$	Two parameter Model
Casson Model	$\sqrt{\tau} = \sqrt{\tau_0} + \sqrt{\mu_p} \times \sqrt{\dot{\gamma}}$	Three Parameter Model
Vocadlo Model	$\tau = \left[\tau_0^{1/n} + k^{1/n} \times \sqrt{\dot{\gamma}}\right]^n$	Three Parameter Model
Hershcel-Bulkley model	$\tau = \tau_0 + k \times \dot{\gamma}^n$	Three Parameter Model
Sisko Model	$\mu = \mu_a + k\,\dot{\gamma}^{n-1}$	Three Parameter Model
Williamson Model	$\mu = \frac{\mu_0}{1+(k\dot{\gamma})^n}$	Three Parameter Model
Vipulanandan Model	$\tau = \tau 0 + \frac{\gamma}{C+D\dot{\gamma}}$	Three Parameter Model

The addition of additives significantly affects the hysteresis path. The area swept by up and down curves in the rheology testing is used to define the cement thixotropic. Additionally, a new concept of cohesion energy of the slurry has been introduced. To calculate the total energy, the area under the shear stress and shear strain rate has been calculated in this thesis.

To predict the shear strain -shear stress behavior, several rheological models have proposed. Based on the accuracy between the predicted and experimental results, each model may be evaluated or compared with each other. In the oil and gas industry, Modified Bingham Model and Herschel- Berkley model are used for knowing the yield stress and plastic viscosity. A new model proposed by Vipulanandan has been suggested in the year 2014, which has extremely high accuracy with the predicted and experimental results. The main features of this model are it predicts the shear thickening and shear thinning behavior based on the model parameters one gets after fitting the equation.

The model suggested by Vipulanandan Model (Vipu et al., 2014) has a limiting shear to any fluid used. The previously proposed model does not have upper limiting shear stress. In this research, the modified Bingham Plastic Model and Vipulanandan Model have been used to model the shear stress and shear strain rate of the cement slurries with additives.

2.5) Review of Additives Used in research.

2.5.1) Cellulose

The mechanism of interaction between cement and cellulose is unusual. The main reasons for the retardation of cement slurry by addition of cellulose is due to change in surface area of hydrating cementing particles. 2) Formation of temporary barriers is formed on the hydrating particles inhibiting the hydration of cement.(Juenger et al., 2002).The adsorption may take place through a process called chelation, where the organic molecules form a complex with the metal ions in cement phases.

Taplin (1962) researched a wide range of retarding agents and found that almost all of them contain HO-C-C=O group. All the reducing cellulose either contain HO-C-C=O group or are readily converted by dilute alkali into saccharinic acids that contain this group. A characteristic feature of this group is that the oxygen molecules can approach each other, a requisite condition for chelation. While many retarding celluloses contain the chelating group, other useful retarding celluloses do not. The capacity of any organic compound to retards directly depends on the number of hydroxyls, carboxylic, and carbonyl groups present in the molecule (Kurdowski, 2014). This is the reason why cellulose is an extremely useful retarder.

Young has suggested the possible cause of retardation of cement slurry addition by cellulose. Cellulose first bonds to the aluminate phases by complexing or chelating, which leads to the dissolution of ions from hydrating calcium silicate phases in solutions. When precipitation of hydration products occurs, its growth is inhibited the adsorption of cellulose. Ultimately, cellulose is incorporated into hydration products slowly, and further hydration of cement occurs (Usmant et al., 2012). Access of water to hydrating material is restricted by the formation of stable and impermeable sheaths of hydration products around hydrating material.

Yang et al. (1997) showed that zeta potential of hydrating cement is positive in the absence of cellulose. Zeta potential of cellulose added cement slurry is negative and it indicates. The difference of zeta potential can be explained by the adsorption of the cellulose onto the hydrating particles. Ramachandran et al. (1981) have reported that cement high in aluminates need a higher dosage of cellulose to achieve retardation. It explains the reason why a lower percentage of cellulose is needed to retard cement hydration.

2.5.2) Polypropylene fibers

Cement strengthened by fibers has high strength against cracks, increased formability, strength against moisture and thermal expansion, enhanced strength against impulse and abrasion (Kakooei et al., 2012). Additionally, the polypropylene fiber augments the concrete resistance to abrasive erosion (Grdic et al., 2012). Further, the addition of fibers has reduced the drying shrinkage of concrete (Banthia et al., 2005). Studies by Patel et al. (2015) and Madhavi et al. (2015) evaluated the properties of polypropylene fiber, and they found that it significantly improves the flexural strength and compressive strength, reduces shrinkage cracks and surface water absorption. Bayasi and Zeng studied the properties of fiber-reinforced concrete with polypropylene fibers and found that volumes less than 0.3%, (3/4) inch-long fibers were suitable for enhancing post-peak resistance. Kakooei et al. (2012) investigated the effect of polypropylene on reinforced concrete structures and found that compressive strength increased in the volume ratio of PP fiber.

Researchers have worked on the mechanical properties of cement with PP fibers. However, the change in electrical properties of cement added with PP has not been explored. Electrical resistivity is good quality control index and the readings can be used to ascertain the changes in mechanical properties (Azarsa et al., 2017). The electrical resistivity measurement shows the interaction PP fibers with the cement at the slurry and hardened stage. Using smart cement, sensitive to AC current different percentages of PP fiber were added into smart cement.

2.5.3) Carboxylated Styrene Butadiene

Latex has been used in oil well cementing operations because of its flexible features, it improves the ant channeling ability of cement slurry, improves the bonding cement and casing and reduces permeability.SBR latex is widely used in oil well cementing as it provides excellent mechanical properties, reduces the shrinkage of cement, reduces fluid loss as SBR particles coalesce. To further improve the bonding properties of SBR, latex emulsion are carboxylate with a strong acid monomer. In this research, the effect of carboxylated styrene-butadiene is evaluated on Class H smart cement.

Baueregger et al. (2002) investigated the influence of carboxylated styrene-butadiene on Portland cement hydration and found that SB particles retard or suppress the silicate and aluminate reactions. Additionally, the presence of carboxylate groups of SB particles chelates calcium ion present in the pore solution. The interaction of polymer on cement and the rate of reaction can be captured by using electrical resistivity. Electrical resistivity is a material property and gives excellent insights about material behavior at various stages of curing.

2.4) Constitutive Models for Concrete Stress- Strain

Various constitutive model has been proposed in the past to predict the stress-strain behavior of cement and concrete. Several models have been proposed to capture the behavior of stress-strain failure of cement. The cement sheath properties which should be tested in the laboratory are compressive strength, tensile strength, young's Modulus, Poisson ratio, and Plasticity Parameter. General industry specification states that 3.45MPa of compressive strength is required to the pipe in the hole, and 13.45MPa is required to provide the resiliency from the shock load of drilling operations (Sabins et al., 1986). The various researcher has studied the effect of additives on oil well cement. The effect of additives on the Class G and H cement are listed below.

To model the stress-strain behavior of the cement, many constitutive models have been suggested. Models proposed for unconfined concrete uniaxial stress-strain failures can be used for modeling the stress-strain behavior of cement. The compressive strength of Class H cement is affected by additives, temperature, and borehole contamination (Labibzadeh et al., 2010). The maximum compressive strength achieved for in oil well cement is around 60 MPa. Concrete Stress-strain models proposed for low(<70MPa) compressive strength, can be applied to model Cement stress-strain model. Models proposed by previous researchers.

1. Smith and Young (1956)

$$f = f_c' \left(\frac{\varepsilon}{\varepsilon_0}\right) \exp\left(1 - \frac{\varepsilon}{\varepsilon_0}\right)$$

Where

f = stress at any strain, f_c' = maximum stress, ε = strain, ε_0 = Strain at the maximum Stress

2. Desayi and Krishman (1964)

$$f = \frac{E\varepsilon}{1 + \left(\frac{\varepsilon}{\varepsilon_0}\right)^2}$$

Where, E = a constant (same as initial tangent modulus)

3. Sargin (1971)

$$\eta = \left[\frac{Ax+(D-1)x^2}{1+(A-2)x+Dx^2}\right]$$

Where

$\eta = \frac{f}{f_c^{'}}$, $x = \frac{\varepsilon}{\varepsilon_0}$, A = Parameter mainly affecting the slope of the ascending branch

$D =$ Parameter mainly affecting the slope of the descending branch

4. Popovics (1973)

$$f = f_c^{'} \frac{\varepsilon}{\varepsilon_0} \frac{AX+BY}{1+CX+DX^2}$$

Where $Y = \frac{f}{f_c^{'}}$, $X = \frac{\varepsilon}{\varepsilon_0}$

$A, B, C, and\ D$ are parameters to be obtained from the boundary condition and test results.

7. Carreira and Chu (1985), Ezeldin et al. (1992), Nataraja et al. (1999)

$$\frac{f}{f_c^{'}} = \frac{\beta\left(\frac{\varepsilon}{\varepsilon_0}\right)}{\beta-1+\left(\frac{\varepsilon}{\varepsilon_0}\right)^{\beta}}$$

Where $\beta = \frac{1}{1-\frac{f_c^{'}}{\varepsilon_0 E_{it}}}$ for $\beta \geq 1.0\ and\ \varepsilon \leq \varepsilon_u$

β is a material parameter that depends on the shape of the stress-strain curve

E_{it} is the initial tangent modulus,ε_u is the ultimate strain or strain at which failure is defined.

8. Hsu and Hsu (1994)

$\eta = \frac{n\beta x}{n\beta - 1 + x^{n\beta}}$ for $0 \leq x < x_d$

Where $\frac{f_c}{f_c^{'}}$,$x = \frac{\varepsilon}{\varepsilon_0}$,$\beta = \frac{1}{1 - \frac{f_c^{'}}{\varepsilon_0 E_{it}}}$ for $\beta \geq 1.0$

β and n are the material parameters. β depends on the shape of the stress-strain diagram, and n depends on the strength of the material. x_d is the strain at $0.3f_c^{'}$ in the descending portion of the stress-strain curve.

9. Wee, Chin and Mansur (1996)

$$\boldsymbol{f} = f_c^{'}\left[\frac{k_1\beta\left(\frac{\varepsilon}{\varepsilon_0}\right)}{k_1\beta - 1 + \left(\frac{\varepsilon}{\varepsilon_0}\right)^{k_2\beta}}\right]$$

Where, $\beta = \frac{1}{1 - \frac{f_c^{'}}{\varepsilon_0 E_{it}}}$,For $f_c^{'} \leq 50MP_a$, $k_1 = k_2$ =1 and For 50$\leq$ $f_c^{'} < 120MP_a, k_1$ = $\left(\frac{50}{f_c^{'}}\right)^3$ and k_2 = $\left(\frac{50}{f_c^{'}}\right)^{1.3}$

10.Vipulanandan Stress-Strain Model.

$$\sigma = \frac{\sigma_{max} \times \left(\frac{e}{ec}\right)}{q_3 + (1 - p_3 - q_3) \times \left(\frac{e}{ec}\right) + p_3 \times \left(\frac{e}{ec}\right)^{\left(\frac{p_3 + q_3}{p_3}\right)}}$$

where σ is the stress (MPa);

σf: compressive stress at failure (MPa);

ρo: initial electrical resistivity (σ = 0 MPa) and p2 and q2 are piezoresistive model parameters.

2.5) Gas Leakage in Oil Wells

The major problem in oil wells in Texas and Pennsylvania are leaking oil wells. Leakage in oil wells is detrimental to the safety of the community and environment. Gas migration frequently occurs in oil wells and accounts for 25 % of job failures. Failure in cementing jobs has led to gas migration in the Gulf of Mexico and many places. The effective way to control gas leakage is to provide zonal isolation for the life oil well. There are several ways of addressing this problem.

The main reasons gas migration in cement slurries are incorrect slurry density, inadequate mud removal, premature gelation, high fluid loss and free water, permeable slurries and high shrinkage, weak bonding.(Bonett et al., 1996) Gas migration starts to occur if there is a hydrostatic imbalance, the establishment of channels for gas flow, development of spaces for gas entrance, weak zonal isolation, and low resistance against gas. Weak bonding in the cement and formation and casing interface, creation of micro annulus in cement due to porosity and stress increment, development of space for gas entrance into cement are pathways where gas can migrate from source to top.

After the cement slurry placement, there is a reduction in hydrostatic pressure. The volume reduction occurs due to shrinkage of cement, loss of water from the slurry to the formation and contamination occurring during placement. Several theories have been published to explain the pressure reduction, such as localized bridging caused by fluid loss (Zichang Li et al., 2016), sedimentation caused by slurry instability and volume reduction caused by fluid loss and chemical shrinkage. The pressure inside the well needs to keep higher than the above the formation pressure, to prevent the gas leakage from cement slurry.

In cementing, the critical phase is the gelation phase. At this stage, cement is something between solid and liquid phases. (Pour et al., 2007) Transition time from a gel state to a hardened state is an essential point in controlling the gas migration. Most of the gas migration control cement has focused on the study of the development of static gel strength of cement slurry. Static Gel strength introduced in classical shear stress theory describes the shear stress at cement/casing. Presently, to minimize the risk of gas migration in oil wells, it is desired to have a shorter SGS based transition time. Although SGS helps to improve the slurry design and cementing practice, it is not sufficient to describe if the cement is gas-tight or prevent gas migration.

Mostly the gas migration occurring inside cement is undetected and leads to failure of structures and oil well. Real-time monitoring is essential to sense gas migration. Acoustic logs measure the cement quality from the degree of acoustic coupling of the cement to casing and formation.(Gowida et al., 2018). CBL provides reliable, functional integrity and zonal isolation but does not detect gas leakage and cement hydration. Fiber Optic Sensors are being researched to monitoring; however, they have limitations. To detect real-time gas leakage, chemo-thermo-smart cement developed by Vipulanandan can be used as a monitoring tool with electrochemical Impedance measurements.

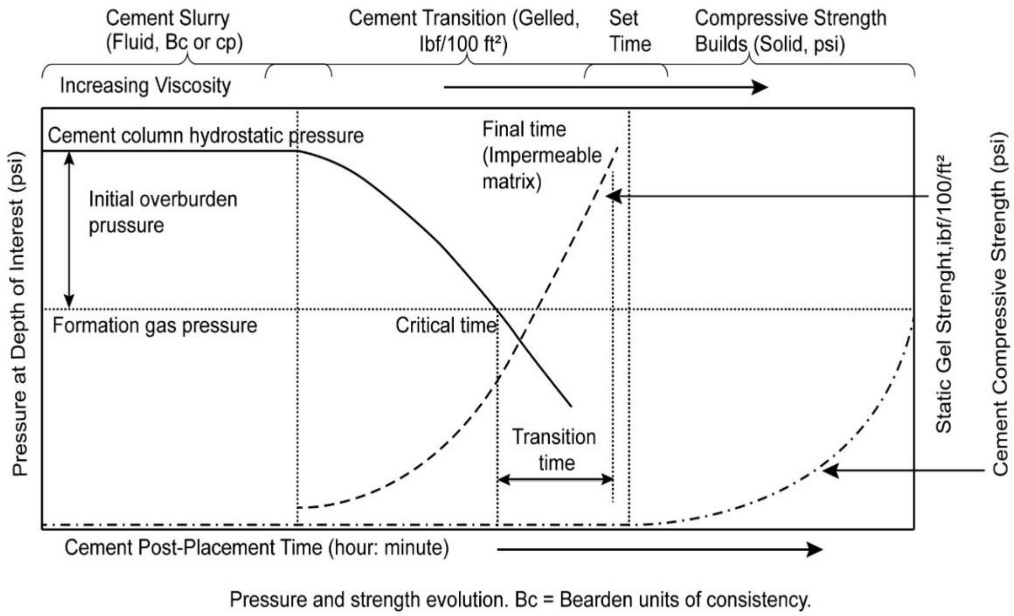

Figure 2-2 Various Physical Phenomenon Developing Inside Oil Well Cement

Typical ways to quantify a gas-tight cement in literature are presented as below.

Fluid Loss- Fluid loss agent is used to preventing early slurry dehydration for HPHT cementing operation. The design criteria for fluid loss control are linked to dynamic filtration rather than static filtration. Maximum fluid loss rates for oil wells are 200 ml per 30 minutes and 50 ml per 30 minutes for gas wells (Hartig et al. 1983).

Static Gel Strength- Static Gel strength is a force needed to move the fluid. SGS is critical if there is an unexpected shutdown and it affects the hydrostatic pressure in the cement slurry. It has been found at SGS 50 Pa, slurry is not able to transmit any hydrostatic pressure and at an SGS OF 250 Pa, it will have sufficient gel strength to inhibit the gas flow. Lower the transition time, the better the slurry is in preventing gas migration.

Slurry Response Number- SRN is defined as the ratio SGS development rate to the fluid loss at the time SGS develops a maximum rate of change. It is written as

SRN = $\frac{\frac{d(SGS)}{dt} / SGS_{maxrate}}{\frac{dl}{dt}/(V/A)}$.

2.6) Permeability of Cement Slurry

Permeability quantifies the capacity of a porous medium to allow the flow of fluid or gases. The unit of measurement for permeability is millidarcy. Permeability is an essential property of cement in influencing the long-term stability, durability and is essential to characterize the hydro-mechanical property of cement. (Banthia et al., 2005) Size of pores, percentage of pores, the connection between pores and overall porosity of the cement affects the permeability. Zonal isolation is the inhibition of fluids to reach different zones outside the casing and is strongly affected by the permeability of cement sheath. To estimate a cement ability to provide zonal isolation both compressive strength and permeability of cement should be investigated.

To calculate the permeability, Darcy law is used. Darcy law can be stated as the relationship between the instantaneous flow rate through a porous medium of permeability k,the dynamic viscosity of the fluid and pressure drop over a given distance in the homogenously permeable medium.It is expressed as,

$$Q = \frac{kA}{\mu}\left(\frac{\partial p}{\partial x}\right).$$

In porous media, where Reynolds number is between 1 and 10, the inertial effect becomes significant and inertial term is added to the equation, known as Forchheimer term. This term accounts for the non-linear term which is expressed as,

$$\frac{\partial p}{\partial x} = -\ \frac{\mu}{k}\,q - \frac{\rho}{k_1}\,q^2.$$

In a porous medium, a thin capillary tube or fine porous medium controls gas leakage. Due to this, the velocity of gas in the velocity layer in the immediate vicinity of solid walls of the capillary or porous medium is not zero, this was observed by Kinkenberg (1941).The mathematical expression is given by

$$K_a = K_\infty \left(1 + \frac{b}{P_m}\right),$$

where Ka is gas permeability, μm^2,K_∞ is Klinkenberg permeability, μm2.Pm is mean pressure, MPa. b is gas slip factor, affected by pressure, temperature, the pore structure of the porous medium, and type of Gas.

2.7) Electrical Resistivity of Cement

Numerous research has been done to apply the electrical resistivity, and resistance concept to study the electrical properties.(McCarter et al., 2000; McCarter et al., 2003; Wei et al., 2012), Electrical properties are not constant throughout as concrete is heterogenous, curing happens over time and there is stratification while placing.(Mc Carter et al., 1994). Electrical Resistivity is used a non-destructive testing tool (Xiao et al., 2008). The electrical resistivity of cement is affected by the pore structure (tortuosity), the composition of the pore solution, the cement content, the proportion of water and cement, and the temperature (Polder et al., 2001). Electrical resistivity is also applied in the geotechnical field. Water content, porosity, and type of mineral in soil affect electrical resistivity (Rhoades et al., 1976). Byson (2005) used the electrical parameters to evaluate the Geotechnical Parameters like plasticity index, dry density, and consolidation Behaviour. Electrical Resistivity shows Material Behavior and can be applied in a lot of diverse application

2.2) Clay soil stabilization by polymer

Introduction

In this study, a literature review is presented on soil treatment by various additives. In our research, polymer treatment is used to treat the clay soil of high plasticity Index. Expansive soil is major problem in Houston area, and soil stabilization is a must for long term durability. In this research, the addition of polymer treatment on compressive strength, tensile strength, swelling behavior, and plastic properties were studied. Another important testing parameter, resistivity is introduced.

2.2.1) Clay Soil

Clay minerals belong to the phyllosilicate family of minerals, which are characterized by their layered structures composed of polymeric sheets of silica tetrahedral attached with octahedral sheets.

Table 2-5 Description of Clay Minerals.

Name of Minerals	Size Shape and Form of Occurrence.
Kaolinite	Well-formed, six-sided flakes, with a prominent elongation in one direction
Halloysite	Tubular units with an outside diameter ranging from 0.04 to 0.15
Smectite	Undulating mosaic sheets.
Illite	Poorly defined flakes commonly grouped together in irregular aggregates
Chrysotiles	Slender tube-shaped fibers having an outer diameter of 100-300 A. Their lengths commonly reach several micrometers.
Palygorskite	Elongated laths, singly or in bundles. Frequently the individual's laths are many micrometers in length and 50 to 100 A in width
Sepolite	Similar lath-shaped units.
Allophane	Very small Spherical particles (30-50 A in diameter), individually or in aggregate
Imogolite	Long (several micrometers in length) thread-like tubes

Traditional stabilizers such as cement lime, fly ash and bitumen have been researched extensively and their stabilizing effects have been understood. In last 50 years other, chemical methods have been developed and researched. The stabilizers are mainly applied in diluted water on soil. A series of non- traditional stabilizers are used nowadays from polymer, enzymes, mineral pitched, salts.

2.2.2) Lime treatment

As per Eades and Grim (1960), lime soil interaction is two-stage process. The first stage, which is known as an immediate or short-term treatment, occurs within a few hours or days after lime is added (Locat et al., 1990; Abdi and Wild, 1993). Three main chemical reactions, namely, cation exchange, flocculation-agglomeration, and carbonation occur at this stage. The second stage requires several months or years to complete and is thus considered the long-term treatment. The pozzolanic reaction is the main reaction at this stage. The drying of wet soil and the increase in soil workability is attributed to the immediate treatment, whereas the increase in soil strength and durability is associated with long-term treatment. The main advantages are Soil-lime mixtures increase soil strength, conserves energy reduce plasticity (increase workability), upgrades the mineral aggregate of the soil and increases soil durability. Also, a considerable reduction in consolidation settlement and improved compressibility characteristics were observed. Major drawbacks of lime treatment are carbonation, sulfate attack and environmental impact. Soil containing sulfates, addition of calcium additives results in heaving and disintegration of soil strength (Firoozi et al., 2017).

2.2.3) Polymer Addition of Soil

In our study, we have attempted to synopsize the work of various researchers using polymers such as polypropylene, Acrylic Polymer, polyurethane polymer, Sodium carboxymethyl Cellulose, Polyacrylamide, Polyethylene Oxide and (bisphenol A/epichlorohydrin) and a polyamide hardener, glycerol. Using these polymers they tested various physical properties of soil such as vane shear test, volumetric shrinkage, desiccation cracks, effect on plasticity, unconfined compressive strength, swelling test, sorption test, erosion test, permeability test Poisson ratio test.

Azzam et al. (2014) used polypropylene polymer on clay soil of high plasticity (CH). The polymer was added to clay soil samples were 0, 3, 6 and 10 %. It was noticed that increasing polymer remarkably increased the dry density while the OMC decreased. Tests like volumetric shrinkage, desiccation cracks, shear strength of clay and plasticity were performed on samples.

Naeini et al. (2011) used acrylic polymer on high and low plasticity clay. Aqueous polymers were chosen 2%, 3%, 4%, and 5% by total weight of the amount of water needed to achieve the optimum moisture content. All the specimen were compacted at their respective maximum dry density. Effect of curing time on UCS, effect of polymer on the USC and stress-strain behavior and effect on plasticity was studied.

Sasaki et al. (2008) studied the effect of polyurethane on expansive soil clay. The shrinkage, volumetric expansion, water absorption and compressive strength of the composite was tested. From the study, it was found that it can be effectively used for soil remediation in the underpinning/grouting industries.

Inyang et al. (2006) applied sodium carboxyl methylcellulose, polyacrylamide, and polyethylene oxide on Na-Montmorillonite. Polymer clay swelling test and polymer test sorption test was performed. Polymers are particularly useful for stabilizing expansive because their sorption in clay is irreversible. Three polymers were applied of which polyacrylamide was most effective against swelling.

Ajayi-Majebi et al. (2007) conducted an experiment designed to determine the effects of stabilizing clay-silt soils with the combination of an epoxy resin (bisphenol A/epichlorohydrin) and a polyamide hardener. The additive mixture was composed of a 1:1 ratio of epoxy resin to polyamide hardener. Reported soil properties included a liquid limit ranging from 37 to 45 and a plasticity index ranging from 13 to 18. From the results, it concluded that admixing up to 4 percent stabilizer into a clay-silt material produced large increases in the load-bearing capacity of the material in terms of its unsoaked California Bearing Ratio (CBR). They observed that increase in the temperature of the curing environment led to increased strength formation. Cure times for the stabilization agent were reported as low as 3 hours

Lin et al. (2012) applied 3 types of polyurethane toluene di-isocyanate, polyethylene glycol and polypropylene on sand-clay mixture (Sand-Clay Mix (1:1, 1:3, 1:5). Sand (D50=.34mm, Cu=2.24, Cc=1.3) and CH (ll-34.5, PI-17.6, Omc-16). Test performed on samples were UCS, shear strength parameters and erosion resistance. With concentrations of 5g/cm^3 polyurethane and sand-clay ratios 1:3, the relative increment of unconfined compressive strength of specimen treated by PUA, PUB and PUC 45.41%, 43.06% and 67.223% in UCS. The cohesion of specimen with (sand: clay) ratio of 1:5 and 5g/cm^3 concentrations of PUA, PUB and PUC were 15.89, 14.02 , 16.01KPa with 8.85KPa for the untreated specimens.

2.2.4) Polyacrylamides polymer

Polyacrylamides are high molecular weight water-soluble or swellable polymers formed from acrylamide or its derivatives. Their glass transition temperature is well above room temperature (> 400 K). The only commercially important polyacrylamide is poly(2-propenamide) which is simply called polyacrylamide or PAM [$-CH_2CH(CONH_2)-$]. It is a non-ionic, water-soluble, and biocompatible polymer that can be tailored to meet a broad range of applications. The polymer can be synthesized as a simple linear chain or as a cross-linked structure. PAM increases the viscosity of water and encourages the flocculation of particles present in water. Polyacrylamide is a cross-linked polymer that can absorb and retain large amounts of water due to the presence of amide groups. Amide groups form strong hydrogen bonds with water molecules. Hydration of polyacrylamide leads to formation of soft gel and thus it is called a water-absorbing polymer. Even though these polymers are called polyacrylamide, they are often copolymers of acrylamide and one or more other monomers

2.3) Summary

1) Existing rheological models do not predict the maximum shear stress. There is a requirement of a model that can predict better yield stress and maximum shear stress.

2) Although the electrical method exists for monitoring the concrete and cementitious system, smart cement with sensing properties enhances the detection of the physical phenomenon occurring in the material.

3) To describe concrete stress-strain, many models are available. Although this model can apply to cement only, however, there is still a requirement of a model which describes the cement mechanical behaviour in tension and compression.

4) Although Class H cement is a class of Portland cement, absence or less percentage of C_3A impart significant changes to cement property. This affects the cement hydration mechanism and resistivity.

5) To quantify cement slurry capacity to prevent gas migration, many quantifications methods are available. The existing method is not able to exactly differentiate the effectiveness of various cement slurries.

6) Lime treatment of clay soil is prevalent, but with soil with high sulphur content, it is not effective. Polymers are the new class of soil stabilizers, and a lot of research is being done on the effectiveness of polymer treatment on soil

7) Concrete corrosion can be detected by electrical methods, but the existing method does not reveal corrosion kinetics and exact location of corrosion.

CHAPTER 3 METHODS AND MATERIALS

In material and method, a brief description of the material used has been provided. The detailed procedure to prepare samples and tests performed on it has been discussed. This chapter has been divided into three parts, which are

3.1) Cementing Studies

3.1.1) Materials Used

3.1.2) Experiment and Mathematical Models to characterize the physical properties.

3.2) Soil Studies

3.2.1) Materials Used

3.2.2) Experiment and Mathematical Models to characterize the physical properties.

3.3) Corrosion Studies

3.3.1) Material and Experiment Performed.

3.3.2) Mathematical Models to characterize the physical properties.

3.1) Cementing Studies

3.1.1) Materials Used

3.1.1.1) Cement

Class H cement is used for the preparation of samples. Three different types of additives influencing the retardation, shrinkage and gas migration control has been used.

The change in setting time due to the addition of retarders has been quantified and related to the resistivity of the material.

3.1.1.2) Cellulose

To retard the setting time of cement, naturally available cellulose has been used. The cellulose percentage has been modified to achieve the optimum combination of compressive strength and setting time.

3.1.1.3) Polypropylene Fiber

It has a linear structure-based one the monomer CnH2n.It is manufactured from propylene gas in the presence of a catalyst such as titanium chloride. Polypropylene fibers are composed of crystalline and non-crystalline regions. Physical properties of polypropylene fiber are presented below

Table 3-1 Physical Properties of Polypropylene fiber

Physical Properties (I)		Physical Properties (II)	
Tensile Strength	3.5 to 5.5	Moisture Absorption	0 to 0.05
Elongation	40 to 100	Softening Point	140
Abrasion Resistance	Good	Electric Insulation	Excellent
Melting Point (C)	165	Relative Density	0.91
Chemical Resistance	Excellent	Thermal Conductivity	6

3.1.1.4) Carboxylated Styrene Butadiene

Commercially available styrene Butadiene is used in the research.The properties are given in table 3-2.

Table 3-2 Properties of Carboxylated Styrene Butadiene.

Physical Properties(I)		Physical Properties (II)	
Physical State	Liquid	Solids by Weight	49%
Color	Milky White	Viscosity	<300cps
pH	8-9	Density	

3.1.2) Experiments Performed.

3.1.2.1) Initial Resistivity

Initial resistivity of the sample was measured using the resistivity probe. Resistivity probe with an accuracy of +/- 1% was used to measure the resistivity of cement slurry with different additives. After year of studies and based on the current study on expansive soil and oil well cement, electrical resistivity (ρ) was selected as the sensing property for soil and cement (Vipulanandan et al., 2005, 2012, 2017). Hence two parameters (resistivity and change in resistivity) were used to quantify the sensing properties which is

$$R = \rho\ (L/A) = \rho\ K\ , \qquad (3\text{-}1),$$

where,R = electrical resistance = Linear distance between measuring points, A = Effective cross-sectional area and K = Calibration parameter is determined based on the resistance measurement method

Normalized change in resistivity with the changing condition can be represented as

$$\Delta\rho/\rho = \Delta R/R.$$

3.1.2.2) **Resistance and Resistivity Measurements**

Using LCR meter, the resistance of the sample is measured over the entire test duration. The measured resistance is converted to resistivity by this equation (3-1) where R = Resistance Measured, A = Area of Cross Section, L = Linear Distance of the Path of Current. Based on experimental results, a theoretical model proposed by Vipulanandan and Paul (1990) was modified and used to predict the electrical resistivity of smart cement during hydration up to 28 days.

To model the resistivity, change due to hydration of cement for any length of the curing period, a curing model developed by Vipulanandan is used, which is

$$\frac{1}{\rho} = \frac{1}{\rho_{min}}\left[\frac{(\frac{t+t_0}{t_{min}+t_0})}{q_1+(1-p_1-q_1)\left(\frac{t+t_0}{t_{min}+t_0}\right)+p_1\left(\frac{t+t_0}{t_{min}+t_0}\right)^{(\frac{p_1+q_1}{p1})}}\right], \quad (3\text{-}2)$$

where ρ: electrical resistivity (Ω-m); t is the curing time (minutes); ρmin: minimum electrical resistivity (Ω-m); tmin: time corresponding minimum electrical resistivity (ρmin), p1, to and q1 are model parameters.

3.1.2.3) Setting Time

Vicat Needle-The Vicat setting test is the most commonly used to identify the initial and final setting time for hydrating cementitious mixtures. It measures the change in the penetration depth of plunger with diameter 1.13+0.05 mm under a constant applied load 300g. As cement solidifies the penetration of needle decreased. A Model proposed by Vipulanandan has been used, which is

$$Tini = T_0 + \frac{\rho}{A+B\rho}, \quad (3\text{-}3)$$

where Tini =Initial Setting Time,

T0, A, and B are material Parameters, ρ = initial resistivity.

3.1.2.4) Shrinkage Measurement

Shrinkage studies were conducted on the hardened specimen for one month, using a commercially available Vernier caliper with an accuracy of 0. 001in.To measure shrinkage, vertical and radial change in dimension were measured over time. Shrinkage happens due to the loss of moisture and the change in resistivity is measured along with this. Two types of shrinkage can be defined 1) Linear Shrinkage, 2) Volumetric shrinkage. It has been quantified by the following formula which is

$$\Delta l = (l(t) - l_0)/l_0 \, , \tag{3-4}$$

where l(t) =Length at any time and l(0)=Initial length.

The expression for volumetric Shrinkage is given by

$$\Delta v = (V(t) - V_0)/V_0, \tag{3-5}$$

where v(t) =Volume at any time and v(0)=Initial Volume.

3.1.2.5) Rheology Measurements

The rheology tests were performed on neat cement slurry and cement slurry with additives. (Cellulose and Carboxylated Styrene Butadiene). Rheology gives an idea to quantity the optimum percentage of the additive into cement and tests were performed on polymer modified cement to estimate the yield point and maximum shear to check the pumpability. Shear stress (τ)− shear strain rate(ϒ) response was monitored during tests. In this study, cellulose and carboxylated styrene Butadiene with different percentages were added into cement slurry. To do rheology test, a couette coaxial cylinder rotational viscometer, manufactured by Offite was used. All tests were repeated twice with a new batch of cement pastes and the results indicate that the tests were repetitive.

The rheology tests were done as per the recent API standard. R1B1 bob and sleeve setup was used to conduct the testing. Testing was done in accordance with API-RB10 testing standards and procedures by mixing the polymer with water first then cement with 0.1% conductive filler dispersed inside was poured into the blender while spinning within 15 s.

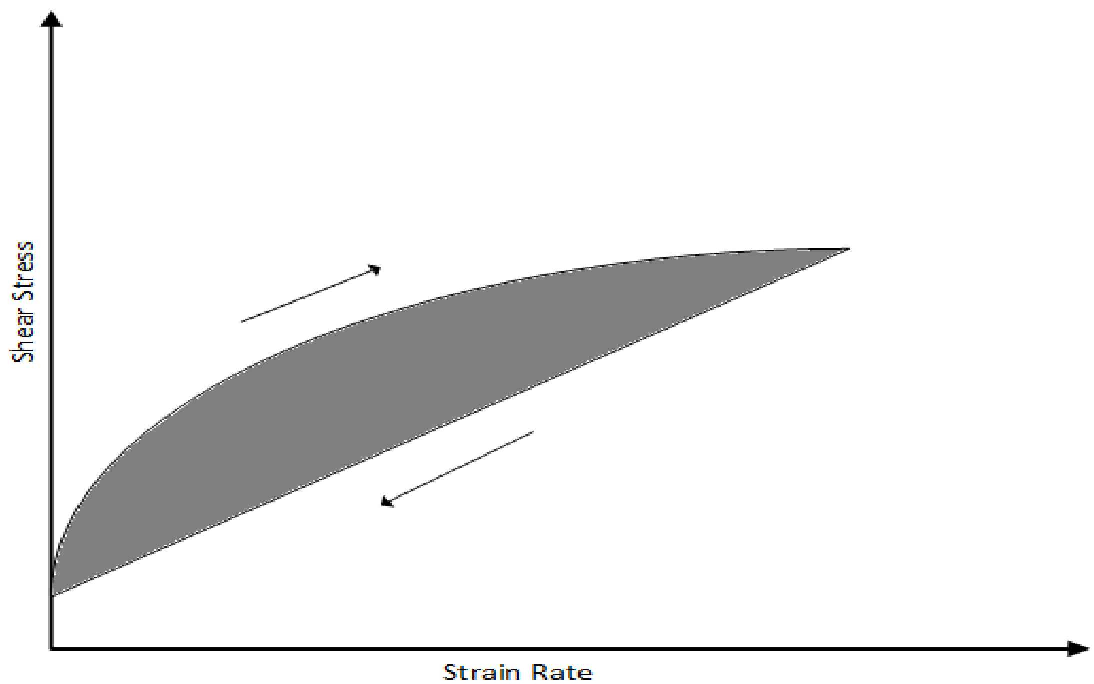

Figure 3-1 Hysteresis Curve Between Up and Down Curve.

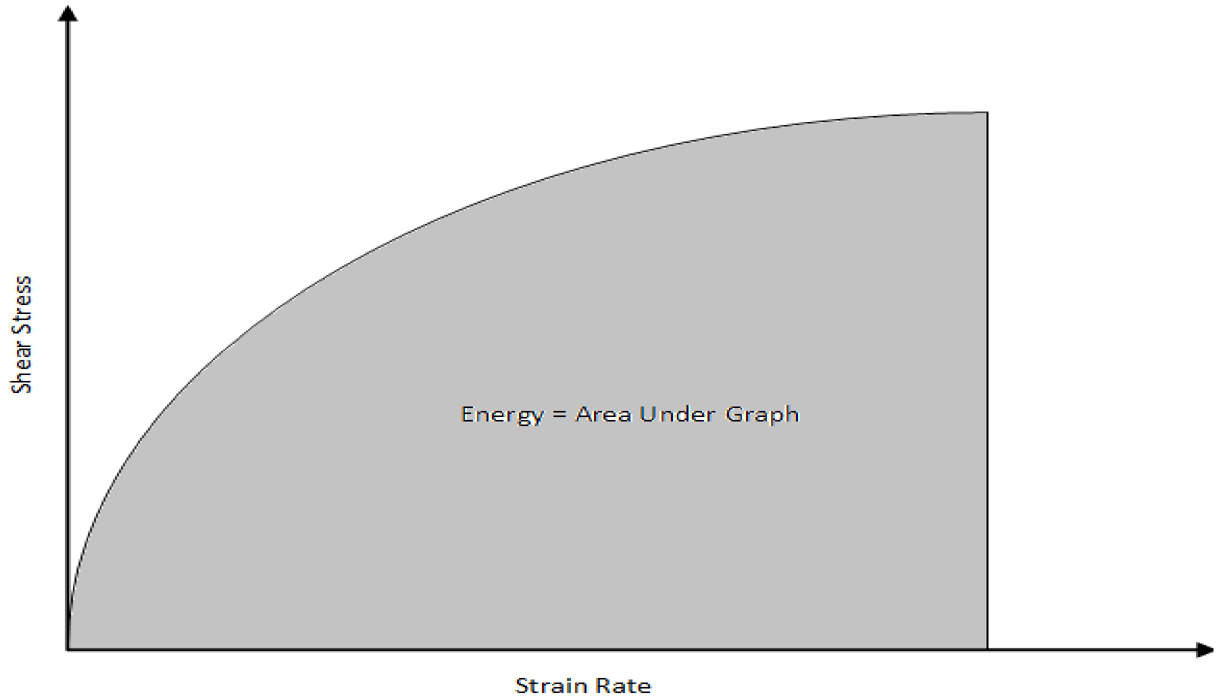

Figure 3-2 Area Under the Shear Stress and Strain Rate

The hysteresis area is the area under the up and down curve of the rheology of cement. The area under the curve is affected by the temperature, type of additive used, and duration of the test. In this, the hysteresis area has been calculated for all the cement slurries under-tested. To know the cohesive energy per unit volume the area under the shear stress and strain rate has been computed. The total energy of the system is essential to know what optimum condition is best for pumping the slurry. The addition of polymer, temperature, and additives affects the energy of the system.

The cement slurry showed non-linear shear thinning behavior with yield stress. Based on the test results, the following conditions have to be satisfied with the model to represent the observed behavior.

Hence the requirements are as follows:

τ = τ_0 when $\dot{\gamma}$ = 0

$$\frac{d\tau}{d\dot{\gamma}} > 0 \quad \text{and} \quad \frac{d^2\tau}{d\dot{\gamma}^2} < 0 \tag{3-6}$$

When $\dot{\gamma} \to \infty \Rightarrow \tau_{max} = \infty$

1) Bingham Model

The Bingham plastic model is used to describe the flow behavior of Bingham plastic fluids. The model is expressed as

$$\frac{d\tau}{d\dot{\gamma}} = k^* > 0 \quad \text{and} \quad \frac{d^2\tau}{d\dot{\gamma}^2} = 0 \tag{3-7}$$

Equation (3-6) is not satisfied, and hence it does not meet the upper limit condition.

When $\dot{\gamma} \to \infty \Rightarrow \tau_{max} = \infty$

2) Vipulanandan Model

The Vipulanandan relationship between shear and shear strain rate for the oil well cement slurry with different temperatures was investigated (Vipulanandan and Mohammed, 2014).The Vipulanandan model is expressed as

$$\tau - \tau_0 2 = \frac{\dot{\gamma}}{C + D^* \dot{\gamma}}, \tag{3-8}$$

$$\frac{d\tau}{d\dot{\gamma}} = \frac{(C + D\dot{\gamma}) - \dot{\gamma}^* D}{(C + D\dot{\gamma})^2} = \frac{C}{(C + D\dot{\gamma})^2} > 0 \Rightarrow C > 0 \tag{3-9}$$

Also, when $\dot{\gamma} \to \infty \Rightarrow \tau_{max} = \frac{1}{D} + \tau_0 2$

where τ is shear stress (Pa); C $(\text{Ps s})^{-1}$ and D $(Pa)^{-1}$: are model parameters (Table 1) and $\dot{\gamma}$ is shear strain rate (s^{-1})

3.1.2.7) Compression Test

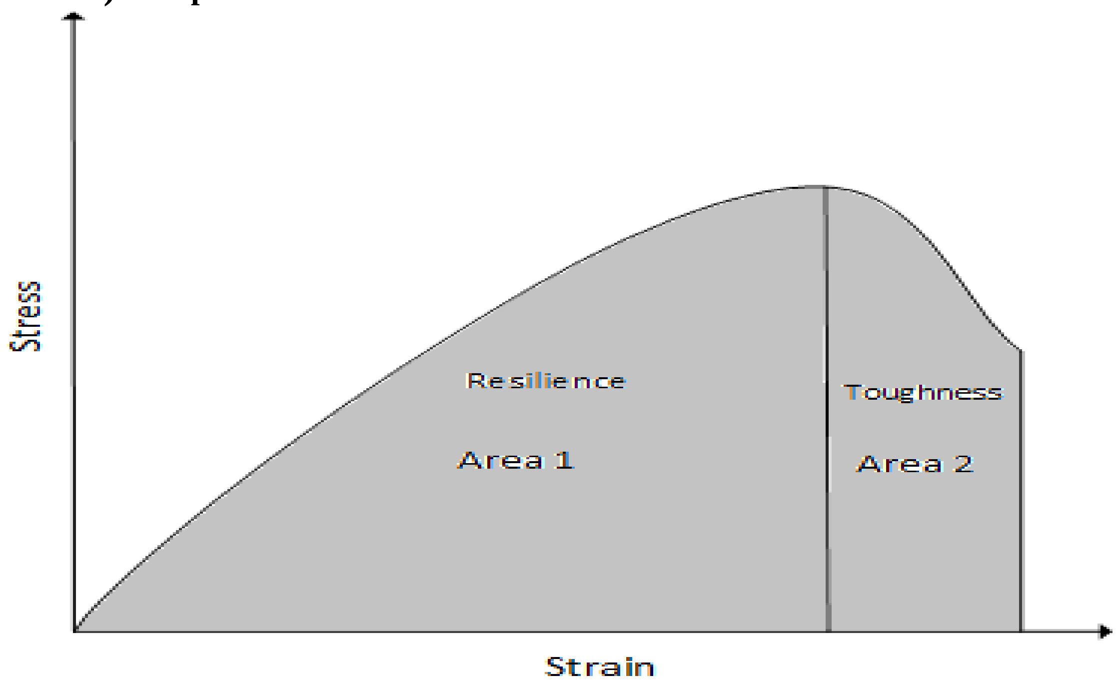

Figure 3-3 Stress Strain Curve of Cement Specimen.

Compressive Stress of the cement specimen was performed using a universal test machine at a displacement rate of 0.125mm/min. The area of the stress-strain curves up to the failure strain is measured, and area after the failure strain is measured.

To capture the stress-strain behavior of the cement, a model was proposed by Vipulanandan. It is a 2 parameter model,which is expressed as

$$\sigma = \left(\frac{\frac{\varepsilon}{\varepsilon_c}}{q+(1-p-q)\left(\frac{\varepsilon}{\varepsilon_c}\right)+p\left(\frac{\varepsilon}{\varepsilon_c}\right)^{(p+q)/p}} \right) \sigma_c \ , \qquad (3\text{-}10)$$

where σ = compressive strength, σ_c, ε_c = compressive strength and corresponding strain, p, q = material parameters.

3.1.2.8) Piezoresistive Behavior

During the uniaxial compression test, using the LCR the resistance is measured for the entire duration of compression testing. The Vipulanandan p-q piezo resistivity model was used to predict the observed trends for the smart cement with and without additives (Vipulanandan et al., 2014).The Vipulanandan p-q piezoresistive model is expressed as

$$\sigma = \frac{\sigma_{max} \times \left(\frac{\left(\frac{\Delta\rho}{\rho}\right)}{\left(\frac{\Delta\rho}{\rho}\right)_{\circ}}\right)}{q_2 + (1 - p_2 - q_2) \times \left(\frac{\left(\frac{\Delta\rho}{\rho}\right)}{\left(\frac{\Delta\rho}{\rho}\right)_{\circ}}\right) + p_2 \times \left(\frac{\left(\frac{\Delta\rho}{\rho}\right)}{\left(\frac{\Delta\rho}{\rho}\right)_{\circ}}\right)^{\left(\frac{p_2 + q_2}{p2}\right)}} , \tag{3-11}$$

where σ is the stress (MPa); σf: compressive stress at failure (MPa);

x= $(\frac{\Delta\rho}{\rho 0})$x100is percentage of change in electrical resistivity due to the stress; xf= $(\frac{\Delta\rho}{\rho 0})$x100 is the percentage of change in electrical resistivity at failure; Δρ: change in electrical resistivity; ρo: initial electrical resistivity (σ = 0 MPa) and p2 and q2 are piezoresistive model parameters.

3.1.2.9) Fluid loss test

The static fluid loss was measured at 25°C with a 500$-m$L HPLT stainless steel filter press cell manufactured by OFI Testing Equipment, Inc. (Houston, TX). The design of this HPHT filter cell and its operation were described in detail in a norm issued by API. After pouring the slurry into the HTHP cell, a differential pressure of 100 psi of N_2 gas was applied at the top of the cell. (API RP 10B $-$ 2 $Specifies$ 70 $bar\ pressure$) Filtration proceeded through a 22.6 cm^2 (3.5-in^2) mesh metal sieve placed at the bottom of the cell. The fluid volume was measured with time till 60 min and Vipulanandan fluid loss model was used to estimate the max fluid loss. But API RP 10B-2 fluid loss is double the volume collected within 30 min.

The API Fluid Loss Model, is expressed as

$$\mathrm{F}L_f - \mathrm{F}L_o = \mathrm{M} * \sqrt{t}\ , \tag{3-12}$$

where FL_f: Volume of fluid loss (mL), FL_o: Initial volume of fluid loss (spurt) (mL)

t: Time (min), M: Model parameter (mL/(min)$^{0.5}$)

The maximum fluid loss FL_{max} when t → ∞ ⇒ F$L_{max} = \infty$

The Fluid Loss Model proposed by Vipulanandan is

$$\mathrm{F}L_f - \mathrm{F}L_o = \frac{t}{D+E*t}\ , \tag{3-13}$$

where D min/mL), and E (mL^{-1}): Model parameters.

From Eqn. 3-13: the maximum fluid loss (FL_{max}) when t → ∞

$$\Rightarrow \mathrm{F}L_{max} = \frac{1}{E} + \mathrm{F}L_o \tag{3-14}$$

3.1.2.10) Gas Leak Test

Gas Migration Apparatus

High Pressure and High-Temperature devices are modified to measure the resistance while the fluid loss test is being done. High Pressure and High-Temperature device with a unique resistance measuring probes were used to measure the resistance change in the dry cement filter after fluid loss. The resistance is converted into resistivity by this formula. During the test, fluid loss is measured, and gas leakage is observed after a definitive loss of fluid. The change in resistance is found during the test.

Gas Migration under Open condition

Case 1- (Presence of Free Fluid Inside Cement Slurry)

When the outlet valve is kept open, the gas is allowed to migrate through the cement slurry. The change in resistivity during this phase is observed. Under the open condition, gas migration initially causes fluid loss in the cement slurry. Precisely, this condition replicates the behavior of gas migration occurring in oil wells. Then the gas leakage after fluid loss is observed. The applied pressure for gas migration under open conditions is kept at 100 psi. The gas migration test is done on cement slurry of w/c of 0.4 and 0.5 after 1hr, 3hr,6hr,12hr, and 24 hours of cement hydration inside the HPHT device.

Case 2- (Absence of Free Fluid in Cement)

After all the free water has been taken out from the cement slurry by a test done in case1, the dried-out cement is subjected to the extremely high pressure of gas. The resistivity changes in the cement slurry and hardened cement due to the applied high gas pressure is measured. In case 2, high-pressure gas migration is done on specimen cured for

1 hour and 24 hours. The tests are done to show the trends observed in resistivity when the cement is at the gel and hardened state.

To control gas migration, it is essential to know the phase conditions inside the cement slurry at different time of curing. As stated in the literature, gas migration starts to occur after there is fluid loss or volume reduction. The purpose of the experiments is to quantify the porosity, moisture content, air void ratio, and water void ratio due to gas migration at different stages of curing.

Phase Change Predictive Model

A new model based on fluid loss has been proposed to quantify the changes happening in the phase diagram (solid, liquid, air).The test is conducted by applying 100psi of gas pressure on the hydrating cement slurry after several hours of curing.(1hr,3hr,6hr,12hr, and 24hr).For complete fluid loss, the duration of pressure application is 30mins. This model can provide useful hindsight of the phase transformation happening inside cement slurry due to cement hydration. The phase change model provides the maximum fluid loss, which can occur inside cement at various stages of curing, with a known water volume inside.

Here, the model is expressed as

$$V(fl) = \frac{t}{Vi/p3+(Vi/q3)*t}\ , \qquad (3\text{-}15)$$

where Vi=Initial Volume of water used; p3and q3 are model parameters at different times. t is the time length of pressure application. When $0< t <30$min, gives detail about the intermediate phase change occurring due applied pressure and t= 30min, complete fluid loss is observed, and model provides absolute phase information at that stage of curing.

Vipulanandan Resistivity Change Model During fluid and Gas Leakage

A new model to quantify resistivity change due to fluid loss is proposed, which is

$$\rho = p4*Vl^{q4} + k \ , \qquad (3\text{-}16)$$

where ,ρ = Resistivity Change Due to Fluid Loss; p4,q4 and k are model parameters.

Vi =is the fluid loss occurring due to gas leakage.

Gas Leak Testing

In order to quantify the gas leak passing through smart cement as a function of both pressure gradient and average velocity, Vipulanandan Fluid Flow Model (Vipulanandan et. al., 2019) was used as

$$U = \frac{\nabla p}{A+B*\nabla P} \ , \qquad (3\text{-}17)$$

where u = Discharge Velocity (m/sec)/(velocity/Area),∇p = Pressure Gradient (MPa/m)

A = Model Parameter 1 (psi.sec/m^2)

B = Model Parameter 2 (sec/m)

Gas Leak Detection and Sensing

The following gas leak correlation is proposed in order to quantify the gas leak velocity in smart cement by monitoring resistivity change.The model is expressed as

$$U = \frac{\frac{\Delta p}{p}}{C+D*(\frac{\Delta p}{p})} \ , \qquad (3\text{-}18)$$

where Δρ/ρ: Change in resistivity (%) ,u: gas leak velocity (m/s)

C and D: Model Parameters (sec/m)

3.2) Materials and Methods for Soil Studies

3.2.1) Houston Clay Soil

Field clays samples were used in the study. To characterize the soil behavior tests such as the Atterberg limit, hydrometer, grain size distribution, and were performed as per the ASTM standards. The test results are summarized in Table 2. Based on the experiments, the soil type was classified

Table 3-3 Test Method and Physical Properties of Soil

	Test Method	Sample 1 (Soil A)	Sample 2 (Soil B)	Sample 3 (Soil C)
Specific Gravity				
LL%	ASTM D 4318	36	86.41	53.91
PI%	ASTM D 4318	18	63.91	35.41
OMC	ASTM D698			
Max-Dry Density	ASTM D698	2.01	1.83	1.95
Soil Type	ASTM D2487	CL	CH	CH

3.2.1.2) Sand

To have proper uniformity and to get consistent results, Ottawa sand conforming to ASTM C778 was used.

3.2.1.3) Bentonite

Commercially available clay was used with a liquid limit of 745% and a plasticity index of 671%.The density of bentonite used is 2.79Mg/m^3 and initial dry density is 1.90Mg/m3

3.2.1.4) Polymer

Commercially available polyacrylamide polymer was used in the study. The polymer solution was prepared with different percentages of polyacrylamide polymer. The effective portion of polymer added into the clay soil was 2.5%,5%, and 7.5% by weight of dry soil.

The soil was pulverized and made dry and kept in oven, then polymer was added into it. For proper dispersion of polymer over pulverized soil, the polymer solution was mixed thoroughly and allowed to dry for one day at room temperature.

To prepare the polymer solution, the following mix of the polymer was used. The polymer solution was prepared by mixing Mix-1 and Mix -2. This polymer solution was applied on the pulverized soil.

Table 3-4 Polymer Preparation Mix.

<table>
<tr><th colspan="2">Mix -1</th><th colspan="2">Mix -2</th></tr>
<tr><td>AV- 100</td><td>2.5%,5%,7.5%</td><td>AV-102</td><td>0.5%</td></tr>
<tr><td>AV -101</td><td>0.5%</td><td rowspan="2">Water</td><td rowspan="2">50ml</td></tr>
<tr><td>Water</td><td>50ml</td></tr>
</table>

3.2.2.1). Electrical Resistivity of Soil

The electrical resistivity of soil is measured using soil conductivity meter of range 0-4000 mS/cm. The temperature range with which it is effective is 0-50 C.

3.2.2.2) Atterberg Limits

The liquid limit, plastic limit, and plasticity index of the field samples were determined before and after treatment. In the case of the field soil sample, 75-80 g was required to find the Atterberg limits.

3.2.2.3) Compaction Test

The compaction characteristics of the untreated and soil samples were carried out using a modified compaction mold based on the available soil samples. The compaction energy was unaltered and equal to the specification of ‘Standard Test Methods for Laboratory Compaction Characteristics of Soil Using Standard Effort (12 400 ft-ibf/ft^3 or 600 kN-m/m^3).

Five different field soil were used have been used to find the OMC and MDD, to characterize the treated soil according to the MDD vs OMC curve. 11b of field soil was used to perform the compaction test. The hammer used for compaction had a weight of 5.5 lbs. The number of blows is reduced, accounting for the change in the dimensions of the mold and the compaction energy was unaltered.

3.2.2.4) Expansion Index

The expansion index test for the filed soil was carried in accordance with ASTM D482911. To do this test, a sample with natural field density was used in the consolidation ring. A seating pressure of 1 psi was used, and dial gauge readings were recorded. As the soil swell, dial gauge reading changed, and the reading was recorded till soil expansion stopped.The equation is given as

$$EI = \frac{\Delta H}{H_1} . 1000 \,, \tag{3-19}$$

where $H_1 - \ the$ initial height of the specimen (in or mm)

$\Delta H -$ Change in height of the specimen (in or mm) and Classification of soils according to the expansion index is detailed

EI Expansion Potential 0 to 20

Very Low 21 to 50

Low 51 to 90

Medium 91 to 130

High >130 Very High.

3.2.2.6) Freezing of Soil

To see the temperature effect on the soft, freeze-thaw test was conducted in a freezer. The change in temperature and resistance was monitored for the entire duration of test. The effect of temperature on electrical behavior was studied.

3.2.2.7) Impedance Model.

Ac measurement is used to characterize the electrical behavior of the material over the frequency range of 20 Hz to 300 kHz. AC measurement provides the resistance and reactance parts of the measurement. The impedance versus frequency curve is plotted for the materials and based on the shape of the curve, (Vipulanandan et al., 2013) equivalent circuits are proposed.

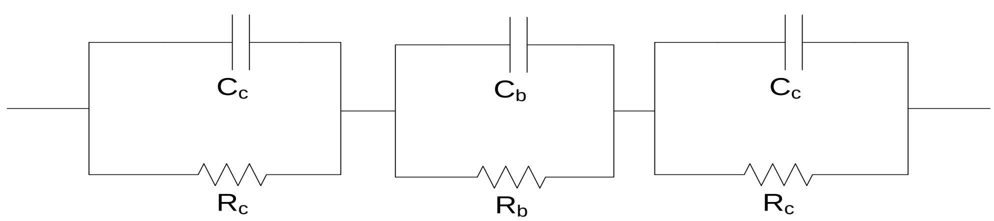

Figure 3-4 Case 1: General Bulk material – Capacitance and Resistance

In the equivalent circuit for case 1, the contact was connected in series, and both the contacts and the bulk material were represented using a capacitor and a resistor connected in parallel. In the equivalent circuit for case 1, R_b and C_b are resistance and capacitance of the bulk material, respectively; and R_c and C_c are resistance and capacitance of the contacts, respectively. Both contacts are represented with the same resistance (R_c) and capacitance (C_c) as they are identical. The total impedance of the equivalent circuit for case 1 (Z_1) can be represented as

$$Z_1(\sigma) = \frac{R_b(\sigma)}{1+\omega^2 R_b^2 C_b^2} + \frac{2R_b(\sigma)}{1+\omega^2 R_c^2 C_c^2} - j\left\{\frac{2\omega R_b^2 C_c(\sigma)}{1+\omega^2 R_c^2 C_c^2} + \frac{\omega R_b^2 C_b(\sigma)}{1+\omega^2 R_b^2 C_b^2}\right\}, \tag{3-20}$$

where ω is the angular frequency of the applied signal. When the frequency of the applied signal is very low, $\omega \to 0$, $Z_1 = R_b + 2R_c$, and when it is very high, $\omega \to \infty$, $Z_1 = 0$.

Case 2: Special Bulk Material – Resistance Only

Case 2 is a special case of case 1 in which the capacitance of the bulk material (C_b) is assumed to be negligible. The total impedance of the equivalent circuit for Case 2 (Z_2) is

$$Z_2(\sigma) = R_b(\sigma) + \frac{2R_c(\sigma)}{1+\omega^2 R_c^2 C_c^2} - j\,\frac{2R_c(\sigma)}{1+\omega^2 R_c^2 C_c^2} \quad , \tag{3-21}$$

where ω is the angular frequency of the applied signal .When the frequency of the applied signal is very low, $\omega \to 0$, $Z_2 = R_b + 2R_c$, and when it is very high, $\omega \to \infty$, $Z_2 = R_b$ (figure 3-5).

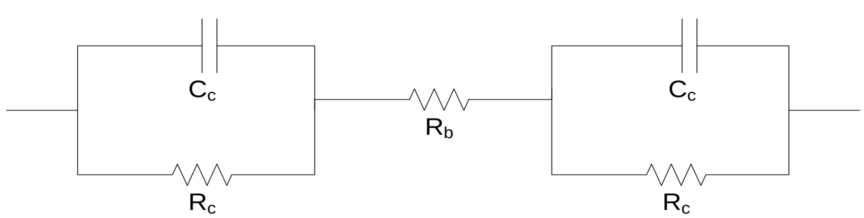

Figure 3-5 Equivalent circuit for case 2

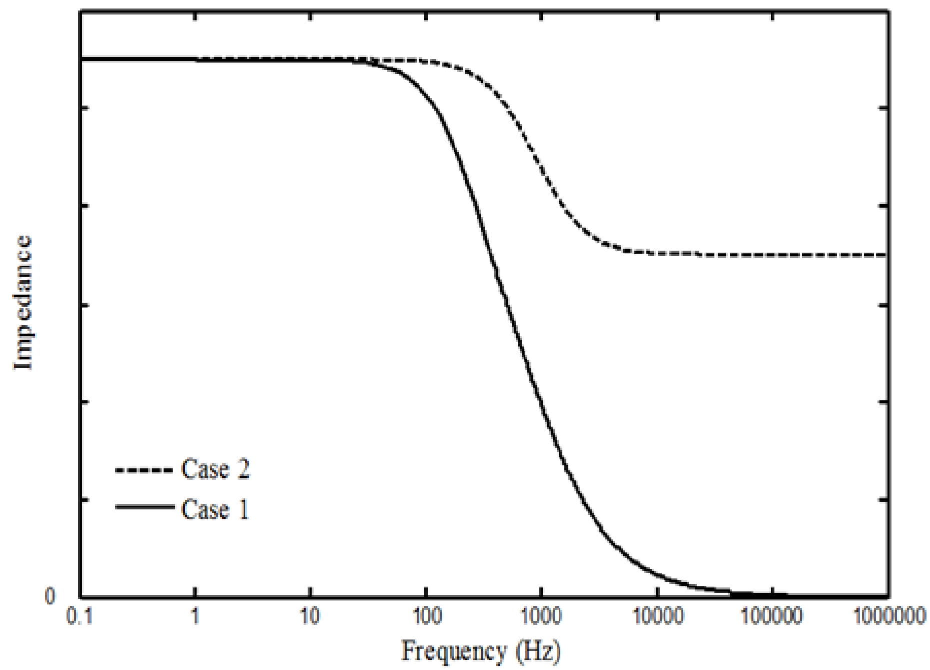

Figure 3-6 Impedance curve of Case 2 and Case 1 materials.

The shape of the curve indicates if the material is case 1 or case 2. In this research, the cement studies and soil studies indicated that these are case 2.

3.3) Material and Method to Study Composite Corrosion.

Materials and Methods.

Cement specimen of dimension 5cmx5cmx20cm was prepared with steel bar embedded in it. The water-cement ratios were 0.4. The cement specimen was room cured in air for one month. Then the sample was immersed in the saltwater of 3.5% concentration to simulate the corrosive environment in actual world. Wires were inserted in the specimen at 4 different locations.

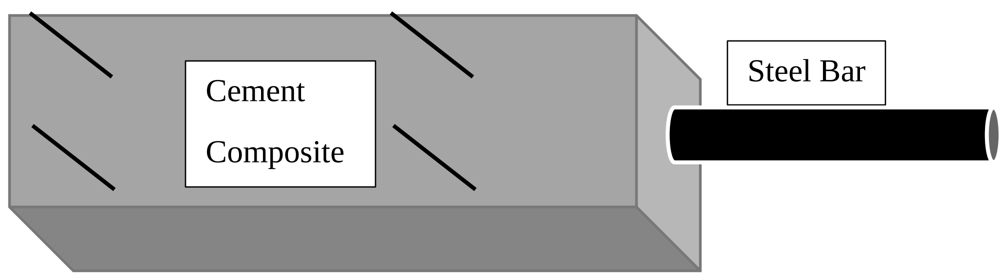

Figure 3-6 Representational figure of Sample Used for Study.

To investigate the effect of corrosion, the electrical impedance response of the steel bar exposed to the saline environment, steel bar and wire A, combinations of wire AB and AC were studied for one year. To quantify the effect of corrosion, before applying the AC current samples were oven dried for one day to diminish the moisture effect on the specimen. To characterize the electrical response the impedance curve with frequency was plotted for all specimens.

A method to quantify the surface corrosion is quantified be measuring the contact capacitance and contact resistance.The resistance (R) and capacitance (C) of a composite material between two points is defined as

$$R = \rho \frac{L}{A} \ , \tag{3-22}$$

where A = cross-sectional area, L = distance between the electrode contacts.

In the other hand the capacitance of the material is defined as

$$C = \varepsilon \frac{A}{L} \ , \tag{3-23}$$

where ε = absolute permittivity of the material .

The product of equation given in (3-22) and (3-23) result as

$$RC = \rho\varepsilon. \tag{3-24}$$

Since ρε in equation (3-22) is material property, RC is also material property. The advantage of equation (3-24) is that we now are able to characterize the material property of the corrosion products at the interface level as without dependence on the geometry factor such as the length or thickness and area.

CHAPTER 4 EFFECT OF CARBOXYLATED STYRENE BUTADIENE POLYMER AND CELLULOSE ON RHEOLOGY OF OIL WELL CEMENTS AT VARIOUS CONCENTRATION AND TEMPERATURE.

Understanding of rheological behaviour of cement systems is essential to design proper cement slurry for formation. There is a need for fundamental and quantitative description of cement paste behaviour. In recent years understanding, measuring, and modeling rheological properties has become more important as the number of additives are applied to modify the cementing properties. In the oil well industry, rheological properties of cement are modeled using Bingham, Herchel-Bulkley model. Although the existing models providing information of yield point and plastic viscosity, most of the models do not predict maximum shear stress. A new fluid model proposed by Vipulanandan predicts the maximum shear stress fluid and yield stress of different types of fluid. It is a two-parameter model and can be used to correlate with other material parameters such as density, resistivity, temperature with the material property.

Rheology

The experimental program consisted of two phases. The first phase concerned the investigation of the effect of Polymer on rheological properties. Different percentages of Polymer were added to study the effect of polymer addition on the rheology of cement pastes. In the second phase, at high temperatures, the behaviour of cement slurry at high temperatures was investigated.

The optimization of oil well slurries requires a number of trial batches to achieve adequate rheological properties. The first phase concerned the investigation of polymer addition into oil well cement and its effect on rheology. In the second phase at high temperature, the impact of polymer addition on the cement rheology is investigated.

4.1) Effect of Temperature on Oil Well Cement

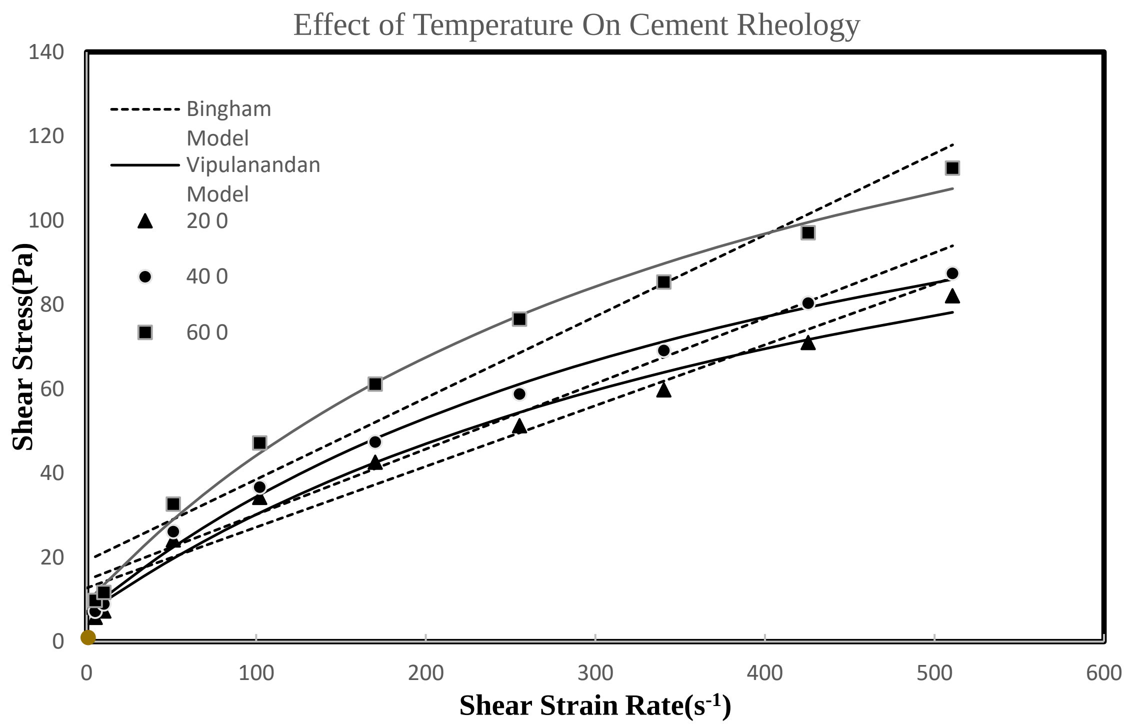

Figure 4-1 Measured and Predicted stress-shear strain rate for Cement Slurry at 20°C, 40°C, and 60°C

Table 4-1 Bingham and Vipulanandan Model Parameter for cement slurry at different temperatures.

Bingham Model					Vipulanandan Model					
Temp	τ_0	k	R^2	RMSE (Pa)	τ_0	C(Pas^{-1})	D(Pas^{-1})	R^2	RMSE (Pa)	τ_{max}
20	12.73	0.14	0.97	4.71	6.66	3.55	0.005	0.98	3.66	149.51
40	14.63	0.16	0.98	4.77	7.05	2.97	0.005	0.99	2.43	154.10
60	19.17	0.17	0.95	7.11	9.89	2.29	0.006	0.98	1.60	209.18

Bingham Plastic Model-

The shear thinning behaviour of smart cement slurry at different temperatures, 20°C, 40°C, and 60°C were modeled using the Bingham Plastic model. The coefficient of determination of (R^2) and root mean square error observed at 20°C, 40°C, and 60°C were 0.97,0.98,0.95 and 4.71Pa, 4.77Pa, 7.11Pa respectively. The average yield stress for the cement slurry at temperature 20°C, 40°C, and 60°C were 12.73Pa,13.01 Pa and 16.18 Pa, respectively. The model parameters were 0.14,0.16,0.17 respectively.

Vipulanandan Model-

The shear-thinning behaviour of smart cement slurry at different temperatures,20°C, 40°C, and 60°C were modeled using the Vipulanandan model. The coefficient of determination of (R^2) and root mean square error observed at 20°C, 40°C, and 60°C were 0.97, 0.98, 0.95 and 4.13Pa, 3.38Pa, 2.29Pa respectively. The average yield stress for the cement slurry at temperature 20°C, 40°C, and 60°C were 8.25Pa, 7.13 Pa, and 5.75 Pa, respectively. The model parameters were (4.13,0.005), (3.38,0.005), and (2.29,0.006), respectively.

Maximum Shear Stress

Based on equation (3-9), the Vipulanandan model has 40°C a limit on the maximum shear stress (τ_{max}). The slurry will produce at a relatively very high rate of shear strain. The τ_{max} for cement slurries at different temperatures 20°C, 40°C, and 60°C was 204.13Pa, 203.13Pa and 168.57Pa, respectively as summarized in Table 4-1.Increasing the temperature of smart cement slurry 20°C to 40°C, 60°C increased the maximum shear stress by --3%,35% respectively.

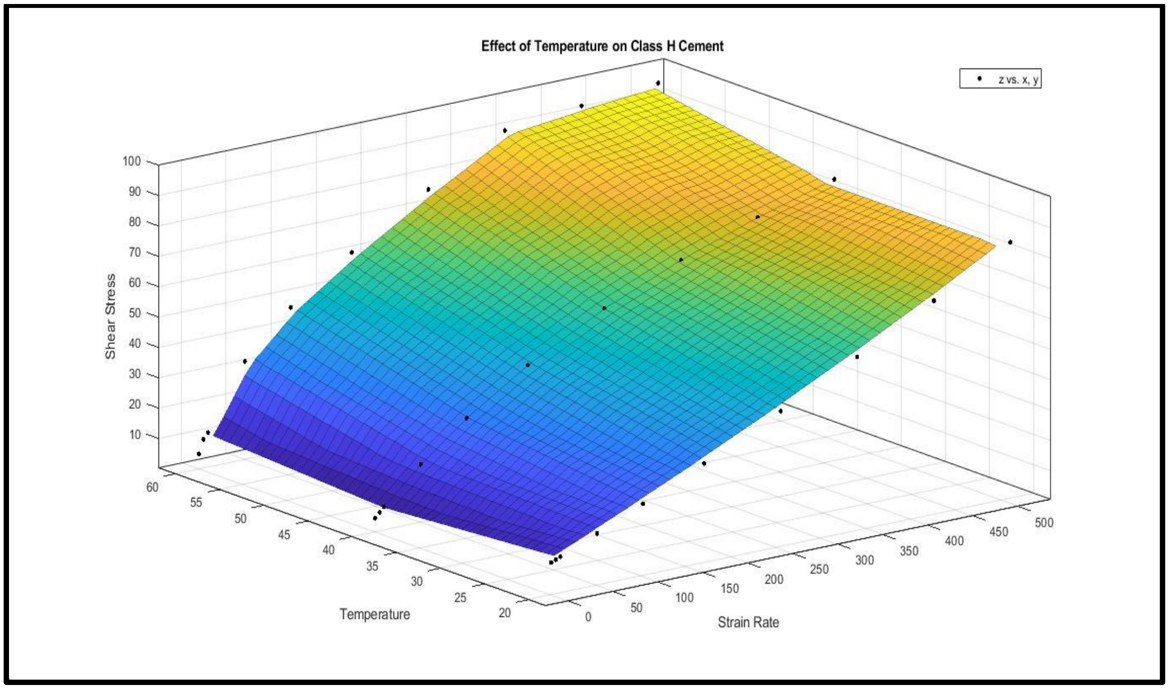

Figure 4-2 Effect of temperaute on the rheology of neat cement.

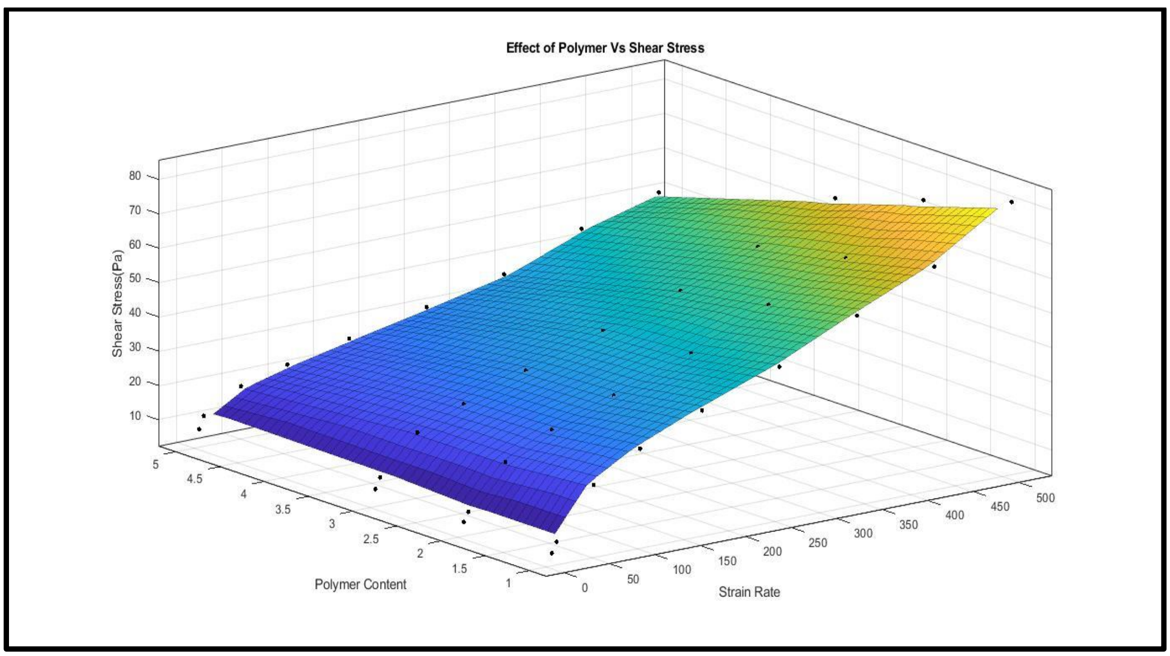

Figure 4-3 Effect of polymer addition on the rheology of neat cement.

4.2) Effect of Polymer (XSBR) Addition on Cement Slurry

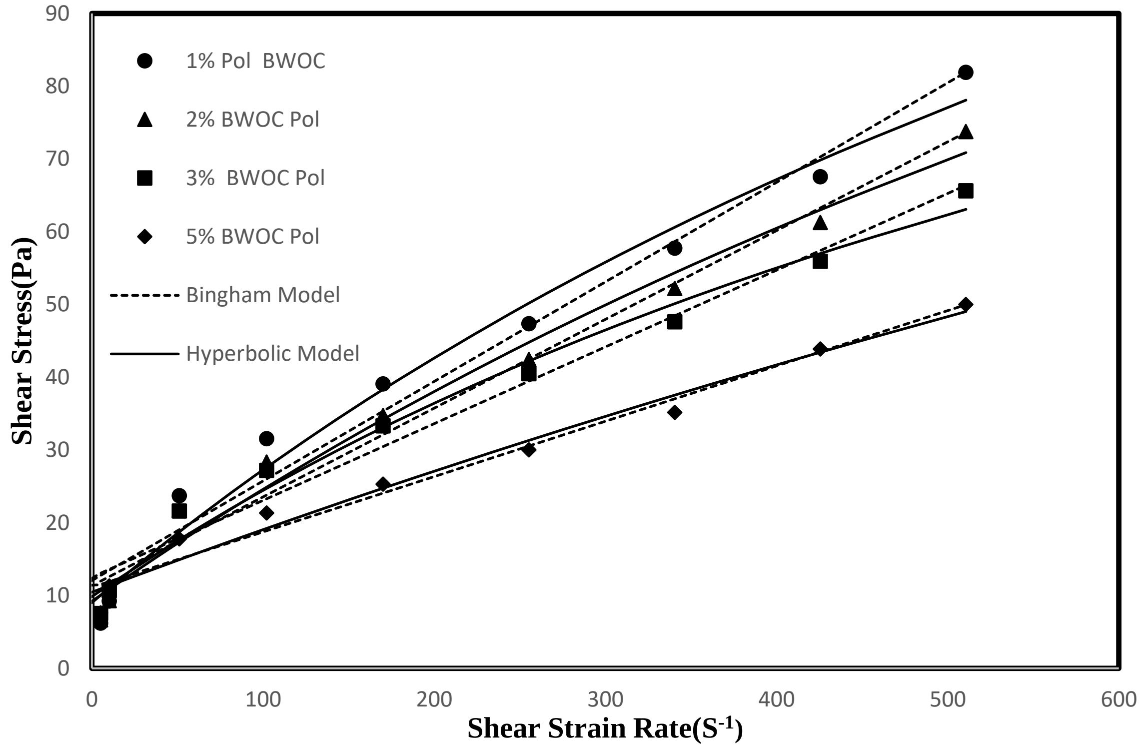

Figure 4-4 Measured and Predicted stress-shear strain rate for Cement Slurry due to addition of 1%,2%,3% and 5% polymer.

Table 4-2 Bingham and Vipulanandan Model Parameter for cement slurry on the addition of Polymer.

	Bingham Model				Vipulanandan Model					
%Pol	τ_0	k	R^2	RMSE (Pa)	τ_0	C(Pas^{-1})	D(Pas^{-1})	R^2	RMSE (Pa)	$\tau_{max(Pa)}$
0	12.73	0.14	0.97	4.71	8.25	4.13	0.005	0.98	3.66	208.25
1%	12.06	0.13	0.98	3.87	9.02	5.01	0.004	0.99	3.23	259.02
2%	11.35	0.12	0.98	3.12	9.21	6.06	0.004	0.99	2.71	259.21
3%	12.53	0.10	0.98	2.98	9.85	6.18	0.0038	0.99	2.32	273.45
5%	11.14	0.07	0.98	1.96	10.4	11.23	0.003	0.99	1.89	343.45

Bingham Plastic Model-

The shear-thinning behaviour of smart cement slurry due to the addition of a different percentage of slurry (1,2,3,5) was modeled using the Bingham model. The coefficient of determination of (R^2) and root mean square error observed due to addition of 1%, 2%, 3% and 5% polymer were 0.97, 0.98, 0.98, 0.95 and 12.06Pa, 12.53Pa, 12.53Pa, 11.14Pa respectively. The average yield stress for the cement slurry at the temperature on the addition of 1%, 2%, 3%, and 5% polymer was 12.73Pa, 13.01 Pa, and 16.18 Pa, respectively. The model parameters for 1%, 2%, 3%, 5% polymer was 0.13, 0.12, 0.10, 0.07.

Vipulanandan Model-

The shear-thinning behavior of smart cement slurry due to the addition of a different percentage of slurry (1, 2, 3, 5) was modeled using the Vipulanandan model. The coefficient of determination of (R^2) and root mean square error observed due to addition of 1%, 2%, 3% and 5% polymer were 0.97, 0.98, 0.98, 0.95 and 9.02Pa, 9.21Pa, 9.85Pa, 11.23Pa respectively. The average yield stress for the cement slurry at the temperature on the addition of 1%, 2%, 3% and 5% polymer was 12.73Pa, 13.01 Pa and 16.18 Pa, respectively. Yield stress increased by 9.33%, 11.65%, 19.35% and 26.78% over The corresponding model parameters for 1%, 2%, 3% and 5% polymer were (5.01, 0.004), (6.06, 0.004), (6.18, 0.006) and (11.23, 0.003) respectively.

Maximum Shear Stress

Based on equation (3-9), the Vipulanandan model has a limit on the maximum shear stress (τ_{max}). The slurry will produce at a relatively very high rate of shear strain. The τ_{max}

for cement slurries at 20^{o}C without and with 1%, 2%, 3% and 5%, respectively, as summarized in Table 4-2. Increasing the polymer dosage by 1%, 2%, 3% and 5% on smart cement slurry increased the $\tau_{(max)}$ by 24.13%, 24.23%, 31.45% and 65.45%.

In the case of the Vipulanandan Model, the yield stress increased consistently with increasing polymer content. This trend confirms the trend reported by Berg et al., (1979), the yield stress and plastic viscosity of cement paste increase as the cement gets finer, which reflects the dominance of the water–cement interface in this system. The addition of Polymer reduces the density as cement volume is occupied by finer polymer particulates. The influence of particle size is a surface area effect in fine-grained pastes and a simple volume effect in the coarser-grained concretes.

4.3) Effect of Temperature on smart cement with different polymer percentages.

4.3.1) Effect of Temperature on Cement Added with 1% slurry.

Bingham Plastic Model-

The shear-thinning behavior of smart cement slurry due to addition 1% polymer at 20^{o}C, 40^{o}C, and 60^{o}C were modeled using the Bingham model. The coefficient of determination of (R^2) and root mean square error observed at 20^{o}C, 40^{o}C and 60^{o}C were and 6.21Pa, 3.89Pa, 8.04Pa, respectively. The average yield stress for the cement slurry at 20^{o}C, 40^{o}C, and 60^{o}C on the addition of 1% polymer was 16.24Pa, 12.35Pa, 24.15Pa, respectively. The corresponding model parameters for Bingham model for 1%, 2%, 3% and 5% polymer were 0.14, 0.08, 0.13 respectively.

Vipulanandan Model

The shear-thinning behaviour of smart cement slurry due to the addition of 1%polymer was modelled using the Vipulanandan model. The coefficient of determination of (R^2) and root mean square error at 20°C, 40°C and 60°C were 0.97, 0.98, 0.98, 0.95 and 8.52Pa, 7.12Pa, 11.23Pa respectively. The average yield stress for the cement slurry at 20°C, 40°C and 60°C temperature on the addition of 1% were 8.52Pa, 7.12 Pa, and 11.31Pa, respectively. The corresponding model parameters for 1% added polymer at 20°C, 40°C and 60°C temperature were (4.59,0.005), (7.12,4.52) and (1.96,0.01) respectively.

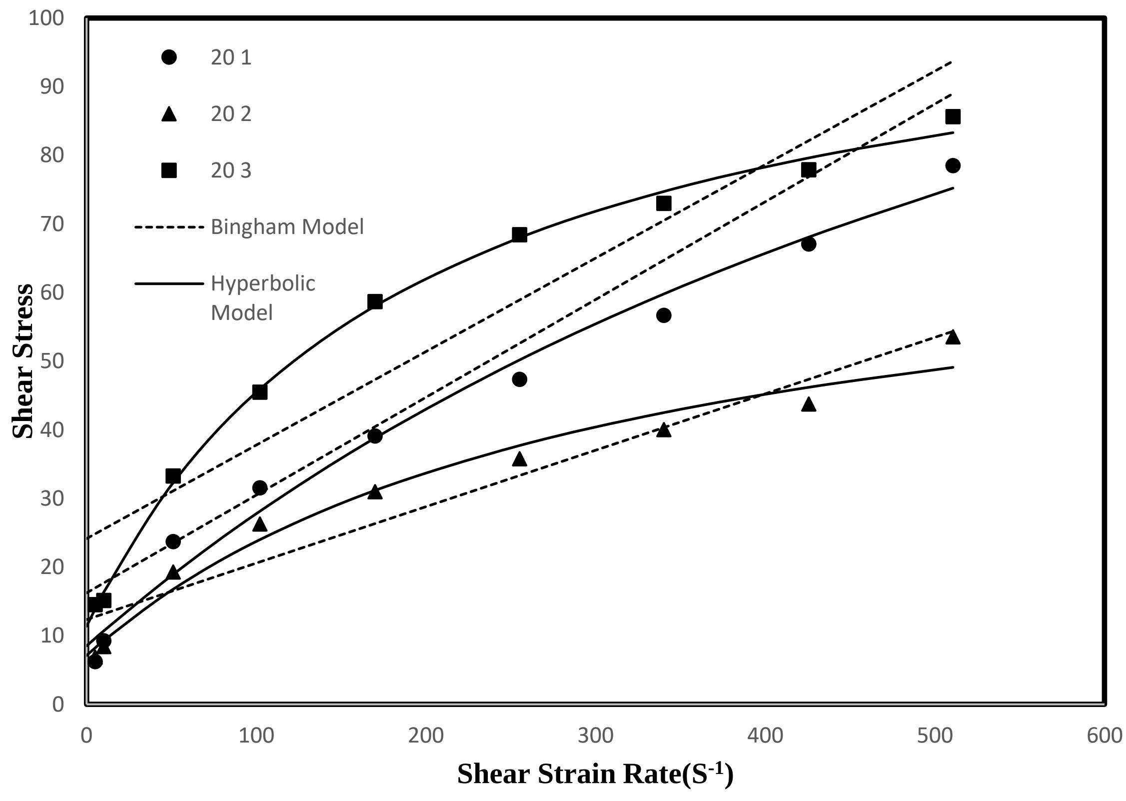

Figure 4-5 Measured and Predicted stress-shear strain rate for Cement Slurry on addition of 1% at 20°C, 40°C, and 60°C.

As the temperature of cement slurry with 1% polymer is raised from 20°C to 40°C, the yield stress decreased. The possible explanation could be the carboxyl group and water affinity of XSBR hinders the ettringite formation. It acts as a plasticizer by enveloping cement particles. (Vitorini et al., 2020). When the temperature was further raised to 60°C, yield stress increased, signifying the dominance of temperature effect on the cement slurry.

Table 4-3 Bingham and Vipulanandan Model Parameter for cement slurry on the addition of 1% and 3% polymer.

% Pol	Bingham Model					Vipulanandan Model					
	Temp	τ_0	k	R^2	RMSE	τ_0	C(Pas^{-1})	D(Pas^{-1})	R^2	RMSE	$\tau_{max(Pa)}$
1%	20	16.24	0.14	0.95	6.21	8.52	4.59	0.005	0.99	2.94	208.52
1%	40	12.35	0.08	0.94	3.89	7.12	4.52	0.01	0.99	2.35	78.54
1%	60	24.15	0.13	0.90	8.04	11.31	1.96	0.01	0.99	1.28	111.31
3%	20	12.32	0.10	0.99	2.97	10.16	6.60	0.004	0.99	2.55	210.53
3%	40	15.84	0.05	0.98	2.75	8.34	6.29	0.02	0.96	1.70	58.34
3%	60	48.32	0.13	0.98	14.04	21.18	0.72	0.01	0.99	1.67	118.53

Maximum Shear Stress

Based on equation (3-9), the Vipulanandan model has a limit on the maximum shear stress (τ_{max}). The slurry will produce at a relatively very high rate of shear strain. The τ_{max} for cement slurries at 20°C without and with 1%, 2% and 3%, respectively as summarized in Table 4-3.

4.3.2) Effect of Temperature on Cement Added with 3% XSBR

Bingham Plastic Model-

The shear-thinning behaviour of smart cement slurry due to addition 3% polymer at 20°C, 40°C, and 60°C were modeled using the Bingham model. The coefficient of determination of (R^2) and root mean square error observed at 20°C, 40°C, and 60°C were and 6.21Pa, 3.89Pa, 8.04Pa, respectively. The average yield stress for the cement slurry at

20^{o}C, 40^{o}C and 60^{o}C on the addition of 1% polymer were 16.24Pa, 12.35Pa, 24.15Pa, respectively. The corresponding model parameters for Bingham model for 1%, 2% and 3% polymer were 0.14, 0.08, 0.13.

Vipulanandan Model-

The The shear-thinning behavior of smart cement slurry due to the addition of 3% polymer was modelled using the Vipulanandan model. The coefficient of determination of (R^2) and root mean square error at 20^{o}C, 40^{o}C and 60^{o}C were 0.97, 0.98, 0.98, 0.95 and 8.52Pa, 7.12Pa, 11.23Pa respectively.

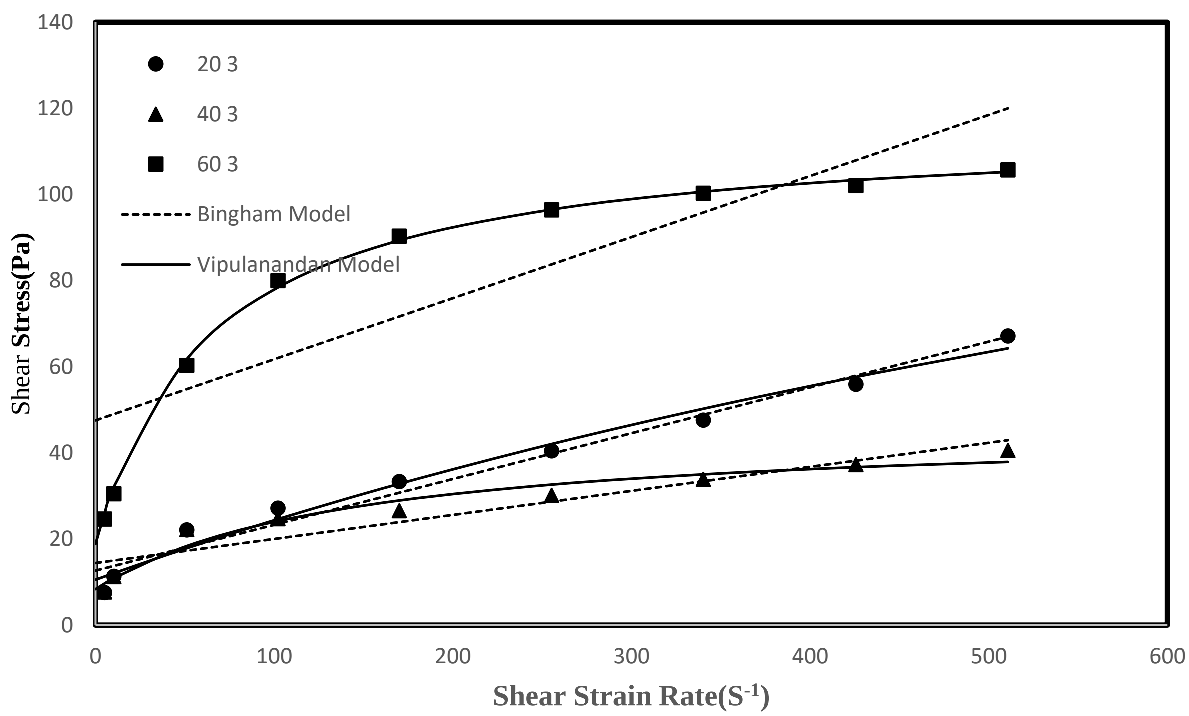

Table 4-4 Measured and Predicted stress-shear strain rate for Cement Slurry on addition of 3% at 20^{o}C, 40^{o}C, and 60^{o}C.

The average yield stress for the cement slurry at 20^{o}C, 40^{o}C, and 60^{o}C temperature on the addition of 1% were 10.16Pa, 12.04Pa, and 21.18Pa, respectively. The corresponding model parameters for 3% added polymer at 20°C, 40°C and 60°C temperature were (6.60,0.005), (6.29,0.02) and (0.72,0.01) respectively.

Maximum Shear Stress

Based on equation (3-9), the Vipulanandan model has a limit on the maximum shear stress(τ_{max}). The slurry will produce at a relatively very high rate of shear strain. The τ_{max} for cement slurries at 20°C, 40°C, 60°C due to 3% polymer addition, is summarized in Table 4.

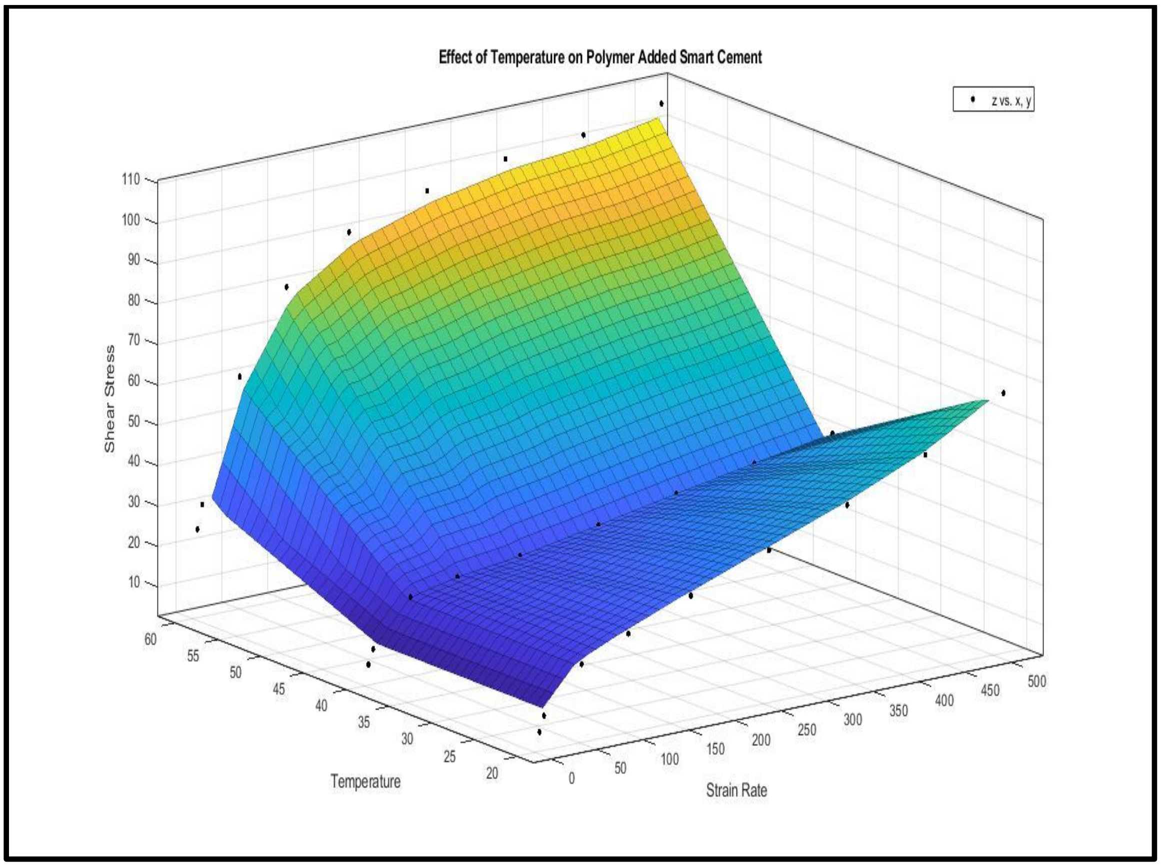

Figure 4-6 Effect of temperature variation on 3% polymer Modified Smart cement.

4.2) Effect of Cellulose on Cement Slurry Rheology.

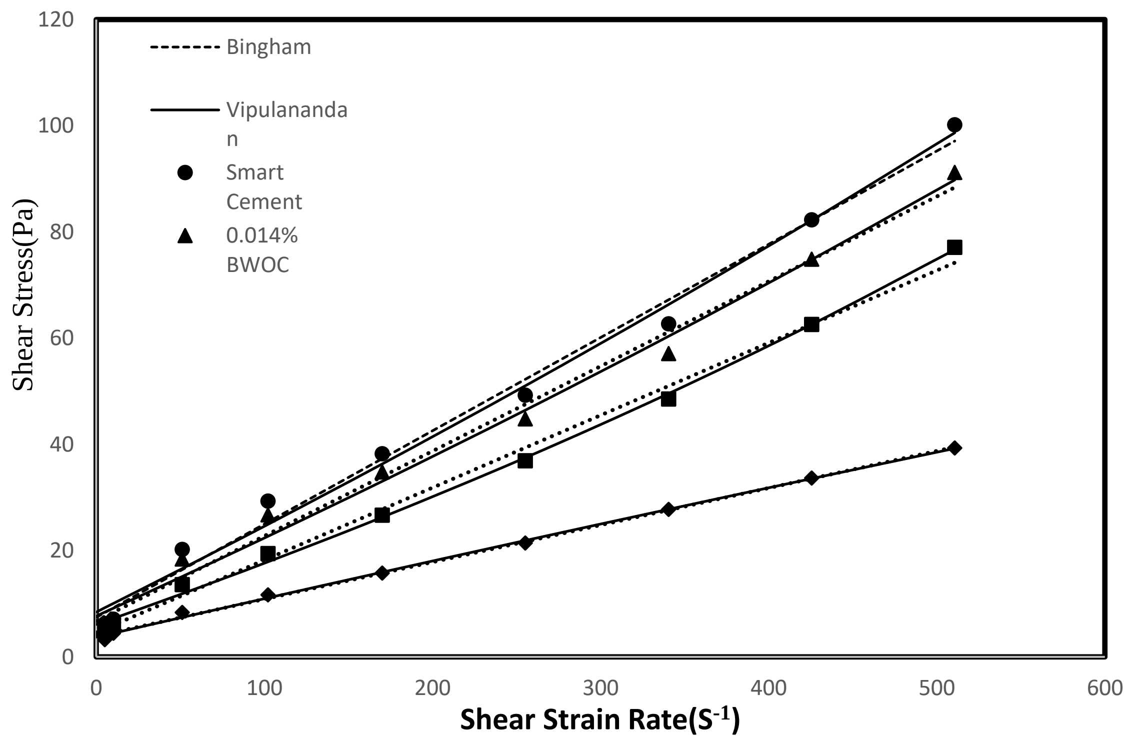

Figure 4-7 Measured and Predicted stress-shear strain rate for Cement Slurry due to addition of 0.014%,0.028% and 0.042% polymer

In figure 4-8, the rheological behavior of cement slurry due to addition of polymer on class H cement at room temperature is shown.

Table 4-5 Bingham and Vipulanandan Model Parameter for cement slurry due addition of Polymer.

	Bingham Model				Vipulanandan Model					
%	τ_0	k	R^2	RMSE (Pa)	τ_0	C (Pas^{-1})	D (Pas^{-1})	R^2	RMSE (Pa)	$\tau_{max(Pa)}$
0	7.44	0.17	0.99	2.96	8.44	6.32	0.005	0.99	2.84	208.8
0.014%	6.77	0.15	0.99	2.70	7.69	6.92	0.0045	0.99	2.58	229.8
0.028%	4.55	0.13	0.99	1.73	6.10	6.10	0.004	0.99	1.07	256.1
0.042%	3.98	0.06	0.99	0.52	3.72	3.72	0.003	0.99	0.50	333.1

Bingham Plastic Model-

The shear-thinning behavior of smart cement slurry due to the addition of a different percentage of slurry (0.014%, 0.028%, 0.042%) was modeled using the Bingham model. The coefficient of determination of (R^2) and root mean square error observed due to addition of 0.014%, 0.028% and 0.042% polymer were 0.99, 0.99, 0.99, 0.99 and 2.96Pa, 2.70Pa, 1.73Pa, 0.52Pa respectively. The average yield stress for the cement slurry at room temperature on the addition of 0.014%, 0.028% and 0.042 cellulose was .44Pa, 6.77Pa, 4.55Pa, 3.98Pa. The model parameters for 0.014%, 0.028% and 0.042% cellulose was 0.17, 0.15, 0.13, 0.06

Vipulanandan Model-

The shear-thinning behavior of smart cement slurry due to the addition of a different percentage of slurry (0.014%, 0.028%, 0.042%) was modeled using the Vipulanandan model. The coefficient of determination of (R^2) and root mean square error observed due to addition of 0.014%, 0.028% and 0.042% cellulose was 0.99, 0.99, 0.99, 0.99 and 2.58Pa, 1.07Pa, 0.50Pa respectively. The average yield stress for the cement slurry at room temperature on the addition of 0.014%, 0.028% and 0.042% polymer was 7.69 Pa, 6.10 Pa and 3.72Pa respectively. Yield stress decreased by 8%, 27%, and 55% over normal smart cement. The corresponding model parameters for 0.014%, 0.028% and 0.042% cellulose was (5.01,0.004), (6.06,0.004), (6.18,0.006) and (11.23,0.003) respectively.

Maximum Shear Stress

Based on equation (3-9), the Vipulanandan model has a limit on the maximum shear stress (τ_{max}). The slurry will produce at a relatively very high rate of shear strain. The τ_{max}

for cement slurries at 20^{o}C without and with 0.014%, 0.028% and 0.042% respectively, as summarized in Table 4-4. Increasing the cellulose dosage by 0.014%, 0.028% and 0.042% on smart cement slurry increased the $\tau_{(max)}$ by 10.13%, 22.23%, and 61.45% and 65.45%.

4.5) Gel Strength of Cement Slurry

Using the rheometer, the gel strength of different cement slurries was evaluated. Gel strength is an indicator, how fast the cement us hydrating.

Table 4-6 Gel Strength of slurries after 10 sec and 10 min.

Slurry Number	Pol% Added	Temperature	Gel 10 sec	Gel 10 min
1	0	20	16	18
2	0	40	20	28
3	0	60	39	74
4	1	20	16	26
5	2	20	18	23
6	3	20	23	28
7	5	20	22	27
8	1	40	17	54
9	1	60	30	84
10	3	40	39	115
11	3	60	74	225

Static Gel Strength is critical in deciding upon the safety factor against unexpected shutdown in cementing job and static gel strength affects the hydrostatic pressure in the cement slurry. The trend observed here shows that with increasing temperature, the gel strength increases. The increase in gel strength indicates at the higher temperature the cement gels faster.

4.6) Area Under the Hysteresis Curve

The effect of polymer addition in oil well cement is studied for various percentages of the Polymer. In addition to that, the temperature effect on the Polymer is investigated to quantify the thixotropy.

Table 4-7 Area Under Hysteresis Loop For Different Slurries

Slurry Number	Pol% Added	Temperature	Hysteresis Area	A1/A
1	0	20	5162	1
2	0	40	10592	2.05
3	0	60	9506	1.84
4	1	20	5073	0.98
5	2	20	3873	0.75
6	3	20	3392	0.65
7	5	20	2037	0.39
8	1	40	5780	1.11
9	1	60	9074	1.75
10	3	40	8371	1.62
11	3	60	10389	2.01

The area of the hysteresis curve at room temperature is considered as 1. The ratio of another hysteresis area over room temperature is calculated. The ratio indicates microstructural changes occurring inside cement slurry with different additives at different temperatures. Cement hydration rate over regular cement can be quantified using the hysteresis area ratio.

i) Smart cement –In the case of smart cement subjected to a higher temperature, the ratio of hysteresis area at 40°C and 60°C over 20°C is 2.05 and 1.84.

ii) Smart Cement + Polymer percentage-In Table 6, slurry number 4, 5, 6 and 7 are prepared by 1%, 2%, 3% and 5% polymer, the ratio of hysteresis area over smart cement is 0.98, 0.75, 0.65 and 0.39 respectively.

iii) Smart Cement +Polymer+Temperaure -In table 4-6, for slurry number 8, 9, 10, 11, the ratio of individual hysteresis area over smart cement was 1.11, 1.75, 1.62 and 2.01, respectively.

The area under the up and down curve indicates structural build-up. As cement slurry start to hydrate, structural build up starts to occur, and the hysteresis area begins to grow up. In the case of cement slurry, with higher temperatures, the hysteresis area gets bigger, indicating that faster structure builds up occurs. Increase in the hysteresis area means more rapid structural build-up. When the Polymer is added into cement slurry, the hysteresis area shows a decreasing trend. The decreasing area indicates the slower structural build-up of the cement slurry when a polymer is added into it, however, with increasing temperature, the area under the hysteresis curve increases.

4.7) Summary

1) Temperature affects the hydration of neat cement slurry. Yield stress and maximum shear stress of cement slurries increased by increasing temperature. Vipulanandan Model predicted the model better than Bingham Plastic with low RMSE values.

2) The addition of Polymer into cement increased the yield stress and maximum shear stress as cement particles were replaced by polymer particulates. In this case, also, the Vipulanandan model predicted model points comparatively better than Bingham Plastic Model.

3) Cement slurry with 1% polymer behaved differently at 20^{o}C, 40^{o}C, and 60^{o}C.This is caused due to the behavior of the polymer at high temperatures. A similar trend was observed with cement slurry with 3% polymer subjected to high temperature. Vipulanandan Model showed better results compared with the Bingham Plastic Model.

4) The addition of cellulose into cement slurry had a super plasticizing effect. The yield stress of cement slurry reduced on the addition of cellulose. Based on Vipulanandan Model, the yield stress decreased by 8%, 27%, and 55% on addition of 0.014%, 0.28% and 0.042% of cellulose.

5) Cement slurries subjected to temperature effect showed an enhanced static gel strength over smart cement.

CHAPTER 5 EFFECT OF ADDITIVES ON SMART CEMENT

Introduction

In this chapter, smart cement is modified by using a retarder, fiber and gas control additive. In detail, the effect of each of the additive has been investigated on the smart cement physical properties. This chapter has been subdivided into three sub sections to highlight the effect of additive on smart cement. Although similar tests and procedures have been followed for quantifying the effect of additives, the materials, research methodology implemented, and models used has been included inside each sub chapter separately. The following subchapter under this subsection are as follows.

1) Effect of cellulose addition on smart cement on electrical resistivity, compressive strength, rheological properties, and piezoresistive behavior.
2) Characterizing smart cement modified by polypropylene fiber for curing, shrinkage control and piezoresistive Behavior using Vipulanandan Models.
3) Impact of Carboxylated Styrene Butadiene on Electrical and Mechanical Properties of Smart Cement.

Under each subchapter, there are specific objectives. Each additive modifies the smart cement physical properties to solve a definitive problem faced in oil well industry regarding cementing problems. The cellulose is used retard the cement setting time and the percentage cellulose addition is optimized to get desired compressive and piezoresistive behavior. Addition of polypropylene finer increases the cement toughness and reduced the shrinkage.

5.1) Effect of cellulose addition on smart cement on electrical resistivity, compressive strength and piezoresistive behavior.

On smart cement, cellulose is added. The cellulose percentage is optimized to optimum effect of cellulose in cement. The effect of cellulose on the setting time and mechanical properties is evaluated. The material behavior is characterized using electrical resistivity.

5.1.2) Electrical Resistivity

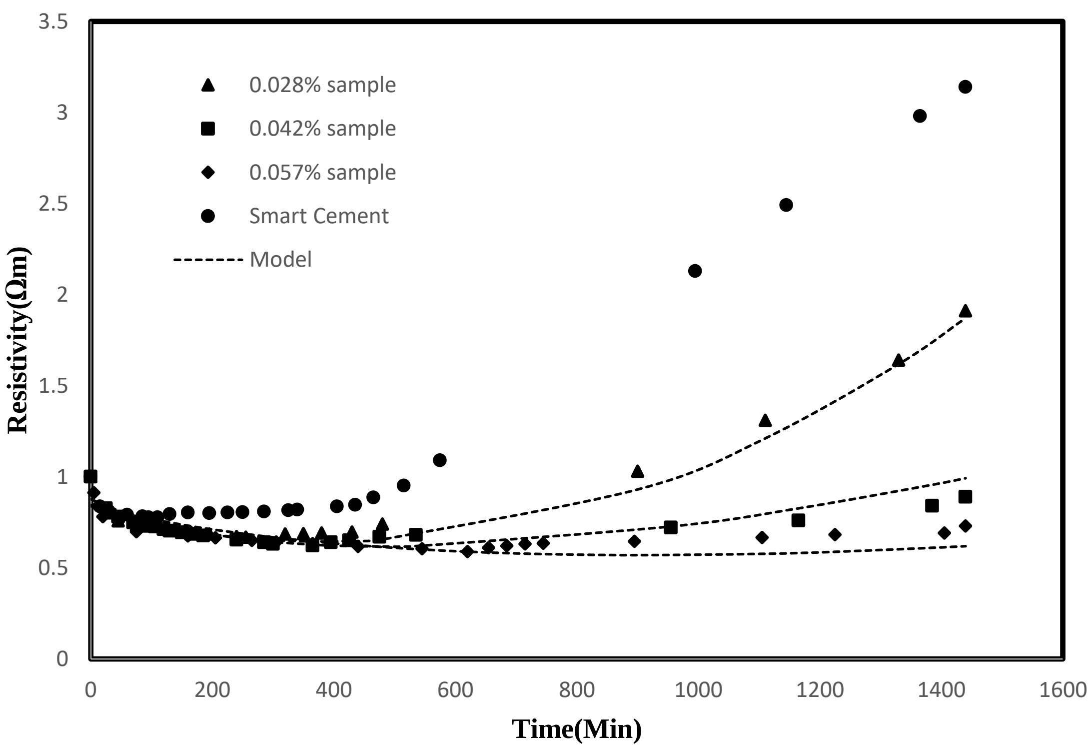

Figure 5-1 One Day Curing of smart cement

Table 5-1 Electrical Resistivity parameters of the smart Cement with Additives.

% Additive	ρ_0	ρ_{min}	t_{min}	ρ_{24}	P1	Q2	t_O	R^2	RMSE	RI_{24h} (%)
0	1.0	.78	90	3.23	0.61	0.42	215.63	0.99	0.19	314.1
0.028%	.99	.67	255	1.89	0.44	0.14	572.45	0.99	0.25	182.09
0.042%	.99	.62	425	.85	0.57	0.31	459.51	0.99	0.15	37.10
0.057%	.99	.58	655	.70	0.44	0.19	886.78	0.99	0.16	20.69

1 Day Resistivity Development

Cement resistivity change is monitored from the preparation stage to hardened stage. As cement hydrates, the resistivity of the material changes. By measuring the electrical resistivity at short interval, the effect of admixtures on cement hydration can be identified. The resistivity development is modelled using equation (3-2) with p1, q1and to as model parameters.

i) Smart Cement- Initial, minimum, and one-day resistivity of the specimen were 1Ωm, 0.78Ωm and 3.23Ωm. Minimum resistivity is noted after 90 min. with (.61,0.42 and 215.63) as model parameters.

ii) Smart Cement +0.028% BWOC- Initial, minimum, and one-day resistivity of the specimen were 1Ωm, 0.67Ωm and 1.89Ωm. Minimum resistivity is noted after 255min. with (0.44,0.14 and 572.45) as model parameters.

iii) Smart Cement +0.042% BWOC- Initial, minimum, and one-day resistivity of the specimen were 1Ωm, 0.58Ωm and 0.85Ωm. Minimum resistivity is noted after 425 min. with (0.57,0.31 and 459.51) as model parameters.

iv) Smart Cement+ 0.056% BWOC- Initial, minimum, and one-day resistivity of the specimen were 1Ωm, 0.78Ωm and 0.70 Ωm. Minimum resistivity is noted after 655min. with (0.44,0.19 and 886.78) as model parameters.

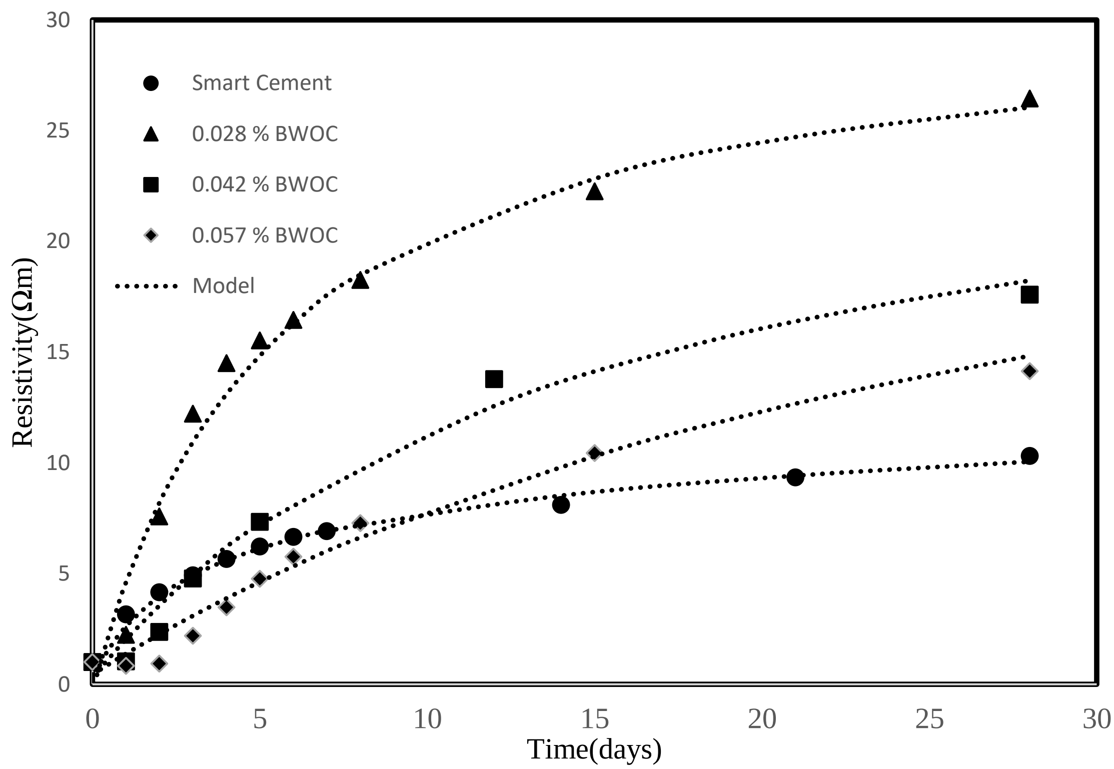

Figure 5-2 Development of Electrical Resistivity of Smart cement composite during 28 days of curing.

28 Long Term Resistivity

In Figure 5-2, the long-term resistivity development of smart cement specimens with and without cellulose is modeled using the equation (3-2) with experimental data.

i) Smart Cement- The resistivity after 28 days is 10.3 Ωm The model parameters as per equation are (0.23, 0.62, 0.001)

ii) Smart Cement +0.028% BWOC- The resistivity after 28 days is 14.14 Ωm. The model parameters as per equation (3-2) are (0.31, 0.68, 0.0001)

iii) Smart Cement +0.042% BWOC- The resistivity after 28 days is 17.58 Ωm. The model parameters as per equation (3-2) are (0.19, 0.31, 0.07)

iv) Smart Cement+ 0.056% BWOC- The resistivity after 28 days is 24.51 Ωm. The model parameters as per equation are (3-2) are (0.20, 0.27, 0.02)

Table 5-2 Model Parameters of P-q Model for evaluating the electrical resistivity of smart cement composites during 28 days of curing.

Additive Content	Initial Resistivity	p1	q1	to	$\rho_{28}(\Omega m)$	R^2	RMSE
0	1.00	0.23	0.62	.001	10.90	.99	0.18
0.028%	.99	0.31	0.68	0.0001	14.14	.94	2.34
0.042%	.99	0.19	0.31	0.07	17.58	.98	1.16
0.057%	.99	0.20	0.27	0.02	24.51	.98	0.71

5.1.3) Cement Setting Time

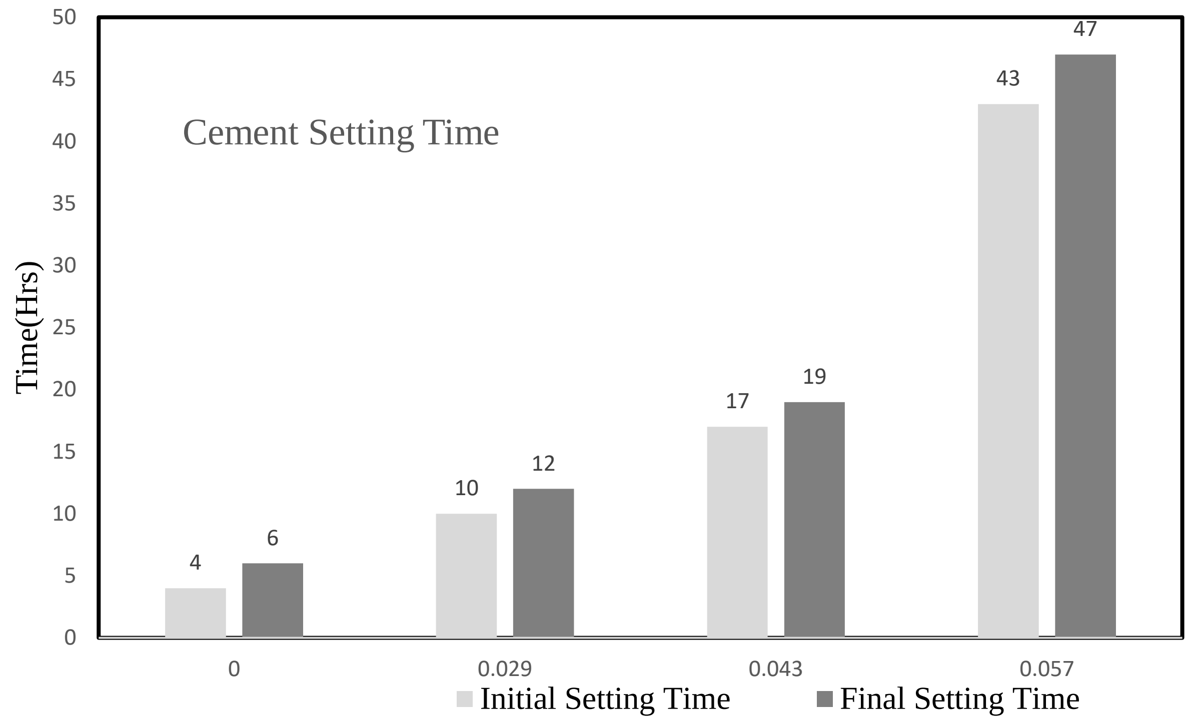

Figure 5-3 Setting Time of Cement Measured by Vicat needle

Using Vicat needle, the setting time of smart cement without and with cellulose is determined.

i) Smart Cement- Initial and Final setting time of smart cement from Vicat needle test was 4 hours and 6 hours, respectively. The corresponding resistivity at the initial and final setting was 1 Ωm and 1.25 Ωm.

ii) Smart Cement +0.028% BWOC- Initial and Final setting time of smart cement with 0.028% BWOC was 10 hours and 12 hours, respectively. The corresponding resistivity at the initial and final setting was 1.13 Ωm and 1.19 Ωm correspondingly.

iii) Smart Cement +0.042% BWOC- Initial and Final setting time of smart cement with 0.042% BWOC was 17 hours and 19 hour, respectively. The corresponding resistivity at the initial and final setting was 1.19 Ωm and 1.27 Ωm correspondingly.

iv) Smart Cement 0.056% BWOC- Initial and Final setting time of smart cement with 0.056% BWOC was 43 hours and 47 hours, respectively. The corresponding resistivity at the initial and final setting was 1.09 Ωm and 1.15 Ωm correspondingly.

5.1.4) Heat of hydration of cement

Hydration of the cement is divided into five periods -pre-induction, induction, acceleration, deceleration, and diffusion. The heat of the hydration curve provides or gives details, how fast the components inside cement are reacting. From the temperature evolution curve, following observation are found on smart cement and cement modified with cellulose. Rate of heat of evolution help to understand the chemical reaction involved in cement hydration.

i) Smart Cement – The peak rate of heat evolution was observed after 700mins from the initial point.

ii) Smart Cement +0.014% Additive- The peak rate of heat evolution was observed at 1444 mins from the start of mixing. Peak time was delayed by 97%compared with smart cement.

iii) Smart Cement +0.028% Additive- The peak rate of heat evolution was observed at 1700 mins from the start of mixing. Peak time was delayed by 133% compared with smart cement.

iv) Smart Cement +0.054% Additive- The peak rate of heat evolution was observed at 1954 mins from the start of mixing. Peak time was delayed by 166%compared with smart cement.

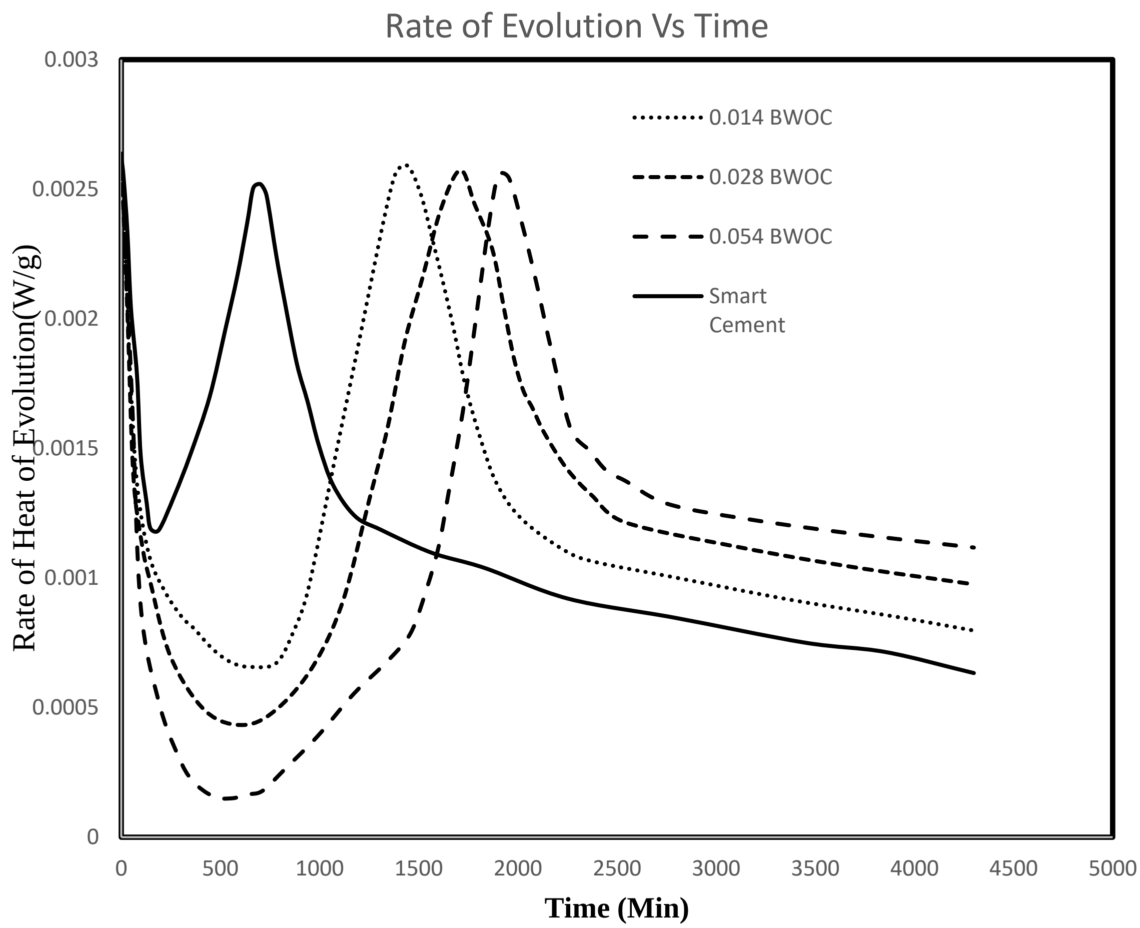

Figure 5-4 Heat Evolution Curve of Smart Cement without and with Additive.

5.1.5) Compressive Strength of Cement

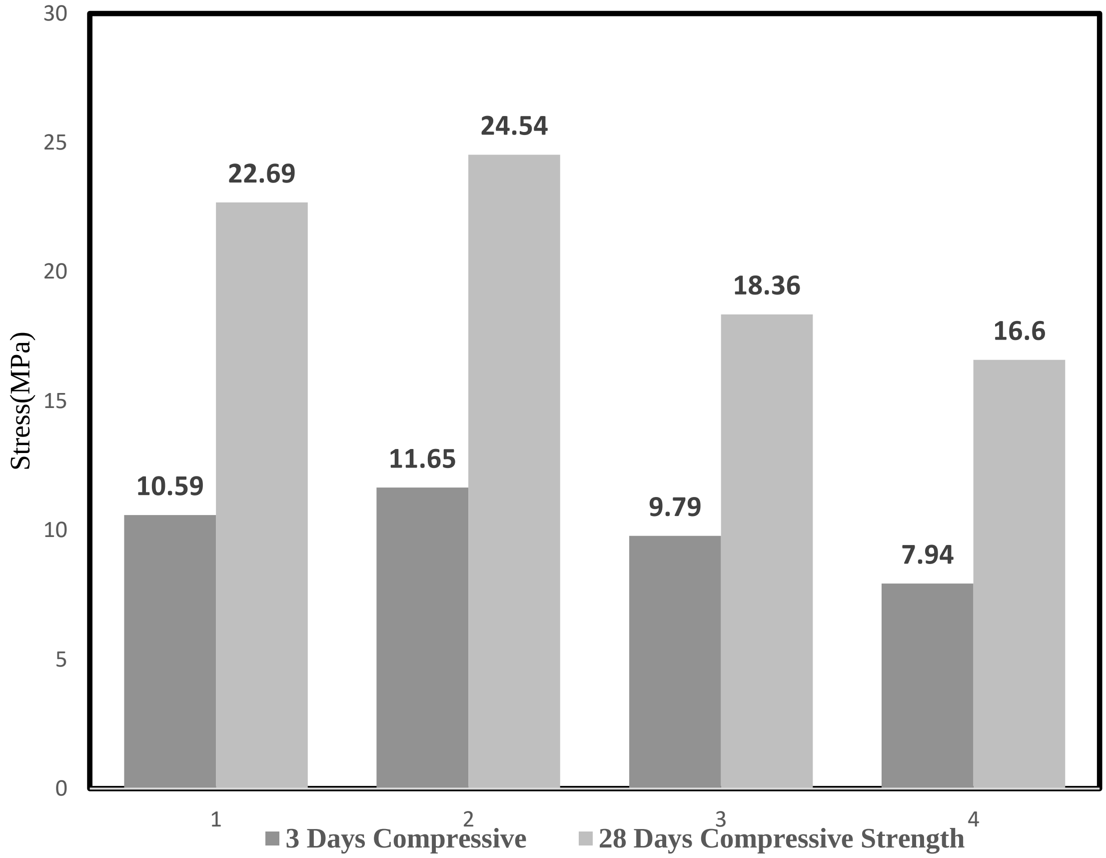

Figure 5-5 Compressive Strength of Cement Composites after 3 days and 28 days.

Compressive test of the specimens was done after 3 days and 28 days of curing.

i) Smart Cement – After 3 days and 28 days, the compressive stress of the specimen was 10.59MPa and 22.69MPa correspondingly.

ii) Smart Cement +0.028% BWOC- After 3 days and 28 days, the compressive strength was 24.54 MPa and 11.65MPa with a 10%, 8% increment over smart cement, respectively.

iii) Smart Cement +0.042% BWOC- After 3 days and 28 days, the compressive strength were 18.36MPa and 9.79MPa with a -7%, -19% reduction over smart cement, respectively

iv) Smart Cement +0.056% BWOC- After 3 days and 28 days, the compressive strength were 16.6MPa and 7.94MPa with a -25%, -26% decrement over smart cement, respectively.

5.1.6) Piezoresistive Behavior of Cement

Piezo resistivity tests were done on samples cured for 3 days and 28 days. The change in resistivity and stress was modeled as per the equation (3-11).

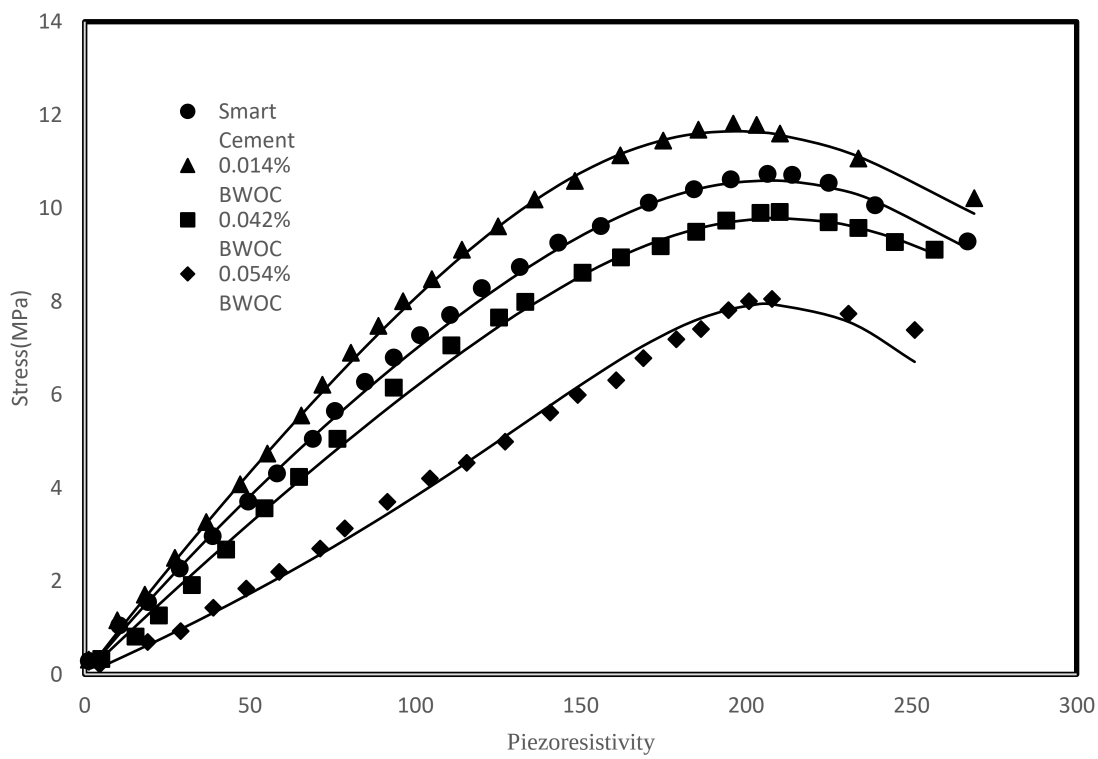

Figure 5-6 Piezoresistive Behavior of 3 Day Cured Specimen.

Table 5-3 Piezoresistive Behavior of cellulose modified smart cement

Smart Cement	P_2	Q_2	R^2	Compressive Strength (MPA)	Ultimate Piezo resistivity	RMSE (MPA)
3 Days Curing						
0	.60	.133	.99	10.59	203	.10
0.028%	.64	.21	.99	11.7	196	.12
0.042%	.68	.17	.99	9.79	210	.15
0.057%	1.20	.226	.99	7.94	209	.23
28 Days Curing						
0	1.05	.25	.99	22.69	193	.32
0.028%	1.03	.11	.99	24.54	170	.59
0.042%	.90	.17	.99	18.34	186	.15
0.057%	1.10	.34	.99	16.61	166	.21

In table 5-3, the summary of the piezoresistive parameters is presented with for different percentages of cellulose addition.The model parameters of the equation 3-11,is provided.

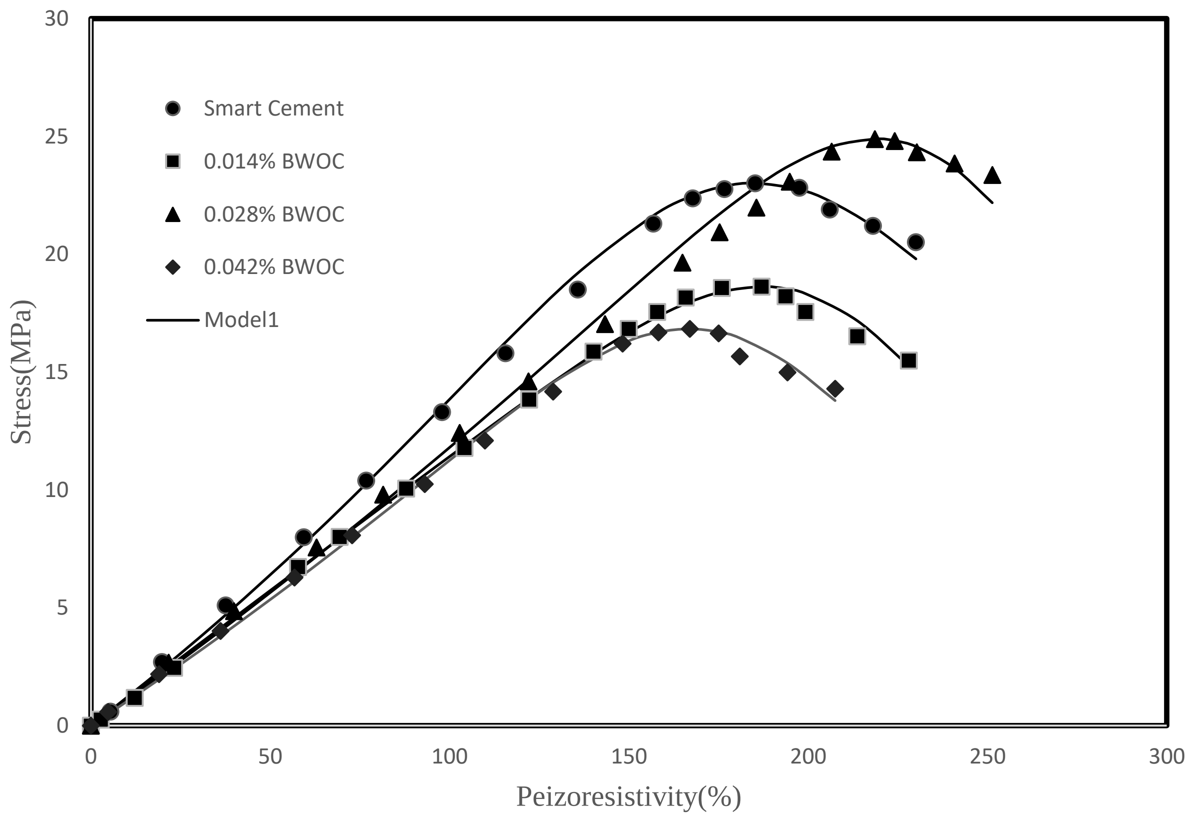

Figure 5-7 Piezoresistive Behavior of 28 Day Cured Specimen.

Piezo resistivity tests were done on samples cured for 3 days and 28 days. The change in resistivity and stress was modeled as per the equation

i) Smart Cement – The Piezo resistivity of smart cement cured after 3 days and 28 days at peak stress of 10.59 MPa and 22.69MPa were 203% and 193% respectively. The model parameters of the equation (3-11), p2 and q2 for 3days and 28 days curing were (0.60, 0.133) and (1.05, 0.25), respectively.

ii) Smart Cement +0.028% – The Piezo resistivity of smart cement cured after 3 days and 28 days at peak stress of 10.59 MPa and 22.69MPa were 203% and 193%, respectively. The model parameters of the equation (3-11), p2 and q2 for 3days and 28 days curing are (0.64, 0.21) and (1.03, 0.11), respectively.

iii) Smart Cement +0.042%– The Piezo resistivity of smart cement cured after 3 days and 28 days at peak stress of 10.59 MPa and 22.69MPa were 203% and 193%, respectively. The model parameters of the equation (3-11), p2 and q2 for 3days and 28 days curing are (0.68,0.17) and (.90,.17), respectively.

iv) Smart Cement +0.057%-The Piezo resistivity of smart cement cured after 3 days and 28 days at peak stress of 10.59 MPa and 22.69MPa were 203% and 193%, respectively. The model parameters of the equation (3-11), p2 and q2 for 3days and 28 days curing are (1.20,0.226) and (1.10,0.34) respectively.

5.2) Characterizing SMART CEMENT modified by polypropylene fiber for Curing, shrinkage control and piezoresistive Behavior using Vipulanandan Models.

The overall objective is to investigate the effects of adding polypropylene fiber into oil well cement. The specific aim is as follows.

1) Effect of polypropylene fiber on the electrical properties of smart cement

2) Effect of polypropylene addition on cement shrinkage compressive stress and tensile stress.

3) Modeling the curing, piezoresistive behavior and strength changes with curing time

5.2.1) Density and Resistivity.

Smart Cement- Initial resistivity and density of smart cement were 1Ωm and 1.96 g/cc.Addition of 0.14% fiber reduced the density to 1.92g/cc and increased the resistivity to 1. 03Ωm.Addition of 0.28% fiber reduced the density to 1.88g/cc and increased the resistivity to 1.09Ωm.

5.2.2) Short Term and Long-Term Electrical Resistivity Development.

One Day Curing of Cement – The cement was allowed to cure for one day, and the change in resistivity is measured. The resistivity change shows the interaction of the additive the Class H cement.

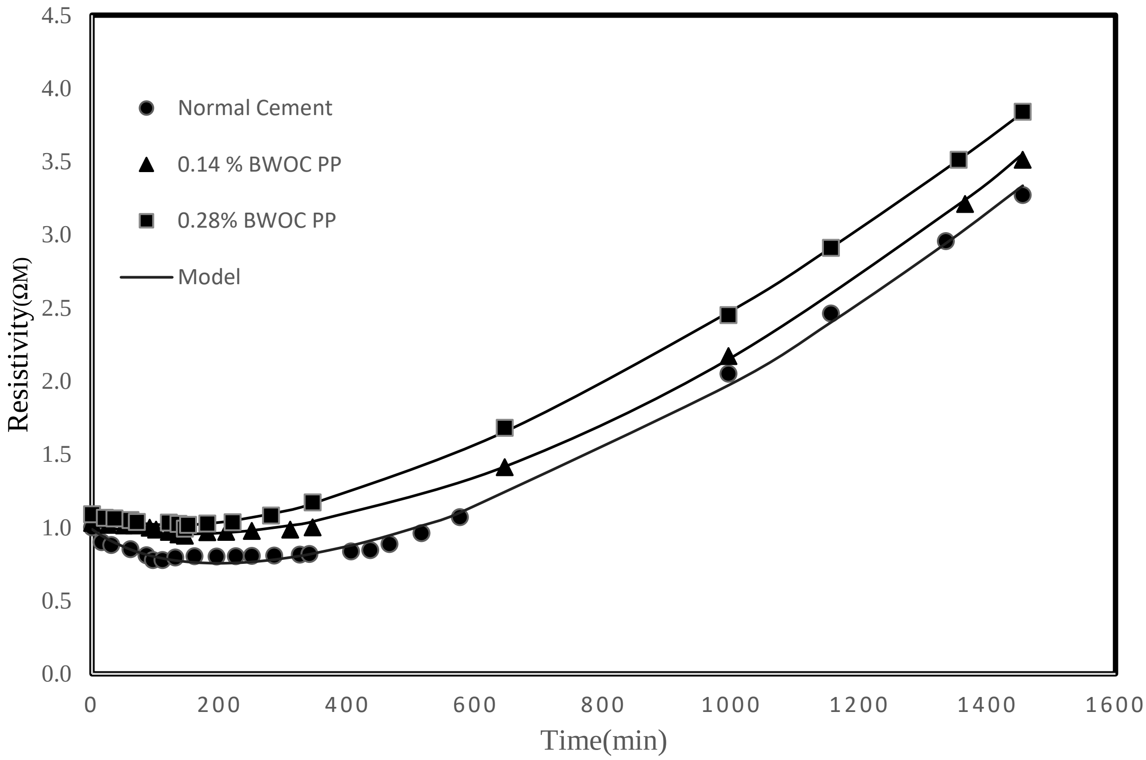

Figure 5-8 One Day Curing of Smart Cement

Table 5-4 Summary of Resistivity Parameters for One Day.

	ρ_{ini}	ρ_{min}	t_{min}	ρ_{24}	p 1	q 1	t 0	R^2	RMSE
Smart Cement	1.0	.78	95	3.27	.30	.21	204.40	.99	0.15
.14% (BWOC)	1.03	.94	130	3.51	.59	.38	264.45	.99	0.14
.28% (BWOC)	1.09	.99	145	3.84	.63	.41	269.51	.99	0.16

1 Day Resistivity Development

Cement resistivity change is monitored from the preparation stage to the hardened stage. As cement hydrates, the resistivity of the material changes. By measuring the electrical resistivity at a short interval, the effect of admixtures on cement hydration can be identified. The resistivity development is modelled using equation (3-2) with p1,q1and to as model parameters.

i. Smart Cement- Initial, minimum, and one-day resistivity of the specimen were 1Ωm, 0.78Ωm, and 3.27 Ωm. Minimum resistivity is noted after 90 min with 0.30, 0.21, 201.41 as model parameters.
ii. Smart Cement +0.028% BWOC- Initial, minimum, and one-day resistivity of the specimen were 1.03Ωm, 0.94 Ωm and 3.51 Ωm. Minimum resistivity is noted after 130min with 0.59, 0.38 and 264.45 as model parameters.
iii. Smart Cement +0.042% BWOC- Initial, minimum, and one-day resistivity of the specimen were 1.09Ωm, 0.99 Ωm and 3.84 Ωm. Minimum resistivity is noted after 145 min with 0.63, 0.41 and 459.51 as model parameters.

28 Days Resistivity Development

The resistivity of the samples was monitored inside and outside the mold. Two set of samples were made, after one day curing one set of samples was demolded and cured in room temperature.

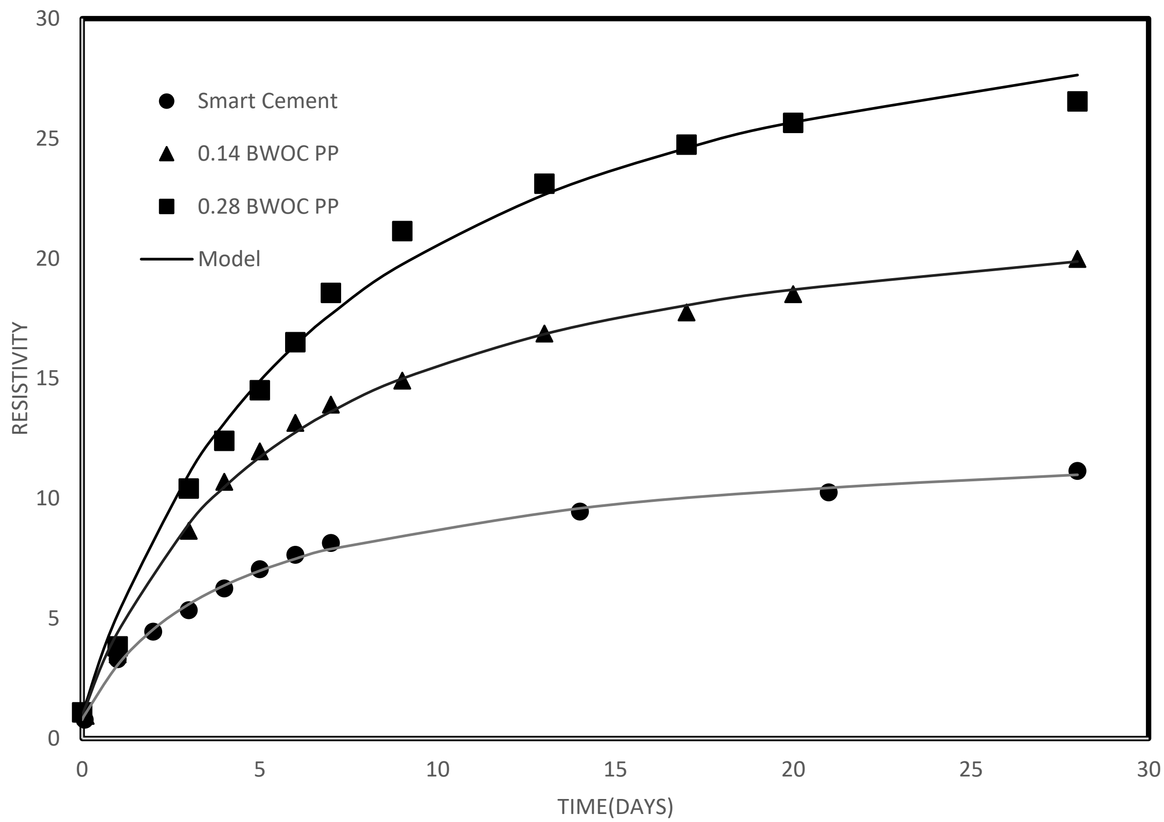

Figure 5-9 Electrical Resistivity Development due to long-term curing (28 days).

Two sets of samples were prepared. One set of samples was cured inside the mold, and another set of samples were cured in open air. To show the effect of fibers to control shrinkage, samples were cured in open air.

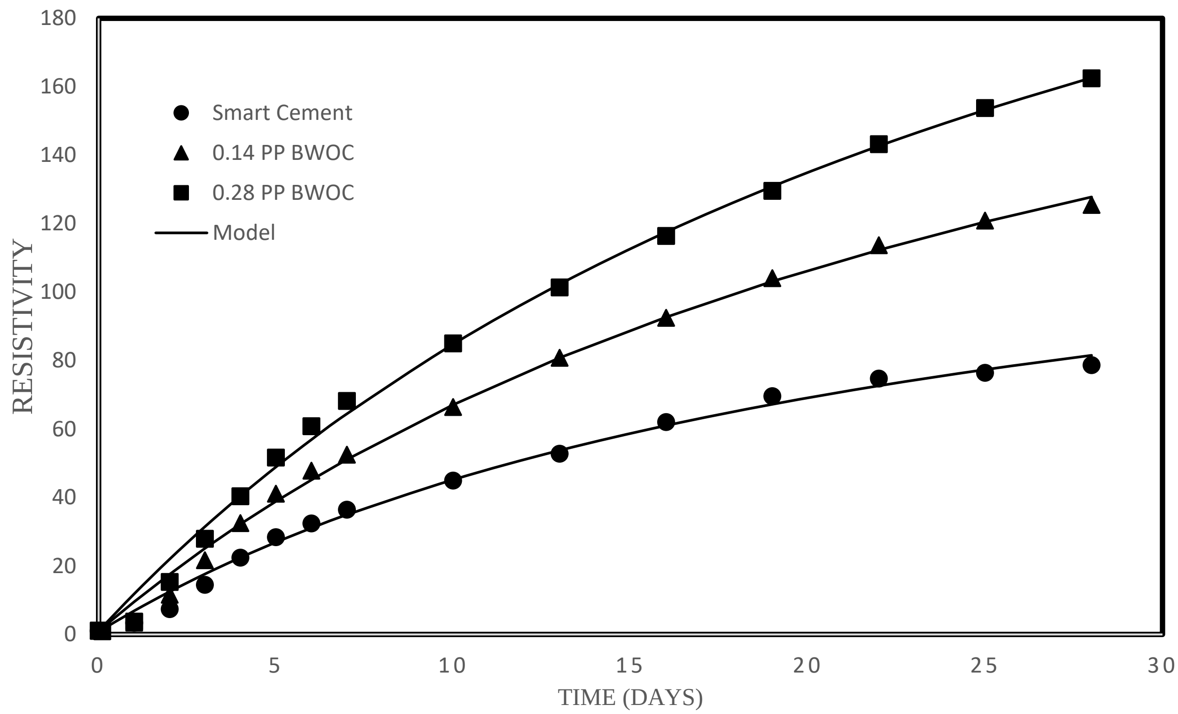

Figure 5-10 Electrical Resistivity Development due long-term curing (Outside Mold)

Table 5-5 Model Parameters for Curing Model of Cement cured Inside Mold and Outside Mold.

	ρ (28)	p2	q2	to	ρ (ini)	R^2	RMSE
Curing Inside Mold							
Smart Cement	10.90	0.23	0.62	.001	1.00	.99	.34
.14% (BWOC)	19.87	0.26	0.63	.001	1.03	.99	.74
.28% (BWOC)	26.45	0.27	0.64	.001	1.09	.99	.18
Open Air Curing							
Smart Cement	81.56	.23	.33	.002	1.0	.99	2.18
.14% (BWOC)	125.66	.25	.35	.002	1.03	.99	2.61
.28% (BWOC)	162.45	.26	.37	.002	1.09	.99	3.19

Long Term Resistivity (Samples Cured Inside Mold)

In Figure 5-4, the long-term resistivity development of samples cured inside mold with and without fiber is modeled using the equation (3-2) with experimental data.

i. Smart Cement- The resistivity after 28 days was 10.90Ωm. The model parameters p2, q2, and to as per equation were 0.23, 0.62 and 0.001, respectively.
ii. Smart Cement +0.14% BWOC- The resistivity of the specimen after 28 days was 19.87Ωm, increased by 54%over smart cement. The model parameters p2, q2 and to as per equation were 0.23, 0.63 and 0.001, respectively.
iii. Smart Cement +0.28% BWOC- The resistivity specimen after 28 days was 26.45Ωm, increased by 98%over smart cement. The model parameters p2, q2, and to as per equation were 0.27, 0.64 and 0.001, respectively.

Long Term Resistivity (Samples Cured Outside Mold)

In Figure 5-5, the long-term resistivity development of samples cured outside with and without fiber is modeled using the equation (3-2) with experimental data.

i. Smart Cement- The resistivity after 28 days was 81.56Ωm. The model parameters p2 and q2 as per equation were 0.23,0.33 and 0.002, respectively.
ii. Smart Cement +0.14% BWOC- The resistivity of the specimen after 28 days was 125.66Ωm, increased 54% over smart cement. The model parameters p2, q2, and to as per equation are 0.25, 0.35 and 0.001, respectively.
iii. Smart Cement +0.28% BWOC- The resistivity of the specimen after 28 days was 162.45Ωm, increased by 98% over smart cement. The model parameters p2, q2 and to as per equation are 0.26, 0.37 and 0.002, respectively.

5.2.3) Volumetric Shrinkage and Resistivity Model

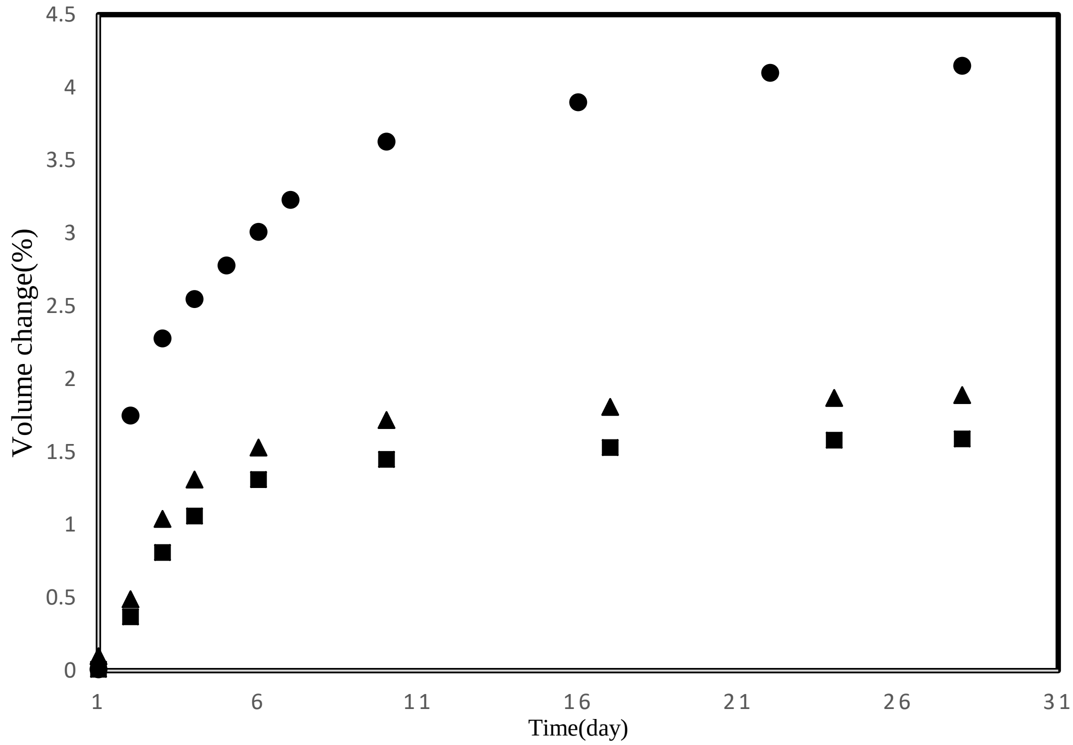

Figure 5-11 Long Term Shrinkage of Smart Cement with and without fibers.

To measure the linear shrinkage and volumetric shrinkage, samples were demolded and allowed to cure in open conditions. Under open conditions, cement samples volume decreased due to shrinkage, and resistivity increased due to the hydration of cement and moisture loss. The change in volume is recorded at every stage of curing. After 28 days of curing the maximum volume loss observed for smart cement, PSC1 and PSC1 were 4.1%, 1.6% and 1.3%, respectively. The addition of polypropylene fibers significantly reduced the volumetric shrinkage of cement.

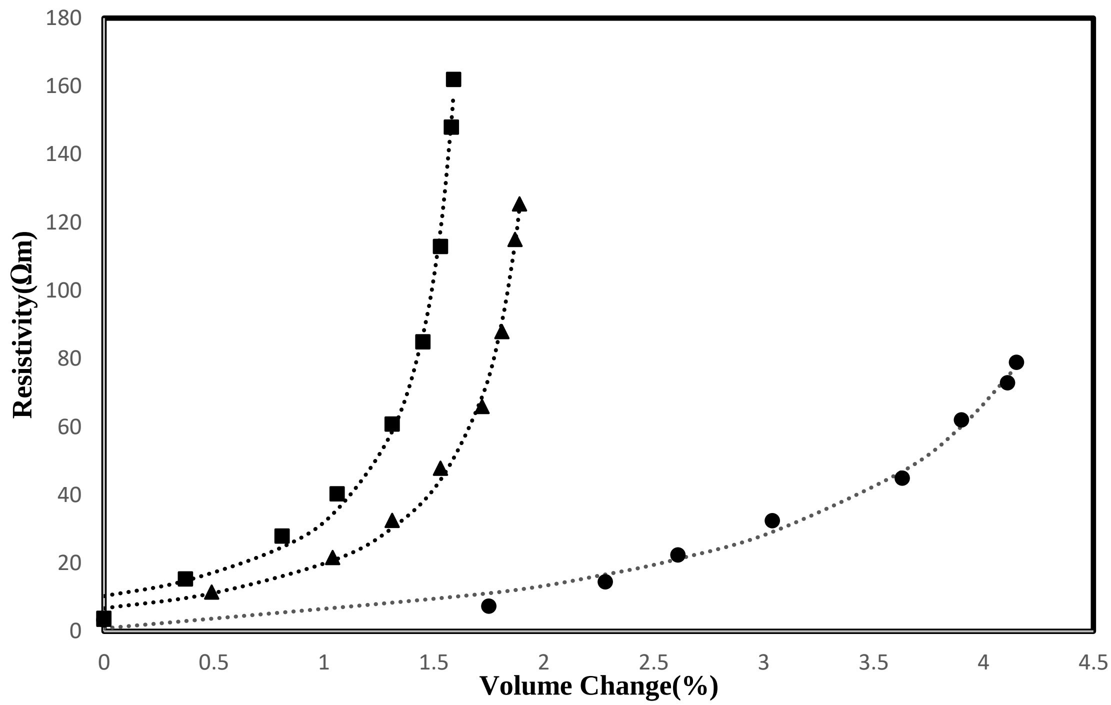

Figure 5-12 Change of Resistivity of cement samples Vs. Resistivity

Table 5-6 Model Parameters for Resistivity Change due to Volume Change.

	A(Ωm)	B	C	R^2	RMSE
Smart Cement	0.87	0.25	-0.014	.99	2.32
0.14 BWOC	6.71	0.14	-0.068	.99	3.67
0.28 BWOC	10.3	0.10	-0.058	.99	2.28

Under open condition, the cement maximum moisture loss occur in the cement specimens, and this also led to volumetric shrinkage in cement. Cement shrinkage and resistivity change are modeled using equation (3-4).

5.2.4) Stress-Strain Behavior of Samples.

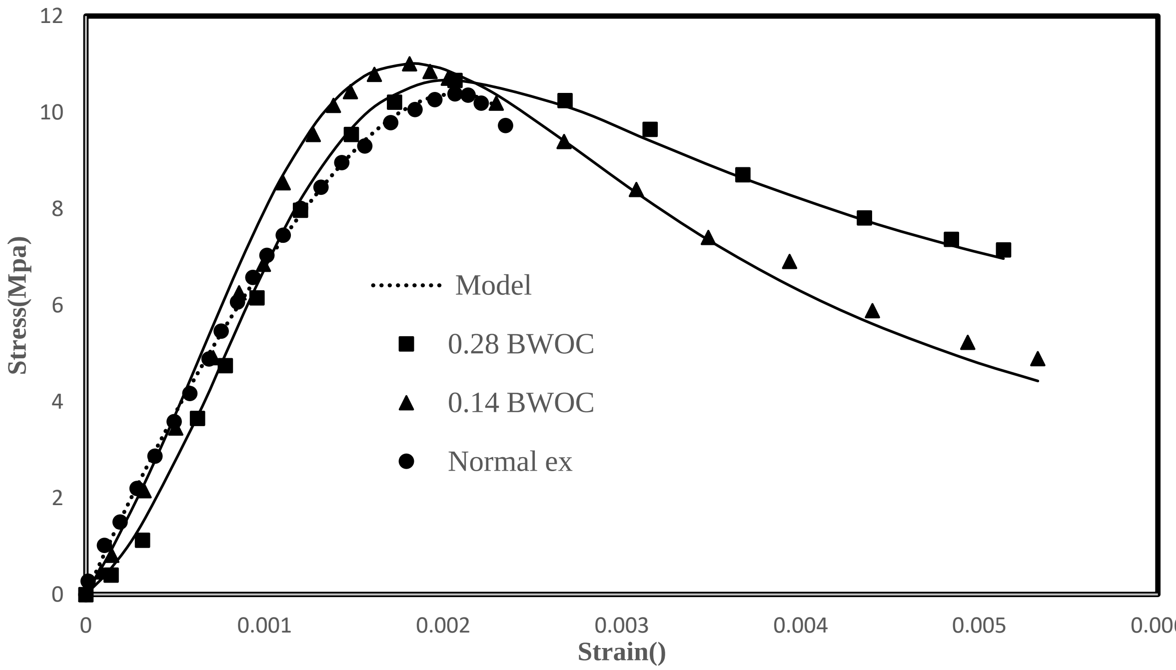

Figure 5-13 Compressive Stress -strain Curve for 1 One day cured specimen.

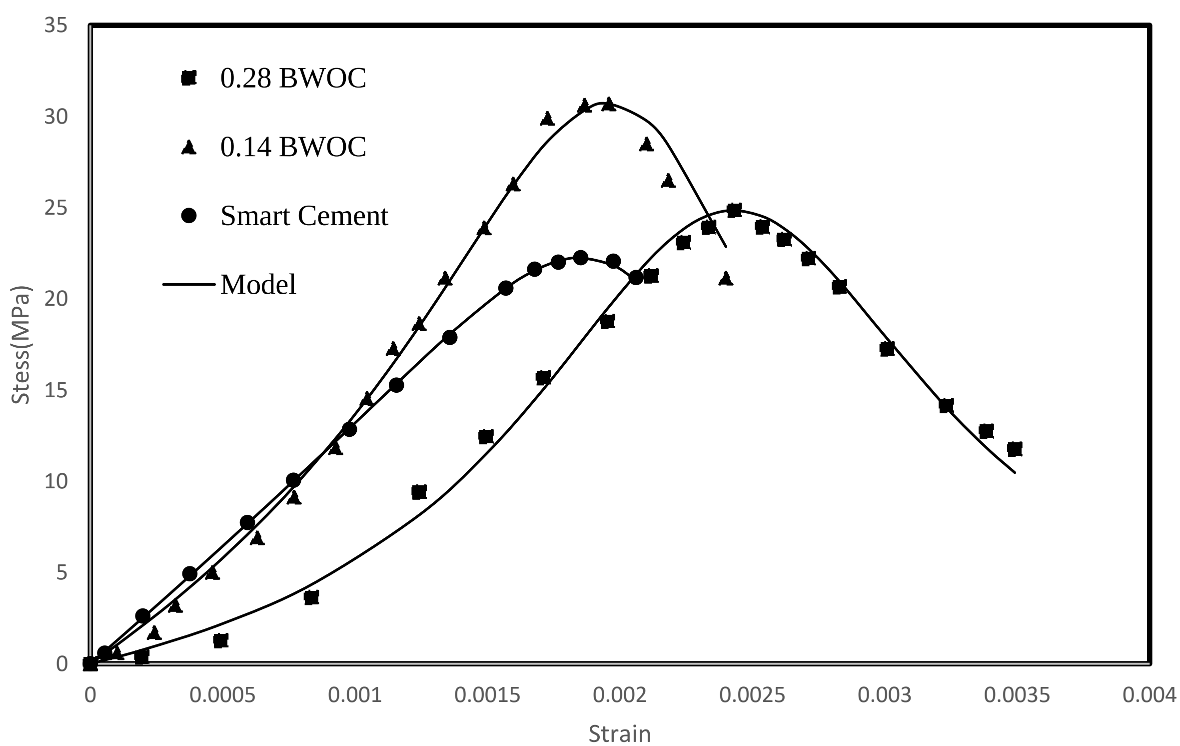

Figure 5-14 Compressive Stress -strain Curve for 28 day cured specimen.

Table 5-7 Compressive Behavior polypropylene modified smart cement

	p3	q3	R^2	Max (MPa)	RMSE (MPa)	Failure Strain	Resilience Modulus	Toughness Modulus
1 Day								
Smart Cement	.55	.07	.99	10.38	.115	0.0020	6.30	1.55
.14% (BWOC)	.64	.35	.99	10.66	.98	0.0019	5.53	13.16
.28% (BWOC)	.59	.40	.99	11.01	.91	0.0020	5.79	14.78
28 Days								
Smart Cement	.90	.09	.99	22.25	0.105	0.0019	12.03	2.46
.14% (BWOC)	2.1	.43	.99	30.24	1.51	0.0021	14.48	3.85
.28% (BWOC)	1.5	.20	.99	24.65	1.34	0.0024	10.30	10.29

The stress-strain curve obtained for the cement mixes is plotted in Figure 5-6 and Figure 5-7. Using the p-q model proposed by Vipulanandan, the stress-strain curve of smart cement, smart cement with 0.14%, and 0.28% of polypropylene fiber cement specimens were modeled. The stress-strain curve obtained for the cement mixes were of a second-degree parabola with vertex as peak stress. The slope of the ascending and descending branches of the curve depended on the volume of fiber added into the cement.

i. Smart cement – Compressive strength and failure strain of smart cement after 1 day and 28 days of curing were 10.38MPa, 0.0020 and 22.25MPa, 0.0019, respectively. The resilience modulus and toughness modulus of the specimen were 6.30, 1.55 and 12.03, 2.46 after 1 day and 28 days of testing. The model parameter obtained from using equation (3-10), were 0.55, 0.07 and 0.90, 0.07 after 1day and 28 days of curing, respectively.

ii. Smart cement + 0.14% fiber – Compressive strength and failure strain of smart cement with 0.14% fiber after 1 day and 28 days of curing were 10.66MPa, 0.0019, and 30.24 MPa, 0.0021 respectively. An increase of 2.7%, 36% in compressive strength, is found over smart cement after 1 and 28 days of curing. The resilience modulus and toughness modulus of the specimen were 5.53, 13.16 and 14.48, 3.85 after 1 day and 28 days of testing. The model parameter from using the equation (3-10), were 0.64, 0.35 and 2.1, 0.43 after 1 day and 28 days of testing.

iii. Smart cement + 0.28% fiber – Compressive strength and failure strain of smart cement with 0.28% fiber after 1 day and 28 days of curing were 11.01MPa, 0.0020 and 24.65MPa, 0.0024, respectively. An increase of 6%,19%in compressive strength, is found over smart cement after 1 and 28 days of curing. The resilience modulus and toughness modulus of the specimen were 5.79, 14.78 and 10.30,10.29 after 1 day and 28 days of testing. The model parameter from using the equation (3-10), were 0.59, 0.40 and 1.51, 0.20 after 1 day and 28 days of testing, respectively.

5.2.5) Piezoresistive behavior of Cement

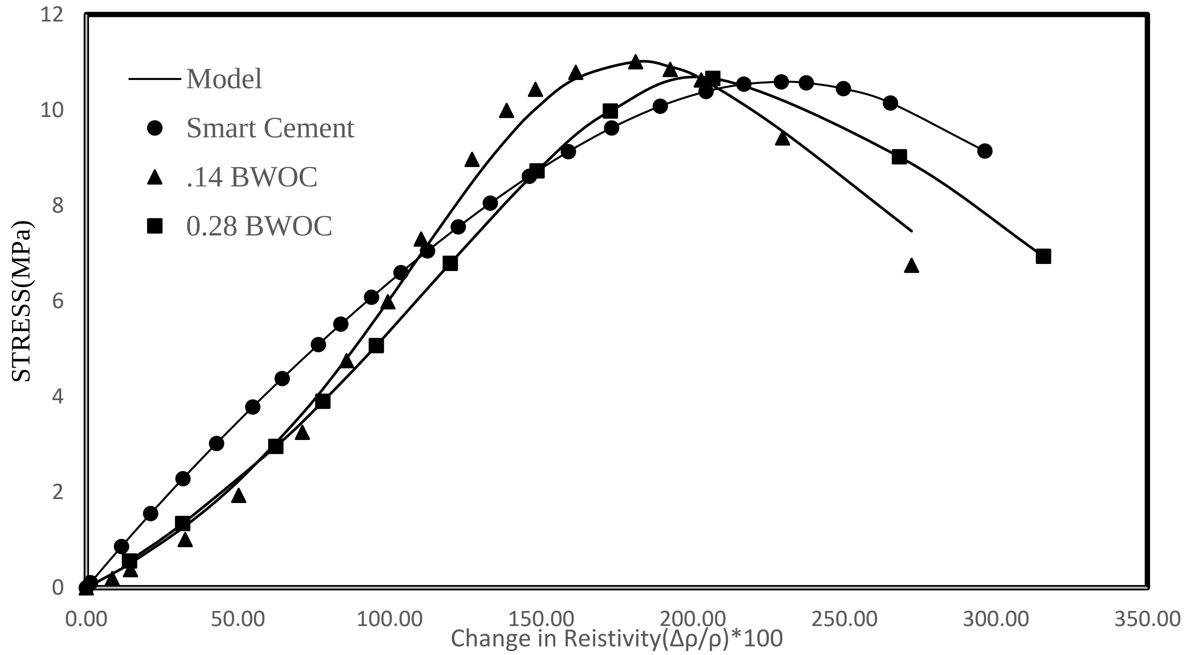

Figure 5-15 Piezoresistive Behavior of 1 Day Cured Specimen.

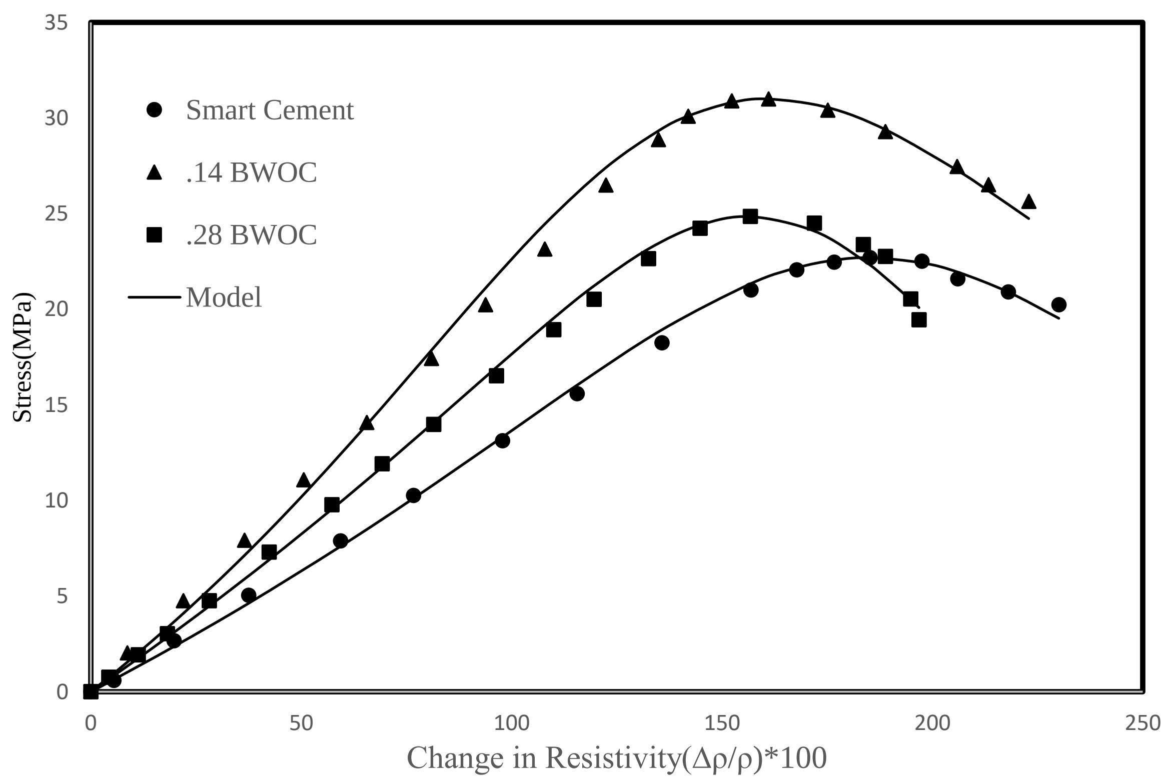

Figure 5-16 Piezoresistive Behavior of 28 Day Cured Specimen.

Table 5-8 Piezo resistivity Model Parameters for the Smart cement with and without fibers.

	Compressive Stress (MPa)	Ultimate Piezo resistivity	p4	q4	R^2	RMSE
Smart Cement	10.38	229	0.57	0.07	.99	
.14% (BWOC)	10.66	181	0.75	0.16	.99	.343
.28% (BWOC)	11.01	179	0.76	0.17	.99	.367
28 Days Curing						
Smart Cement	22.25	185	0.72	0.18	.98	.32
.14% (BWOC)	30.24	161	0.86	0.13	.99	.68
.28% (BWOC)	24.65	156	0.80	0.19	.99	1.18

i) Smart Cement – The Piezo resistivity of smart cement cured after 1 day and 28 days at peak stress of 10.59MPa and 22.69MPa were 203% and 193%, respectively. The model parameters of the equation (3-11), p2 and q2 after 1 day and 28 days of the test were 0.57, 0.07 and 0.72, 0.18, respectively.

ii) Smart cement + 0.14% fiber – The Piezo resistivity of smart cement cured after 1 day and 28 days at peak stress of 10.59 MPa and 22.69MPa were 229% and 185%, respectively. The model parameters of the equation (3-11), p2 and q2 after 1 day and 28 days of the test were 0.75, 0.16 and 0.86, 0.13, respectively.

iii) Smart cement + 0.28% fiber – The Piezo resistivity of smart cement cured after 1 day and 28 days at peak stress of 10.59 MPa and 22.69MPa were 181% and 161%, respectively. The model parameters of the equation (3-11), p2 and q2 for 3days and 28 days curing are 0.76, 0.17 and 0.80, 0.19 respectively.

5.3) Impact of Carboxylated Styrene Butadiene on Electrical and Mechanical Properties of Smart Cement.

Overall objective is to investigate the effects of adding XSBR to oil well cement. The specific objective are as follows.

1) Characterize the electrical resistivity of smart cement with and without polymer. Quantify the effect of cement hydration on the resistivity of specimen for one day and 28 days of curing.
2) Investigate the effect of polymer addition on the compressive strength of smart cement with and without polymer after one day and 28 days of curing.
3) Quantify the effect of polymer addition on the fluid loss behavior of cement with and without polymer using API fluid loss model and Vipulanandan Model.
4) The effect of polymer addition on compressive strength, piezoresistive behavior is investigated. Using Vipulanandan Piezoresistive model, the piezo resistivity is investigated.

5.3.1) Materials

To characterize the material, their initial density and resistivity is measured. The density and resistivity of polymer used was Initial resistivity and density of smart cement were 1Ωm and 1.96 g/cc. Addition of 1% polymer reduced the density to 1.89g/cc and increased the resistivity to 1.05Ωm. Addition of 3% polymer reduced the density to 1.79g/cc and increased the resistivity to 1.11Ωm. Addition of 5% polymer reduced the density to 1.74g/cc and increased the resistivity to 1.23Ω polymer addition replaces the cement particles for a specific volume and makes it lighter. This leads to a reduced density with addition of polymer.

5.3.2) Short Term and Long-term electrical resistivity Development.

One Day Resistivity

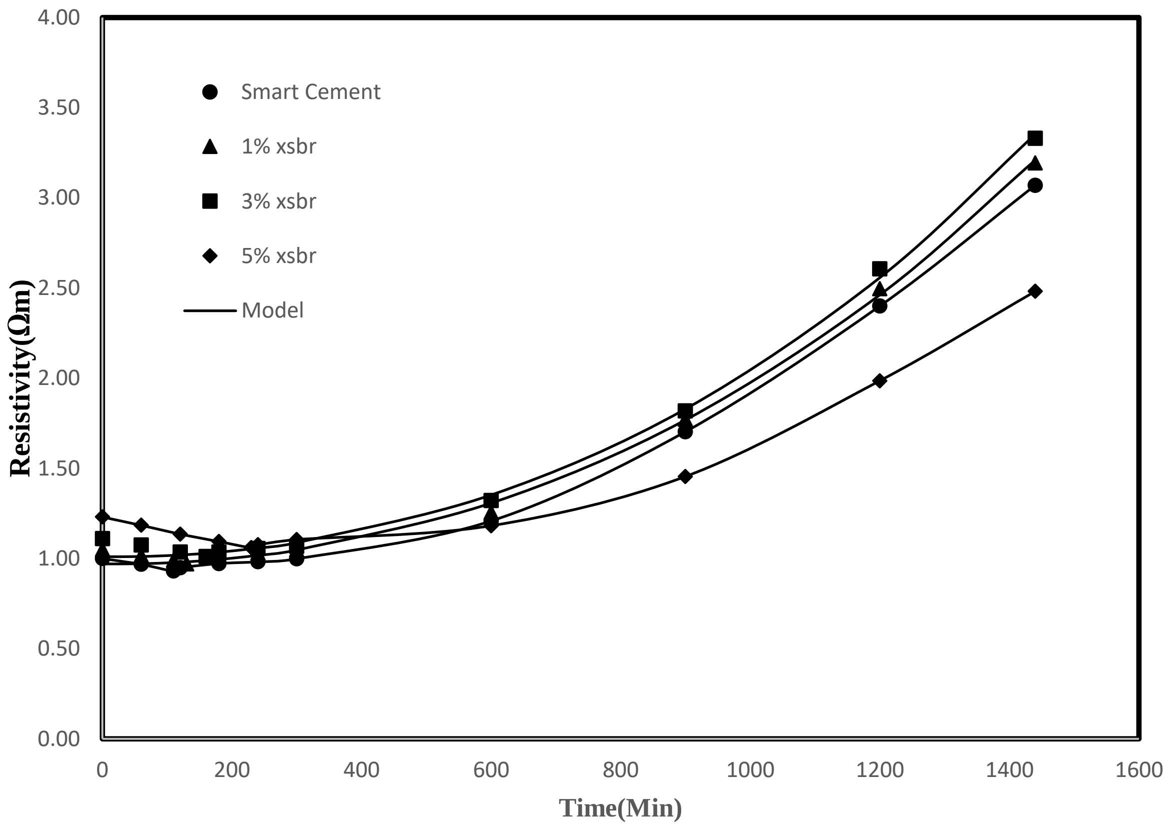

Figure 5-17 One Day Curing of samples.

The one day resistivity of smart cement and smart cement modified by 1%, 3% and 5% polymer is shown in figure 5-17.

Table 5-9 Model Parameters for 1 day cured smart cement modified XSBR

	ρ (Ωm)	ρ_{min}	t_{min}	ρ_{24}	p 1	q 1	t_0	R^2	RMSE
Class H	1.00	0.84	95	3.07	.69	.21	1168	.99	0.03
1%XSBR	1.05	0.99	120	3.24	.72	.21	1250	.99	0.03
3%XSBR	1.11	1.01	160	3.43	.74	.20	1322	.99	0.04
5%XSBR	1.23	1.06	230	2.91	.44	.15	999	.99	0.06

One Day Resistivity Development

Cement resistivity change is monitored from the preparation stage to the hardened stage. As cement hydrates, the resistivity of the material changes. By measuring the electrical resistivity at a short interval, the effect of admixtures on cement hydration can be identified. The resistivity development is modeled using equation (3-2) with p1,q1and to as model parameters.

i. Smart Cement- Initial, minimum, and one-day resistivity of the specimen were 1Ωm, 0.84Ωm, and 3.07 Ωm. Minimum resistivity is noted after 90 min. with 0.61, 0.42 and 1168 as model parameters.
ii. Smart Cement +1% XSBR BWOC- Initial, minimum, and one-day resistivity of the specimen were 1.05Ωm, 0.99 Ωm and 3.24 Ωm. Minimum resistivity is noted after 120min. with 0.44, 0.14 and 1250 as model parameters.
iii. Smart Cement +3% XSBR BWOC - Initial, minimum, and one-day resistivity of the specimen were 1.11Ωm, 1.01 Ωm, and 3.43 Ωm. Minimum resistivity is noted after 160 min with 0.74, 0.21 and 1322 as model parameters.

iv. Smart Cement+ 5% XSBR BWOC - Initial, minimum, and one-day resistivity of the specimen were 1.23Ωm, 1.06 Ωm and 2.91 Ωm. Minimum resistivity is noted after 230min. with 0.44, 0.15 and 999 as model parameters.

28 Days Change in Resistivity

Long Term Resistivity

In Figure 5-18, the long-term resistivity development of smart cement specimens with and without cellulose is modeled using the equation (3-4) with experimental data.

i. Smart Cement- The resistivity after 28 days was 9.62 Ωm The model parameters as per equation were

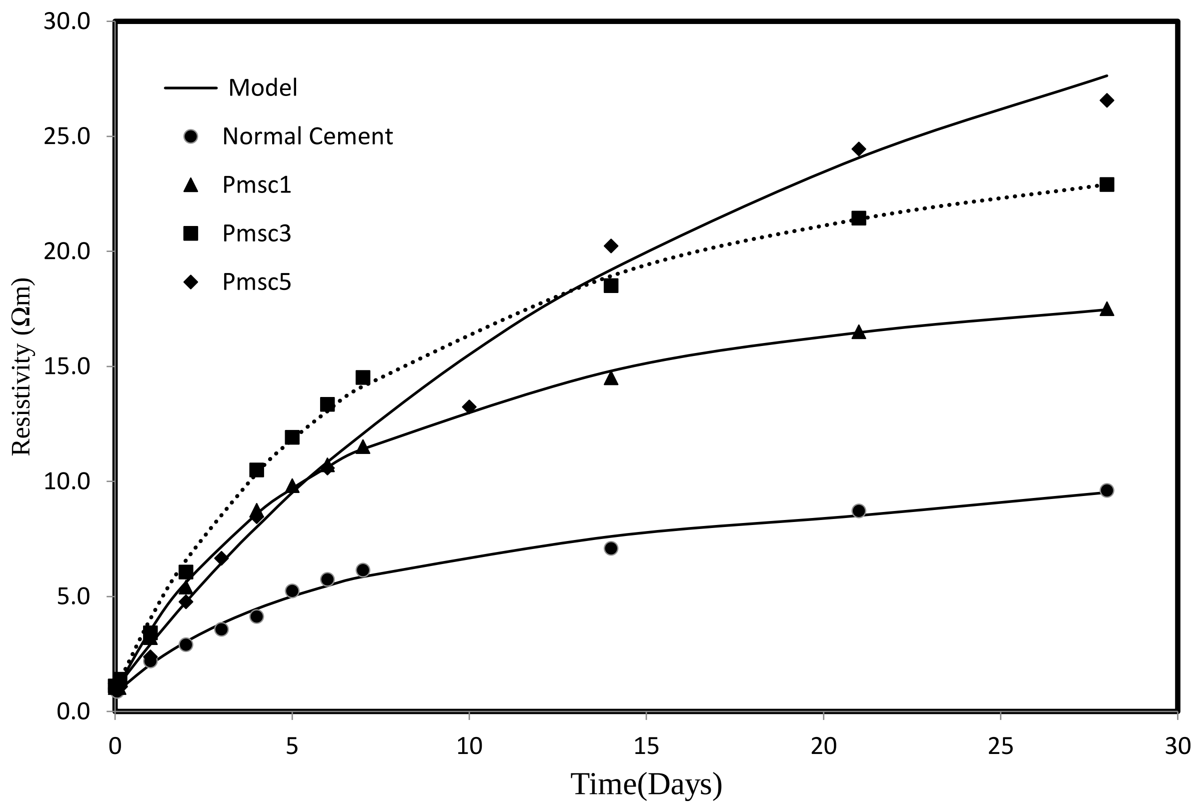

Figure 5-18 Long Term Curing of samples

Table 5-10 Models Parameter for long Term curing of Smart Cement Modified XSBR

	ρ (ini)	ρ (28)	p2	q2	to	R^2	RMSE
Class H	1.00	9.62	0.49	0.23	6.83	.99	0.18
1%XSBR	1.05	17.46	0.25	0.61	0.004	.99	0.83
3%XSBR	1.11	22.91	0.29	0.64	0.005	.99	1.11
5%XSBR	1.23	26.57	0.16	0.25	0.013	.99	1.03

ii. Smart Cement +1% XSBR BWOC- The resistivity after 28 days was 17.46 Ωm, increased over 81% smart cement. The model parameters as per equation were 0.25, 0.61, 0.004 respectively.

iii. Smart Cement +3% XSBR BWOC – The resistivity after 28 days was 22.91 Ωm, increased over 135% smart cement. The model parameters as per equation were 0.29, 0.61, 0.004 respectively.

iv. Smart Cement+ 5% XSBR BWOC - The resistivity after 28 days was 26.57 Ωm, increased over 176% smart cement. The model parameters as per equation were 0.16, 0.25, 0.013 respectively.

5.3.3) Fluid Loss Test

Using the HPHT device, the fluid loss up to 60 min (API 13A and API 13 B) was measured. The gas migration starts to occur only after the loss of a specific water percentage from the cement slurries. The volume los fluid after which gas migration occurs is termed as Critical Fluid Loss.

Table 5-11 Vipulanandan and API fluid loss model parameters for smart cement and Polymer Modified smart cement.

	API Model					Vipulanandan Model						
Cement Type	**M mL/min$^{0.5}$**	**FL_0 mL**	**FL_{30} mL**	RMSE	R^2	**D min/mL**	**E mL^{-1}**	**FL_0 mL**	**FL_{30} mL**	**FL_{max} mL**	R^2	RMSE
Smart Cement	15.64	32.93	118.6	14.34	.76	0.26	0.012	0.009	98.9	103.0	.99	.35
1%XSBR	12.89	27.72	98.3	11.81	.76	0.61	0.014	0.011	81.8	85.1	.99	.12
3%XSBR	10.56	18.90	76.8	8.12	.99	0.78	0.023	0.015	64.0	67.2	.99	.40
5%XSBR	9.45	7.42	59.2	4.04	.97	0.16	0.077	0.016	53.3	62.2	.99	.12

In table 5-11, the model parameters of API model and Vipulanandan model are summarized. In the model, it can be observed that Vipulanandan model, predicted the maximum fluid loss and gives better RMSE compared to API model.

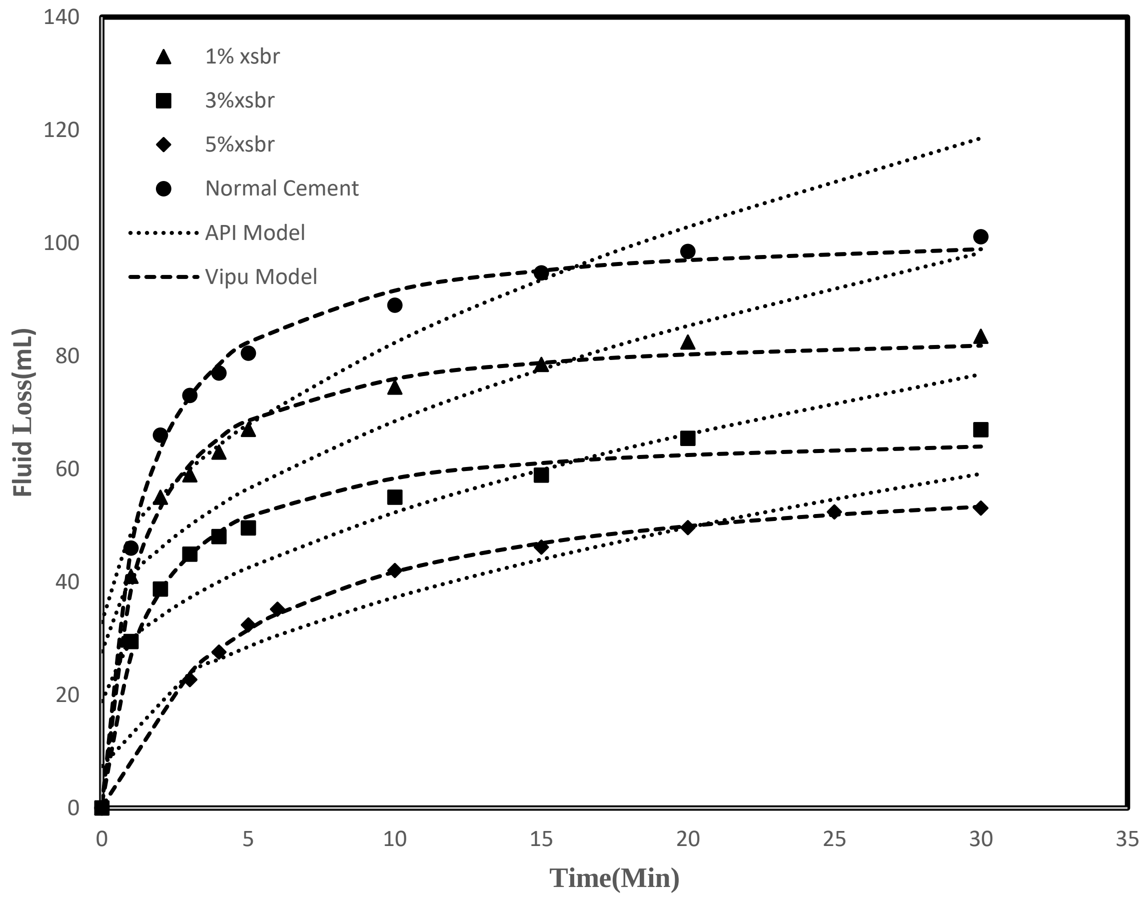

Figure 5-19 API Fluid Loss and Vipulanandan Model.

Fluid loss test performed on smart cement, smart cement with 1% XSBR,3% XSBR and 5% XSBR is modeled over the experimental fluid loss observed from the test. It can be seen that addition of polymer significantly reduced the fluid loss on smart cement.

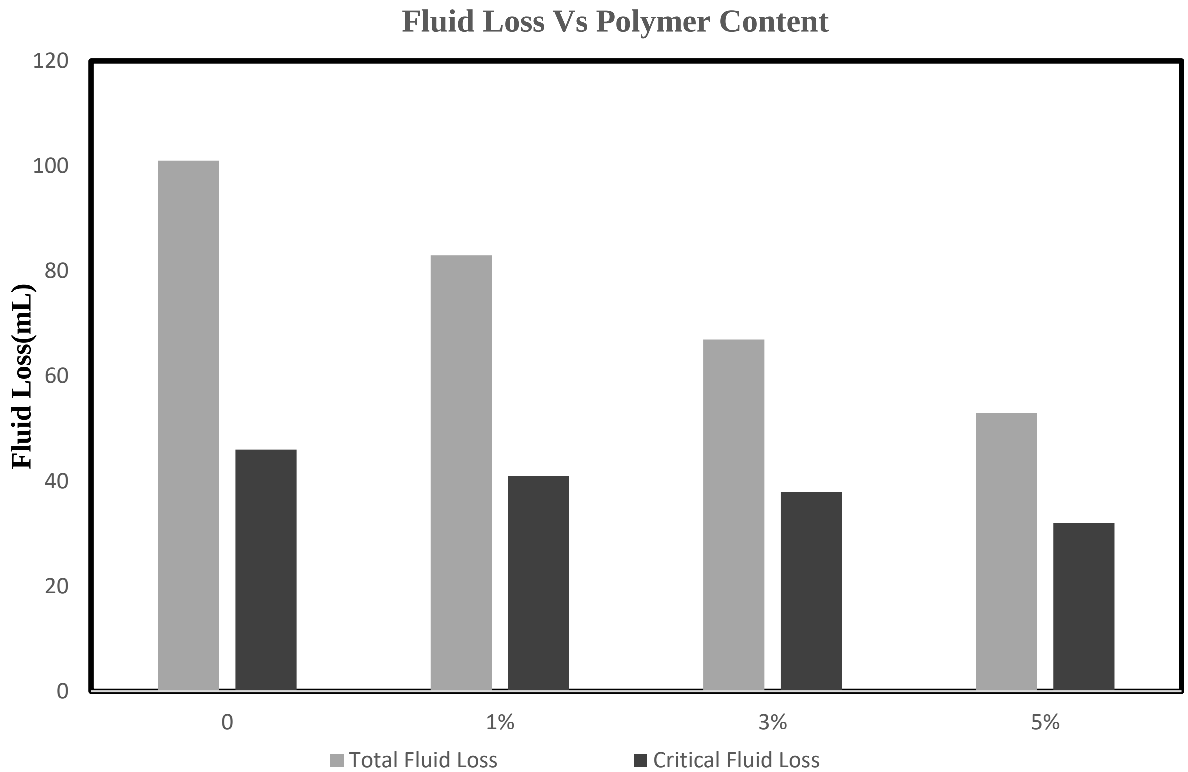

Figure 5-20 Total Fluid loss and Critical Fluid loss of Smart cement with and without polymer.

Fluid Loss of smart cement with and without Polymer

In Figure 5-19 and table 5-11, the experimental fluid loss observed has been modeled as per equation (3-14).

i. Smart Cement- The experimental fluid loss, fluid loss predicted by API, and Vipulanandan model were 101ml, 118.6ml and 103ml, respectively. The corresponding model parameters for API and Vipulanandan model were 15.64, 32.93 and 0.26, 0.012, 0.009, respectively. The ratio of critical fluid loss to total fluid loss was 0.45

ii. Smart Cement +1% XSBR BWOC- The experimental fluid loss, fluid loss predicted by API, and Vipulanandan model were 81ml, 98.3ml and 81.8ml, respectively. The corresponding model parameters for API and Vipulanandan model were 12.89, 27.72 and 0.61, 0.014, 0.011, respectively. The ratio of critical fluid loss to total fluid loss was 0.49.

iii. Smart Cement +3% XSBR BWOC – The experimental fluid loss, fluid loss predicted by API, and Vipulanandan model were 67ml, 76.8ml and 64ml, respectively. The corresponding model parameters for API and Vipulanandan model were 10.56, 18.90 and 0.78, 0.023, 0.015, respectively. The ratio of critical fluid loss to total fluid loss was 0.56.

iv. Smart Cement+ 5% XSBR BWOC - The experimental fluid loss, fluid loss predicted by API, and Vipulanandan model were 53.5ml, 59.2ml and 62.2ml, respectively. The corresponding model parameters for API and Vipulanandan model were 9.45, 7.42 and 0.16, 0.077, 0.016, respectively. The ratio of critical fluid loss to total fluid loss was 0.60.

The ratio between the critical fluid loss to total fluid loss increased from 0.45, 0.49, 0.5, and 0.60. The increasing percentage shows the effect of polymer to resist gas leak. Based on R^2 and RMSE summarized in table 4 for cement slurries with and without polymer, the Vipulanandan model better predicts the fluid loss.

Resistivity Correlation with Fluid Loss

Using the hyperbolic model, the change in fluid loss is correlated with the resistivity change which occurs occurring measured during the test.

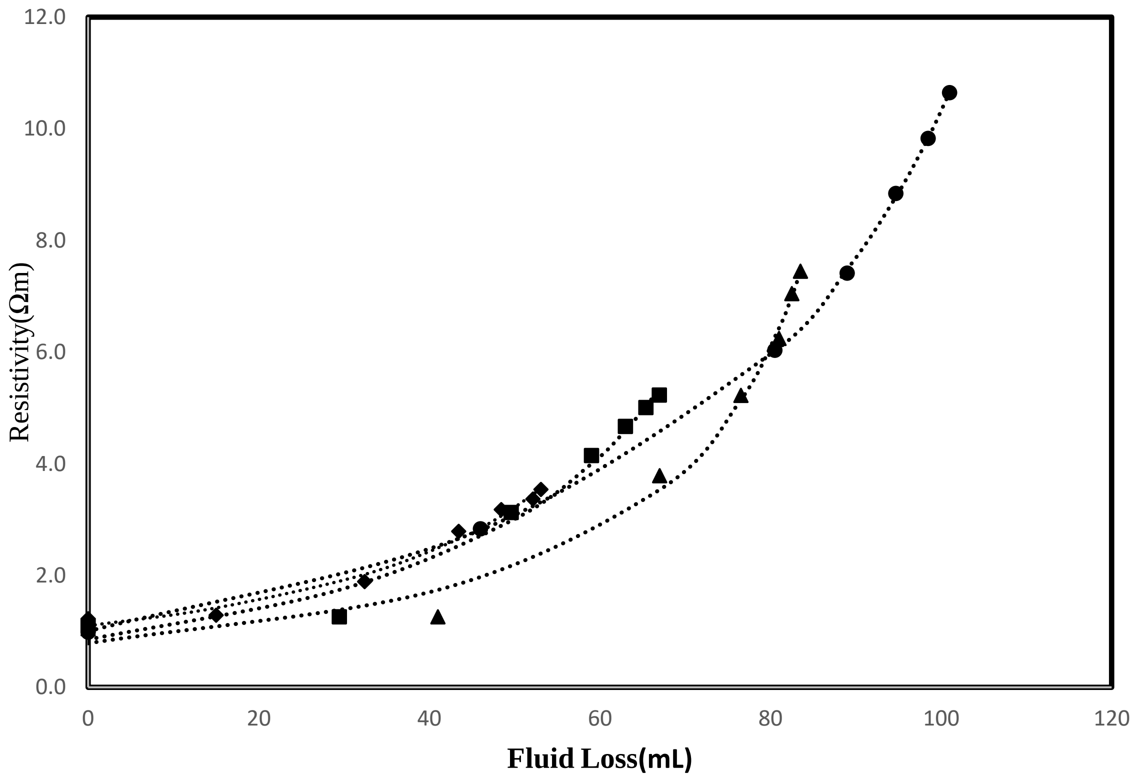

Figure 5-21 Change of Resistivity in Cement slurry Due to Fluid Loss.

Table 5-12 Model Parameters for Resistivity and Fluid Loss Model

Cement Type	A	B	C	R^2	RMSE
Smart Cement	1	37.92	-.27	.99	0.03
1%XSBR	.78	72.31	-.71	.99	0.24
3%XSBR	.85	47.31	-.48	.99	0.22
5%XSBR	1.1	56.73	-.66	.99	0.11

Due to the applied pressure of gas, fluid loss occurs in smart cement and polymer modified smart cement. This fluid leads to a change in resistivity of cement. In Figure 6 , it is observed that the higher the fluid loss, the higher is the resistivity change. The change in resistivity is modeled for the fluid loss using equation (3-16),

i. Smart Cement- The resistivity changed from 1Ωm to 10.65Ωm due to applied pressure. The model parameters for this were 1, 37.92 and -0.27 respectively.

ii. Smart Cement +1% XSBR BWOC- The resistivity changed from 1.05Ωm to 7.45Ωm due to applied pressure. The model parameters for this were 1,37, 0.92 and -0.71 respectively.

iii. Smart Cement +3% XSBR BWOC – The resistivity changed from 1.11Ωm to 5.23Ωm due to applied pressure. The model parameters for this were 0.85, 47.31 and -0.48 respectively.

iv. Smart Cement+ 5% XSBR BWOC - The resistivity changed from 1.23Ωm to 3.54Ωm due to applied pressure. The model parameters for this were 1.11, 56.73 and -0.66 respectively.

5.3.4) Compressive Stress-Strain of 1 day and 28 cured specimen

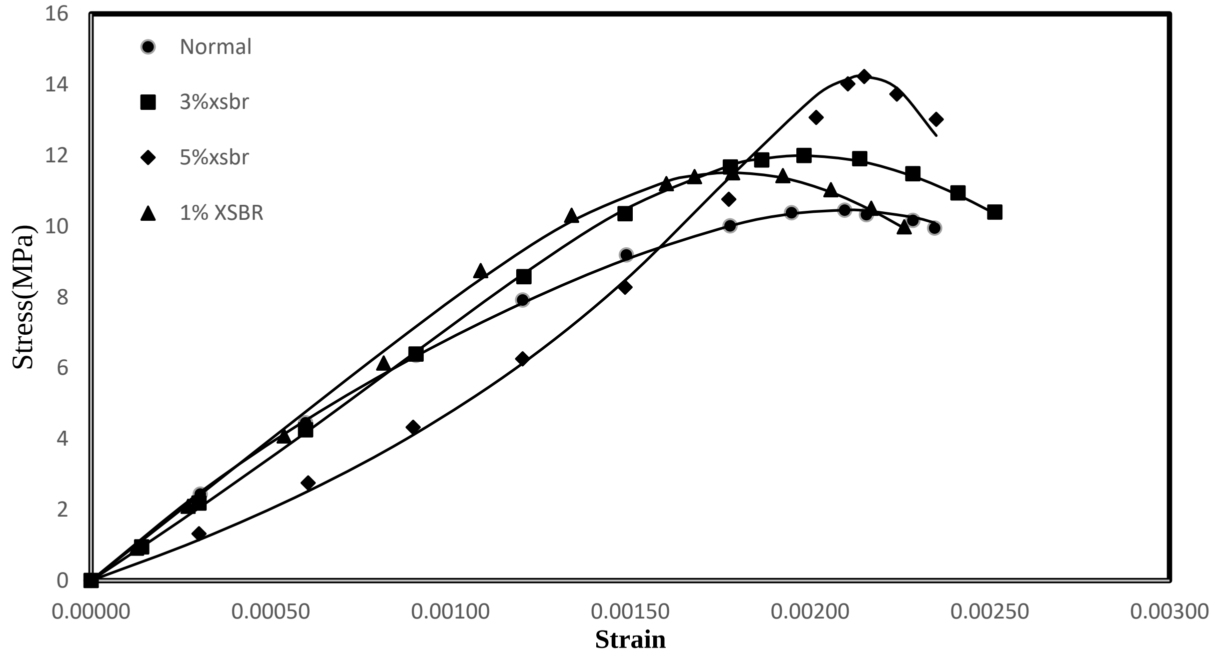

Figure 5-22 Compressive Stress -strain Curve for 1 One day cured specimen.

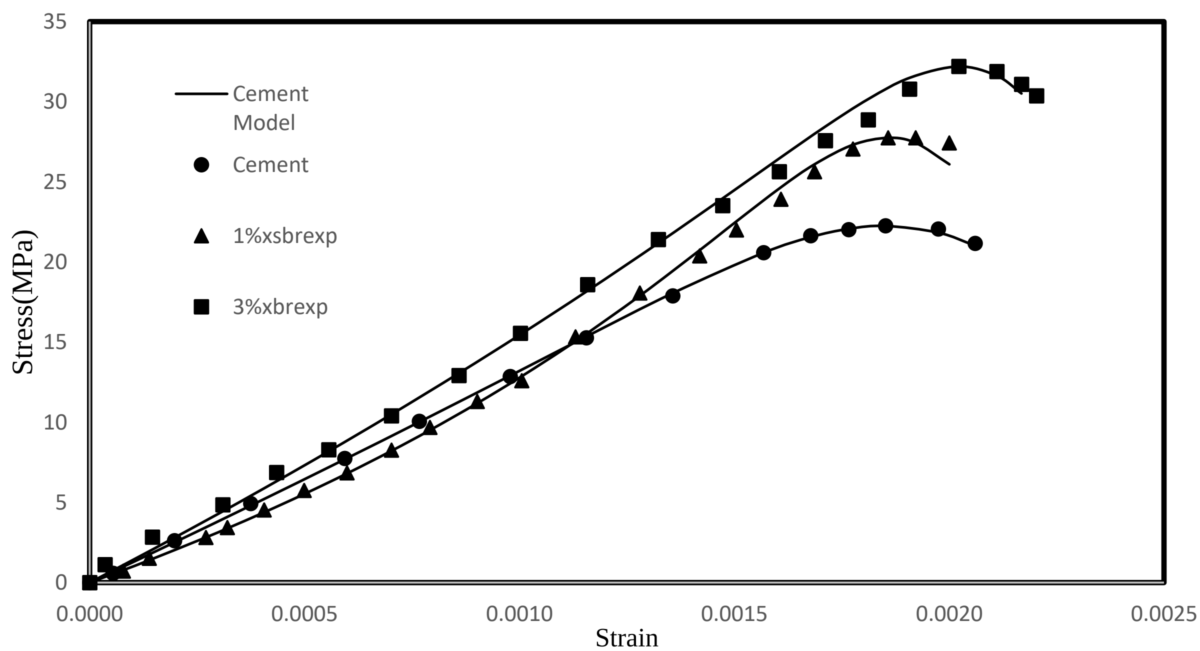

Figure 5-23 Compressive Stress-Strain Curve for 28 days cured specimen.

Table 5-13 Compressive Stress of Smart Cement Modified by XSBR

	Ultimate Compressive Strength (MPA)	p3	q3	R^2	RMSE
One Day					
Smart Cement	10.33	.55	0.08	.99	0.07
1% XSBR	11.52	.75	0.16	.99	0.15
3%XSBR	12.00	.95	0.04	.99	0.85
5%XSBR	14.23	.81	0.18	.99	0.13
28 Days					
Smart Cement	22.25	0.90	0.09	.99	0.177
1% XSBR	27.75	0.93	0.04	.99	1.91
3%XSBR	31.89	0.94	0.05	.99	1.01
5%XSBR	34.45	0.95	0.05	.98	1.04

i. Smart cement – Compressive strength and failure strain of smart cement after 1 day and 28 days of curing were 10.53MPa and 22.25MPa, respectively. The model parameter obtained from using the equation (3-10), were (0.55, 0.08), respectively.

ii. Smart Cement +1% XSBR BWOC – Compressive strength and failure strain of smart cement with 0.14% fiber after 1 day and 28 days of curing were 11.52 MPa and 27.73MPa, respectively. An increase of 7.7%, 26.75%in compressive strength, is found over smart cement after 1 and 28 days of curing. The model parameter obtained from using the equation (3-10), were (0.55, 0.08) and (0.93, 0.09) for 1 day and 28 days cured specimen, respectively.

iii. Smart Cement +3% XSBR BWOC – Compressive strength and failure strain of smart cement with 0.14% fiber after 1 day and 28 days of curing were 12.0 MPa and 31.89MPa, respectively. An increase of 11%, 30.89% in compressive strength, is found over smart cement after 1 and 28 days of curing. The model parameter obtained from using the equation (3-10), were (0.81, 0.18) and (0.94, 0.05) for 1 day and 28 day cured specimen, respectively.

iv. Smart Cement +5% XSBR BWOC – Compressive strength and failure strain of smart cement with 5%XSBR after 1 day and 28 days of curing were 12.0 MPa and 31.89MPa, respectively. An increase of 30.89%, 54% in compressive strength, is found over smart cement after 1 and 28 days of curing. The model parameter obtained from using the equation (3-10), were (0.81, 0.18) and (0.94, 0.05) for 1 day and 28 days cured specimen, respectively.

Piezoresistive of Smart Cement

The piezo resistivity tests were done to determine the sensing properties of the cement with and without polymer.

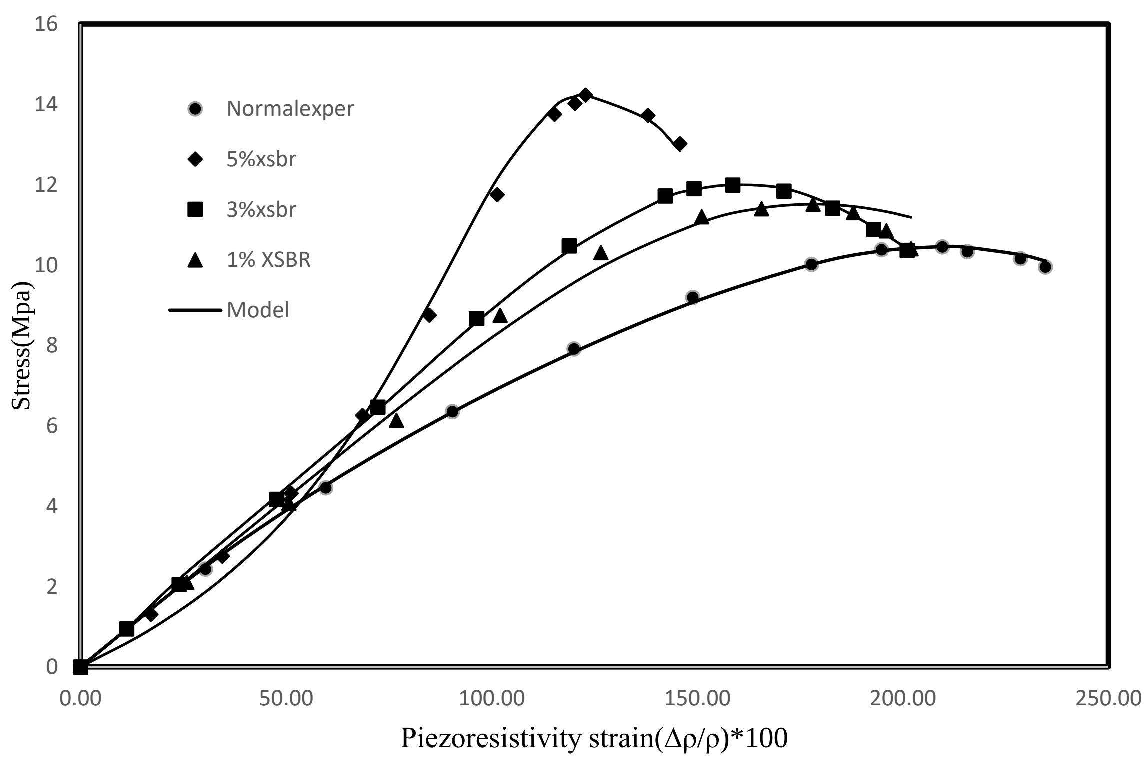

Figure 5-24 Piezoresistive Behavior of One Day Cured Specimen.

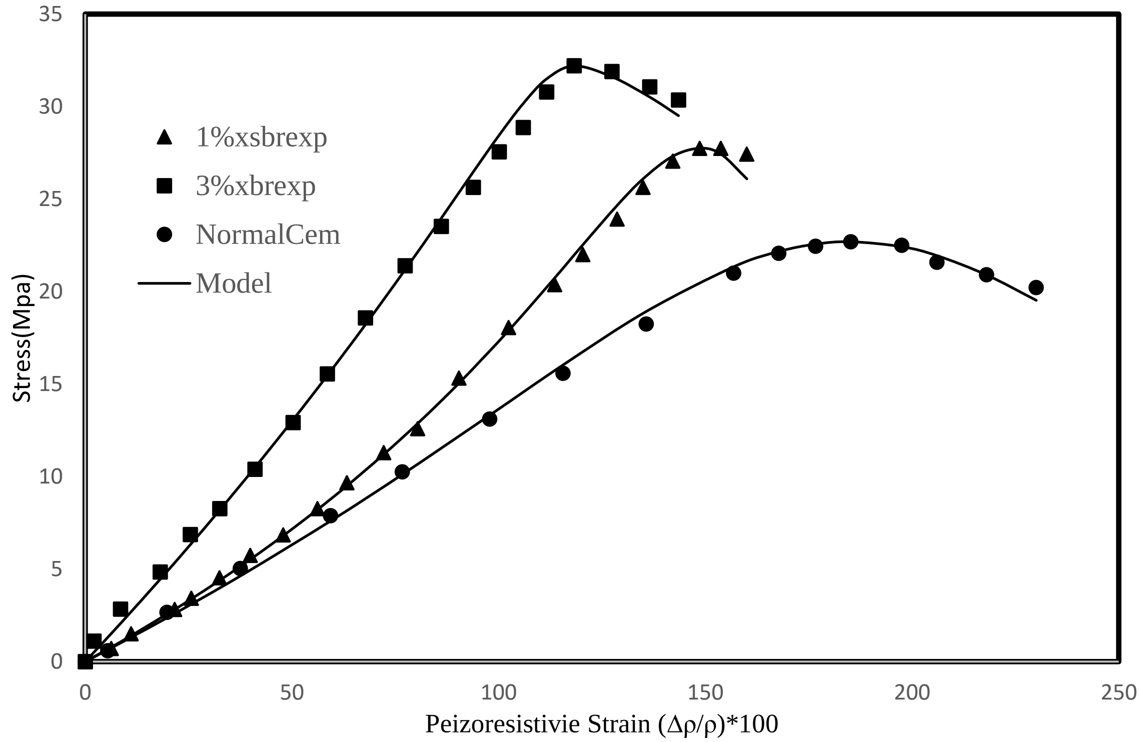

Figure 5-25 Piezoresistive Behavior of 28 Days Cured Specimen.

The piezo resistivity tests were done on specimen cured after 1 day and 28 days.

Table 5-14 Piezo resistivity Model Parameters for Smart cement with and without Polymers.

	UCS (MPa)	Ultimate Piezo resistivity	p4	q4	R^2	RMSE
Smart Cement	10.33	209	0.58	0.12	0.99	0.07
1% XSBR	11.52	178	0.77	0.22	0.99	0.32
3%XSBR	12.00	158	0.83	0.19	0.99	0.07
5%XSBR	14.23	118	0.89	0.17	.99	0.65
28 Days						
Smart Cement	22.25	185	0.85	0.14	.99	0.17
1% XSBR	27.75	148	0.90	0.03	.99	1.91
3%XSBR	31.89	118	0.91	0.05	.99	1.01
5%XSBR	34.25	105				

Piezo resistivity tests were done on samples cured for 3 days and 28 days. The change in resistivity and stress was modeled as per the equation

i. Smart Cement – The Piezo resistivity of smart cement cured after 1 day and 28 days at peak stress of 10.33 MPa and 22.25MPa were 209% and 185% respectively. The model parameters of the equation (3-11), p2 and q2 for 3days and 28 days curing were (0.60, 0.133) and (1.05, 0.25), respectively.
ii. Smart Cement +1% XSBR BWOC – The Piezo resistivity of smart cement cured after 1 day and 28 days at peak stress of 11.52 MPa and 27.75MPa were 178% and 148%, respectively. The model parameters of the equation (3-11), p2 and q2 for 3days and 28 days curing are (0.77, 0.22) and (0.9,0.03), respectively.
iii. Smart Cement +3% XSBR BWOC – The Piezo resistivity of smart cement cured after 1 day and 28 days at peak stress of 12 MPa and 31.89MPa were 158% and 118%, respectively. The model parameters of the equation (3-11), p2 and q2 for 3days and 28 days curing are (0.83, 0.19) and (0.91, 0.05), respectively.
iv. Smart Cement +5% XSBR BWOC -The Piezo resistivity of smart cement cured after 1 day and 28 days at peak stress of 14.23 MPa and MPa were 118% and %, respectively. The model parameters of the equation (3-11), p2 and q2 for 3days and 28 days curing are (0.89, 0.17) and (0.91, 0.05) respectively.

5.4) Summary

1) Addition of cellulose into smart did not affect the initial resistivity and density of smart cement.

2) The minimum resistivity ρ_{min} of the smart cement decreased due to addition of 0.014%,0.028% and 0.42% of cellulose. The tmin increased due to addition of cellulose by 183%,372% and 627%. The one day resistivity index (RI $_{24hours}$) were 182%, 37% and 20% on addition 0.014%, 0.028% and 0.42% of cellulose.

3) After 1 month of curing the resistivity of samples were monitored. Resistivity increased by 39%, 73% and 141% on addition of 0.014%, 0.028% and 0.42% of cellulose. This shows that after the retardation effect is diminished, normal hydration starts to occur in cellulose added cement.

4) Addition of cellulose 0.014%, 0.028% and 0.42% delayed the final setting time over 101%, 216% and 683% over normal smart cement due to addition of cellulose.

5) The heat of hydration curve showed significant slowdown in cement reduction due to addition of cellulose. The peaks curve in hydration curve were observed 1444 min,1700 min and 1954 min from the start of mixing.

6) The compressive strength increased on addition of 0.014% of cellulose and decreased on further addition of cellulose. Addition of cellulose increased the ultimate piezo resistivity marginally. Thus, cellulose addition does not affect the sensing properties.

7) Addition of polypropylene fibers increased the resistivity of smart cement and reduced the density, as fibers replaced the cement particulates inside the cement slurry.

8) The minimum resistivity ρ_{min} of the smart cement decreased due to addition of 0.14% and 0.28% polypropylene fibers on smart cement. The tmin increased due to addition of fibers by 36% and 115%.The one day resistivity index (RI $_{24hours}$) were 319.23%,329% and 365% on addition 0%,0.28% and 0.42% of fibers into smart cement.

9) After 1 month of curing the resistivity of samples were monitored. Samples cured inside mold, the resistivity increased by 82% and 142% over smart cement. Samples which were cured in room temperature (without mold), the resistivity increased by 54% and 99% over smart cement by addition of 0.28% and 0.42% fibers . This indicates the resistivity is affected by curing conditions.

10) An addition of 0.028% and 0.42% of fibers polypropylene fibres increased the compressive strength and toughness of smart cement. A significant change was observed in post failure mode in case of fiber added into smart cement, indicating high strain tolerance and ductile.

11) The addition of polypropylene fiber reduced the piezoresistivity of smart cement after 1 day and 28 days of testing. Piezo resistivity decreased by 20% ,21% and 12%,15% after 1 day and 28 days of testing, respectively. The sensing properties of smart cement were reduced by the addition of polypropylene fibers.

12) The addition of polypropylene fibre significantly reduced the shrinkage of class H cement. The addition of 0.28% and 0.42% of fibres reduced the volumetric shrinkage by 54% and 61% respectively.

13) Addition of XSBR polymer increased the resistivity of smart cement and reduced the density. The change in density is due to the replacement of cement particles by the polymer.

14) The minimum resistivity ρ_{min} of the smart cement decreased due to the addition of 1%, 3% and 5% of XSBR polymer. The tmin increased due to the addition of cellulose by 183%,372%, and 627%. The one day resistivity index (RI $_{24hours}$) were 182%,37% and 20% on addition 0%,1%,3% and 5% XSBR on smart cement.

15) Change in resistivity was monitored up to 1 month. The resistivity of samples modified by 1% XSBR,3%XSBR, and 5% XSBR on smart cement increased the resistivity by 26%,68% and 142% over smart cement.

16) Polymer modified cement is used to control the gas leakage, and the addition of polymers reduced the fluid loss of smart cement. Increasing the polymer loading over smart cement reduced the fluid loss of smart cement. The fluid loss was modeled using API and Vipulanandan model. Vipulanandan model predicted better R^2 and RMSE values.

17) A new model was made to predict the resistivity change due to fluid loss. The model was verified by using the coefficient of determination and root mean square error.

18) The compressive stress of smart cement increased due to the addition of polymer content. After 28 days compressive strength of polymer modified smart cement increased by 26.75%,30.45% and 50.54% over smart cement on the addition of 1%,3%, and 5% of XSBR The stress-strain behavior of cement specimens is modeled using the Vipulanandan Model. Polymer addition increased the failure strain of smart cement.

19) To sense the material behavior, piezoresistive behavior of cement is tested. The addition of polymer into smart cement decreased the piezoresistive behavior. The piezoresistive behavior is modeled using Vipulanandan piezoresistive model. Using R^2 and RMSE,the model was verified.

CHAPTER 6 DETECTION AND QUANTIFICATION OF GAS LEAKS IN SMART CEMENT AT VARIOUS STAGES OF CURING

The main objective is to study the behavior hydrating cementing slurry when subjected to gas pressure at different times of hydration under different conditions. Understanding the mechanism of gas migration is vital; offering a solution is only possible if the concept is well understood. It is essential to study the electrical behavior; for this smart cement was used, which is sensitive to stress. Changes in electrical resistivity of smart cement at different stages of curing are known, and the effect of gas migration on it is studied. Gas migration affects the resistivity of the cement at the slurry and hardened stage. By monitoring the resistivity of cement, gas invasion occurring inside the cement can be ascertained. In this chapter, the behavior of smart cement at slurry and the hardened stage is observed. Significant changes in resistivity are observed. To control gas migration, it is essential to know the phase conditions inside the cement slurry at a different time of curing. As stated in the literature, gas migration starts to occur after there is fluid loss or volume reduction. The purpose of the experiments is to quantify the porosity, moisture content, air void ratio, and water void ratio due to gas migration at different stages of curing.

The change in void ratio, water content, and porosity has been investigated from the experiment. Phase diagram of curing cement before and after gas migration is plotted. A correlation is found between the initiation point of gas migration and phase diagram. Further, discharge velocity from the cement at various stages of curing has been observed. A new non-linear model called the Vipulanandan flow model has been used to predict the discharge velocities and compared them with the Darcy model. To simulate actual ground conditions, gas migration is studied in closed and open conditions.

6.1) Materials and Methods

Class H cement with water/cement ratio of 0.4 and 0.5 is used to prepare the cement slurry. Conductive fillers are added to cement to get sensing properties, and cement slurry were prepared by the API standard. The prepared cement slurry is poured into the mold of size with four wires inserted into it. The resistivity of the cement slurry is measured for 24 hours.

6.2) Resistivity Measurements

The electrical resistivity of smart cement is measured using API resistivity meter in the range of 0.01Ω-m to 400Ω-m. Using the conductivity probe, also the conductivity of the cement slurry is measured.

Resistivity Change Model

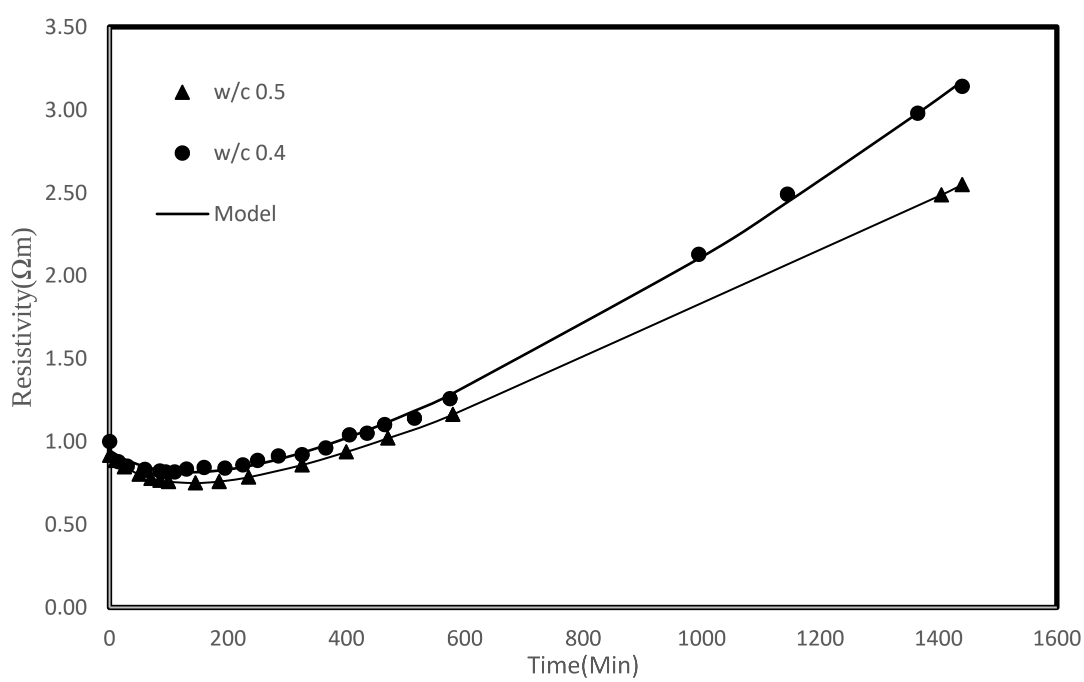

Figure 6-1 One Day Curing with w/c of 0.4 and 0.5

Table 6-1 Summary of Bulk resistivity of cement with various W/c ratios.

w/c	ρ_0 (Ωm)	ρ_{min}(Ωm)	tmin	p 1	q 1	to	R^2	RMSE	ρ_{24h}(Ωm)
0.4	1	.80	85	0.61	0.42	215.63	0.99	0.19	3.15
0.5	.91	.75	145	0.55	0.47	162.45	0.99	0.23	2.54

One Day Resistivity Development

Cement resistivity change is monitored from the preparation stage to the hardened stage. As cement hydrates, the resistivity of the material changes. By measuring the electrical resistivity at short interval, the effect of different w/c ratios on cement hydration can be identified. The resistivity development is modeled using equation (3-4) with p1, q1and to as model parameters.

i. Smart Cement(w/c0.4)- Initial, minimum, and one-day resistivity of the specimen were 1Ωm, 0.78 Ωm and 3.23 Ωm. Minimum resistivity is noted after 90 min. with (0.61, 0.42 and 215.63) as model parameters.
ii. Smart Cement (w/c0.5) - Initial, minimum, and one-day resistivity of the specimen were 0.91Ωm, 0.78 Ωm, and 2.54 Ωm. Minimum resistivity is noted after 145 min with (0.55, 0.47 and 162.45) as model parameters.

6.2) Piezoresistive behavior of Smart Cement-Smart cement was tested after one day to get the piezoresistive behavior

The change in piezo resistivity after one day curing of water/cement of 0.4 and 0.5 is shown in figure 6-2.

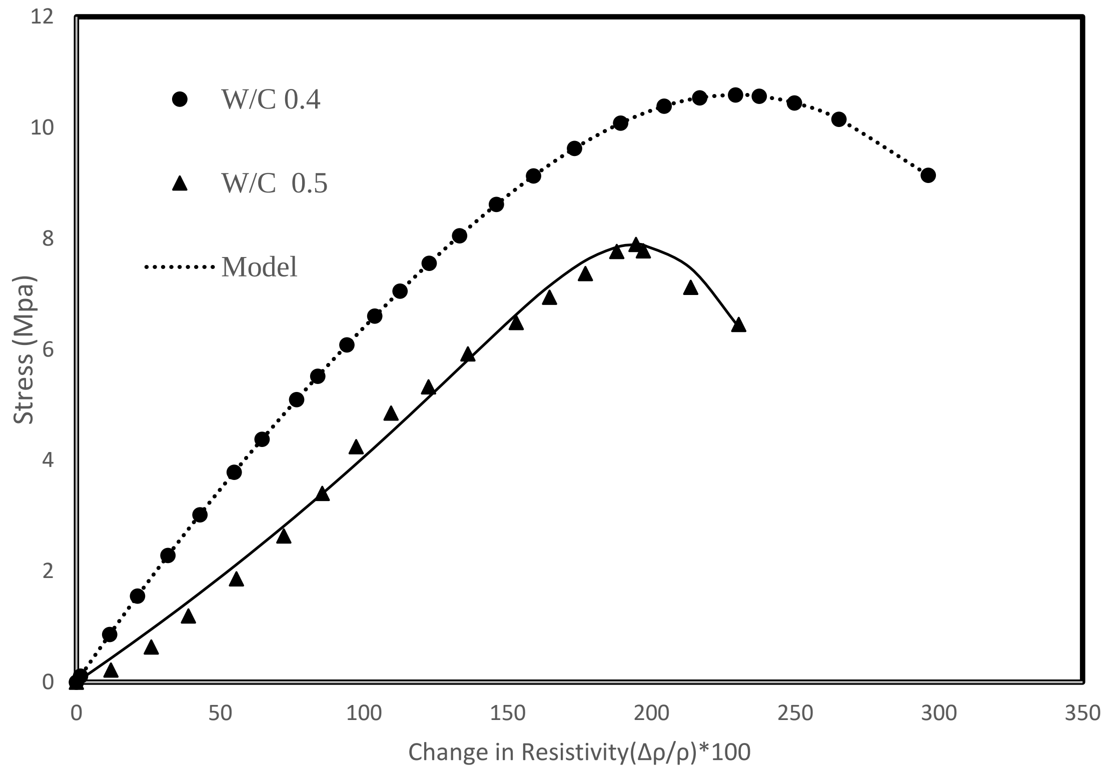

Figure 6-2 Piezoresistive behavior of Smart cement with w/c of 0.4 and 0.5

Table 6-2 Piezoresistive Behavior of Smart Cement with W/c of 0.4 and 0.5

	p 2	q 2	R^2	RMSE	Ultimate Strength (MPA)	Ultimate Piezo resistivity
w/c 0.4	.60	.133	0.99	.195	10.59	230
w/c 0.5	0.91	0.08	0.99	.201	7.89	191

i. Smart Cement(w/c0.4) – The Piezo resistivity of smart cement of w/c 0.4 cured after 1 day at peak stress of 10.59 MPa was 230%. The model parameters of the equation (3-11), p2, and q2 for 1day were (0.60, 0.91).

ii. Smart Cement(w/c0.5) – The Piezo resistivity of smart cement of w/c 0.5 cured after 1 day at peak stress of 7.89 MPa was 191%. The model parameters of the equation (3-11), p2, and q2 for 1day were (0.91, 0.08).

6.3) Fluid Loss from Hydrating Cement

Due to the applied pressure of 100psi for 30 mins on the cement slurry at various hours of curing on different W/c ratios of 0.4 and 0.5, fluid loss is observed in the cement slurry. This Fluid loss is basically the free fluid, which is removed from the slurry. After a specific threshold fluid loss from the slurry, gas leakage is observed.

Table 6-3 Model Parameters to Quantify Fluid Loss at different Time interval for W/c of 0.4 and 0.5.

	Vi	P3	Q3	R^2	RMSE	P3/q3
W/c 0.4						
1 hour	160	12252.92	16614.53	.99	1.636	0.74
3 hours	160	9852.77	12781.08	.99	1.3048	0.77
6 hours	160	5480.03	10982.79	.99	1.7452	0.50
12 hours	160	3782.80	9731.51	.99	1.5181	0.39
24 hours	160	496.70	5978.71	.99	0.4332	0.08
W/c 0.5						
1 hour	175	19068.87	20104.06	.99	3.4728	0.95
3 hours	175	6683.30	16061.20	.99	2.3236	0.42
6 hours	175	5316.07	13853.73	.99	1.7101	0.38
12 hours	175	5665.81	12900.35	.99	0.7478	0.44

Discussions

As shown in Figure 3a, constant gas pressure is applied after 1 hour, 3 hours, 6 hours,12 hours, and 24 hours of curing of cement slurry inside the HPHT cell, the objective of the test is to determine the fluid loss at which the gas starts to leak. This volume of the loss of water due to applied pressure is the critical fluid loss due to constant pressure, after volume loss and total volume loss was determined. As cement is constantly hydrating, the critical volume loss and total fluid loss decreases over time. The fluid loss test also provides the existing phase of solid, liquid volume at various stages of curing. Initially, there is no air present inside the hydrating cement, as high pressure is applied, it leads to the formation of air voids which were previously occupied by water. Through this test, critical air volume has been found out, where an interconnected network of pores occurs, leading to gas leakage at different stages of curing.

For w/c of 0.4, the critical fluid loss was 47ml, 25ml, 17ml, 15ml and 11ml after 1 hours, 3 hours, 6 hours, 12 hours and 24 hours of cement hydration and total fluid loss observed from the test were 101ml, 77ml, 66ml, 58ml and26ml. The percentage of volume loss (Vw/V) at which gas migration starts to occur after 1 hour, 3 hour, 6 hours,12 hours and 24 hours is 14.92%, 7.94%, 5.41%, 4.76% and 3.49% respectively.

In case of w/c of 0.5, the critical fluid loss observed was 66ml, 43ml, 35ml, 22ml and 18ml and total fluid loss observed was 115ml, 88ml, 73ml, 65ml and 48ml after 1 hour, 3 hours, 6 hours, 12 hours and 24 hours of curing. The percentage of volume loss (Vw/V) at which gas migration starts to occur after 1hour, 3hour, 6 hour, 12 hours and 24 hours is 22.76, 14.83%, 12.07%, 7.59% and 6.21% respectively

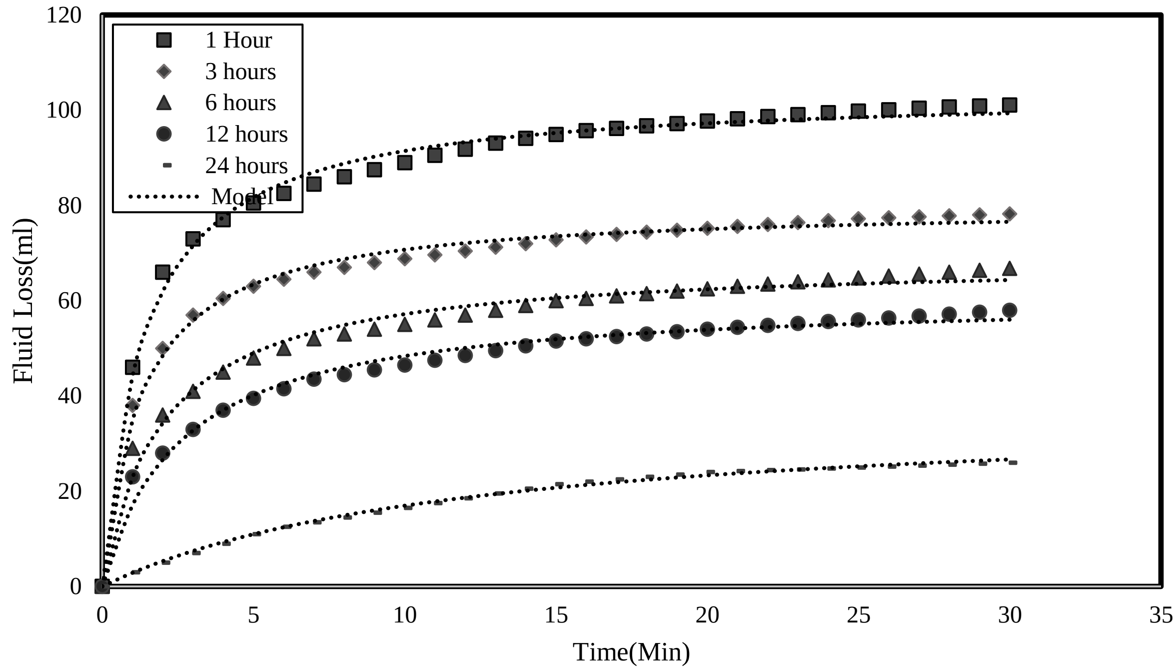

Figure 6-3a Fluid Loss of cement slurry cured for 1hr,3hr,6hr,12hr and 24hr for w/c 0.4

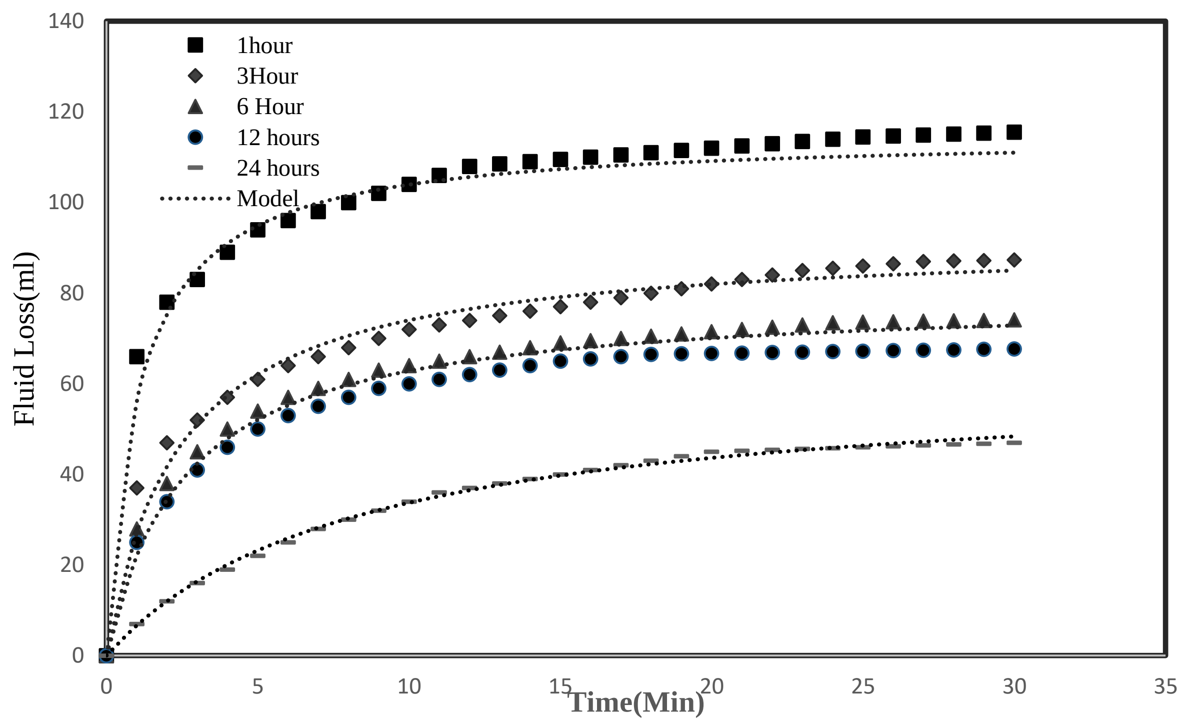

Figure 6-3b Fluid Loss of cement slurry cured for 1hr,3hr,6hr,12hr and 24hr for w/c 0.4

6.4) Phase Diagram of Cement Slurry at different Stages of Curing has been shown.

By doing fluid loss experiments at stage 3, complete sets of phase diagrams can be established for cement at various stages of curing. The phase diagram gives a complete picture of the existing solid volume, water volume (unhydrated free water inside pores which can be taken out), and air volume inside the cement slurry at various stages of curing. When gas pressure is applied, an interconnected network of pores is created before gas leakage takes place. This interconnected network of pores can be quantified in terms of total air volume existing in the material before gas leakage takes place. When gas leakage occurs inside cement slurry, both air and water volume exist inside cement slurry. In the phase diagram of W/c of 0.4 and 0.5 the phase of solid and liquid existing before and after gas leakage has been shown. This phase diagram always changes, as cement is hydrating. When cement hydrates, the porosity of cement decreases over time, and pore volume decreases with time.However, when gas pressure is applied, it causes the water to leak, and then gas starts to leak as an interconnected of pores has been created. The volume loss of water after which gas migration takes place, is referred to as gas breakout volume. From the tests, .it was observed that gas break out volume gradually decreased with time as cement hydration occurred.

For Smart cement w/c ratio of 0.4, the gas breaks out volume percentage was 15.41%, 8.20%, 5.57%, 4.92% and 3.61% after 1 hour, 3 hour, 6 hour, 12 hour and 24hours of curing. The total free fluid volume (the fluid which can be taken out by applying high pressure) at 100 psi is 33.15%, 25.64%, 23.90%, 19.02%, and 8.52%, respectively.

In case of smart cement w/c ratio of 0.5, the gas breaks out volume percentage was 22.76%, 14.83%, 12.07%, 7.59%, and 6.21% after 1hour, 3hour, 6hour, 12hour and

24hours of curing. The total free fluid volume for W/c of 0.5 is 33.15%, 25.64%, 23.90%, 19.02% and 8.52% after 1 hour, 3 hours, 6 hours ,12 hours and 24 hours of curing. It is observed that a higher volume is required to have gas leakage in W/c of 0.5 compared with W/c of 0.4. The phase diagram shows the changes happening inside the cement slurry, how applied air pressure creates air void in the system. Cement resistivity change is always positive whenever free water (Water Which can be taken out) is present inside cement slurry, this explains why the positive change in resistivity is observed in case of fluid loss from cement slurry at various stages of curing.

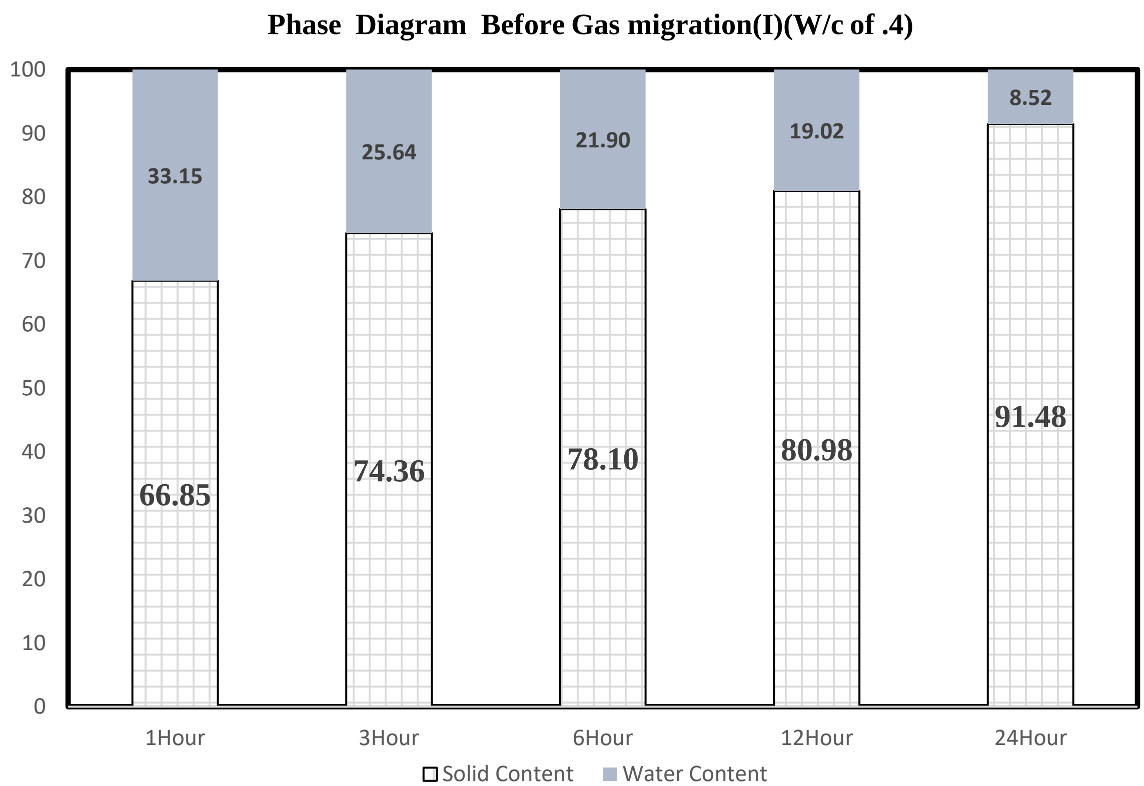

Figure 6-2 Phase Diagram of the cement Slurry after 1hr,3hr,6hr,12hr and 24hr of curing for W/c of 0.4.

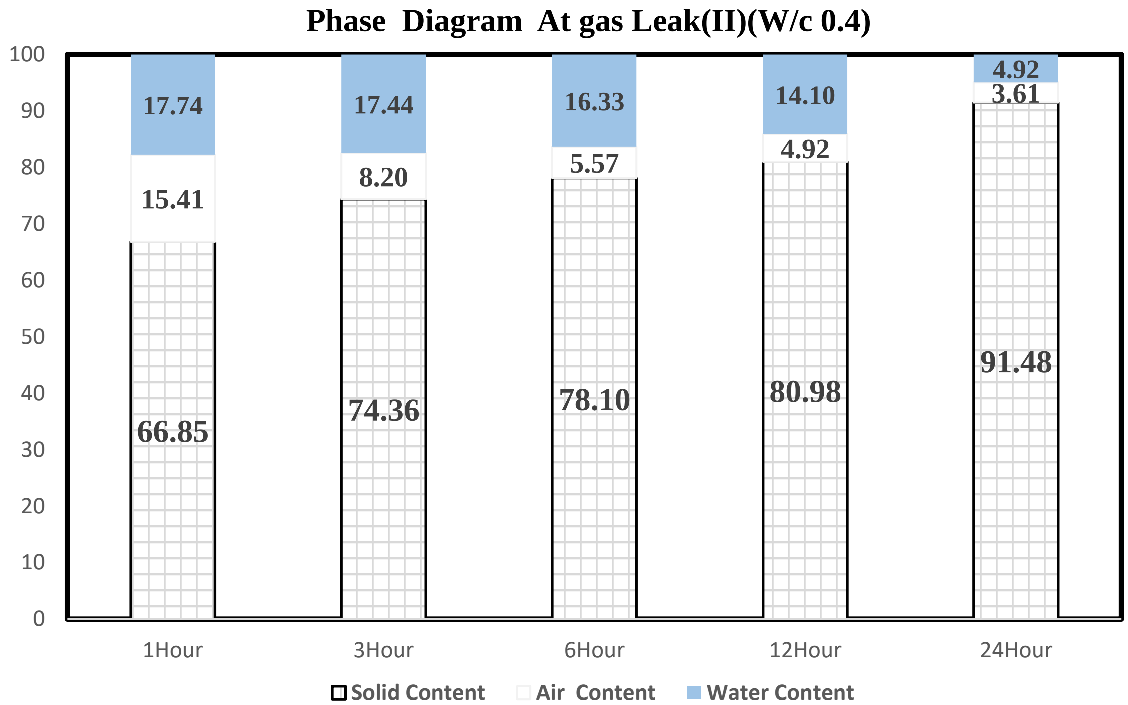

Figure 6-3 Phase Diagram of the cement Slurry before gas migration after 1hr,3hr,6hr,12hr and 24hr of curing for W/c of 0.4.

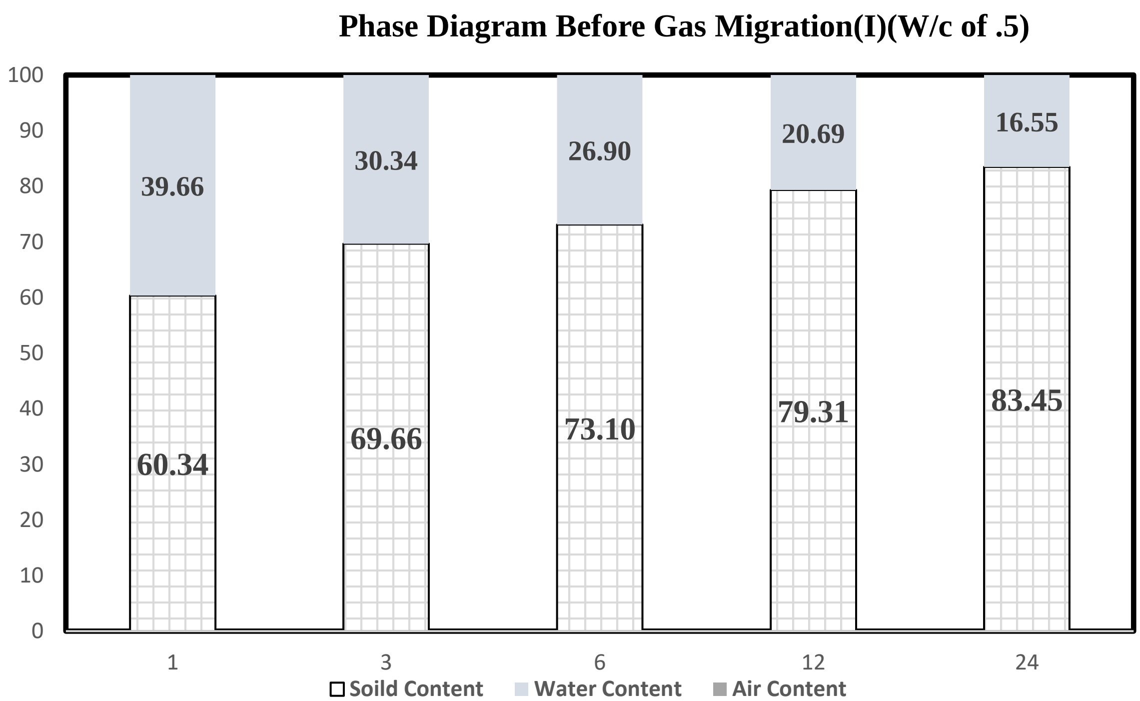

Figure 6-4 Phase Diagram of the cement Slurry after 1hr,3hr,6hr,12hr and 24hr of curing for W/c of 0.5.

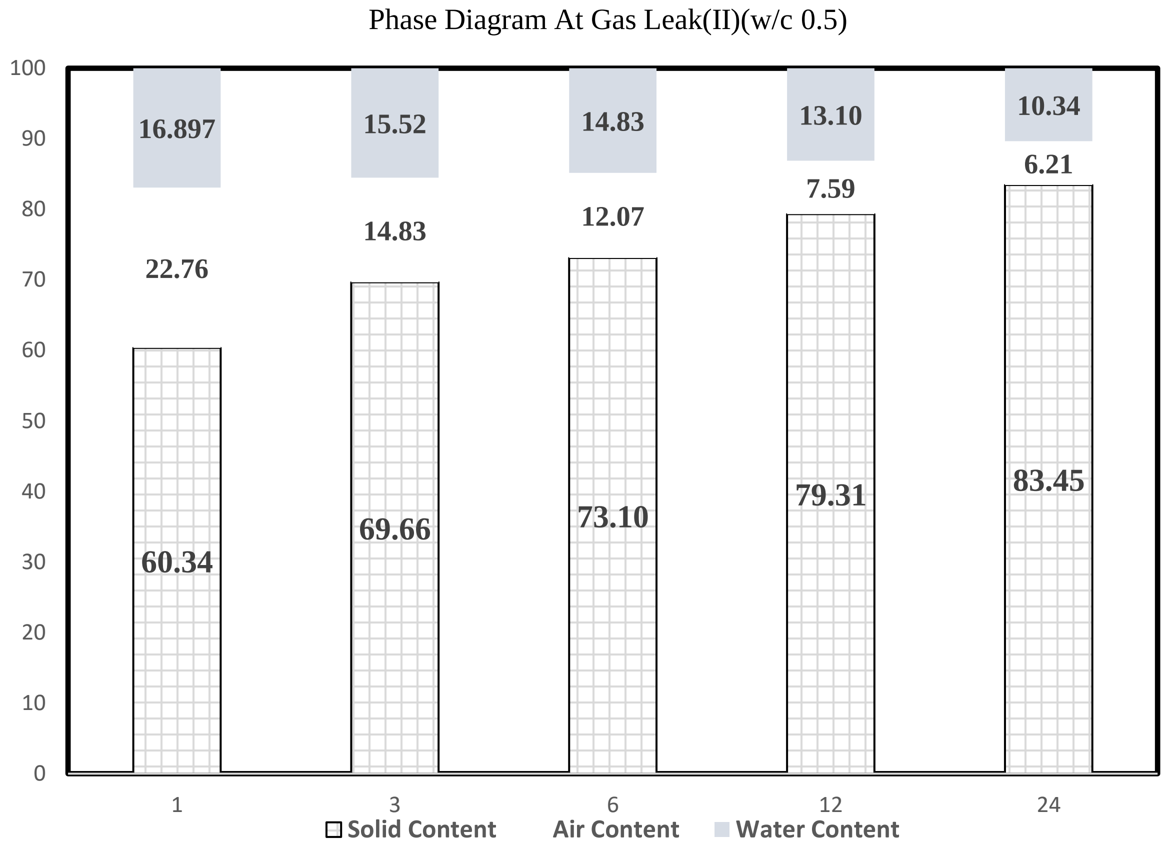

Figure 6-5 Phase Diagram of the cement Slurry before gas migration after 1hr,3hr,6hr,12hr and 24hr of curing for W/c of 0.5.

From the phase diagrams at various stages of curing,the porosity of the cement is calculated.Porosity change of cement at all stages of curing is shown and the porosity at which gas starts to leak is identified from the experiment. A novel concept of critical porosity is presented at which gas starts to leak for water cement ratio of 0.4 and 0.5.In figure 6-8 and 6-9 ,the critical porosity and total porosity of smart cement at w/c 0.4 amd 0.5 is presented.

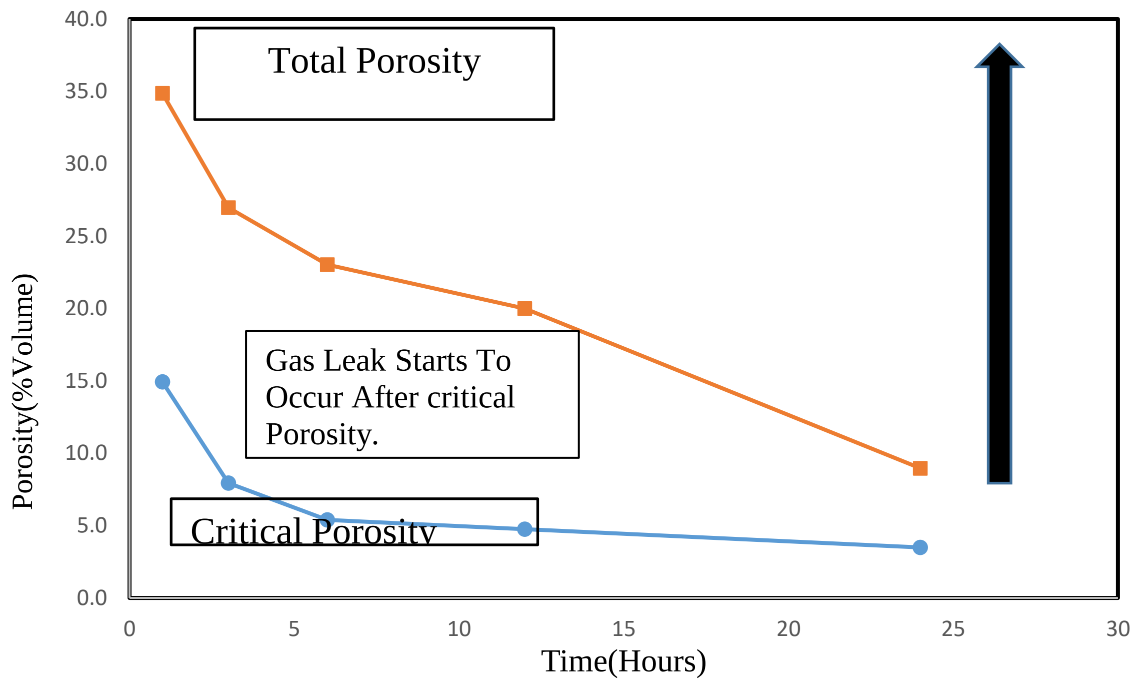

Figure 6-8 Fluid Loss affecting porosity of Cement at Various Stages of Curing.

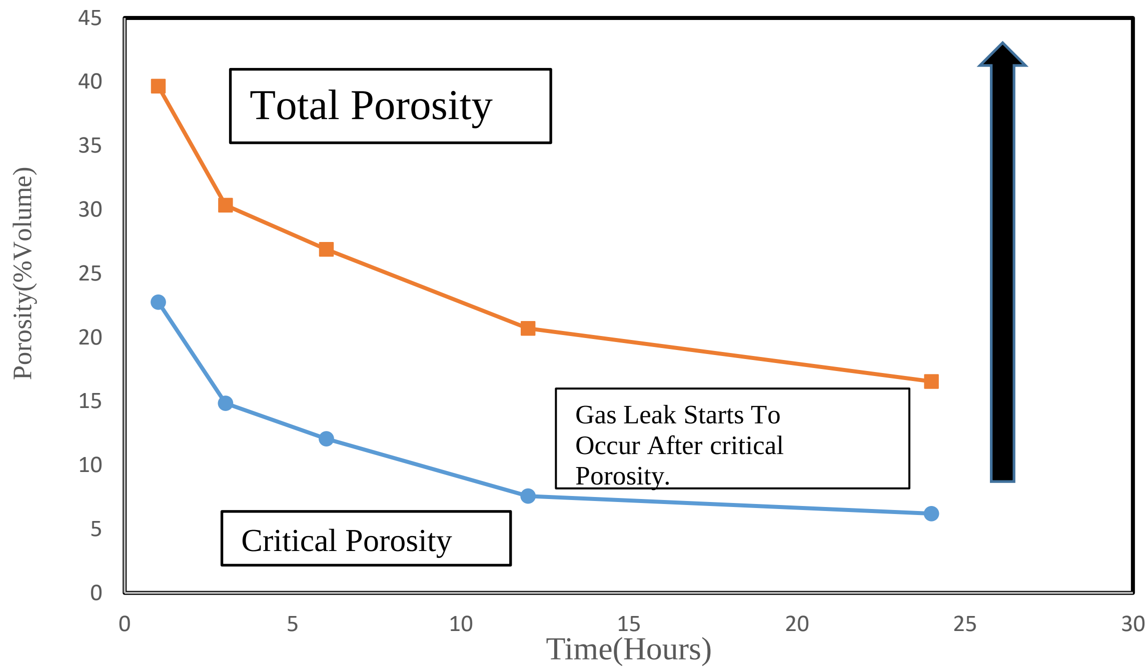

Figure 6-9 Fluid Loss affecting porosity of Cement at Various Stages of Curing.

6.5) Gas Leakage in Dry Slurry

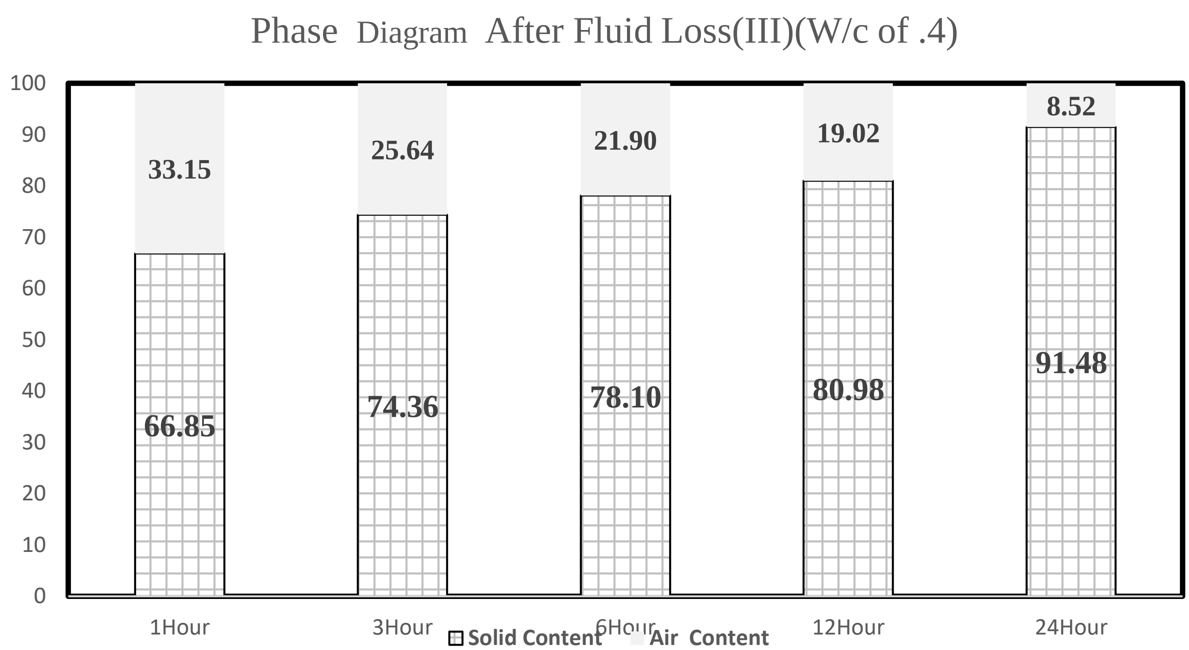

Figure 6-6 Phase Diagram after the complete fluid loss of samples cured 1Hour,3hour,6hour,12 hours and 24 hours.

`

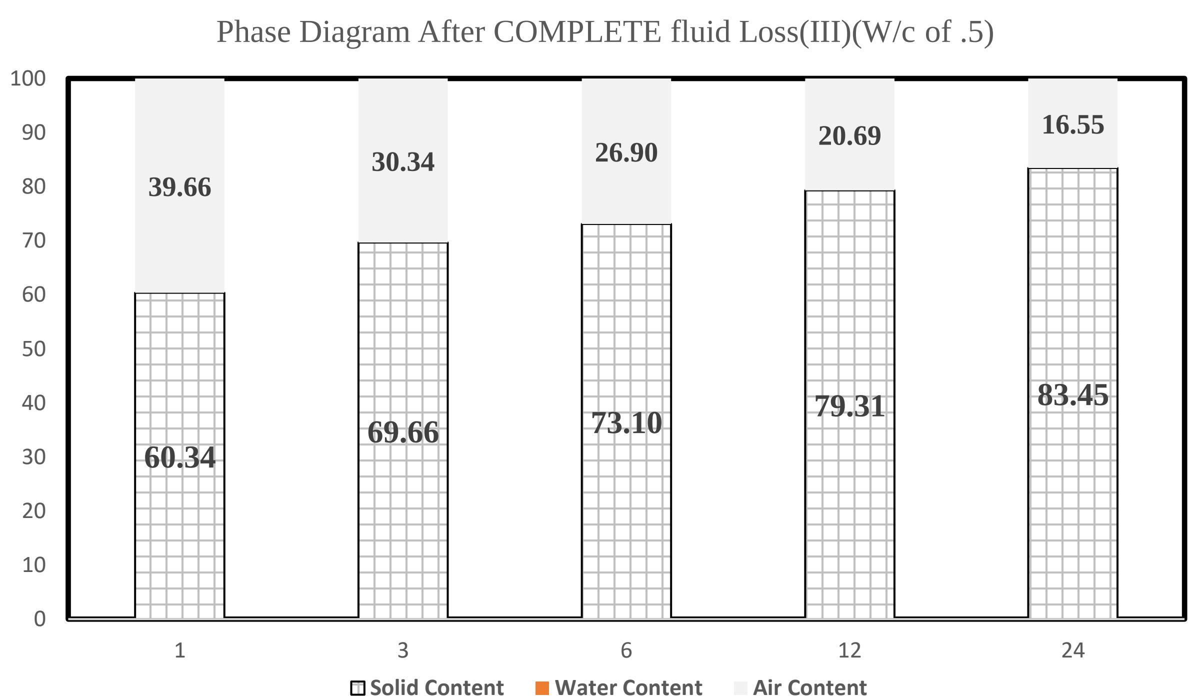

Figure 6-7 Phase Diagram after the complete fluid loss of samples cured 1Hour,3hour,6hour,12 hours and 24 hours.

After all the water has been expunged from the cement slurry, the resistivity of dry slurry is measured by allowing the gas to flow through the system at high pressure. The change in resistivity due to gas flowing through a cement slurry after 1 hour of curing and hardened cement is presented to show how resistivity is a sensitive parameter to detect gas leakage. In this stage, gas leakage is observed immediately as pressure is applied. The phase diagram before the test is shown to show the existing air void in the Cement. Gas leakage test is performed at this stage with increasing pressure after 1 hour and 24 hours of curing.

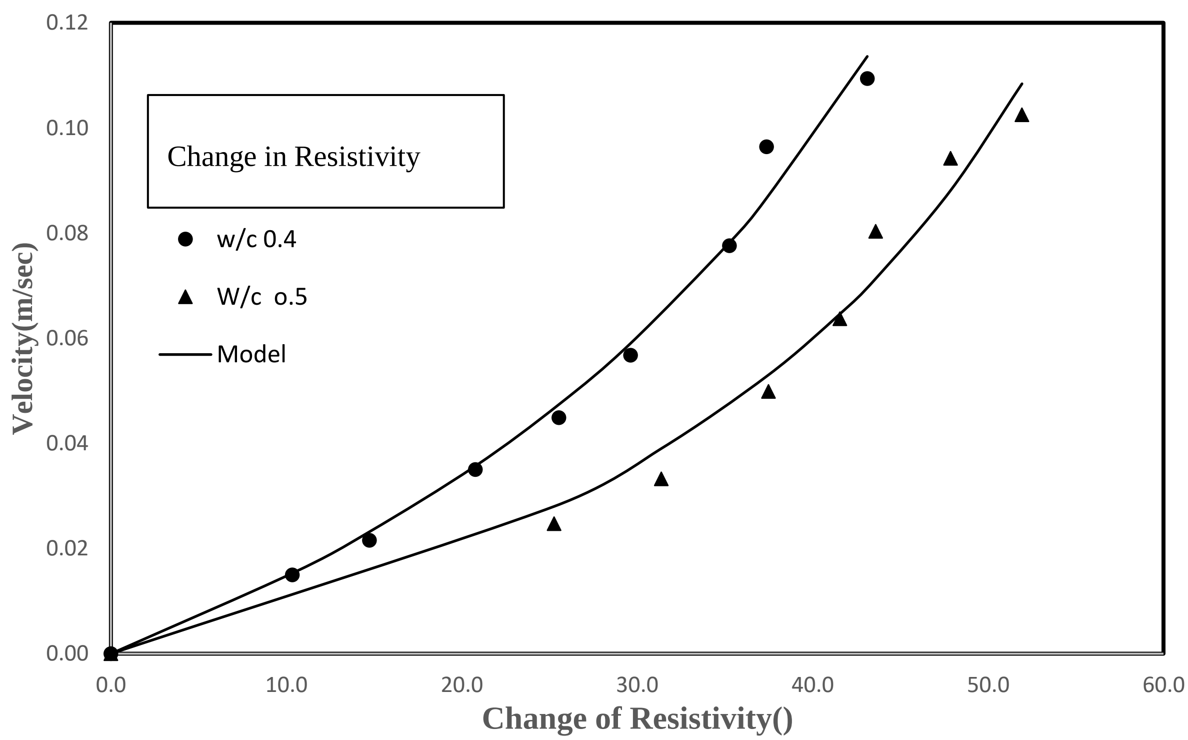

Figure 6-8 Change in Resistivity Due Applied Pressure in HPHT Cell after 1 Hour of Curing

Resistivity Change due to Gas Leakage After 1 Hour Curing

i. Smart Cement (w/c0.4)- Positive change in resistivity is observed due to applied gas pressure. At a gas leak velocity of 0.11m/sec, the resistivity change was 43.11%. The model parameters as are per equation were (769.95, -9.05)

ii. Smart Cement (w/c0.5)- Gas Leakage After 1 Hour Curing- Positive change in resistivity is observed due to applied gas pressure. At a gas leak velocity of 0.10m/sec, the resistivity change was 51.93%. The model parameters as are per equation were (1299.31, -15.82)

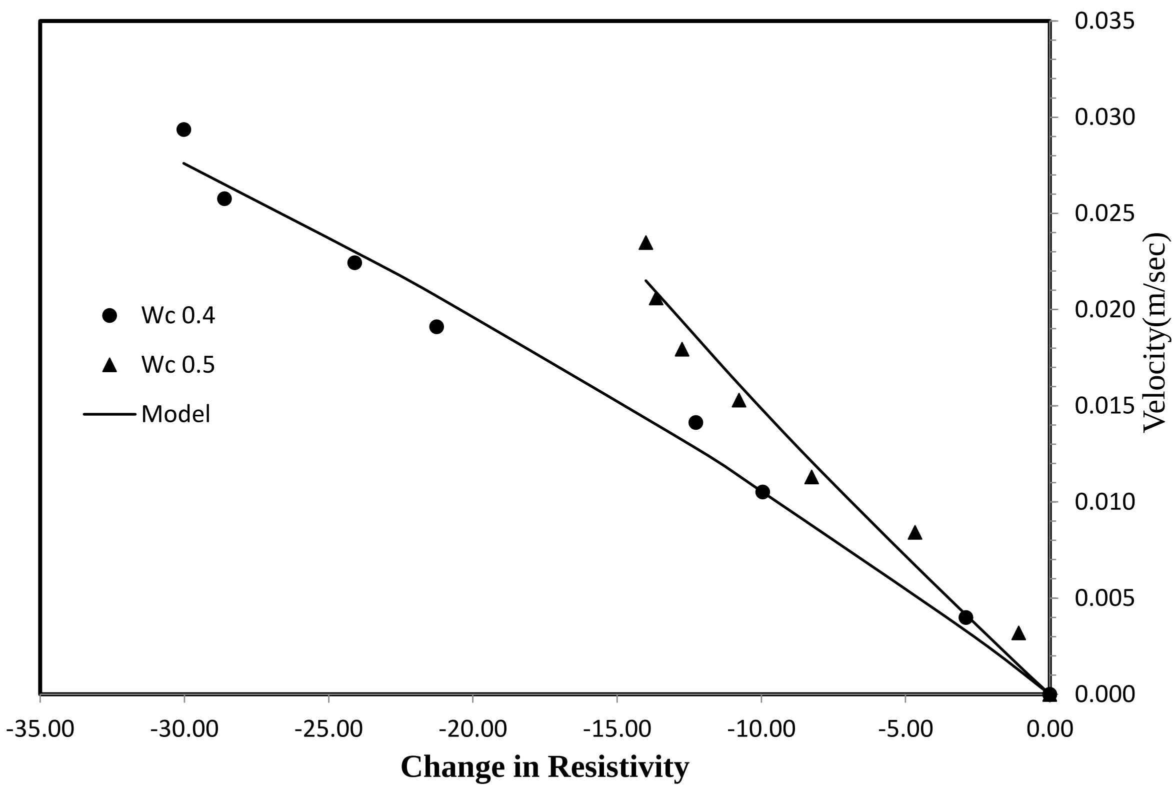

Figure 6-9 Change in Resistivity after 24 hours of curing (no free water) due to high gas pressure.

Resistivity Change due to Gas Leakage After 24 Hour Curing

i. Smart Cement (w/c0.4)- At the hardened stage, a negative change in resistivity is detected due to applied gas pressure. At a gas leak velocity of 0.029m/sec, the resistivity change was -30.02%. The model parameters as are per equation were (-874.45,7.11)

ii. Smart Cement (w/c0.5)-Similarly, a negative change in resistivity is observed due to applied gas pressure. At a gas leak velocity of 0.10m/sec, the resistivity change was 51.93%. The model parameters as are per equation were (-717.37, -5.46)

Table 6-4 Gas Leak Correlation Model.

	A sec/m	B sec/m	R^2	RMSE	Figure
1 Hour Curing					
0.4 W/c	769.95	-9.05	0.99	0.0038	6c
0.5 W/c	1299.31	-15.82	0.99	0.0051	6c
24 Hour Curing					
0.4 W/c	-874.45	7.11	0.99	0.0011	6b
0.5 W/c	-727.37	-5.46	0.99	0.0013	6b

6.6) Gas Flow Model

A model has been proposed by Vipulanandan to quantify the gas leakage in the porous medium. This model is a non-linear model, and aptly describes the velocity with applied pressure. The model parameters were compared with Darcy ‘s law.

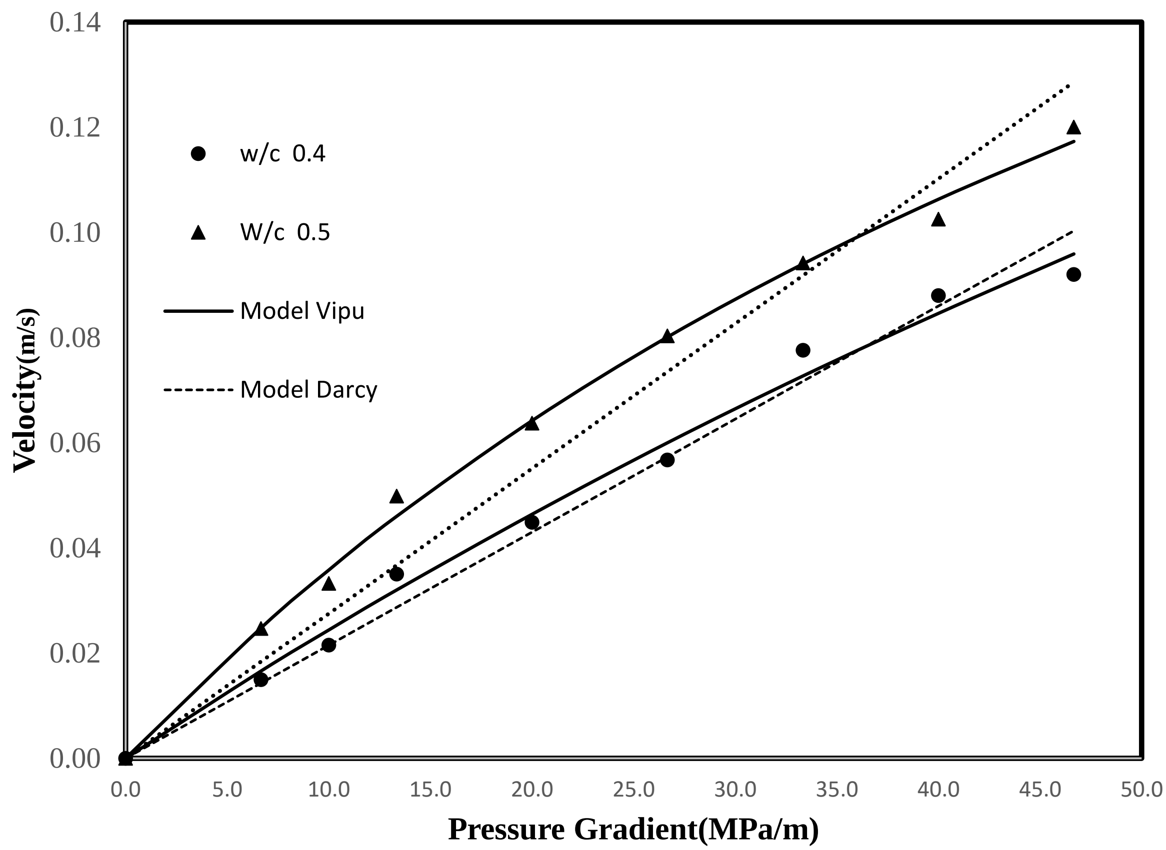

Figure 6-10 Velocity of Discharge after 1 Hour of Curing.

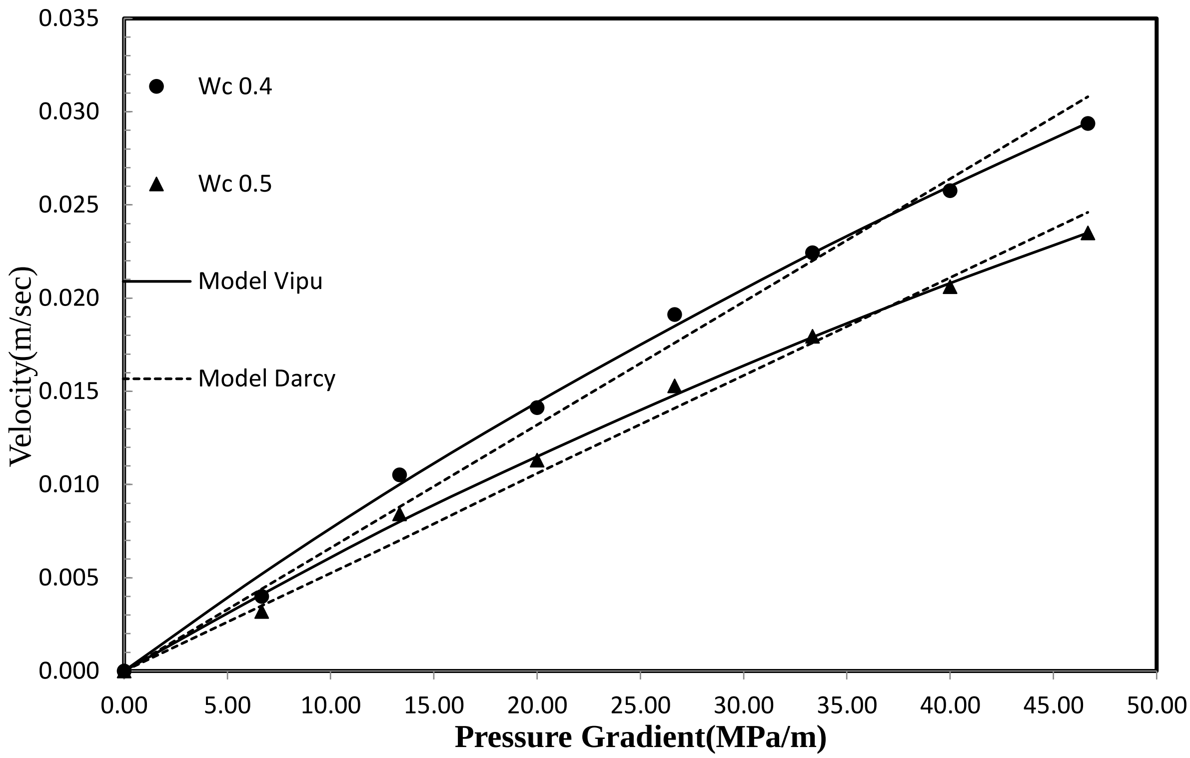

Figure 6-11 Velocity of Discharge after 24 Hour of Curing.

Due to continuously applied pressure, a gas leak occurs from the porous cement slurry and hardened cement. The gas leak velocity at the slurry stage and the hardened stage is modeled as per Darcy's law and Vipulanandan Fluid Flow Model. Gas leak velocity is modeled with Darcy's law and Vipulanandan model after 1 hour and 24 hours. RMSE error observed in the case of the Vipulanandan model was less compared with Darcy's law.

Table 6-5 Gas Leak Test Model Parameters for Darcy's Law and Vipulanandan Fluid Flow

	Darcy 's Law			Vipulanandan Fluid Model				
	k (m/sec)	R^2	RMSE (m/s)	C psi.sec/ft^2	D sec/m	R^2	RMSE (m/s)	Figure
1-hour Curing								
	0.0022	0.99	0.0033	422.32	0.49	0.99	0.0032	7a
	0.0027	0.99	0.0037	246.86	3.23	0.99	0.0022	7a
24 Hour Curing								
	0.00066	0.99	0.0011	1237.95	7.50	0.99	0.0005	7b
	0.00052	0.99	0.0008	1547.45	9.38	0.99	0.0004	7b

Due to continuously applied pressure, a gas leak occurs from the porous cement slurry and hardened cement. The gas leak velocity at the slurry stage and the hardened stage is modeled as per Darcy's law and Vipulanandan Fluid Flow Model. Gas leak velocity is modeled with Darcy's law and Vipulanandan model after 1 hour and 24 hours. RMSE error observed in the case of the Vipulanandan model was less compared with Darcy's law.

Gas Leak Due to Applied Pressure After 1 and 24 Hours Curing.

i. Smart Cement (w/c0.4)- The velocity of gas leak reduced significantly as cement hardened. Permeability obtained from Darcy law after 1hour and 24 hours of curing were 0.0022m/s and 0.00066m/s. Model parameters for the Vipulanandan Model after 1 hour and 24 hours of curing were (422.32, 0.49) and (1237.5, 7.50), respectively.

ii. Smart Cement (w/c0.5)- The velocity of gas leak reduced significantly as cement hardened. Permeability obtained from Darcy law after 1hour and 24 hours of curing were 0.002m/s and 0.00052m/s. Model parameters for the Vipulanandan Model after 1 hour and 24 hours of curing were (246.86, 1547.5) and (1237.5, 7.50), respectively.

6.7) **Summary**

1) Initial resistivity of w/c of 0.5 is lower than the initial resistivity of W/c of 0.4. The compressive strength of cement is reduced with increasing w/c ratio, and consequently, the piezo resistivity is reduced.

2) Cement with higher w/c 0.5, has more water for hydration. Thus more water is required to be expunged from the cement slurry at various stages of curing compared with w/c 0.4.It indicates that cement slurry with higher W/c ratios is more capable of withstanding gas migration compared with lower W/c ratios.

3) Gas Migration initially causes fluid loss in the cement slurry, and a positive change in resistivity is observed. As the cement hydrates, fluid loss decreases, and change in resistivity decreases. The trends observed for different w/c ratios are similar.

4) At all duration of curing, it was noted that there is a critical fluid loss, the fluid loss volume at which there is a formation interconnected pores. Gas leakage is observed after critical fluid loss.

5) In the second stage of gas migration test (free water is absent due to removal in 1st stage), the applied pressure gradient is increased and the change in velocity and resistivity is observed. After one hour of curing, the difference in resistivity is positive, and after 24 hours, the change in resistivity of the hardened cement is negative.

6) Gas leak occurring in cement due to application of pressure has been modeled on Darcy Law and Vipulanandan Gas Leak Model. In the Vipulanandan model, the permeability is pressure-dependent and more accurately predicts the velocity of the gas flow as it has a low RMSE compared with Darcy Law.

CHAPTER 7 SOIL

In this chapter, the mechanism of clay soil treatment with polymer has been investigated by measuring the changes in the electrical properties of soil. The effect of polyacrylamide polymer addition onto clay soil is described by studying the electrical properties. Standard compaction and swelling test were done as per the ASTM standard to check the behavior of soil. The change in the plasticity index of soil, the resistivity of soil, the electrical impedance curve of untreated and treated saturated soil has been examined. Additionally, the electrical impedance of the untreated and treated soil is investigated and using equivalent circuits, the bulk and contact resistance is predicted.

Additionally, in this chapter the electrical impedance method has applied detect the freezing of soft soil. Artificial laboratory made soft soil is exposed to temperature variations below sub xero conditions and the change in electrical measurements is quantified using electrical impedance method, the change in stress due to freezing is modelled using p-q model.

This chapter is subdivided into sub chapters which are

7.1) Electrical Characterization of Polymer Treated Expansive Clay.

7.2) Characterizing the effect of Ground Freezing on the clay soil Behavior.

7.1) Electrical Characterization of Polymer Treated Expansive Clay.

7.1.1) Index Properties.

After polymer treatment onto the dry soil, the liquid limit and plastic limit test are repeated on the treated soil. The test results are summarized below.

Table 7-1 Index Properties of Soil after Polymer Treatment.

% Polymer Treated	Soil A			Soil B			Soil C		
	LL	PL	PI	LL	PL	PI	LL	PL	PI
0	36	18	18	86.41	22.5	63.91	53.91	18.5	35.41
2.5	34.5	17.6	16.9	68.81	20.5	48.31	47.21	17.5	29.71
5	32.5	17	15.5	56.05	19.5	36.55	43.21	16.5	26.71
7.5	30.5	16.75	13.75	51.04	18	33.04	39.41	16	23.41

The liquid limit and plastic limit of soil A, soil B, and Soil C showed a similar trend. Addition of 2.5%, 5% and 7.5% polymer on soil A reduced the LL by 4.16%, 9.72%and 15.21, on soil B polymer addition reduced the LL by 20.36%, 35.13% and 40.93%and on soil C polymer addition reduced the liquid limit by 7.75%, 12.38% and 16.78%.Similarly, trends were observed in case of Plastic Limit. Reduction in liquid limit and plasticity index leads to a decrease in the plasticity index. Plasticity index is reduced by 6.1%,13.8% and 23.6% respectively for Soil A, 24.2%, 42.3% and 48.3% respectively for Soil B and 16.09%, 24.5% and 33.88% respectively for Soil C respectively for addition of 2.5%, 5% and 7.5% polymer into soil.

From the Atterberg tests, it is clearly observed that polymer addition affects the index properties of soil. Based on the plasticity index, the soil expansivity can be classified using Holtz and Gibbs and Chen criteria.

Table 7-2 Expansivity Characterization Based On Holtz & Gibbs and Chen Criteria.

Soil A	Holtz and Gibbs	Chen Criteria	**Soil B**	Holtz and Gibbs	Chen Criteria	**Soil C**	Holtz and Gibbs	Chen Criteria
0%	Low	Low	0%	Very High	Very High	0%	Very High	Very High
2.5%	Low	Low	2.5%	Very High	Very High	2.5%	Medium	Medium
5%	Low	Low	5%	Very High	Medium	5%	Medium	Medium
7.5%	Low	Low	7.5%	Medium	Medium	7.5%	Medium	Medium

The addition of polymer coats the clay particle and inhibits their ability to coagulate. A coat formation occurs on top of clay particles.

7.1.2) Compaction Test

Compaction test were performed on Soil A, Soil B and Soil C, after polymer treatment. Using ASTM standard, all the tests were performed. The effect of polymer addition on the dry densisyt and optimum moisture content of soil is investigated.

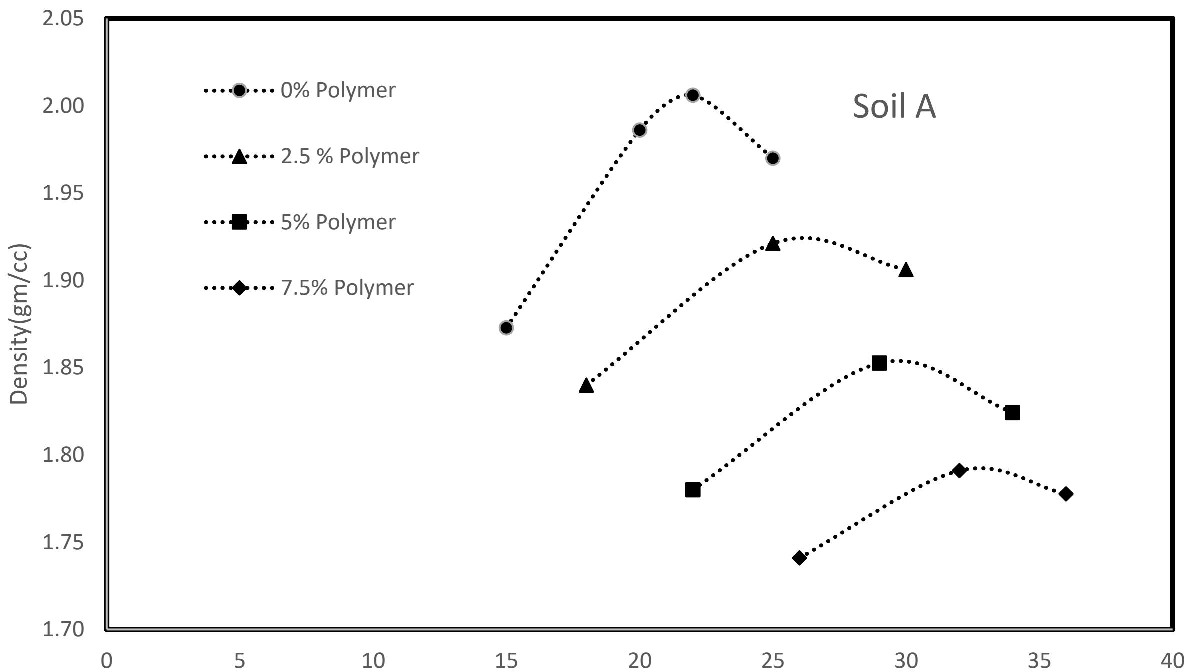

Figure 7-1 Density of treated and untreated Soil A.

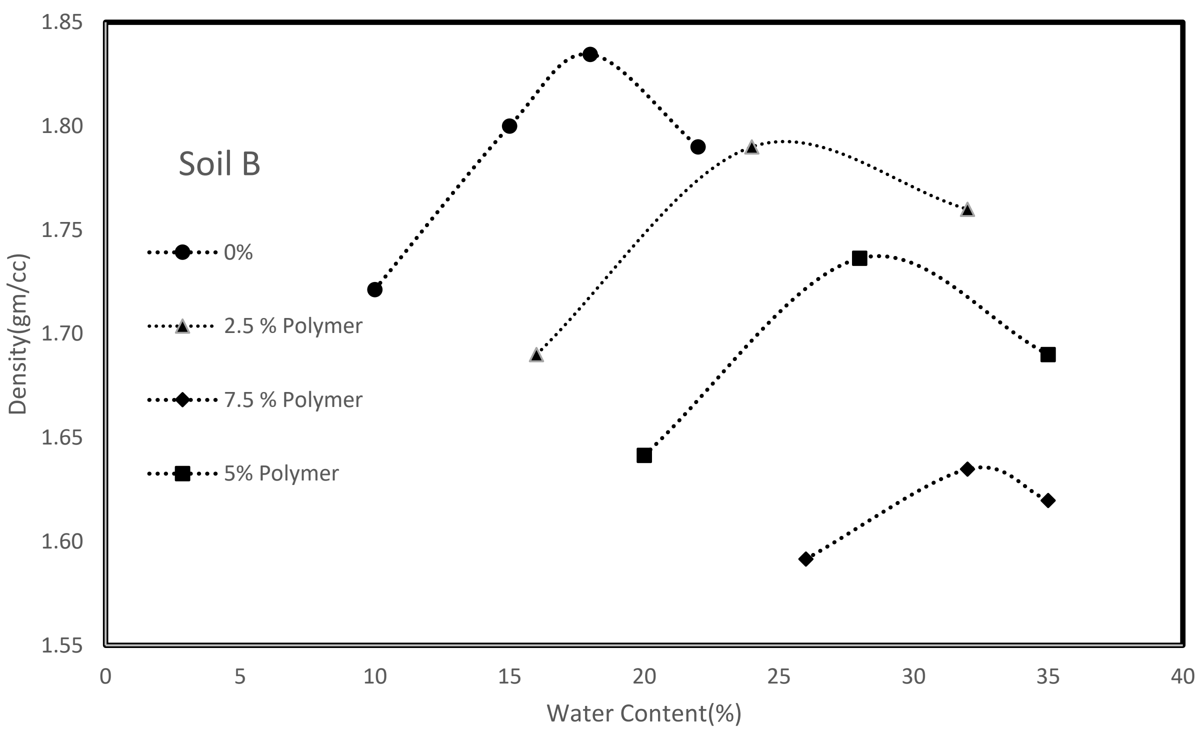

Figure 7-2 Density of treated and untreated Soil B.

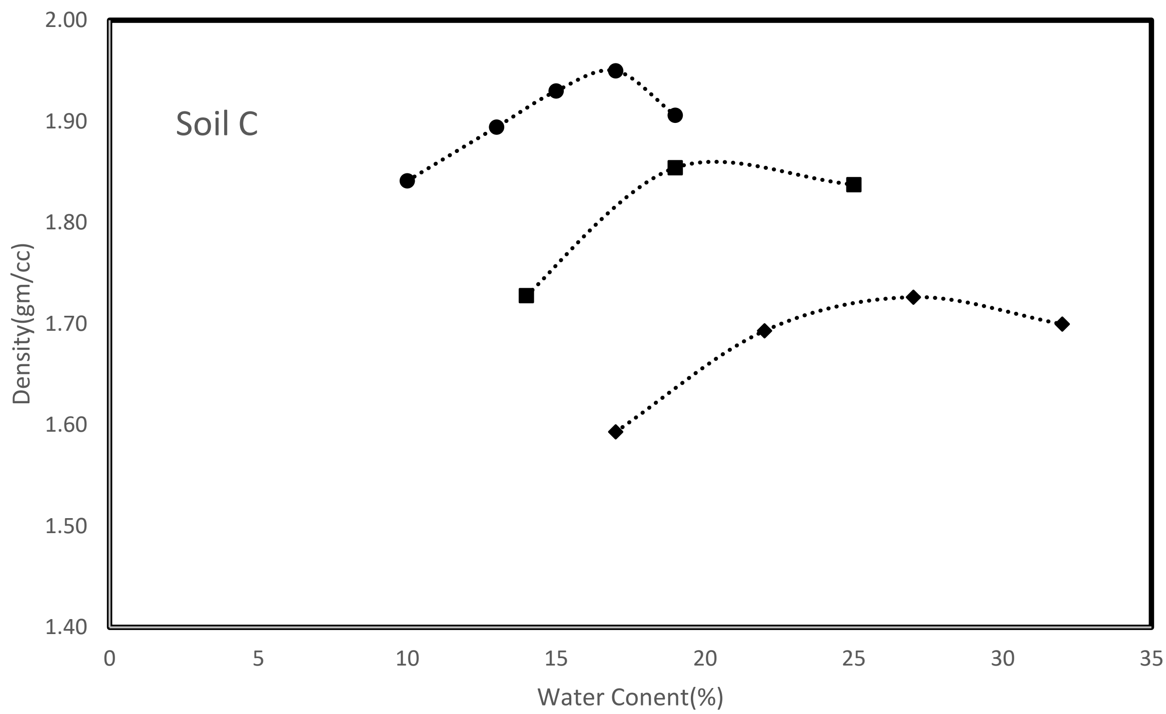

Figure 7-3 Density of treated and untreated Soil C

The compaction test of soil samples before and after polymer treatment has been analyzed. The maximum dry density for untreated sample and treated sample with 2.5%, 5% and 7.5% polymer by weight was 2.01(gm/cc), 1.92(gm/cc), 1.85(gm/cc) and 1.79(gm/cc) with optimum moisture content of 22, 25, 29 and 32 respectively. In case of soil B, maximum dry density of soil treated by polymer with 0%, 2.5 %, 5% and 7.5% was 1.83(gm/cc), 1.79(gm/cc), 1.74(gm/cc) and 1.63(gm/cc) with an optimum moisture content of 18%, 24% ,28% and 33%, for soil B, the maximum dry density was 1.89((gm/cc), 1.85(gm/cc), and 1.73(gm/cc) with on optimum moisture content of 17%, 19% and 27% respectively. Polymer treatment reduced the density of treated soil and in increase in optimum moisture content is observed.

The polymer addition of soil reduces the dry density of soil, and there is an increase in optimum moisture content. With increasing polymer content, dry density gets reduced, and water content increases.

7.1.3) Electrical Impedance curve of the Soil Treated by Polymer.

The electrical properties of soil are measured with different polymer percentage and water content. The impedance and resistivity of all the soil with varying moisture content were measured and it was found to be Case II.AC measurement was used to measure the change in electrical properties of soil due to polymer additions. The electrical impedance curve for Soil treated with polymer at 10% moisture content is plotted. At a particular moisture content, impedance curves soil with and without treatment is plotted. Impedance curve show a definitive trend. Impedance curves for soil A, soil B and soil C with different percentages of polymer is shown.

i. Soil A- The impedance curve of soil A with different polymer content followed Case 2 electrical model. With the addition of polymer on Soil A, the Rb, Rc and Cc at different polymer content were plotted in Table 7-3
ii. Soil B- The impedance curve of soil B with different polymer content followed Case 2 electrical model. With the addition of polymer on Soil A, the Rb, Rc and Cc at different polymer content were were plotted in Table 7-3
iii. Soil C- The impedance curve of soil A with different polymer content followed Case 2 electrical model. With the addition of polymer on Soil A, the Rb, Rc and Cc at different polymer content were were plotted in Table 7-3

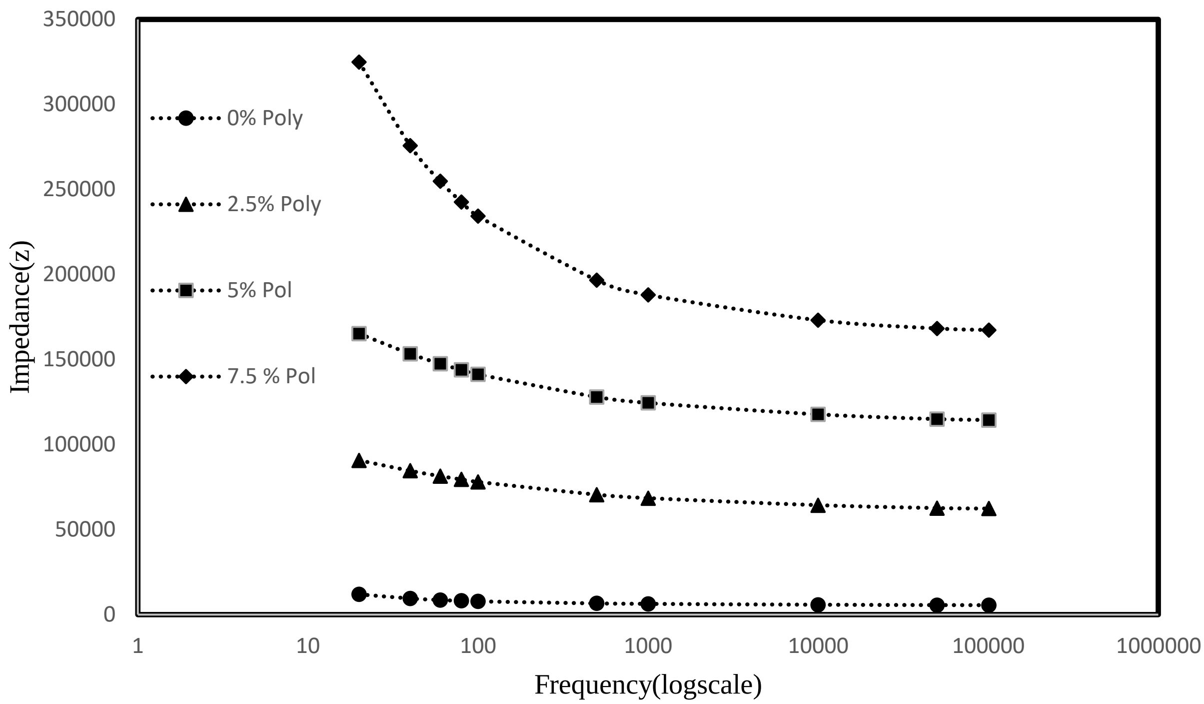

Figure 7-4 Impedance Curve of Soil A with varying polymer content at 10% moisture content.

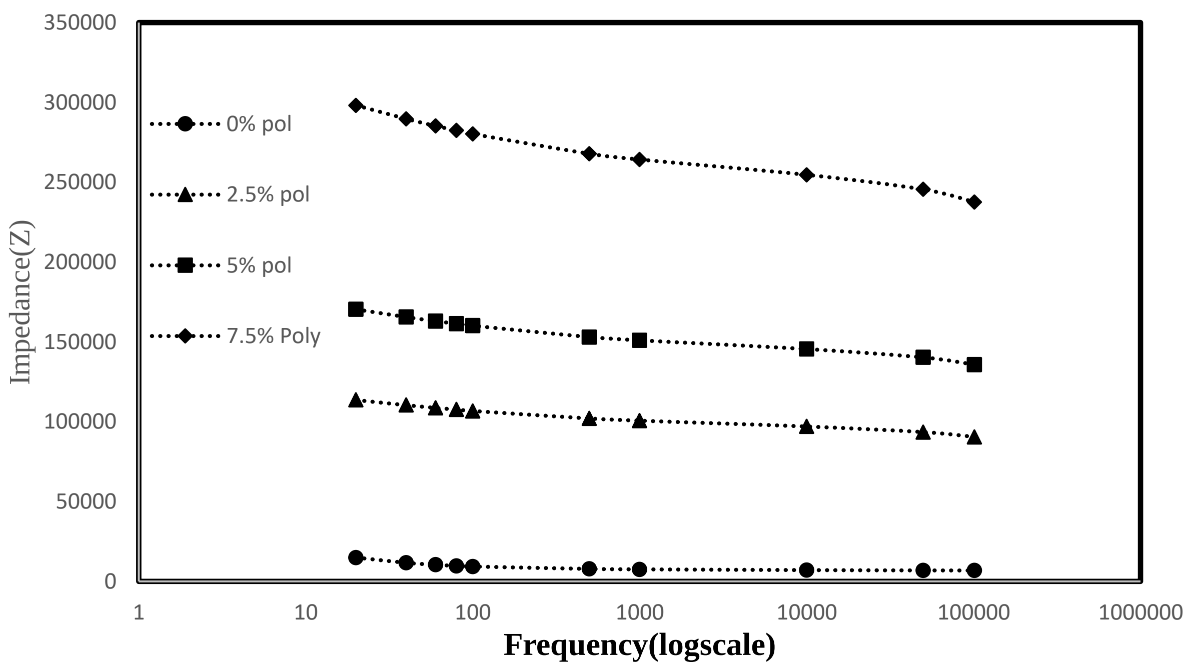

Figure 7-5 Impedance Curve of Soil B with varying polymer content at 10% moisture content.

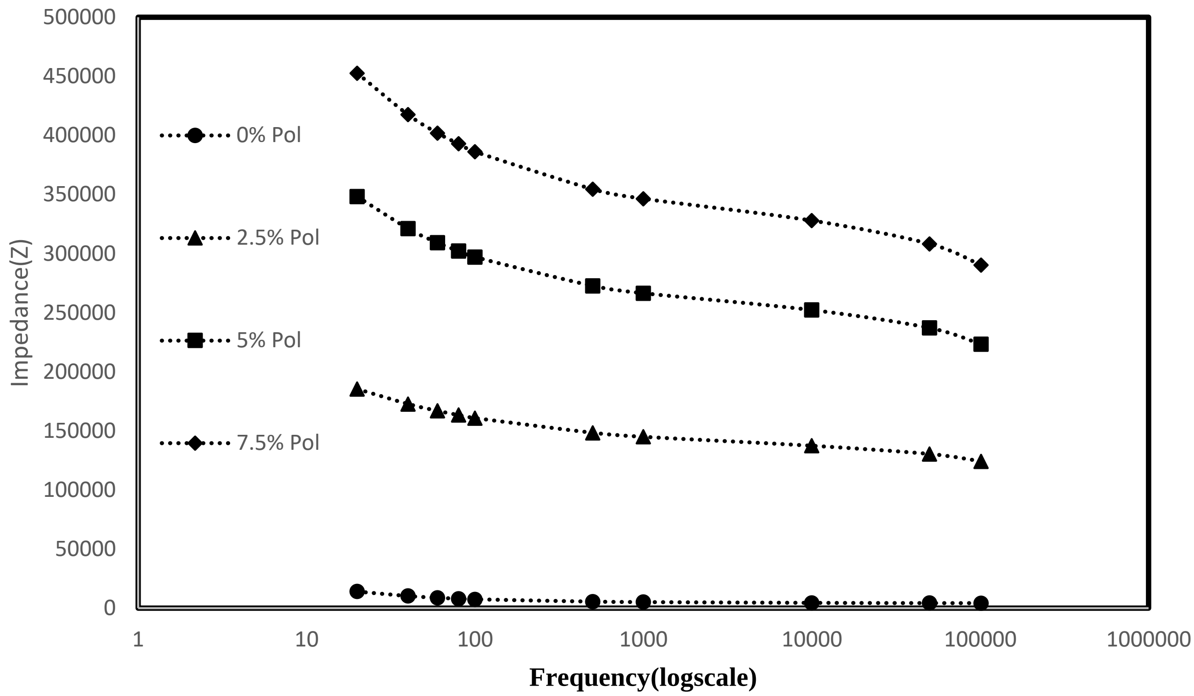

Figure7-6 Impedance Curve of Soil B with varying polymer content at 10% moisture content.

In soil samples, it was observed that the addition of polymer increased the resistivity of the soil. Similarly, trends were observed for all soils. With increasing water content, the resistivity of the soil decreased. Increasing moisture content on polymer treated soil reduced the resistivity. Polymer treatment of soil increases the resistivity by coating the soil particles with the polymer. Measuring resistivity of soil after polymer treatment can be used as a quality control measure in field applications. The addition of polymer onto soil increased the electrical resistivity. All the soil showed a similar pattern with increased polymer content. Electrical measurement can be used as a method for the detection and measurement of polymer treated soil.

Table 7-3 Electrical Resistivity of Soil Treated with Polymer at Different Moisture Content.

Soil Type	% Polymer Content	10% Moisture Content	20% Moisture Content	30% Moisture Content	40% Moisture Content.
SOIL A	0	35.33	8.38	5.71	3.22
	2.5	528.51	17.61	7.84	3.65
	5	650.94	20.05	10.56	7.27
	7.5	786.96	23.66	12.16	8.45
SOIL B	0	43.80	7.40	4.40	1.80
	2.5	521.20	44.30	9.50	3.40
	5	861.30	56.00	11.40	5.30
	7.5	1185.70	72.00	13.30	6.10
SOIL C	0	27.41	7.78	6.51	2.82
	2.5	687.11	30.10	10.96	4.29
	5	1177.88	41.82	12.16	5.95
	7.5	1468.75	60.38	16.12	7.50

In table 7-3, in soil A ,soil B and soil C the resistivity of the smaple calculated after measuring the impedance curve is tabulated. The change in resistivity of soil is affected by the percentage of polymer applied and varying moisture content.

7.1.4) Swelling Test of Soil

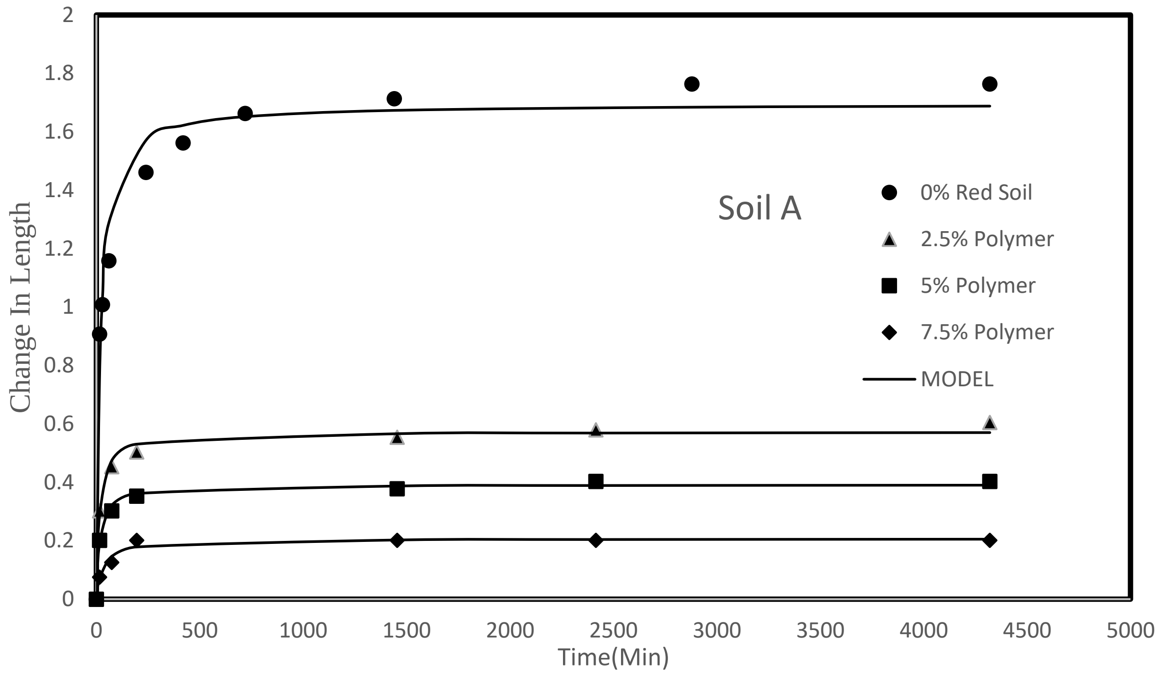

Figure 7-7 Swelling Behavior of Soil A treated by different percentages of polymer.

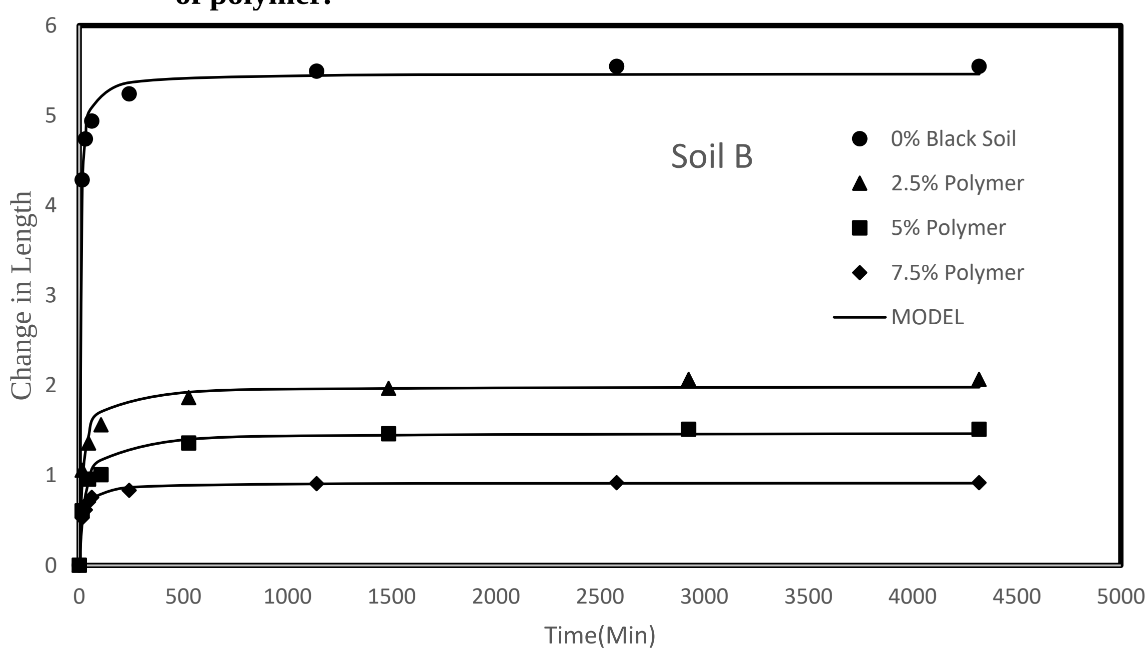

Figure 7-8 Swelling Behavior of Soil A treated by different percentages of polymer

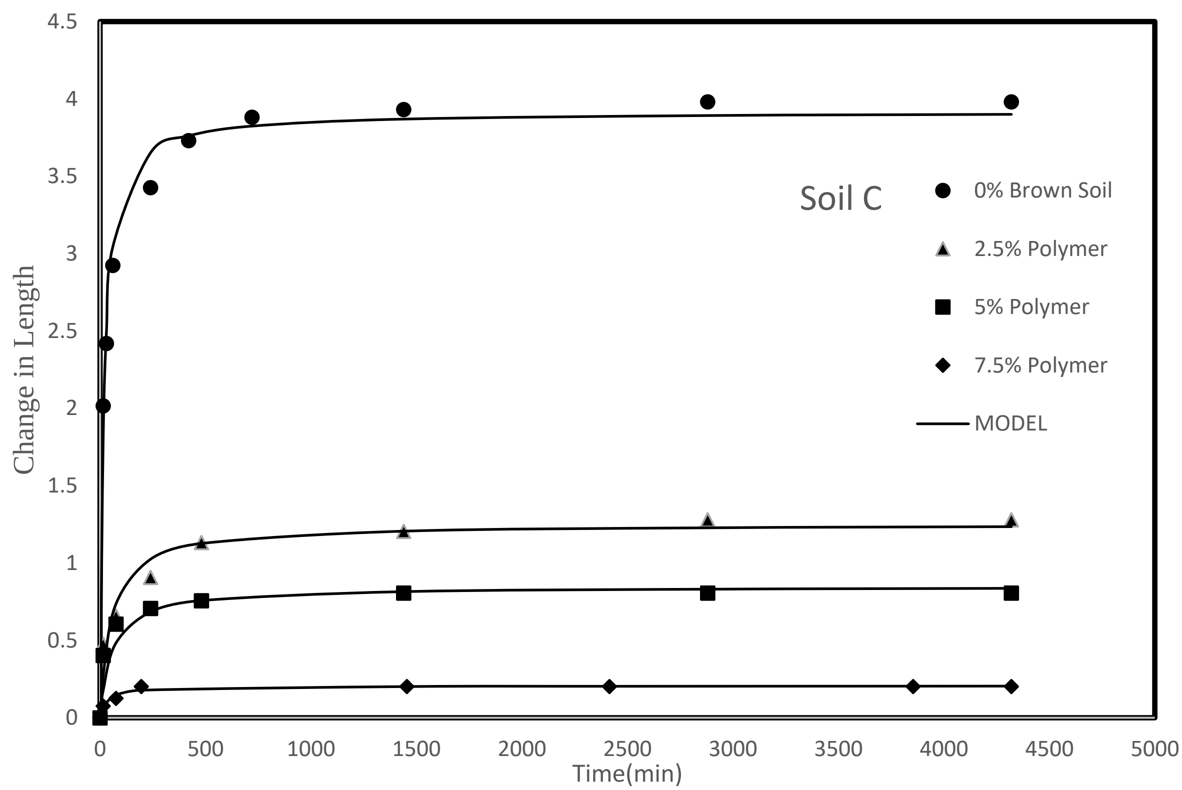

Figure 7-9 Swelling Behavior of Soil C treated by different percentages of polymer

The swelling test was carried in accordance with ASTM D4829-11. The sample for expansion index test was performed on the dry side of Optimum moisture content for 72hours. Using the hyperbolic model, the expansion of the clay was predicted with actual results. As expected, the maximum deflection was seen in the case of untreated soil and swelling behavior was reduced considerably with the addition of polymers. In case of soil A , 2.5%, 5%, and 7.5% polymer addition reduced the swelling index by 65%, 77% and 88% respectively. For soil B and Soil C, the addition of 2.5%, 5% and 7.5% polymer resulted in the reduction of 62%, 72% , 83% and 67%, 78%, 89% respectively.

The swelling behavior of soil is influenced by the type and percentage of clay minerals present in the clay. Polymer treated soil showed less swelling as polymer particles covered the soil particles and prevented it from swelling. Additionally, the ionic nature of polymer makes it effective in controlling the swelling potential of clayey soils.

Table 7-4 Model Parameters of Swelling Soil.

Soil Type	Polymer Addition	A	B	R^2
Soil A	0% Pol	11.86	0.58	.99
Soil A	2.5% Pol	26.75	1.74	.99
Soil A	5% Pol	41.57	2.55	.98
Soil A	7.5% Pol	148.28	4.83	.98
Soil B	0% Pol	0.81	0.18	.98
Soil B	2.5% Pol	8.70	0.50	.98
Soil B	5% Pol	18.42	0.62	.99
Soil B	7.5% Pol	15	1.09	.97
Soil C	0% Pol	4.40	0.25	.95
Soil C	2.5% Pol	42.10	0.79	.98
Soil C	5% Pol	67.01	1.17	.99
Soil C	7.5% Pol	146.81	4.85	.96

Discussion of Swelling Test- Using the hyperbolic model, the swelling behavior of soil is modeled. The model parameters are listed in Table 7-4. The model parameters can be used to predict the swelling behavior of soil. For soil A, soil B, and soil C, it is observed that with the increment of polymer, the model parameters also increased.

7.2) Characterizing the effect of Ground Freezing on the clay soil Behavior.

7.2.1) Electrical Characterization

Using LCR machine, the impedance of soil between 20-100Khz is measured. The measurement from LCR provides the real and imaginary parts of the circuit at different frequency ranges. By measuring the impedance curve, we separate the bulk resistance and contact resistance of the circuit. Impedance measurement.

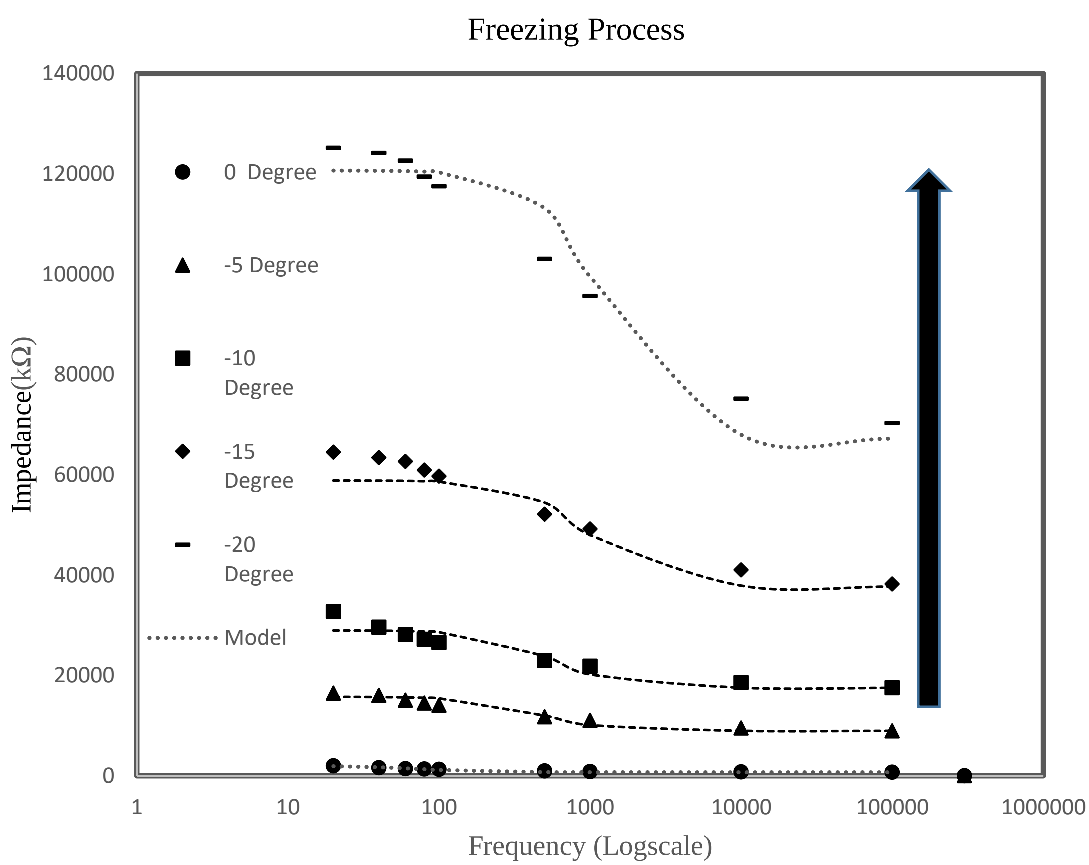

Figure 7-10 Electrical Impedance curve of Soft Soil at Different Temperatures

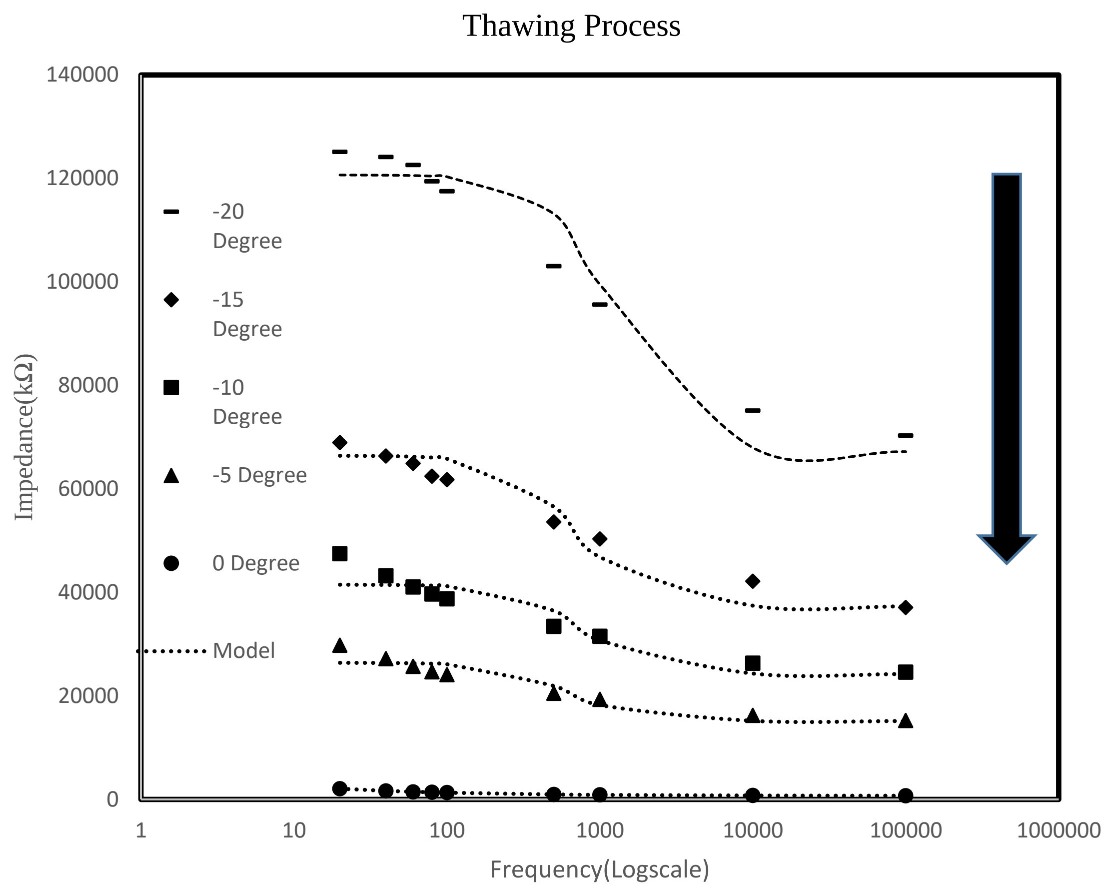

Figure 7-11 Electrical Impedance curve of Soft Soil at Different Temperatures While Thawing

In Figure 7-10 and Figure 7-11, the sensitivity of the measurement is shown while freezing soil. The impedance curves of soil at various temperatures are plotted. As temperature decreased the impedance curve increased upwards. Clearly, the change in impedance curve trends shows that the electrical impedance method can be used to detect the freezing of soil. Further, the same procedure is repeated for the thawing process. In the thawing process, the impedance curve of the soil samples followed the opposite trend. The change in bulk resistance of soil can be used as an indicator for determining and monitoring the freezing activity in soil.

Using the equation of 2, the Rb and Rc have been calculated. Additionally, the contact capacitance has been quantified. The change in resistance of soil can be used to monitor the soil condition while freezing.

Table 7-5 Model Parameter of The Impedance Curve

Freezing Process					
Temperature	Rb(Ω)	Rc(Ω)	Cc	R^2	RMSE
0^oC	702.45	646.24	3.28e-06	0.99	102.42
$-5\,^oC$	8939.54	3397.14	1.04e-07	0.98	1091.12
$-10\,^oC$	17445.7	5731.18	5.01e-08	0.98	1701.51
$-15\,^oC$	37111.65	10582.72	1.51e-08	0.99	3171.54
$-20\,^oC$	67916.54	26746.45	4.81e-09	0.99	5541.31
Thawing Process					
$-20\,^oC$	67916.45	26746.45	4.81e-09	0.93	5541.31
$-15\,^oC$	37452.52	14568.29	1.56e-08	0.98	2991.41
$-10\,^oC$	24335.65	8639.31	2.36e-08	0.98	2631.35
$-5\,^oC$	15193.62	5634.31	4.59e-08	0.99	1621.12
$0\ ^oC$	711.15	687.52	3.21e-06	0.99	115.41

To check the sensitivity of the measurements, a cyclic process of freezing and thawing is followed over the soft soil. The measurements are made at an interval of 5^0C, from 0^0C up to -20^0C. From the impedance curve, by using the equation, the bulk resistance and contact resistance were calculated. In the case of the freezing process, an increase in bulk resistance and contact resistance is observed with the drop of temperature. From the model, the contact capacitance is calculated. The contact capacitance decreased with an increase in temperature. When the reverse process is followed, the temperature is increased from -20^0C.Similarly, the temperature reading was taken at an interval of 5^0C. In this case, the bulk resistance and contact resistance are significantly reduced when compared. The contact capacitance increased when the temperature rises from -20^{0}C. Electrical impedance spectra is sensitive to temperature changes.

Electrical Resistivity of Soil

The electrical resistivity of the soil is calculated from the initial parameters. The change in electrical resistivity of the soft can be associated with the temperature.

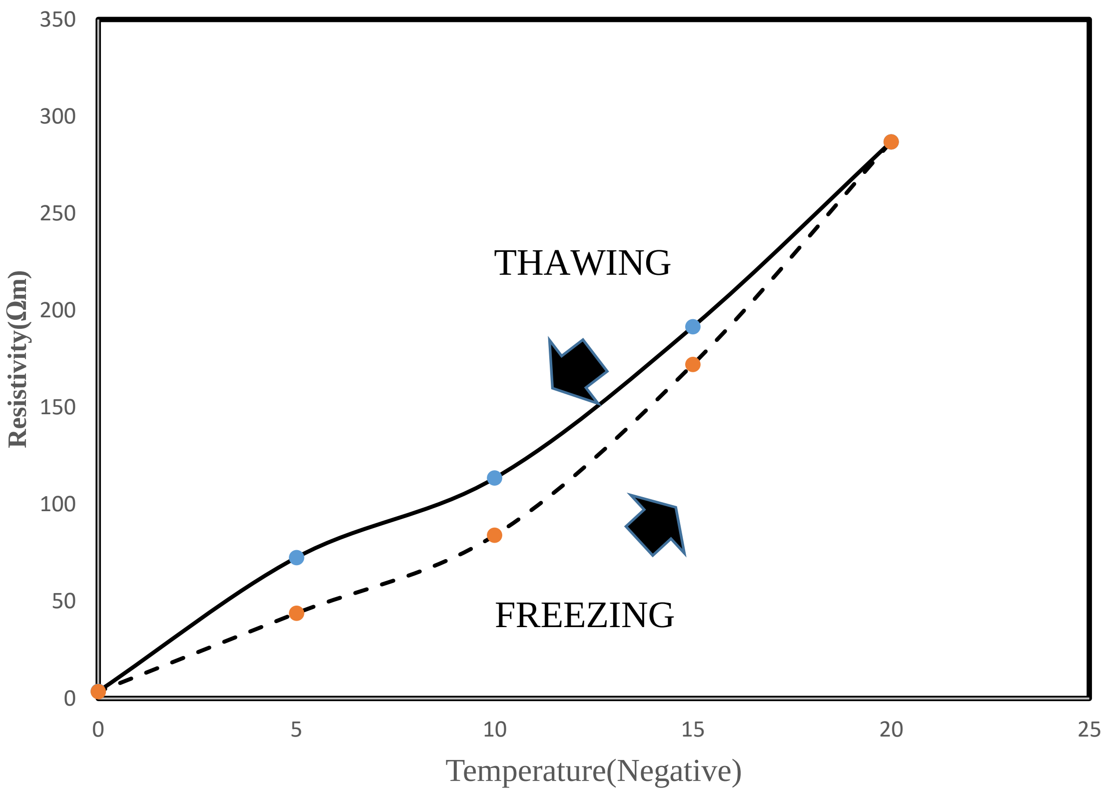

Figure 7-12 Effect of Temperature on Resistivity of Soil While Freezing and thawing.

In Figure 3, the effect of temperature on the freezing and thawing is provided.The resistance of the soil is converted to resistivity.Using Rb, the resistivity of the soil is calculated.The change in resistivity of during the freezing and thawing process is calculated.From the resistivity change, the temperature of the soil can be predicted.

Electrical Impedance Method is useful in monitoring the soil condition of soil. The sensitivity of electrical resistivity can be seen in the freezing and thawing process. In the freezing process, as the soft soil was frozen, the resistivity increased from 3.5Ω-m to 43.96 Ω-m, 84.08 Ω-m, 172.19 Ω-m, 286.89 Ω-m, when the temperature of soft soil was lowered to -5^{o}C, -10 ^{o}C, -15 ^{o}C and -20 ^{o}C. Then the thawing process is implemented, and the temperature is increased. When the thawing process is performed, the resistivity of the soil specimen reduces from 286.89 Ω-m to 189.3 Ω-m, 112.2 Ω-m, 71.8 Ω-m, 3.5 Ω-m when the temperature of soil specimen is increased to -15^{o}C, -10^{o}C, 5^{o}C and 0 ^{o}C.

7.2.2) Stress-Strain Curves for the soil

With decreasing the stiffness of soil increased. This change in stiffness was modeled using P-q model. As soil freezes, its strength increases. A compressive test on soil was conducted at different temperatures. Using the stress-strain model, the compressive strength of freezing soil com be predicted. The model parameters for the compression test at 0 ^{o}C, -5^{o}C, -10 ^{o}C, -15 ^{o}C and -20 ^{o}C were (0.39,0.22), (0.40,0.35), (0.50,0.49), (0.53,0.46) and (0.57,0.42) respectively. The coefficient of determination and root mean square error at 0 ^{o}C, -5^{o}C, -10 ^{o}C,-15 ^{o}C and -20 ^{o}C were 0.99, 0.99, 0.99, 0.99, 0.99 and 10.5 Pa, 33.27Pa, 10.76Pa, 10.71Pa and 52.1Pa.

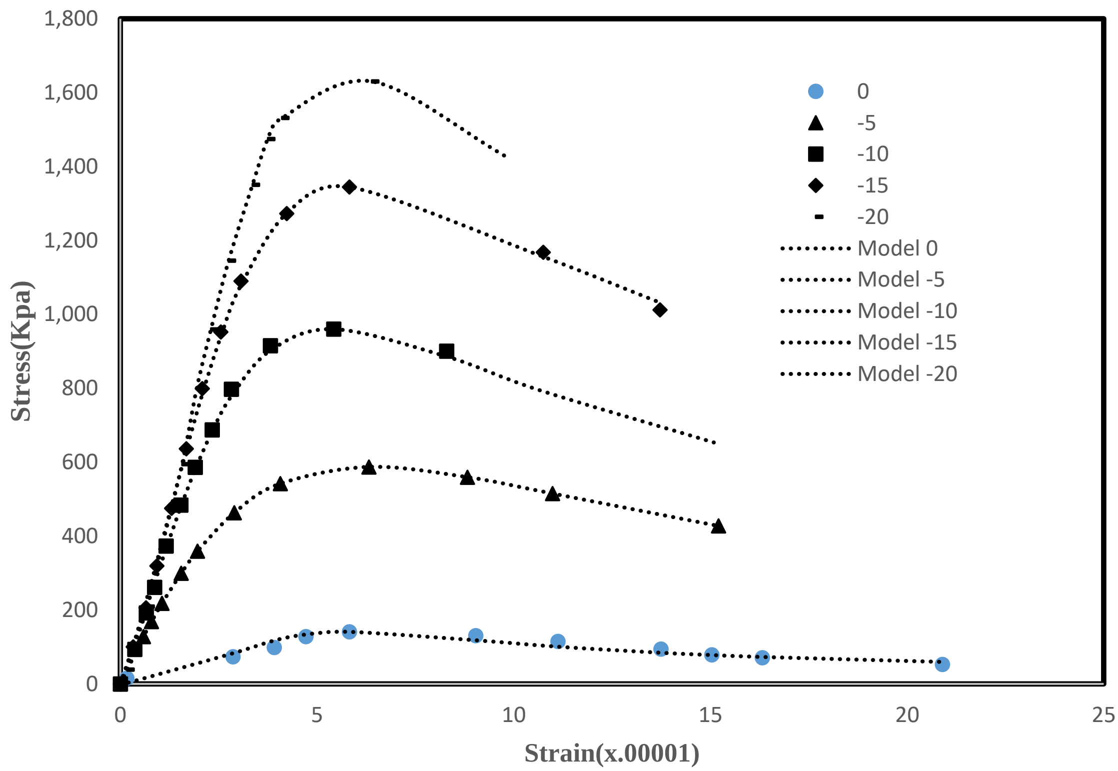

Figure 7-13 Using P-Q Model, the stress Strain Behavior is modeled.

Table 7-6 Stress-strain Model Parameters of Soft Soil at Different Freezing Temperature.

Temperature	p	q	σ (max)	R^2	RMSE(Pa)
0 Degree	0.39	0.22	140	.97	10.5
-5 Degree	0.40	0.35	587	.99	33.27
-10 Degree	0.50	0.49	959	.99	10.76
-15 Degree	0.53	0.46	1344	.99	10.71
-20 Degree	0.57	0.42	1630	.99	52.1

The compressive strength of soil increased from 140(KPa) to 587(KPa), 959(KPa), 1344(KPa), 1630(KPa) as the temperature was lowered from 0 ^{0}C, -5 ^{0}C, -10 ^{0}C,.-15 ^{0}C and -20 ^{0}C. Stress-strain.

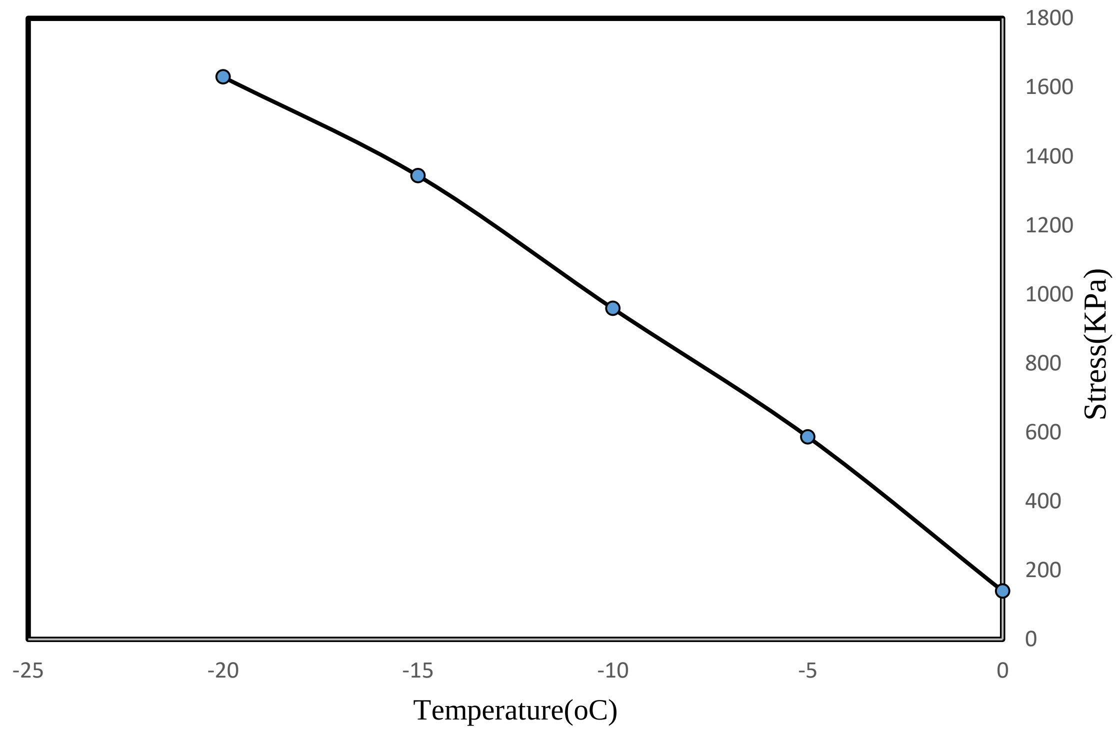

Figure 7-14 Effect of Reduction in Temperature on Compressive Stress of Soil.

It is evident in Figure 7-14, as the temperature was reduced from 0 ^{0}C to -20 ^{0}C, the compressive strength increased from 140 KPa to 1630KPa, an increase of 1064% is observed. The tensile strength of ice varies from 0.7–3.1 MPa and the compressive strength varies from 5–25 MPa over the temperature range –10C to –20C.The freezing of ice lead to enhanced compressive strength in soft.

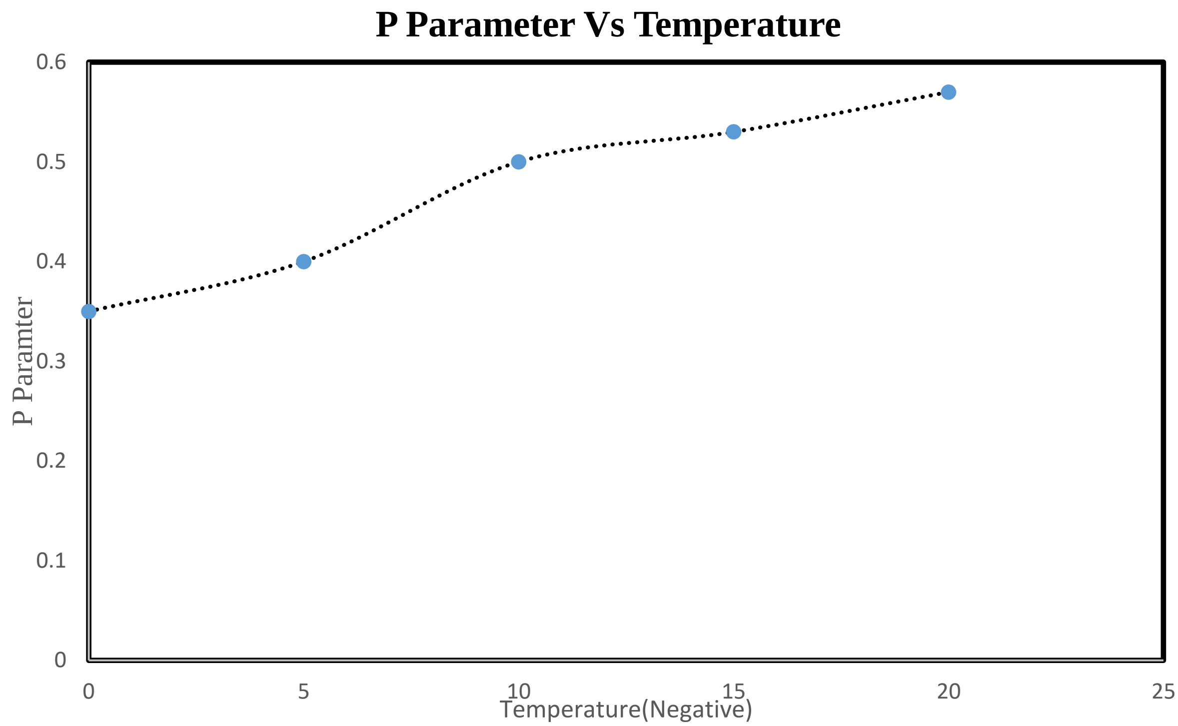

Figure 7-15 Correlation of P parameter with Freezing temperature.

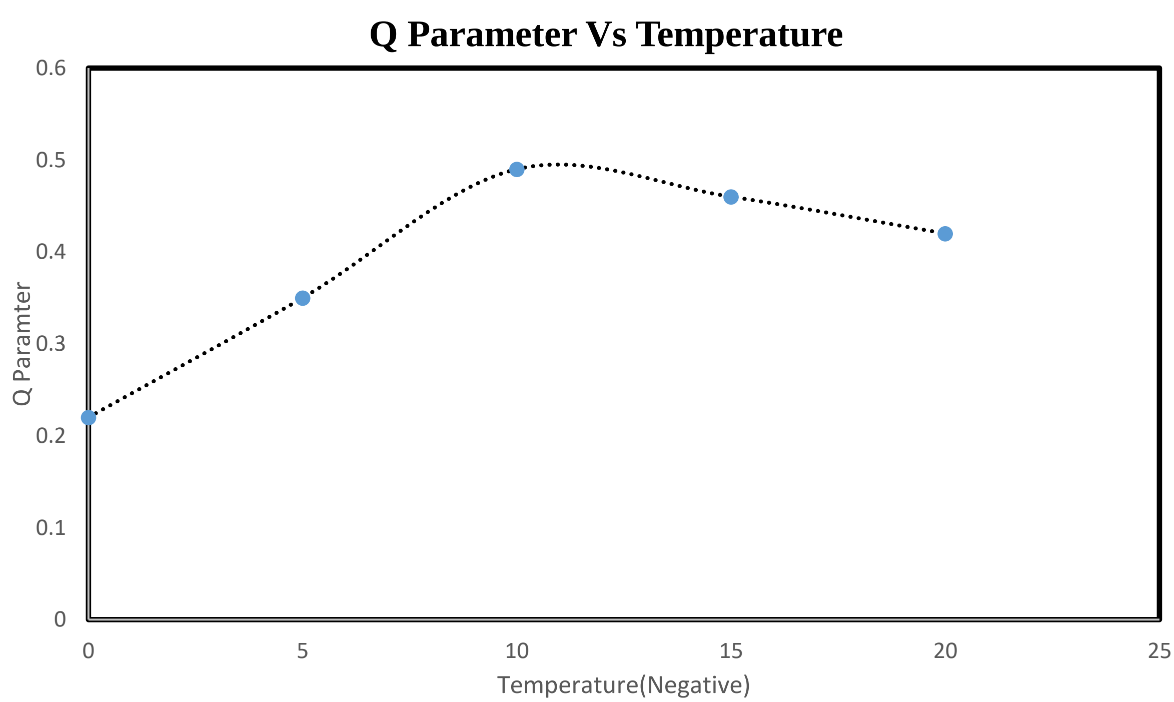

Figure 7-16 Correlation of q parameter with Freezing temperature

The model parameter can be effectively correlated with the temperature of the soil specimen. A definitive trend is being observed.

7.3)Summary

1) Polymer treatment of soil significantly affected the index properties of soil. Polymer treatment leads to a reduction in the plasticity index of soil.

2) Polymer treatment of soil affected the dry density of soil and the optimum moisture content of soil treated. A regular trend was found in the case of dry density and the optimum moisture content of soil. Polymer particles coated soil particles, which lead to an increased density at higher optimum moisture content.

3) The swelling test on polymer treated soil showed that polymer treatment of soil is beneficial in reducing the modified swelling index of soil. Polymer treatment on Soil A reduced the swelling by 65%, 77%, 88% respectively, on Soil B a reduction of 62%, 72%, 88% was observed and on soil C polymer treatment lead to a reduction of swelling by 67%, 78%, 89%.

4) The measurement of electrical measurement showed all the soil treated by using polymer showed CASE 2 behavior. Due to polymer addition, the electrical Impedance of the curve increased. Similar trends were observed for Soil A, Soil B, and Soil C.

5) The resistance measured by the impedance measurement can be used to measure the resistivity of soil, which is a material property.Soil resistivity increased with polymer addition at different moisture content. Further resistivity can be used in field applications as a quality control tool.

6) Electrical Impedance can be successfully employed to measure the freezing of soil at different temperature. By measuring the bulk resistance of soil specimens, the temperature of soil can be predicted which would be useful in artificial ground freezing monitoring.

7) Additionally, the electrical resistivity of the soil can be measured from the electrical impedance method. Electrical resistivity is a material property and can successfully employ to monitor the freezing of soil. The resistivity of the soil increased when the temperature of the soil is lowered down and reduces when the temperature is increased.

8) The compressive strength of soil increased due to freezing. Using the Vipulanandan model the stress-strain relationship was modeled. The model was used the coefficient of determination, and root mean square method.

9) The model parameters of stress-strain model showed correlation with the temperature of the soil specimen. Using the model parameter, the compressive stress of the soil specimen can be predicted for intermediate points.

CHAPTER 8 CORROSION OF COMPOSITES

Introduction

In this chapter, the composite corrosion has been investigated over 1 year. The samples are exposed to a rigorous process of cyclic corrosion. The effect of corrosion on electrical impedance curve over the time duration has been studied and monitored. The change in resistance, contact resistance, contact capacitance and resistivity is quantified in this chapter using Vipulanandan Model. Additionally, a high temperature investigation of steel plate has been put to quantify the effect of temperature on steel coupon corrosion.

This chapter has been subdivided into two subchapters

8.1) Corrosion Quantification in Cement Composites by electrical Impedance Method treated in a saline environment.

8.2) Corrosion quantification and detection of steel coupons exposed in high-temperature electrolytes.

8.1) Corrosion Quantification in Cement Composites by electrical Impedance Method treated in saline environment.

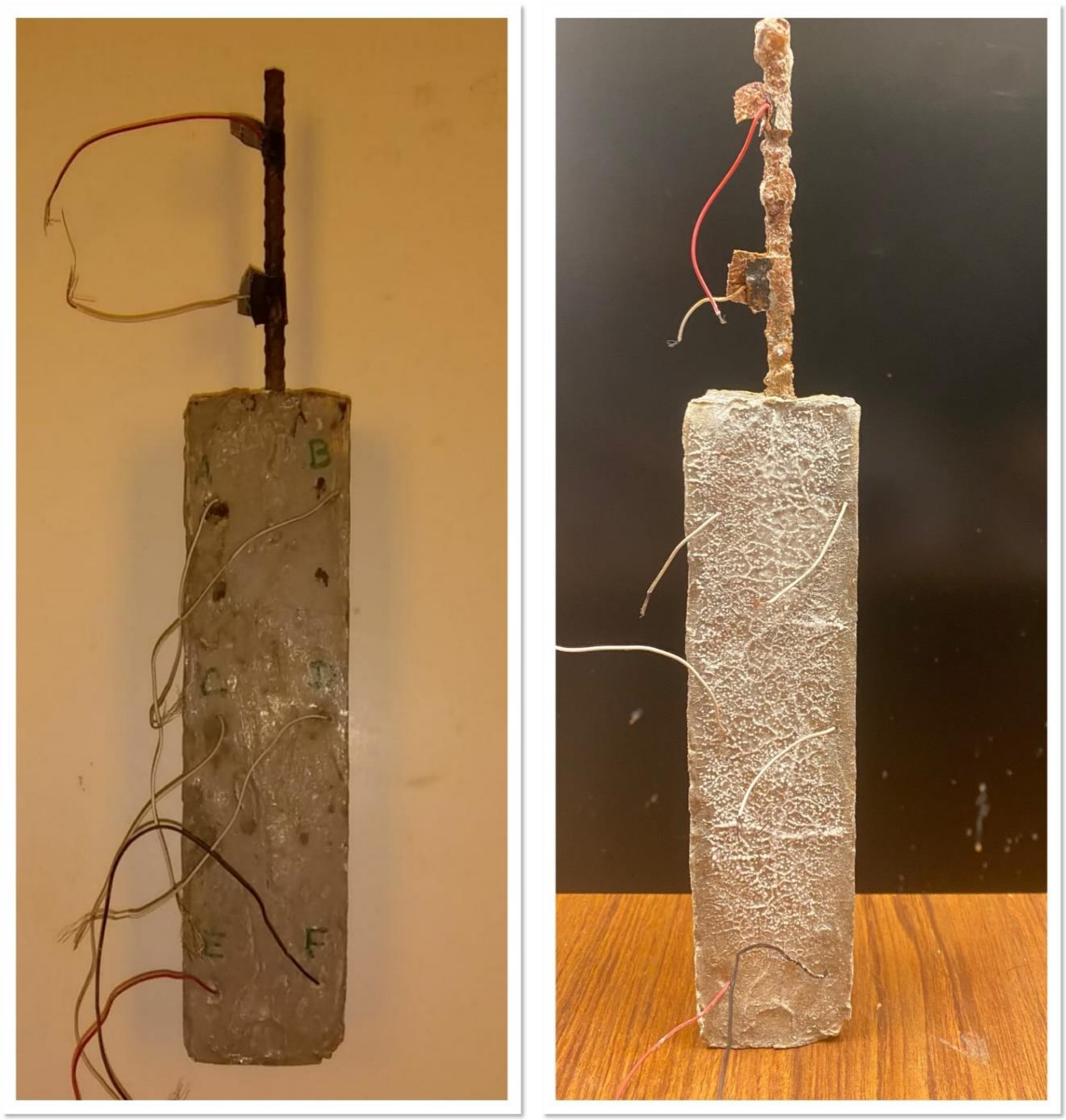

Figure 8-1 Image of cement composite before and after corrosion.

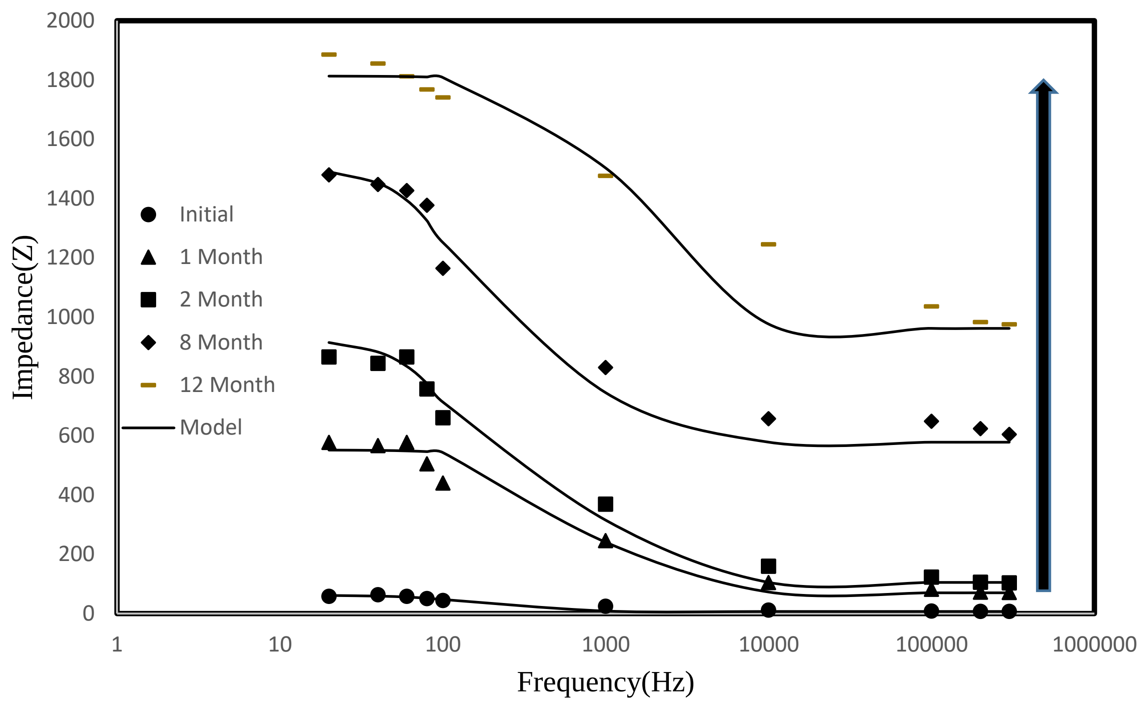

Figure 8-2 Impedance behavior of exposed steel in Cement Composite.

Table 8-1 Model Parameters of the equivalent circuit for the exposed steel.

	Rb(Ω)	Rc(Ω)	Cc	R^2	RMSE(Ω)
Initial	7.07	27.45	3.45e-05	0.94	5.78
1 Month	70.71	240.92	8.92e-06	0.96	48.16
2 Month	103	410.61	2.29e-06	0.94	86.71
8 Month	578	465.51	2.10e-06	0.93	97.14
12 Month	942	489.41	2.58e-07	0.92	100.02

After immersion, the initial resistance was 7.07Ωm, and it increased to 70.71 Ω,103 Ω,578 Ω and 942 Ω after 1month,2 month,8 months and 12 months immersion in a saltwater solution. Similarly, the contact resistance values also increased from 240.92 Ω,410.61 Ω, 463.31and 550Ω after 1month,2 months,8 months, and 12 months respectively. The change in resistance activity shows the ongoing phenomenon of corrosion inside the cement specimen. Similarly, the contact capacitance also decreased from the initial observed value of 3.45e-05F to 8.92e-05F, 2.29e-06F, 2.10e-06Fand 2.58E-07 F.

In terms of resistivity change, the resistivity of the sample increased by 777%, 1395%, 1587% and 1904% after 1month ,2 month ,8 month and 12 months of immersion. The coefficient of determination and root mean square error observed after the immersion interval of 1month, 3month, 8months and 12months were 0.99, 0.96, 0.92, 0.96, 0.98 and 22.96Ω, 6.97Ω, 10.46Ω, 91.57Ω, 294.75Ω respectively. The significant increase in resistance values indicate formation of corrosion products over the steel bar and inside the specimen.

8.1.2) Corrosion Between Steel and Cement Interphase.

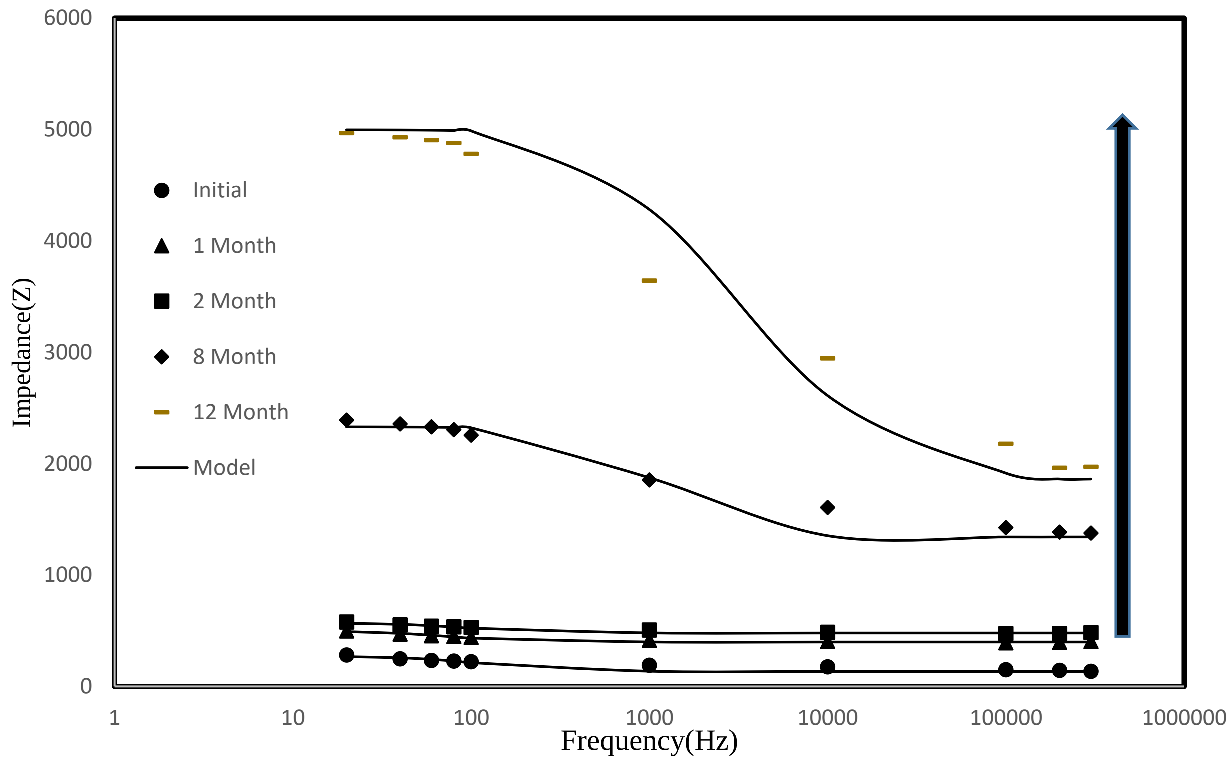

Figure 8-3 Impedance Behavior of Horizontal Combination interphase over time.

Table 8-2 Model Parameters of the equivalent circuit for the interphase.

	Rb(Ω)	Rc(Ω)	Cc	R^2	RMSE(Ω)
Initial	135	68	1.31e-05	0.99	22.96
1 Month	401	51	1.99e-05	0.96	6.97
2 Month	480	45	3.66e-07	0.92	10.46
8 Month	1342	494	2.29e-07	0.96	91.57
12 Month	1862	1567	5.52e-08	0.98	294.75

Figure 8-4 Impedance Behavior of Horizontal Combination CD over time.

After immersion, the initial resistance was 135 Ωm, and it increased to 401 Ω,480 Ω,1342 Ω and 1862 Ω after 1month,2 month,8 months and 12 months immersion in a saltwater solution. Similarly, the contact resistance values also increased from 68 Ω,51 Ω,494 Ω, and 1567 Ω after 1month, 2 months, 8 months and 12 months respectively. The change in resistance activity shows the ongoing phenomenon of corrosion inside the cement specimen. Similarly, the contact capacitance also decreased from the initial observed value of 1.31e-05F to 1.99e-05F, 3.66 e-07F, 2.29e-07F and 5.525.52e-08 F.

In terms of resistivity change, the resistivity of the sample increased by 197%,255%,894% and 1279% after 1month ,2 month ,8 month and 12 months of immersion. The coefficient of determination and root mean square error observed after the immersion interval of 1month, 3month, 8months and 12months were 0.99, 0.96, 0.92, 0.96, 0.98 and 22.96Ω, 6.97Ω, 10.46Ω, 91.57Ω, 294.75Ω respectively.

The significant increase in resistance values indicate formation of corrosion products over the steel bar and inside the specimen. The corrosion is affected by the concentration of salt, temperatures, electric conductivity of electrolyte.The interphase reading between the embedded steel bar and cement base is affected by the steel corrosion and deterioration of cement.This combination stimulates the oil well casing embedded inside the cement sheath.

8.1.3) Corrosion in Cement Measured Along Horizontal Direction.

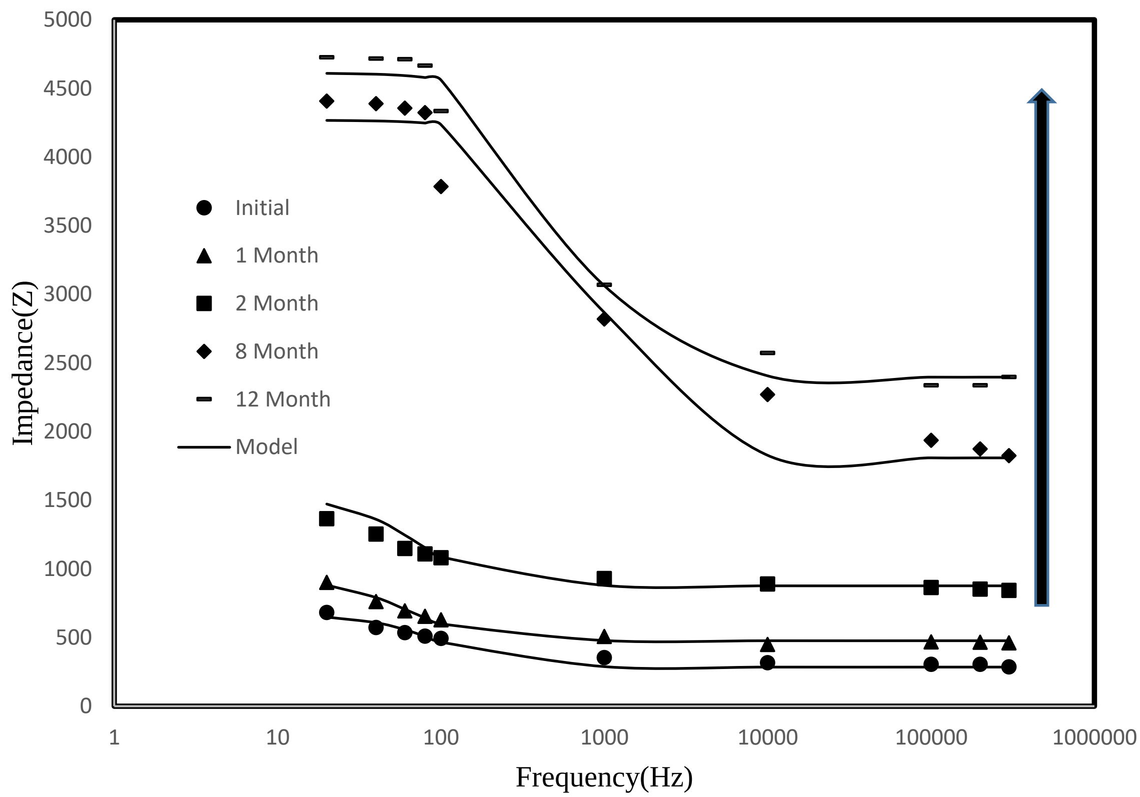

Figure 8-5 Impedance Behavior of Horizontal Combination AB over time.

Table 8-3 Model Parameters of the equivalent circuit for the Horizontal combination

	Rb(Ω)	Rc(Ω)	Cc	R^2	RMSE(Ω)
Initial	285	190	8.75e-05	0.99	30.88
1 Month	458	224	1.15e-05	0.99	20.15
2 Month	837	322	7.07e-06	0.86	90.21
8 Month	1809	1229	1.48e-07	0.98	217.31
12 Month	2396	1107	1.11e-07	0.97	171.08

After immersion, the initial resistance was 285 Ω and it increased to 458 Ω,837 Ω ,1809 Ω and 2396 Ω after 1month,2 month,8 months and 12 months immersion in a saltwater solution. Similarly, the initial contact resistance of 190 Ω values also increased to 224 Ω,322 Ω a 1229 Ω and 1331 Ω after 1month,2 month,8 months, and 12 months respectively. The change in resistance activity shows the ongoing phenomenon of corrosion inside the cement specimen. Similarly, the contact capacitance also decreased from the initial observed value of 1.31e-05F to 1.99e-05F, 3.66e-07F, 2.29e-07F, and 5.525.52e-08 F.

In terms of resistivity change, the resistivity of the sample increased by 197%,255%,894% and 1279% after 1month, 2 months, 8 month and 12 months of immersion. The coefficient of determination and root mean square error observed after the immersion interval of 1month, 3month, 8months, and 12months were 0.99, 0.99, 0.86, 0.98, 0.97 and 30.88Ω, 20.15Ω, 90.21Ω, 217.31Ω, 171.08Ω, respectively.

Over time the chloride ions get absorbed on the C-S-H surface, these adsorption causes the cement resistivity to increase over time. Continuous immersion of cement specimen inside saltwater affects the cement microstructure(Lia et al., 2015 and Yoshida et al., 2002) and leads to the formation of products which affect the cement strength and increases cement resistivity.

8.1.4) Corrosion in Cement Measured Along Vertical Direction.

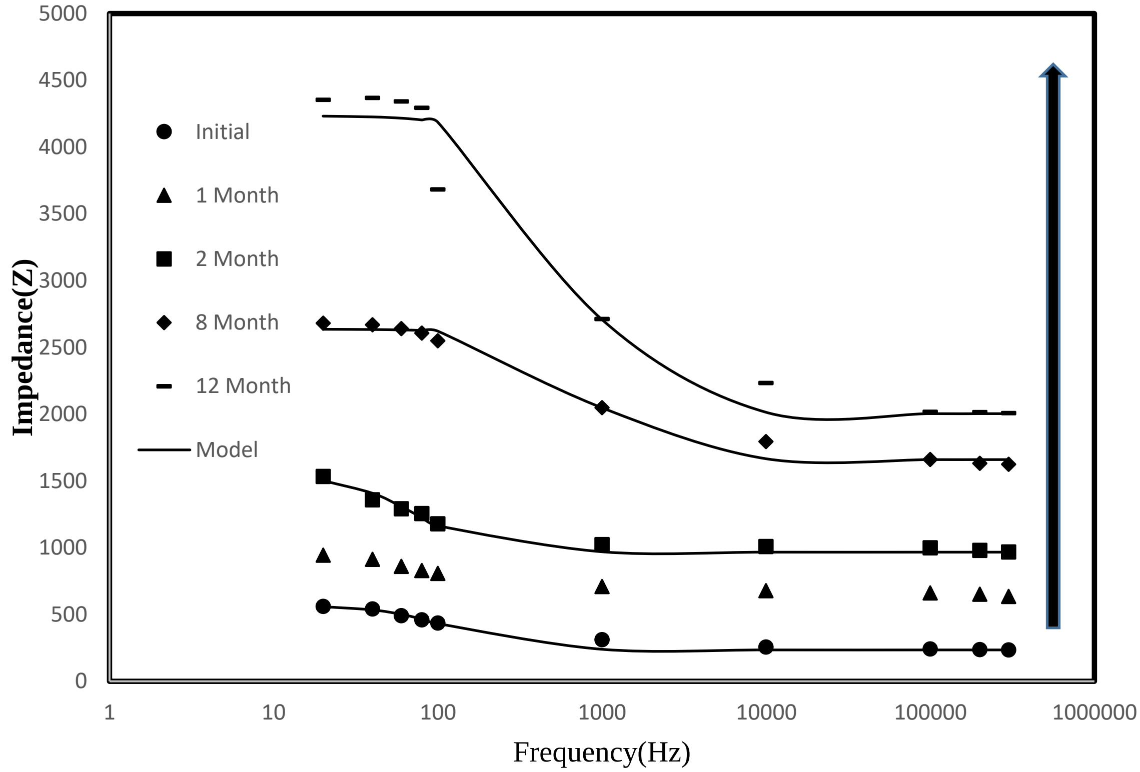

Figure 8-6 Impedance Behavior of vertical Combination AC over time.

Table 8-4 Model Parameters of the equivalent circuit for the Horizontal combination

	Rb(Ω)	Rc(Ω)	Cc	R^2	RMSE(Ω)
Initial	235	186	9.7e-05	0.97	24.12
1 Month	631	180	8.7e-05	0.99	39.41
2 Month	967	289	1.1e-05	0.99	32.16
8 Month	1905	488	4.0e-07	0.86	52.75
12 Month	2007	1114	2.1e-07	0.98	189.45

After immersion, the initial resistance was 135 Ω, and it increased to 631 Ω, 967 Ω, 1905 Ω and 2007 Ω after 1month,2months,8 months, and 12 months immersion in a saltwater solution. Similarly, the contact resistance values also increased from 186 Ω to 180Ω,289 Ω, 488 Ω, and 1114 Ω after 1month, 2 months, 8 months and 12 months respectively. The change in resistance activity shows the ongoing phenomenon of corrosion inside the cement specimen. Similarly, the contact capacitance also decreased from the initial observed value of 9.7e-05 to 8.7e-05F, 1.1e-05F, 2.29e-07F, 4.0e-07F and 2.1e-07F.

In terms of resistivity change, the resistivity of the sample increased by 197%, 255%, 894%, and 1279% after 1month,2 months,8 month and 12 months of immersion. The coefficient of determination and root mean square error observed after the immersion interval of 1month, 3month, 8months and 12months were 0.99, 0.96 ,0.98, 0.86, 0.98 and 24.12Ω, 39.41 Ω, 32.16Ω, 52.75Ω, 189.45Ω, respectively.

The vertical direction readings also show similar trends as compared to horizontal readings.The changes in measurement is actually due to the formation of by products inside cement due to seepage of electrolyte inside the cement composite.

8.1.5) Surface Characterization

The contact resistance is characterized by the product of RcCc. The contact resistance characterized the surface condition.

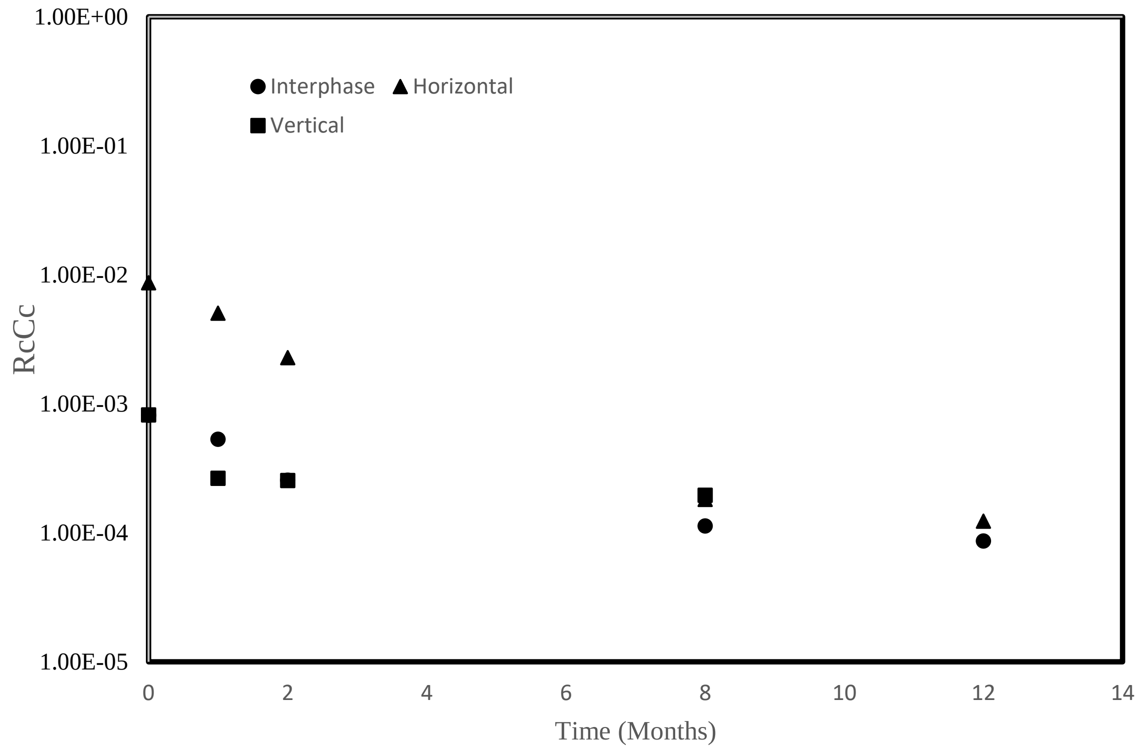

Figure 8-7 RcCc Development over Time for Interphase, horizontal, and vertical combinations.

The RcCc index for horizontal combination decreased by 41.3%, 73.45%, 97.90%, 98.58% over 1month,2month,8month and 12 months. Similarly, the RcCc index for vertical combination decreased by 67.6%, 69.03%, 76.18%, 87.66% over 1month, 2month, 8month and 12 months. The decrease in RcCc can be attributed towards the sharp decrease in contact capacitance over the immersion period. The change in Cc for the various combinations is plotted in figure 8-7.

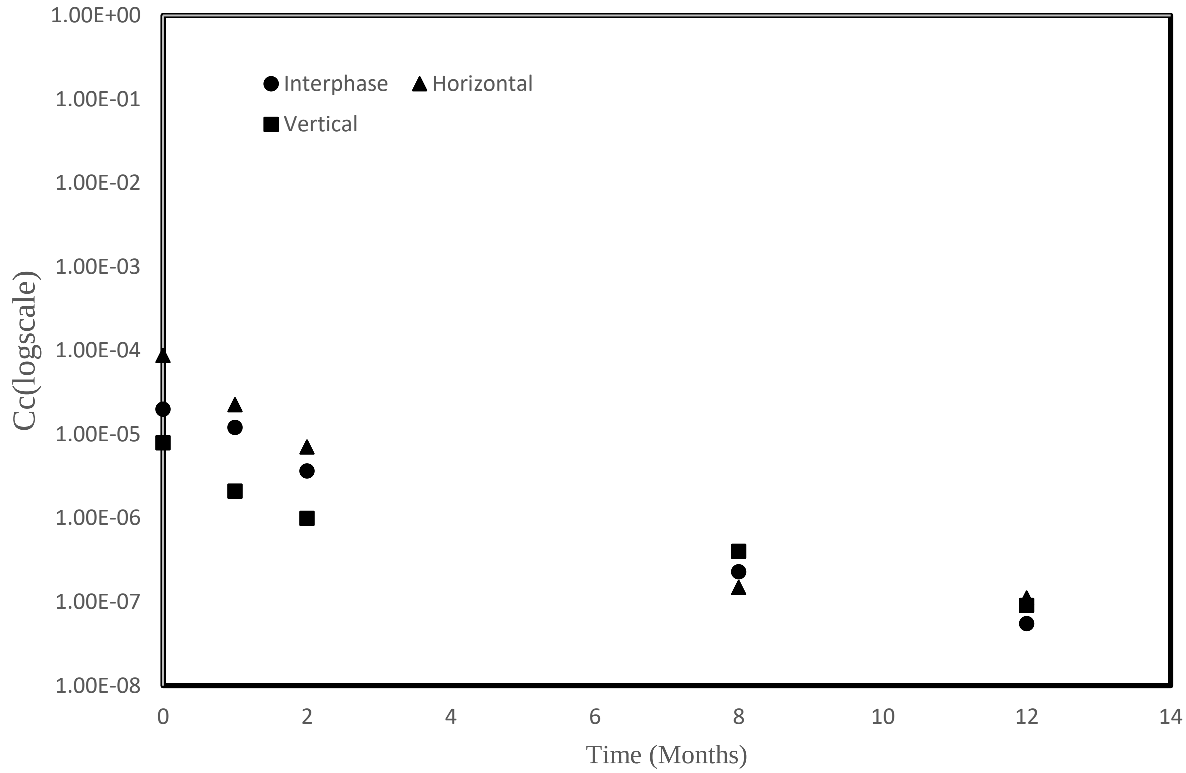

Figure 8-8 Change in contact capacitance over immersion time.

The decreases in contact capacitance explains the reasons behind decrement in RcCc. The contact capacitance decreased over 197% , 255%, 894% and 1279%; 41%, 735, 97%, 98% and 100%; 67%, 69%, 76% and 87% along interphase, horizontal and vertical directions after immersion of 1 month,2 month,8 month and 12 months. The change in contact capacitance of the material is an indicator that corrosion is occurring on the cement surface.

8.1.6) Resistivity Change Due to Corrosion

The resistivity change of the corroding steel bar and combination AA is calculated over the entire duration of immersion. The change observed in resistivity and percentage resistivity change indicates how fast the sample is corroding. Bulk resistance obtained from the impedance measurement was used to calculate the resistivity. Then electrical resistivity (ρ) is related to the measured electrical resistance (R) by the equation (3-), the change in resistivity of the steel bar and cement is calculated. The change in resistivity observed for the corroding embedded steel bar is 900%, 1356%, 8075% and 13223% after 1 month,2 month ,8 month and 12 months. In case of cement, the change in resistivity observed is 160%, 293% , 634% and 840% after 1 month,2 month ,8 month and 12 months. The change in resistivity of cement only measurements increases because of formation of deleterious products inside the cement.

The resistivity change compared with other methods like open circuit potential and weight change method shows significant change. This change indicates indicates the corrosion kinetics occurring inside cement specimen.The corrosion occurring on the surface ,as well as the bulk corrosion can be quantified be measuring the resistivity and and surface index changes.

8.2) Corrosion quantification and detection of steel coupons exposed in high-temperature electrolytes.

Steel coupon were immersed inside the saline water and corrosion behavior was studied at high temperatures. The change in electrical impedance was investigated and correlated with the resistivity change of material. The impedance change was compared with the normal steel corrosion occurring in saline environment at room temperature.The corrosion occurs in the surface and also in the bulk,Although corrosion occurs in x,y and z direction ,in this study the corrosion along the y direction is investigated.The effect of temperature effect on the corrosion of steel bar has been quantified.

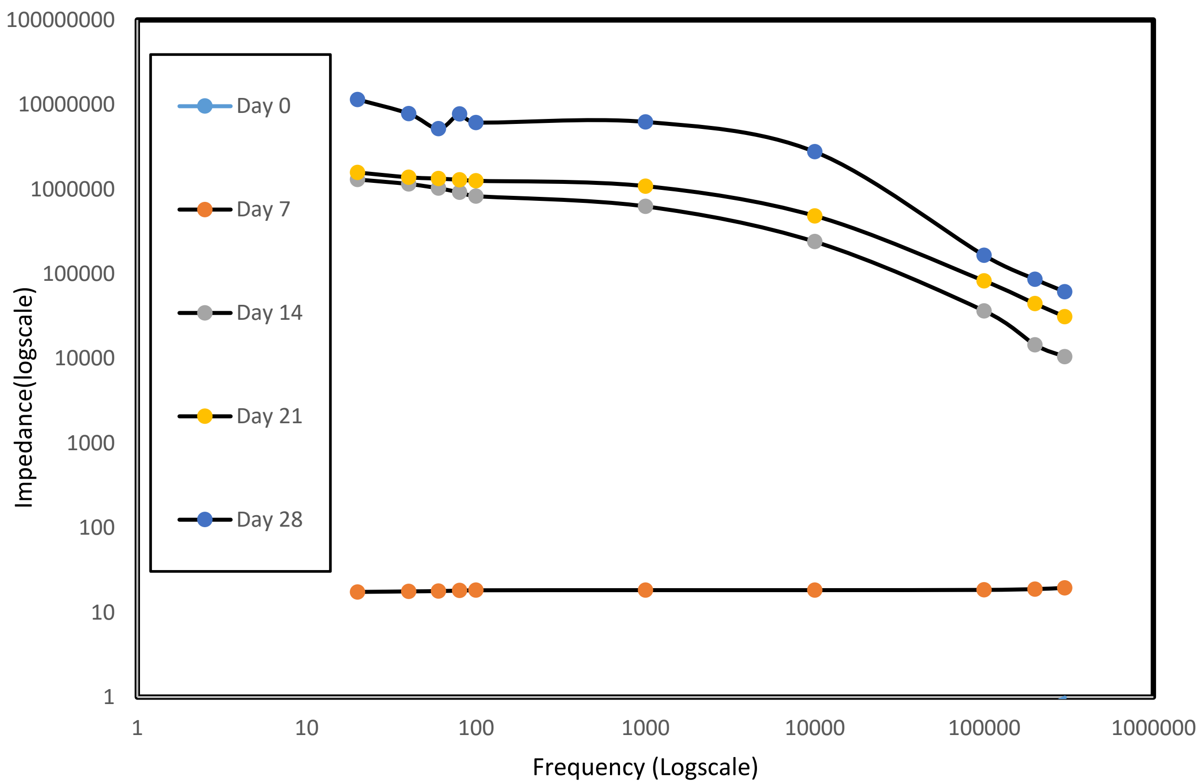

Figure 8-9 Change in Impedance curve due to Corrosion in steel coupons immersed at high temperatures.

The bulk resistance of the sample changed by 149%,1299%,15475%, and 19722% on immersion in saline water at 40^{o}C. Compared with the weight change method, the electrical impedance method is capable of detecting microscopic changes occurring on the steel surface. During the course of corrosion due to immersion inside saline water, the surface corrosivity index increased by 0.85%, 132%, 151%, and 428% over a period of 28 days. RcCc index characterized the surface corrosion occurring on the surface of steel. The contact resistance increased by 56%, 34x10^6%, 67x10^6% and 179x10^6% over the period of corrosion. Similarly, the contact capacitance decreased significantly over 1 month due to the corrosion of steel. This great change in resistance and resistivity is due to the high temperature of the electrolyte.

Figure 8-10 Image of steel coupons on Day 1.

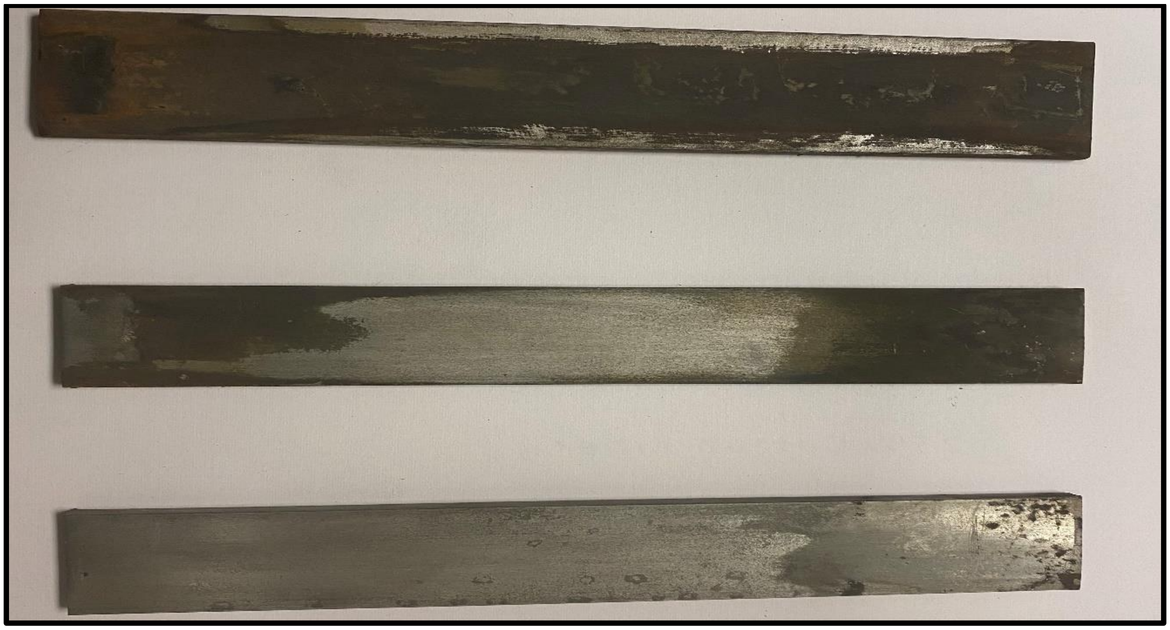

Figure 8-11 Image of steel coupons After 1 week.

Figure 8-12 Image of steel coupons After 3 week.

Figure 8-13 Image of steel coupons After 4 week.

In figure 8-10,the image of of samples before testing are shown. Samples 1 and 2 are put in saline water at an temepraure of 40^{o}C. As corrosion starts to occur the surface of the steel loses its shine,resistance and resistivity starts to increases.Figure 8-11, shows the corrosion after one week and the surface deterioration is clearly visible after one week.Similarly,the samples 1 and 2 show further deterioration after 3 weeks and 4 weeks of immersion as visible in in figure 8-12 and 8-13.Present methods like weight loss or weight gain do not show significant changes as compared with electrical impedance method.

Summary

1) The cement composite was allowed to corrode in the actual saline environment. To measure the impedance measurement of samples, these were dried to take out the existing moisture left inside due to immersion in the electrolyte.
2) A huge change in resistivity of exposed steel bar and cement was observed due to corrosion occurring inside the cement composite due to embedded steel and cement deterioration. The contact resistance increased for all the cases, and contact capacitance decreased for all cases.
3) In the case of steel coupon immersed inside the hot saline electrolyte, the corrosion was accelerated.

CHAPTER 9 CONCLUSION AND RECOMMENDATION

1) Cement rheology depends significantly on testing procedures and methods. It is affected by the temperature, the additive used. Vipulanandan model predicts the maximum shear stress and can be used for rheological prediction like yield stress and plastic viscosity.
2) The hysteresis area in the rheological test significantly suggests the structural build-up or break down. Setting time of cement of slurries can be ascertained by the ratio of hysteresis area over normal cement.
3) The addition of cellulose significantly retards the setting time of cement. Proper mixing procedure and optimum percentage of cellulose can be an effective solution for achieving delayed setting time in oil well cement. Electrical measurement techniques can be successfully employed to measure retardation of cement. Cellulose addition does not affect the sensing properties of oil well cement.
4) Polypropylene fiber addition to cement reduces the shrinkage. The optimum percentage of polypropylene fiber increase ductility and compressive strength of smart cement. Cement sensing properties gets reduced due to the addition of polypropylene fibers.
5) A new class of polymers called carboxylated styrene-butadiene is added to control gas leakage in oil well cementing is explored. The addition of carboxylated reduces the gas leakage over normal cement, and the addition of polymers reduced the sensing properties.
6) Gas leakage in cement slurry occurs only after the loss of critical fluid or volume. The ratio of critical fluid loss to total fluid loss of increased with polymer addition.

7) Gas leakage tests at different curing times of cement showed there is a critical porosity after which gas leak starts to occur. At this juncture, there is the formation of interconnected pores that allow the gas to leak through. Thus, there exists critical porosity, after which gas leak starts to occur.

8) Gas flow and leak rate can be detected by highly sensing smart cement. By measuring the electrical properties, gas flow can be ascertained. Positive change in resistivity is observed due to fluid loss, whereas the negative change in resistivity is observed at the hardened stage.

9) A non-linear model proposed by Vipulanandan shows a better prediction of gas leak rate compared with Darcy’s law. This model essentially confirms that permeability is non-linear and depends upon a lot of physical factors.

10) Polyacrylamide polymer drastically reduces the shrinkage of clay soil. Polymer application methodology is extremely important to get the desired reduction in shrinkage. Polymer addition affects the compaction results of clay soil. A significant reduction in index properties is observed due to polymer addition.

11) The electrical resistivity of soil increased due to the addition of polymer. Polymer addition coats soil particles and increases the soil resistivity of soil. Electrical resistivity can be used in field application for quality control

12) For detection and quantification of artificial ground freezing, the electrical impedance method can be deployed. Electrical resistivity is affected by the freezing and thawing process in soil.

13) Electrical Impedance method shows the corrosion kinetics and evolution of corrosion over time. The electrical impedance model circuit proposed by Vipulanandan predicts the bulk corrosion and surface corrosion.

RECOMMENDATION

1) All the additives used in this study and percentages of additive have been optimized Class H Cement. The effectiveness of additives may vary on change of cement.
2) Rheological properties of cement are essential in deciding the percentage of the addition of additives, especially in case of oil well cementing. The hysteresis area created by the ramp up and ramp down provides a knowledge of structuration occurring inside cement slurry.
3) Cement slurry evaluation can be done based on its capacity of critical fluid loss. The ratio of critical fluid loss to total fluid loss of the slurries can be used as a useful parameter to distinguish between slurries ability to prevent gas migration.
4) Polymer application can be used to prevent the swelling of clay soil. Widescale application of polymer for rapid treatment is suggested.
5) Electrical resistivity may be used as quality control in the filed applications pertaining to soil stabilization and contamination.
6) Artificial ground freezing can be easily detected by an electrical impedance method.Its sensitivity to physical changes is well demonstrated in the thesis.
7) Electrical impedance method significantly captures the corrosion kinetics and can complement existing methods for corrosion detection.

FUTURE STUDIES

1) The rheology of cement slurries may be investigated at extremely high temperatures.

2) Gas Migration test can be done at high-temperature to oversee the effect of gas leal on cement slurry.

3) Ramp up and ramp down models for rheology may be modeled with existing rheological models.

4) Corrosion of steel cement composite can be investigated at extremely high temperatures.

References

Aguwa, J. I. Effect of hand mixing on the compressive strength of concrete. *Leonardo Electronic Journal of Practices and Technologies*.

Ahmad, O. A., & Awwad, M. The Effects of Polypropylene Fibers Additions on Compressive and Tensile Strengths of Concrete. *International Journal of Civil and Environmental Engineering*, *37*(1), 1701–8285.

Al Ramadan, M., Salehi, S., Kwatia, G., Ezeakacha, C., & Teodoriu, C. Experimental investigation of well integrity: Annular gas migration in cement column. *Journal of Petroleum Science and Engineering, 179*(March), 126–135.

Alimardani, Mohammad, and Foroud Abbassi-Sourki. "New and Emerging Applications of Carboxylated Styrene Butadiene Rubber Latex in Polymer Composites and Blends: Review from Structure to Future Prospective." *Journal of Composite Materials*, vol. 49, no. 10, 2014, pp. 1267–1282.

Al-Yami, A. S. An innovative cement formula to mitigate gas migration problems in deep gas wells: Lab studies and field cases. *Society of Petroleum Engineers - SPE Kuwait Oil and Gas Show and Conference*.

Amarasinghe, P. M., Katti, K. S., & Katti, D. R. Insight into Role of Clay-Fluid Molecular Interactions on Permeability and Consolidation Behavior of Na-Montmorillonite Swelling Clay. *Journal of Geotechnical and Geoenvironmental Engineering*, *138*(2), 138–146.

Asuri, S., & Keshavamurthy, P. Expansive Soil Characterisation: an Appraisal. *INAE Letters*, *1*(1), 29–33.

Azzam, W. R. Utilization of polymer stabilization for improvement of clay microstructures. *Applied Clay Science*, *93–94*, 94–101.

Baueregger, Stefan. “Influence of Carboxylated Styrene–Butadiene Latex Copolymer on Portland Cement Hydration.” *Cement and Concrete Composites*, vol. 63, 2015, pp. 42–50.

Baueregger, Stefan.“Impact of Carboxylated Styrene–Butadiene Copolymer on the Hydration Kinetics of OPC and OPC/CAC/AH: The Effect of Ca2 Sequestration from Pore Solution.” *Cement and Concrete Research*, vol. 73, 2015, pp. 184–189.

Bermudez, M. Effect of Sugar on the Thickening Time of Cement Slurries. In *SPE Annual Technical Conference and Exhibition*.

Bishop, M., & Barron, A. R. Cement hydration inhibition with sucrose, tartaric acid, and lignosulfonate: Analytical and spectroscopic study. *Industrial and Engineering Chemistry*.

Bonett, A., & Pafitis, D. Getting to the root of gas migration. *Oilfield Review*, *8*(1), 36–49.

Bruere, G. M. Set-retarding effects of sugars in Portland cement pastes. *Nature*.

Deshmukh, V. V. A Laboratory Analysis of Permeability of Typical Cement Mixtures Used in the Permian Basin.

Firoozi, A. A., Guney Olgun, C., Firoozi, A. A., & Baghini, M. S. Fundamentals of soil stabilization. *International Journal of Geo-Engineering*, *8*(1).

Garci Juenger, M. C., & Jennings, H. M. New insights into the effects of sugar on the ydration and microstructure of cement pastes. *Cement and Concrete Research*.

Gowida, A. H., Ahmad, Z., Elkatatny, S., Mahmoud, M., & Fahd, K. *SPE- 192360 -MS Cement Evaluation Challenges*.

Graybeal, B., & Tanesi, J. A Cementitious Long-Life Wearing Course to Reduce Frequency of Maintenance Works on High-Traffic Roads. *Transport Research Arena Europe 2008*, *1561*(February), 454–461.

Han, C. G., Hwang, Y. S., Yang, S. H., & Gowripalan, N. Performance of spalling resistance of high performance concrete with polypropylene fiber contents and lateral confinement. *Cement and Concrete Research*, *35*(9), 1747–1753.

Han, L., Ye, G. L., Li, Y. H., Xia, X. H., & Wang, J. H. In situ monitoring of frost heave pressure during cross passage construction using ground-freezing method. Canadian Geotechnical Journal, 53(3), 530-539.

Heinold, T., Dillenbeck, R. L., & Rogers, M. J. The Effect of Key Cement Additives on the Mechanical Properties of Normal Density Oil and Gas Well Cement Systems. *SPE - Asia Pacific Oil and Gas Conference*, 400–411.

Kakooei, S., Akil, H. M., Jamshidi, M., & Rouhi, J. The effects of polypropylene fibers on the properties of reinforced concrete structures. *Construction and Building Materials*, *27*(1), 73–77.

Kochova, K., Schollbach, K., Gauvin, F., & Brouwers, H. J. H. Effect of saccharides on the hydration of ordinary Portland cement.

Kolay, P. K., Dhakal, B., Kumar, S., & Puri, V. K. Effect of Liquid Acrylic Polymer on Geotechnical Properties of Fine-Grained Soils. *International Journal of Geosynthetics and Ground Engineering*, *2*(4), 1–9.

Kong, Xiangming. “Effect of Polymer Latexes with Cleaned Serum on the Phase Development of Hydrating Cement Pastes.” *Cement and Concrete Research*, vol. 84, 2016, pp. 30–40.

Konrad, J. M. Prediction of freezing-induced movements for an underground construction project in Japan. Canadian Geotechnical Journal, 39(6), 1231-1242.

Labibzadeh, M., Zahabizadeh, B., & Khajehdezfuly, A. Early-age compressive strength assessment of oil well class G cement due to borehole pressure and temperature changes. *Shahid Chamran University, 6*(7), 38–47.

Lackner, R., Amon, A., & Lagger, H. Artificial ground freezing of fully saturated soil: thermal problem. Journal of Engineering Mechanics, 131(2), 211-220.

Lee, I. Complete stress-strain characteristics of high performance concrete. *ProQuest Dissertations and Theses*, 119-119 p.

Li, H. N., Li, D. S., & Song, G. B. Recent applications of fiber optic sensors to health monitoring in civil engineering. Engineering structures, 26(11), 1647-1657.

Li, H., & Ou, J. The state of the art in structural health monitoring of cable-stayed bridges. Journal of Civil Structural Health Monitoring, 6(1), 43-6

Li, Z., Vandenbossche, J. M., Iannacchione, A. T., Brigham, J. C., & Kutchko, B. G. Theory-Based review of limitations with static gel strength in cement/matrix characterization. *SPE Drilling and Completion, 31*(2), 145–158.

Lijah Abalaka, A. Effects of Sugar on Physical Properties of Ordinary Portland Cement Paste and Concrete. *Au J.T.*, *14*(3), 225–228.

Liu, J., Shi, B., Gu, K., Jiang, H., & Inyang, H. I. Effect of polyurethane on the stability of sand-clay mixtures. *Bulletin of Engineering Geology and the Environment*.

Lyomov, S. K., Backe, K. R., Skalle, P., Lile, O. B., Justnes, H., & Sveen, J. Shrinkage of oil well cement slurries. *Annual Technical Meeting 1997, ATM 1997*.

Md Zahri, A., & Zainorabidin, A. An overview of traditional and non traditional stabilizer for soft soil. *IOP Conference Series: Materials Science and Engineering*, *527*(1).

Milind V. Mohod. Performance of Polypropylene Fibre Reinforced Concrete. *IOSR Journal of Mechanical and Civil Engineering (IOSR-JMCE)*, *12*(1), 28–36.

Mousavi, F., Abdi, E., & Rahimi, H. Effect of polymer stabilizer on swelling potential and CBR of forest road material. *KSCE Journal of Civil Engineering*, *18*(7), 2064–2071.

Murvay, P. S., & Silea, I.A survey on gas leak detection and localization techniques. *Journal of Loss Prevention in the Process Industries*, *25*(6), 966–973.

Naeini, S. A., Naderinia, B., & Izadi, E. Unconfined compressive strength of clayey soils stabilized with waterborne polymer. *KSCE Journal of Civil Engineering*, *16*(6).

Namkon, L., Abhinav, P., Gary, O. K. C., Juhyuk, M., Min-Hong, Z., Arthur, C. C. H., Hau, K. K. Experimental design of a well cement slurry for rapid gel strength development. *Construction and Building Materials*, *191*, 1093–1102.Pakeetharan, S. *Characterization of Sensing Repair Materials*. 138.

Panda, G., and C. Vipulanandan Effect of Polypropylene Fiber on Oilwell Cement Behavior.CIGMAT-2018 Conference & Exhibition.

Panda, G., and C. Vipulanandan. Annual Daily Temperature Prediction using the ANN with and without Hurricane.THC-IT-2019 Conference & Exhibition.

Panda, G., and C. Vipulanandan. Moisture Healing Efficiency of Polymer Modified Smart Cement. CIGMAT-2018 Conference & Exhibition.

Panda, G., and C. Vipulanandan. Applying Electrical Impedance technique for Structural Health Monitoring. THC-IT-2017 Conference & Exhibition.

Panda, G., and C. Vipulanandan. Characterizing Initial Steel Corrosion in Polymer Modified Smart Cement.THC-IT-2018 Conference & Exhibition

Panda, G., and C. Vipulanandan. Clay Soil Stabilization by Polymers. CIGMAT-2016 Conference & Exhibition.

Panda, G., and C. Vipulanandan. Clay Soil Treatment using Water Soluble Polymer. CIGMAT-2017 Conference & Exhibition.

Panda, G., and C. Vipulanandan. Detection and quantification of Gas leak in Smart Cement. CIGMAT-2019 Conference & Exhibition.

Panda, G., and C. Vipulanandan. Effect of Cellulose Material on Oil Well Smart Cement THC-2016 Conference & Exhibition.

Panda, G., and C. Vipulanandan. Effect of Dewatering on the phreatic surface in the sand in a confined area. THC-2019 Conference & Exhibition.

Panda, G., and C.Vipulanandan. Factor Influencing Surface Soil Settlement Due to Dewatering.THC-IT-2019 Conference & Exhibition

Panda, G., and C. Vipulanandan. Quantifying Gas Flow through Soils. THC-IT-2018 Conference & Exhibition.

Panda, G., and C. Vipulanandan. Verification of load-displacement Response of Augur Cast Pile in Clay.CIGMAT-2019 Conference & Exhibitio

Papakonstantinou, S., & Anagnostou, G. Numerical interpretation of temperature distributions from three ground freezing applications in urban tunnelling. Tunnelling and Underground Space Technology, 28, 57-69.

Pour, M. M., & Moghadasi, J. New cement formulation that solves gas migration problems in Iranian south pars field condition. *SPE Middle East Oil and Gas Show and Conference, MEOS, Proceedings, 3*(March 2007), 1368–1375.

Qi, J., Ma, W., & Song, C. Influence of freeze–thaw on engineering properties of a silty soil. Cold regions science and technology, 53(3), 397-404.

Qu, Xiaoling, and Xuguang Zhao. "Influence of SBR Latex and HPMC on the Cement Hydration at Early Age." *Case Studies in Construction Materials*, vol. 6

Ramalho, Ramón Victor Alves. "Evaluation of Mechanical Properties of Cement Slurries Containing SBR Latex Subjected to High Temperatures." *Journal of Petroleum Science and Engineering*, vol. 178, 2019, pp. 787–794.

Roy, S S, Dash, SR. Dynamic Behavior of Multi Span Continuous Girder Bridge with Isolation Bearings. International Journal of Bridge Engineering.

Roy, S S., Sawab, J., Zhou, T., Mo, Y. L., Hsu, T. T. C.. Performance of Skew Reinforcing in Inverted-T Bridge Caps. Transportation Research Record, 2672(41).

Ratu, R. N., Of, M., & Science, A. Development of Polypropylene Fiber As Concrete Reinforcing Fiber, (April).

Rehman, S. K. U., Ibrahim, Z., Memon, S. A., & Jameel, M. Nondestructive test methods for concrete bridges: A review. Construction and Building Materials, 107, 58-86.

Rhoades, J. D., Raats, P. A. C., & Prather, R. J. Effects of Liquid-phase Electrical Conductivity, Water Content, and Surface Conductivity on Bulk Soil Electrical Conductivity1. *Soil Science Society of America Journal*, *40*(5), 651.

Russo, G., Corbo, A., Cavuoto, F., & Autuori, S. Artificial ground freezing to excavate a tunnel in sandy soil. Measurements and back analysis. Tunnelling and Underground Space Technology, 50, 226-238.

Sabins, F. L., & Sutton, D. L. Relationship of Thickening Time, Gel Strength, and Compressive Strength of Oil Well Cements. *SPE Production Engineering*, *1*(2),

Samudio, M. Modelling of an oil well cement paste from early age to hardened state : hydration kinetics and poromechanical behaviour.

Spaulding, R. A Quantitative Assessment of Atmospherically generated Foam Cements: Insights, Impacts, and Implications of Wellbore Integrity and Stability.

Sridharan, A., & Prakash, K. Classification procedures for expansive soils. *Proceedings of the Institution of Civil Engineers: Geotechnical Engineering*, *143*(4), 235–240.

Taha Jawad, I., Raihan Taha, M., Hameed Majeed, Z., & A. Khan, T. Soil Stabilization Using Lime: Advantages, Disadvantages and Proposing a Potential Alternative. *Research Journal of Applied Sciences, Engineering and Technology*, *8*(4), 510–520.

Thomas, P. J. Quantifying Properties and Variability of Expansive Soils in Selected Map Units by of Expansive Soils in Selected Map Units. *Analysis*.

Velayati, A., Tokhmechi, B., Soltanian, H., & Kazemzadeh, E. Cement slurry optimization and assessment of additives according to a proposed plan. *Journal of Natural Gas Science and Engineering*, *23*, 165–170.

Vipulanandan, C, and A Mohammed. "Smart Cement Modified with Iron Oxide Nanoparticles to Enhance the Piezoresistive Behavior and Compressive Strength for Oil Well Applications." *Smart Materials and Structures*, vol. 24, no. 12, June 2015, p. 125020.

Vipulanandan, C., and A. Mohammed. "Rheological Properties of Piezoresistive Smart Cement Slurry Modified with Iron-Oxide Nanoparticles for Oil-Well Applications." *Journal of Testing and Evaluation*, vol. 45, no. 6, 2017.

Vipulanandan, C., and P. Prashanth. "Impedance Spectroscopy Characterization of a Piezoresistive Structural Polymer Composite Bulk Sensor." *Journal of Testing and Evaluation*, vol. 41, no. 6, 2013, p. 20120249

Vipulanandan C, A Aldughather, Guru Panda**,** G Wong. Real-Time Gas Leak Detection and Quantification Using Smart Cement. International Petroleum Technology Conference,2020

Vipulanandan C, Guru Panda, AR Maddi, G Wong, A Aldughather. Characterizing Smart Cement Modified with Styrene Butadiene Polymer for Quality Control Curing and to Control and Detect Fluid Loss and Leaks Using Vipulanandan Models. Offshore Technology Conference,2019

Vipulanandan C,, C Ganapathy, KA Gebreselassie, D Pan, Guru Panda. New Rapid Nondestructive Testing Method for Detecting and Quantifying with Material Property Changes Using Vipulanandan Impedance Corrosion Model.Offshore Technology Conference,2019

Vitorino, Fabrício De C. "Hydration at Early Ages of Styrene-Butadiene Copolymers Cementitious Systems." *Journal of Thermal Analysis and Calorimetry*, vol. 131, no. 2, 2017, pp. 1041–1054.

Vondran, G. L., Nagabhushanam, M., & Ramakrishnan, V.. Fatigue Strength of Polypropylene Fiber Reinforced Concretes. *Fiber Reinforced Cements and Concretes: Recent Developments*, (Journal Article), 533–543.

Weyer, H. J., Müller, I., Schmitt, B., Bosbach, D., & Putnis, A. Time-resolved monitoring of cement hydration: Influence of cellulose ethers on hydration kinetics. *Nuclear Instruments and Methods in Physics Research, Section B: Beam Interactions with Materials and Atoms*, *238*(1–4).

Wilcox, Bomá. "HPHT Well Integrity and Cement Failure." *SPE Nigeria Annual International Conference and Exhibition*, 2016.

Yan, Q., Wu, W., Zhang, C., Ma, S., & Li, Y. Monitoring and Evaluation of Artificial Ground Freezing in Metro Tunnel Construction-A Case Study. KSCE Journal of Civil Engineering, 1-12.

Yan, Q., Xu, Y., Yang, W., & Geng, P. Non-linear transient analysis of temperature fields in an AGF project used for a cross-passage tunnel in the Suzhou metro. KSCE Journal of Civil Engineering, 1-11.

Yang, B. han, Weng, X. zhong, Liu, J. zhong, Kou, Y. nan, Jiang, L., Li, H. lei, & Yan, X. cheng. Strength characteristics of modified polypropylene fiber and cement-reinforced loess. *Journal of Central South University*, *24*(3), 560–568

Yang, P., Ke, J. M., Wang, J. G., Chow, Y. K., & Zhu, F. B. Numerical simulation of frost heave with coupled water freezing, temperature and stress fields in tunnel excavation. Computers and Geotechnics, 33(6-7), 330-340.

Yao, X., Qi, J., & Ma. Influence of freeze-thaw on the stored free energy in soils. Cold Regions Science and Technology, 56(2-3), 115-119.

Appendix A:Ramp Up and Ramp Down Results of Rheology

The ramp up and ramp down models for the rheology ae modelled and presented below. In this appendix the model ramp- up and ramp -down are modelled. It is modelled using Bingham plastic and Vipulanandan Model.

Table 1 -Model Parameters for ramp up and ramp down model.

	Bingham Model					Vipu Model				
	Temp	τ1	k	R^2	RMSE(Pa)	τ1	C	D	R^2	RMSE(Pa)
UP Curve	20	10.30	0.13	0.97	4.53	10.73	7.65	-0.001	0.97	4.52
	40	9.99	0.14	0.92	7.52	11.15	8.11	-0.002	0.92	7.49
	60	11.56	0.15	0.94	7.01	5.01	3.22	0.006	0.96	5.74
Down Curve	20	15.16	0.05	0.95	6.34	6.01	2.59	0.007	0.97	2.23
	40	16.04	0.18	0.94	8.46	6.04	2.35	0.005	0.99	3.96
	60	20.80	0.18	0.91	10.16	7.02	1.80	0.006	0.99	3.82

Table 2 -Model Parameters for ramp up and ramp down model with different polymer Content.

		Bingham Model				Vipulanandan Model				
		τ1	k	R^2	RMSE(Pa)	τ1	C	D	R^2	RMSE(Pa)
UP Curve	20 1	9.48	0.13	0.97	4.13	10.89	9.34	-0.003	0.971	3.99
	20 2	8.92	0.11	0.97	3.45	10.48	10.74	-0.004	0.976	3.31
	20 3	9.75	0.11	0.96	4.14	12.56	14.46	-1.01	0.971	3.45
	20 5	9.71	0.07	0.97	2.24	10.93	17.81	-0.009	0.980	1.94
Down Curve	20 1	14.67	0.14	0.96	5.36	7.37	3.13	0.007	0.992	2.34
	20 2	13.74	0.12	0.96	4.41	8.09	3.89	0.008	0.989	2.31
	20 3	13.21	0.11	0.97	3.86	10.01	5.35	0.006	0.977	3.21
	20 5	12.57	0.07	0.96	2.92	9.07	6.27	0.018	0.982	1.84

Table 3 -Model Parameters for ramp up and ramp down model with different polymer Content.

	Bingham Model					Vipulanandan Model				
	Temp	τ1	k	R^2	RMSE	τ1	C	D	R^2	RMSE
Up Curve	20 1	9.48	0.13	0.97	4.14	10.83	9.34	-0.003	0.97	3.99
	20 3	9.75	0.11	0.96	4.14	12.56	14.46	-0.011	0.97	3.45
	40 1	10.22	0.08	0.89	4.81	12.41	22.97	-0.020	0.90	4.62
	40 3	10.4	0.04	0.80	4.14	5.93	3.19	0.013	1.00	0.92
	60 1	15.52	0.14	0.95	6.03	8.64	3.2	0.006	0.98	4.25
	60 3	46.33	0.15	0.98	12.75	23.68	0.95	0.009	0.98	4.96
Down Curve	20 1	14.67	0.14	0.96	5.37	7.33	3.13	0.007	0.99	2.34
	20 3	13.215	0.12	0.97	3.87	10.01	5.37	0.006	0.98	3.21
	40 1	13.68	0.09	0.92	5.12	5.93	3.19	0.013	1.00	0.941
	40 3	21.27	0.05	0.79	5.37	13.69	3.19	0.021	0.95	2.57
	60 1	30.7	0.15	0.89	9.57	16.62	1.78	0.009	0.99	2.35
	60 3	83.23	0.09	0.77	9.62	72.69	2.39	0.013	0.89	6.61

Appendix B: Error Plots of Effect of PP fiber on Smart Cement.

The error plots for the work in polypropylene fibers is presented. Here the range of experimental data have been shown over the sample of test performed. In this appendix the initial resistivity plot, long term curing ,1 day compressive stress-strain,28 days compressive stress-stain ,piezo resistivity and 28 days piezo resistivity is plotted for reference.

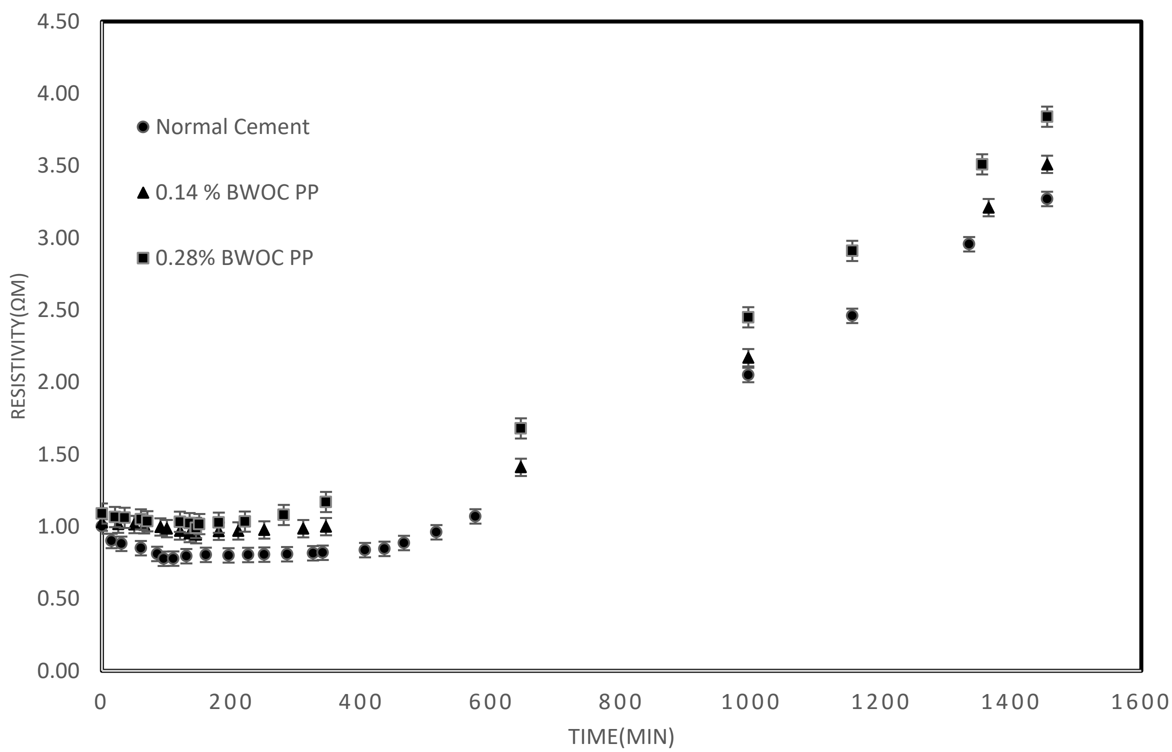

Figure 1 -One Day Curing of Smart Cement

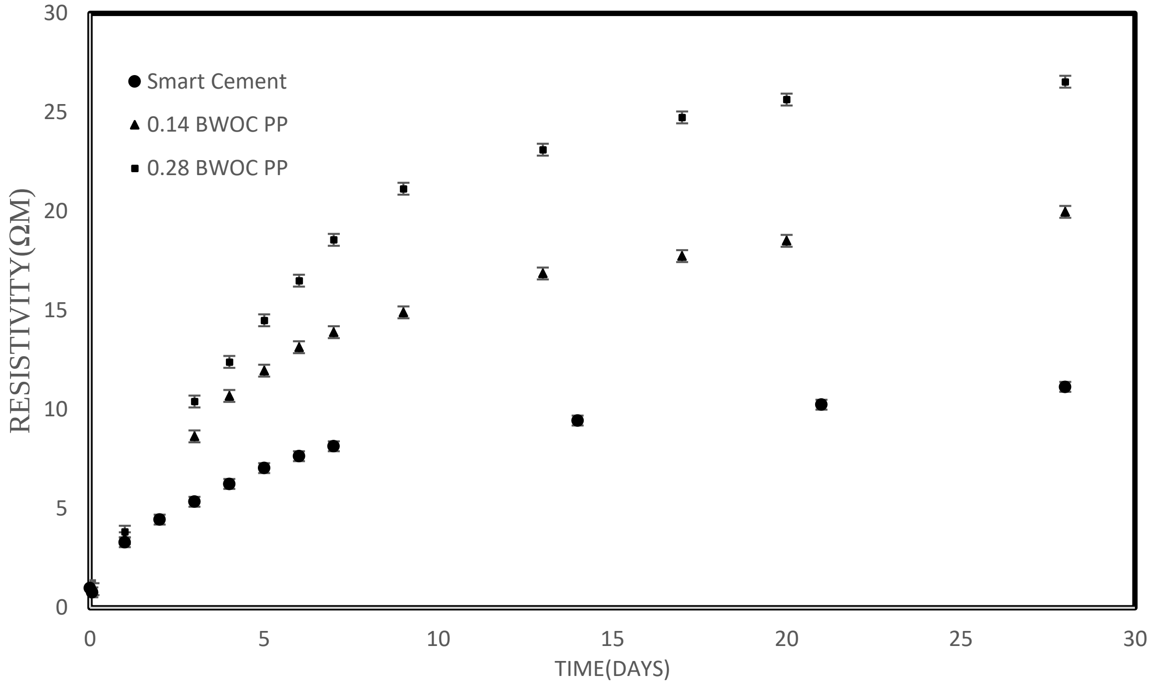

Figure 2-Long Term Curing Model (samples are kept Inside mold)

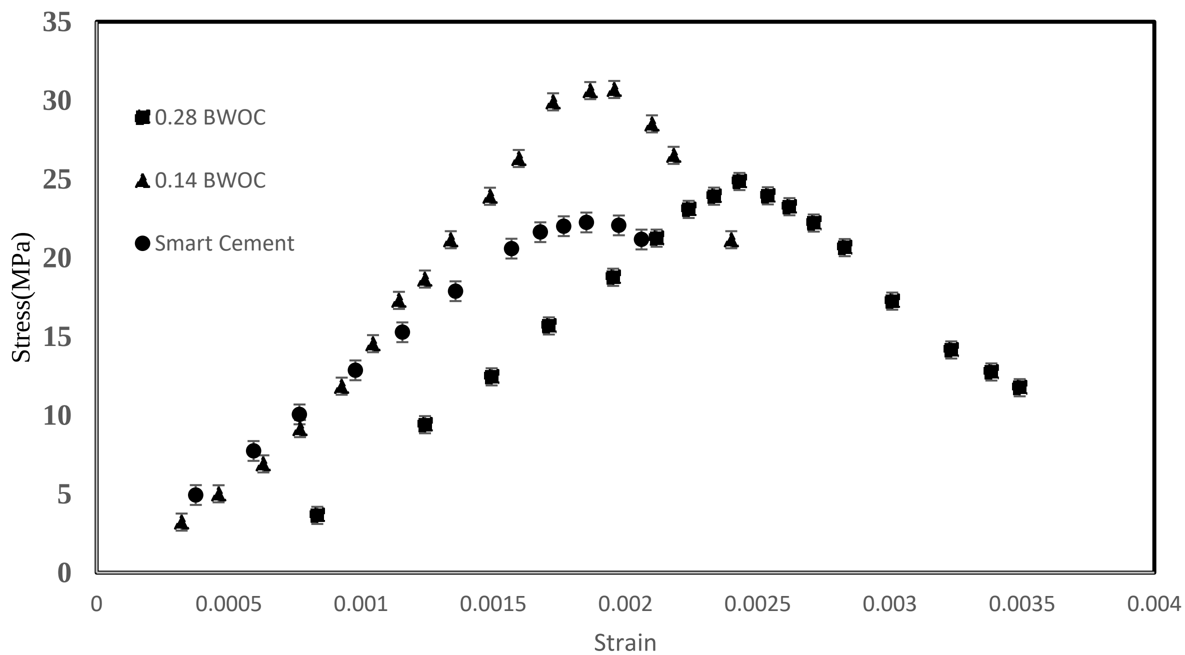

Figure 3-Compressive strength of smart cement,0.14% and 0.28% BWOC after 1 day

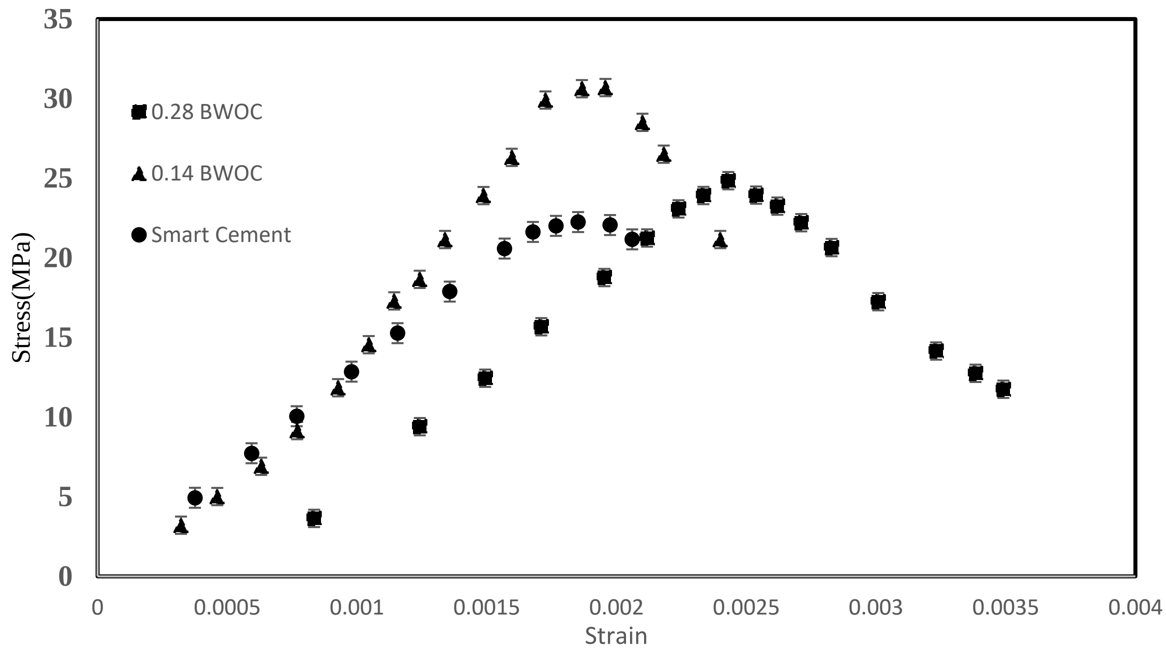

Figure 4-Compressive strength of smart cement,0.14% and 0.28% BWOC after 28 day

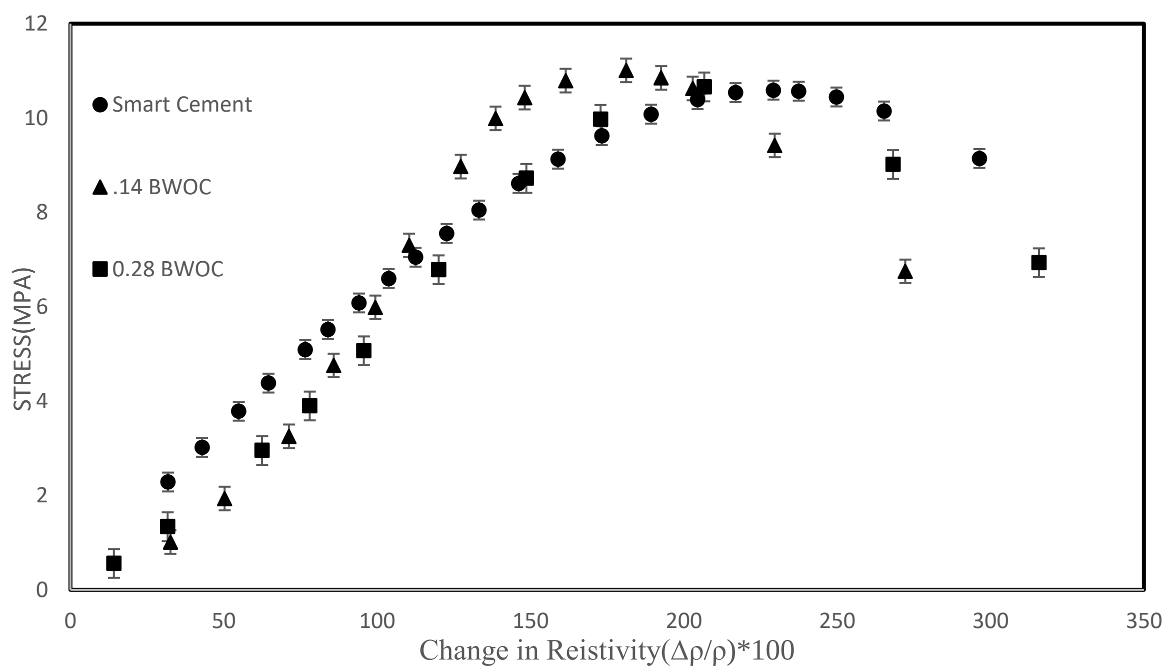

Figure 5 – Piezoresistive behavior of smart Cement after one Day of Curing

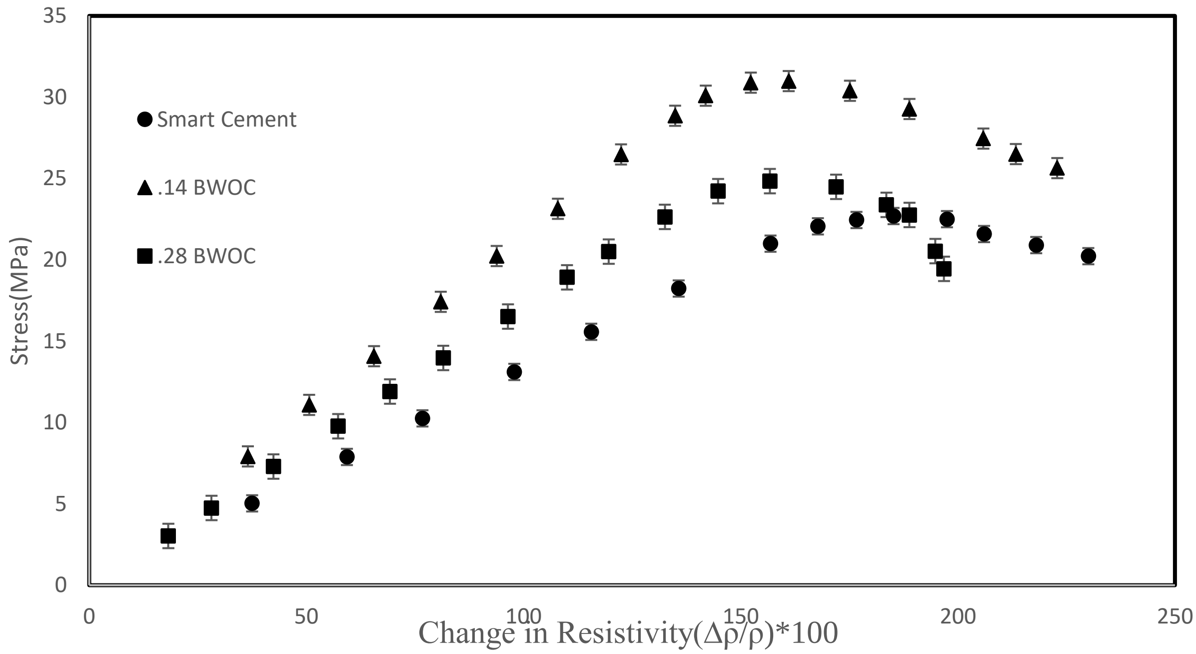

Figure 6 – Piezoresistive behavior of smart Cement after 28 Days of Curing.

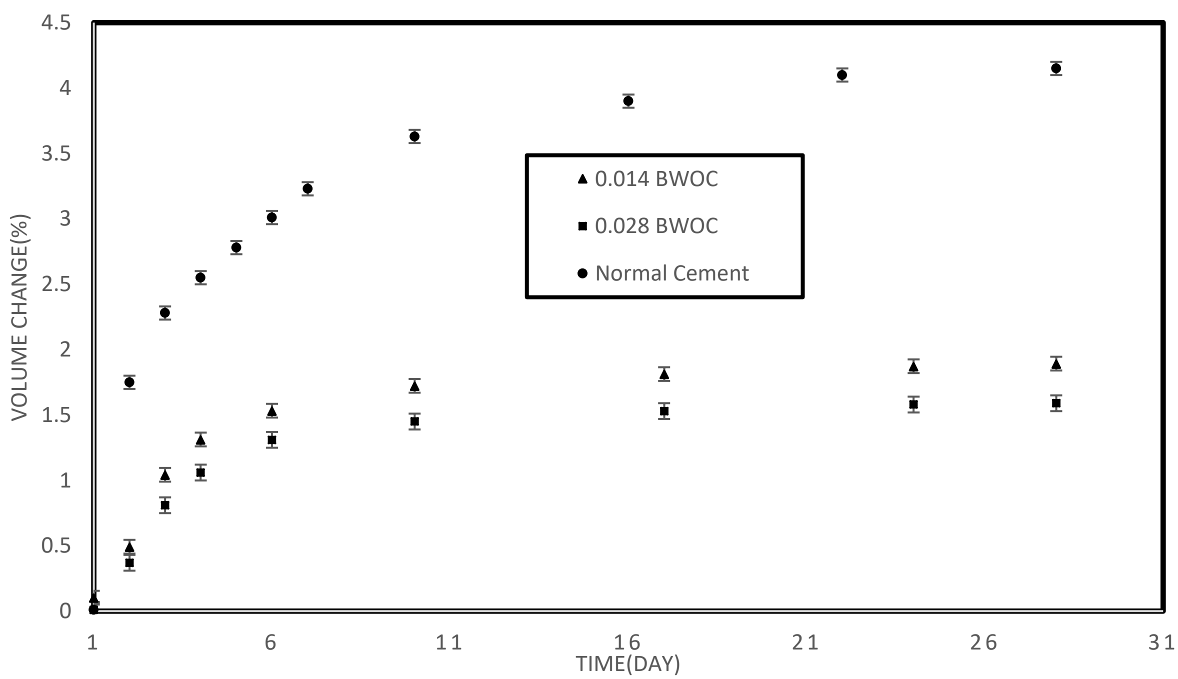

Figure 7 -Long Term Shrinkage of Smart Cement with and without fibers.